

# Reactive fluorescent dye systems for single-molecule studies

Dissertation  
zur Erlangung des Grades  
des Doktors der Naturwissenschaften  
der Naturwissenschaftlich-Technischen Fakultät III -  
Chemie, Pharmazie, Bio- und Werkstoffwissenschaften  
der Universität des Saarlandes

von  
**Alexander Schmitt**

Saarbrücken  
2009



Die folgende Arbeit entstand unter der Anleitung von Herrn Professor jun. Dr. Gregor Jung in der Abteilung Biophysikalische Chemie der Fachrichtung 8.1 Chemie der Universität des Saarlandes in Saarbrücken von Oktober 2005 bis August 2009.

Mein besonderer Dank gilt:

Herrn Prof. jun. Dr. Gregor Jung für die Aufnahme in seinen Arbeitskreis und die interessante, breitgefächerte Themenstellung, die Möglichkeit zur Teilnahme an internationalen Kongressen, seine Geduld und die immer vorhandene Bereitschaft zur Diskussion und Beratung.

Frau Babette Götzendorfer (ehemals Hinkeldey) danke ich für die Jahre der Zusammenarbeit, der Hilfsbereitschaft und Freundschaft und für all den Spass, den wir im Arbeitsalltag, auf Tagungen und in Kneipen hatten.

Frau Nicole Bach für ihre freundschaftliche Hilfe und Unterstützung bei Forschung und Arbeitskreisorganisation.

Frau Dagmar Auerbach für die Unterstützung bei all dem Organisatorischen und Ihre STETS vorhandene Bereitschaft zur Diskussion.

Frau Silke Altmeier, Herrn Benjamin Hötzer, Herrn Matthias Basters und Herrn Stephan Gerharz für die Jahre der Hilfe und Unterstützung in Forschung und Leben.

All den Studis, Vertiefern und Hiwis, die mir über die Jahre bei den Synthesen und Analysen unter die Arme gegriffen haben.

Herrn Rainer Wintringer, Herrn Josef Wilhelm, Herrn Norbert Ochs, Herrn Jens Wiegert und Herrn Peter Skohutil für die schnelle Hilfe in technischen Fragen.

Herrn Harald Toader für das Korrekturlesen und das geduldige Ausbessern meiner Englischkenntnisse.

All meinen Freunden und bekannten Nicht-Chemikern dafür, dass sie mich in schweren Zeiten immer geduldig ertragen haben.

Zuletzt meiner Familie für ihre liebevolle Unterstützung und dafür, dass sie immer hinter mir standen.

“Wenn eine Idee am Anfang nicht absurd klingt, dann gibt es keine Hoffnung für sie.”

-Albert Einstein-

**meinen Eltern Melitta und Harald**

# Table of Contents

|          |  |           |
|----------|--|-----------|
| <b>1</b> | <b>Abstract</b>  | <b>1</b>  |
| <b>2</b> | <b>General Part</b>  | <b>3</b>  |
| 2.1      | Introduction . . . . .   | 3         |
| 2.2      | The BODIPY dye system . . . . .  | 5         |
| 2.2.1    | General and historic information . . . . .   | 5         |
| 2.2.2    | The BODIPY system and its structure . . . . .  | 6         |
| 2.2.3    | Chemistry and characteristics of BODIPYs . . . . .   | 7         |
| 2.2.4    | Syntheses of BODIPY dyes . . . . .   | 9         |
| 2.2.5    | BODIPYs for fluorescent model systems . . . . .  | 13        |
| 2.3      | Fluorescence spectroscopic investigations . . . . .  | 20        |
| 2.3.1    | Interactions of light and matter . . . . .   | 20        |
| 2.3.2    | Classical optical spectroscopy: . . . . .  | 21        |
|          | Absorption . . . . .   | 21        |
|          | Excitation/Emission . . . . .  | 21        |
| 2.3.3    | Modern optical spectroscopy: . . . . .   | 25        |
|          | Fluorescence Correlation Spectroscopy (FCS) . . . . .  | 25        |
|          | Time Correlated Single Photon Counting (TCSPC) . . . . .   | 29        |
| 2.3.4    | Ratiometric Methods . . . . .  | 30        |
| 2.3.5    | Excited state reactivity (ESPT) . . . . .  | 32        |
| 2.3.6    | The Solvatochromic Comparison Method . . . . .   | 35        |
|          | The Kamlet-Taft-equation . . . . .   | 36        |
|          | Differential solvatochromism . . . . .   | 37        |
|          | The Ooshika-Lippert-Mataga-Equation . . . . .  | 39        |
| <b>3</b> | <b>Publications of the results</b>   | <b>42</b> |
| 3.1      | <i>Comparative Photostability Studies of BODIPY and Fluorescein Dyes by Using Fluorescence Correlation Spectroscopy</i> ; Babette Hinkeldey, Alexander Schmitt, Gregor Jung*; <i>ChemPhysChem</i> <b>2008</b> , 9, 2019-2027 . . . . . | 43        |

|          |   |            |
|----------|---|------------|
| 3.2      | <i>Synthesis of the Core Compound of the BODIPY Dye Class: 4,4-Difluoro-4-bora-(3a,4a)-diazas-indacene; Alexander Schmitt, Babette Hinkeldey, Mandy Wild, Gregor Jung*; J. Fluoresc. 2009, 19, 755-758 . . . . .</i>                                | 79         |
| 3.3      | <i>Disabling Photoinduced Electron Transfer in 4,4-Difluoro-8(-4'-hydroxyphenyl)-1,3,5,7-tetramethyl-4-bora-3a,4a-diazas-indacene by Phosphorylation; Michaela Jacob, Alexander Schmitt, Gregor Jung*; J. Fluoresc. 2008, 18, 639-644 . . . . .</i> | 90         |
| 3.4      | <i>Solvent-dependent steady-state fluorescence spectroscopy for searching ESPT-dyes: Solvatochromism of HPTS revisited; Gregor Jung*, Stephan Gerharz, Alexander Schmitt; Phys. Chem. Chem. Phys. 2009, 11, 1416- 1426 . . . . .</i>                | 103        |
| 3.5      | <i>Fluorescent Probes for Chemical Transformations on the Single-Molecule Level; Gregor Jung*, Alexander Schmitt, Michaela Jacob, Babette Hinkeldey; Ann. N. Y. Acad. Sci. 2008, 1130, 131-137 . . . . .</i>  | 129        |
| 3.6      | <i>A ratiometric fluorescent substrate for mechanistic studies of oxidation reactions; Alexander Schmitt, Babette Hinkeldey, Benjamin Hötzer, Gregor Jung*; J. Phys. Org. Chem. 2009, accepted . . . . .</i>  | 142        |
| <b>4</b> | <b>Appendix</b>   | <b>163</b> |
| 4.1      | Research in progress: A BODIPY dye for metathesis screening . . . . .   | 163        |
| 4.1.1    | The metathesis reaction . . . . .   | 163        |
| 4.1.2    | A BODIPY dye as a probe for metathesis catalysis  | 165        |
| 4.1.3    | BODIPYs and Grubbs reactions . . . . .  | 167        |
| 4.1.4    | Conclusion on metathesis . . . . .  | 173        |
| 4.2      | Bibliography . . . . .  | 174        |
| 4.3      | List of Figures . . . . .   | 181        |
| 4.4      | List of Equations . . . . .   | 185        |

# 1 Abstract

Die Einzelmolekülspektroskopie ist eine in der Physik und den Lebenswissenschaften etablierte Methode. Anwendungen auf mechanistische Fragestellungen in der Chemie sind selten, was auf das Fehlen geeigneter Fluorophore zurückzuführen ist. Deshalb stand in dieser Arbeit die Entwicklung eines reaktiven Systems zur späteren Visualisierung von chemischen Reaktionen auf dem Einzelmolekülniveau im Vordergrund. Es wurden Farbstoffsysteme auf der Basis der BODIPY Fluorophore dargestellt. Erstmals wird hier die Synthese der Stammverbindung dieser Farbstofffamilie beschrieben. Methylierte Derivate der Stammverbindung wurden hinsichtlich ihrer Photostabilität charakterisiert und als überlegen gegenüber Fluorescein eingestuft. Photophysikalische Elementarprozesse wurden auf ihre Eignung als Auslesemechanismus für das Projektziel untersucht. Hier konnte ein Substrat für Phosphorsäureesterspaltungen entwickelt werden, bei dem die Reaktion durch eine Änderung der Fluoreszenzlebensdauer detektiert werden kann. Ein anderer Auslesemechanismus beruht auf dem Wechsel der Fluoreszenzfarbe durch chemische Reaktionen. Hier konnten entsprechende Substrate für Oxidationsreaktionen wie auch für Metathesereaktionen entwickelt werden. Diese Systeme stellen vielversprechende Kandidaten für die projektierte Verfolgung individueller Reaktionsabläufe durch ultrasensitive Fluoreszenzspektroskopie dar.

Single-molecule spectroscopy is a well established method in physics and life sciences. Appliances on mechanistic problems in chemistry are rare, which can be traced back to the lack of suitable fluorophores. Therefore the development of a reactive system for future imaging of chemical reactions on a single-molecule level had top priority in this work. Dye systems based on the BODIPY fluorophore were prepared. For the first time, the synthesis of the core compound of this dye family is presented here. Methylated derivatives of this core compound have been characterized concerning

## 1. Abstract

their photostability and were categorized as superior to fluorescein. Elementary photophysical processes have been examined for their suitability as read-out mechanism for the project aim. Here a substrate for phosphorester cleavage has been developed where the reaction could be detected by a change of fluorescence lifetime. Another read-out mechanism was based on the change of fluorescence colour by chemical reactions. Appropriate substrates for oxidation reactions and metathesis reactions could be developed. The systems are promising candidates for the projected pursuit of individual reaction processes by ultrasensitive fluorescence spectroscopy.

## 2 General Part

### 2.1 Introduction

In recent years technical advances in imaging technology, due to advances in the design of optical systems and the remarkable increase of computational power, made achievements in natural sciences possible that could not be reached before [Bin82, Moe89, Orr90, Upp99, Nie94, Bet93]. It is quite common nowadays to observe the interactions of individual proteins in living cells. The field of research today is even close to pursuit reactions on a single-molecule level [Gre05, Yu06, Xie06, Lea06, Sot07]. But the technical evolution might have been useless if there hadn't been an advancement in chemical research and synthesis as well. The usage of optical systems applied on imaging techniques requires fluorescent probes or labels, so that the products or educts of a chosen reaction could even be seen. Therefore fluorescent dye systems are needed that fulfill the desired requirements for their application in special reaction environments and conditions. These include high photophysical, thermal and chemical stability, high fluorescence quantum yield, a fluorescence in the visual spectrum of light, etc.. [Kon82, Sun97, Tsi98, Hua05, Hau02]

In this work the efforts to establish fluorescent dye systems are presented. These can be used for explanation of processes that occur during a reaction by the analysis of the photophysical properties of products and educts. These efforts all have in common the usage of a distinct fluorescent dye system for mechanistic studies, the Borondipyrromethene (BODIPY, BDP) dyes. This dye class found widespread interest in science in the past 20 years. Since the fact, that living biological tissue is relatively transparent for emission wavelengths higher than 800 nm, the synthesis of fluorescent dyes, which emit above this threshold, are aspired. In addition, for labeling the manifold different biological molecules like enzymes and their substrates with fluorescent moieties, appropriate functional groups have to be added to the dye molecules. Therefore most of the re-

## 2.1 Introduction

search projects involve the synthetic derivation of the basic BODIPY fluorophore to tune the emission or absorption wavelength depending on the biological application and the functionalisation of the core with adequate anchor groups.

Our research motivation was a different one. Our aim is to use the BODIPY dye system to trace chemical reactions on a single-molecule level. The far main goal of this work was to establish fluorescent dye systems, where both educt and product of a chosen reaction would differ clearly in their photophysical properties, what would make them distinguishable by different spectroscopic means and methods. The BODIPY dye family seemed to be a promising system, due to its intrinsic, prerequisite photophysical properties.

Our first approach was to analyze the differences in photophysical behavior of fluorescent dyes in dependence of the structure of the dyes. The changes of photophysical variables as rate constants, like e.g.  $k_{21}$  or  $k_{23}$ , were observed on BODIPY dye systems with different substitution patterns.

In cooperation with the workgroup of Prof. Dr. B. Dick, Institute for Physical and Theoretical Chemistry, Laserspectroscopy and Photochemistry from the University of Regensburg, we synthesized the unsubstituted core compound of the BODIPY-dye class. The workgroup applies high-resolution line narrowing spectroscopy to ultracold molecules in supersonic jets and in rare gas matrices with the aim of understanding the photochemical reactivity and deactivation of electronically excited states in detail. An unsubstituted BODIPY-core-molecule therefore is a valuable target for these applications, due to the lack of disturbing vibrational signals of substituents like e.g. methyl groups.

Next, we have shown that the donor ability of a phenol moiety in a BODIPY molecule, which enables photoinduced electron transfer (PeT) and quenches fluorescence, could be switched off by phosphorylation. The aim was to establish a proof of principle if photoester cleavage could be studied with dyes which are also suitable for single-molecule detection. The effects that could directly be observed are the changes in fluorescence lifetime  $\tau_{Fl}$  and fluorescence quantum yield  $\Phi_{Fl}$ .

Another reaction which could be studied by means of fluorescence is excited state proton transfer (ESPT). We used the variation of photophysical properties in dependence of the used solvents, i.e. solvatochromism, to predict the ESPT behaviour of fluorescent dyes. Conclusions could be drawn by the comparison of solvatochromism of classical methylated and hydroxylated pyranine dyes as opposed to the solvatochromism of *p*-hydroxylated styryl-BODIPY-dyes.

Finally, a main motivation of this work was to evolve a concept to combine single-molecule detection and chemistry of fluorescent dyes. Therefore, we synthesized a BODIPY dye system as a sensitive probe for reactive species. Here the fluorescent dye contains a functional group that is a target for distinct chemical agents. This functional group is also part of the expanded chromophoric system. By shortening of the chromophoric system upon reaction the dye should experience a visible change in fluorescence colour. Two BODIPY dye systems were established as a target for two substrate classes. At first we verified the effect of oxidizing species like hydrogenperoxide or reactive metallate oxides ( $\text{KMnO}_4$ ,  $\text{OsO}_4$ ), performing hydroxylation reactions, to the chromophore. Furthermore a fluorescent probe molecule for metathesis catalysts was developed. This work is still in progress.

## 2.2 The BODIPY dye system

### 2.2.1 General and historic information

As mentioned, successful research for imaging processes in living cells is limited by the available fluorescent probes. The BODIPY-dye system is a class of fluorescent molecules which show high extinction coefficients, high fluorescence quantum yields and fluorescence spectra with sharp peak forms [Lou07, Ulr08]. The facts, that the fluorophore lacks any functional groups which are sensitive to environmental influences, and that the molecule itself is not charged, makes its photophysical properties almost insensitive to fluctuations of pH or polarity of the solvents. On the other hand, by the addition of functional groups with donor or acceptor character to the fluorophore, a tuning of its fluorescence characteristics can be achieved

by a relatively small synthetic effort.

The BODIPY dye class was first discovered in 1968 by Treibs and Kreuzer [Tre68]. During an effort to acetylate dimethyl-pyrrole in boiling acetanhydride in the presence of borontrifluoride, they isolated a green fluorescent by-product. As this was not their desired product, it received not much attention. As a matter of fact, for almost twenty years the interest in this dye class was generally limited to a few publications which had the topic of examining difluoradducts of dipyrromethenes.

In the 1980's, applications of sulfonated, water soluble BODIPY dyes for biologic applications and the usage of BODIPY dyes as active media in dye lasers made the dye class more popular [Boy89, Mor93]. Especially because of their photophysical properties and high photostability, BODIPY dyes added to the established laser dyes like rhodamine or coumarine [Lou07, Ulr08]. Also, a commercial application of BODIPYs by the company *Molecular Probes* [Pro00] as fluorescent tags for labeling proteins, modification of nucleotides or fluorescing enzyme substrates, etc. took place.

In the 1990's then BODIPY dyes gained more and more the reputation of being one of the most versatile fluorophores which, especially in biochemistry and biology, became a highly fluorescent and photostable alternative for the long time used dyes, like e.g. fluorescein [Lou07, Ulr08]. This development is reflected in the steadily increasing number of publications that describe the usage of the BODIPY fluorophore for the most different and multifaceted applications.

This versatility is due to its almost unique set of photophysical properties. Departing from this, a wide field of research involving the BODIPY dye system emerged until today, represented by about thousand journal articles per year since 2006 [Lou07].

### 2.2.2 The BODIPY system and its structure

Chemically the BODIPY fluorophore consists of two pyrrole rings which are linked in 2-position by a methene bridge and are held in one plane by the complexation of the molecule with a borondifluoride moiety via the pyrrole nitrogen atoms [Pic90]. Thus BODIPY stands

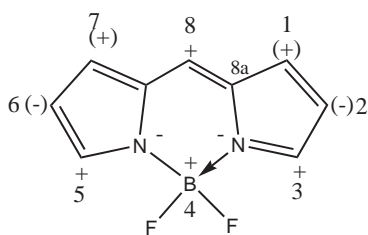


Fig. 2.1: BODIPY fluorophore with atom numbering

| C8    | C8a   | C1    | C2    | C3    | N     | B     | F     |
|-------|-------|-------|-------|-------|-------|-------|-------|
| -0,14 | +0,01 | +0,03 | -0,07 | +0,32 | -0,56 | +1,29 | -0,52 |

Fig. 2.2: Relative polarisation of the atoms in the BODIPY core framework [Kol99]

for BORon-DI-PYrrromethene. The systematic, chemically correct, name of the structure is 4,4-Difluoro-4-bora-3a,4a-diaza- *s*-indacene (Figure 2.1). Hence, the fluorophore consists of a planar carbon framework with  $C_{2v}$  symmetry. Observations have been made that the dipyrromethene cation, where the boron atom is replaced by two protons, exhibits a similar fluorescence spectrum as the BODIPY fluorophore. But fluorescence appears only at very low temperatures where the conformational freedom of the cation is inhibited [Par85]. This shows that the planar complexation of the dipyrromethene by the boron atom adds to the fact that the BODIPY dyes fluoresces at room temperature. But due to the lack of free p-orbitals, the boron atom does not add to the conjugation of the molecule [Kol99]. The presence of nitrogen and boron bonds in the molecule and the thus resulting inhomogeneous charge distribution leads to positive and negative polarised, i.e. electrophilic (Pos. 1,3,5,7) and nucleophilic (Pos. 2,6), sites on the molecule. This opens the door to a wide range of synthetic derivatisations which can be applied to the molecule. These polarisations may also be made responsible for the fact that the unsubstituted BODIPY core framework was unknown until this work, due to its assumed vulnerability to electrophilic attacks [Lou07].

### 2.2.3 Chemistry and characteristics of BODIPYs

An adequate choice of electrophilic and nucleophilic substituents hence opens the possibility to tune the chemical and photophysical properties of the fluorophore without the loss of its fluorescence. Typically applied substitutions are made at the *meso*-position (Pos.

8) of the molecule where usually functional groups are added that function as anchor groups to biomolecules for labeling purposes [Lou07]. Substitutions at the 1-,3-,5- and 7-positions with donor and/or acceptor moieties usually lead to a change of absorption and emission maxima, where even BODIPY dyes with infrared emission spectra could be isolated [Roh06a, Qin06, Bar05]. Variations at the 2- and 6-positions are less common. The most known may be the addition of sulfonyl groups to improve the water solubility of the generally poorly water soluble core molecule. Also common is inserting halogens like bromine or iodine to observe their heavy atom effect to the fluorescent moiety or to enable cross coupling [Li98, Wan03, Roh06b].

In contrary to many other applied fluorescent dyes, like e.g. coumarine, rhodamine or fluorescein dyes, the particular small BODIPY molecule exhibits strong absorption and fluorescence with extinction coefficients over 70.000 l/mol · cm and fluorescence quantum yields over 90% [Lou07, Ulr08]. It also exhibits a great amount of chemical robustness and photochemical and thermal stability.

Our success in the synthesis of the BODIPY core compound allowed us to characterize the fluorophore completely by NMR and crystallographic methods (Figure 2.3).

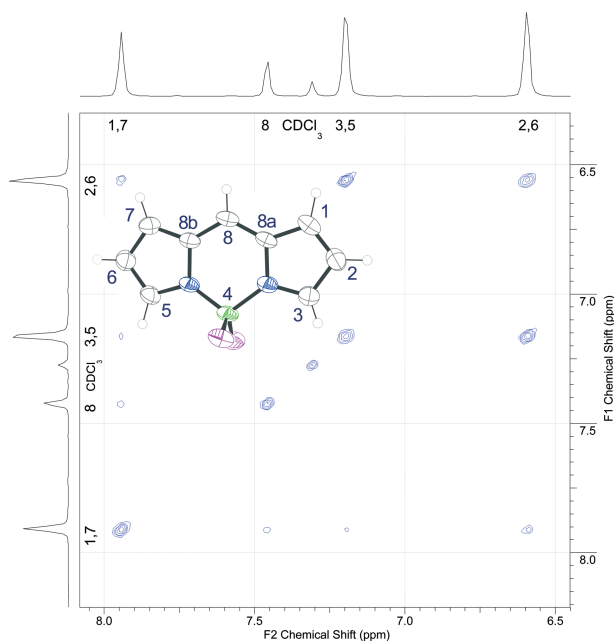


Fig. 2.3: 2D-HH-COSY-NMR-spectrum of the BODIPY core compound and its crystallographic structure with atom numbering

### 2.2.4 Syntheses of BODIPY dyes

Generally two synthetic approaches for the generation of the BODIPY fluorophore are available. The first approach involves the condensation of acyl chlorides with pyrroles to prepare “symmetric” fluorophores where, dependent on the selection of the acyl chloride, specific substitutions in *meso*-position can be achieved [Lou07, Ulr08]. This maintains the  $C_{2v}$  symmetry. The preparation involves the generation of unstable dipyrromethene hydrochloride salts which are not generally isolated. The following complexation with boron trifluoride yields the now stable fluorescent dye (Figure 2.4). The

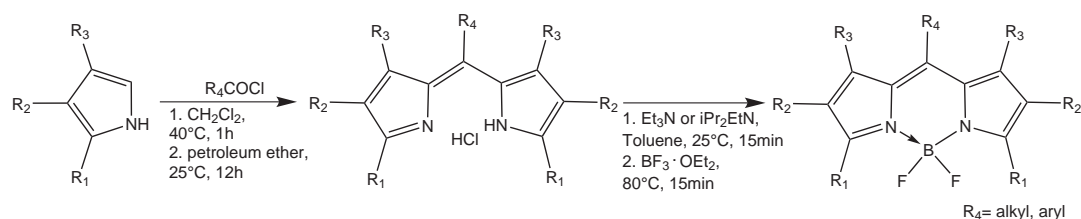


Fig. 2.4: Synthesis of symmetric BODIPY dyes from pyrroles and acid chlorides or anhydrides

usage of acyl chlorides bears the advantage that the resulting intermediate salt is already formed on the right oxidation level, the dipyrromethene. The usage of aldehydes follows almost the same reaction path with the exception that, after acid catalyzed condensation a dipyrromethane salt is formed which has to be oxidized in an additional step (Figure 2.5) [Kan93, Ulr04, Mor93]. Thanks to the wide range of commercially available pyrroles, acid chlorides or aldehydes the symmetric path opens the door to an open range of modifications on the *meso*-position of the dye. During this work

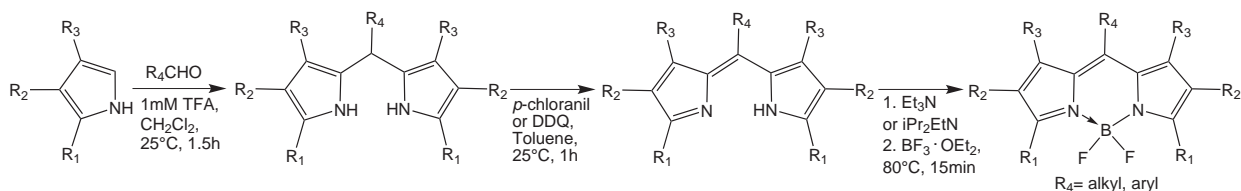


Fig. 2.5: Synthesis of BODIPY dyes from pyrroles and aldehydes, involving an additional oxidation step

different BODIPY core molecules were prepared via the symmet-

ric route (Figure 2.6). The second synthetic approach leads to

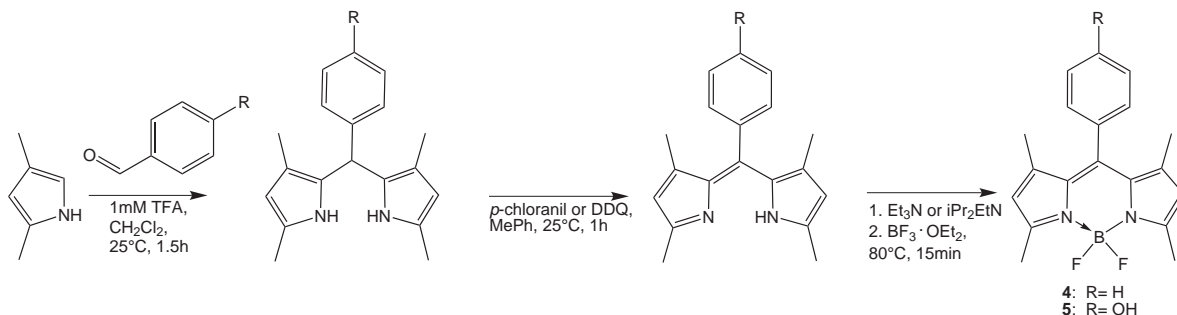


Fig. 2.6: Performed synthesis of BODIPY core compounds via the symmetric route

“asymmetric” BODIPY fluorophores [Lou07, Ulr08]. Here a aldehyde containing pyrrole component is directly condensated by a pyrrole with a free 2-position, also forming an intermediate already on the dipyrromethene level. Further complexation yields a BODIPY moiety with different substituents on the two pyrrole components (Figure 2.7) [Hau88, Mon89, Pro00]. Also, during this work different

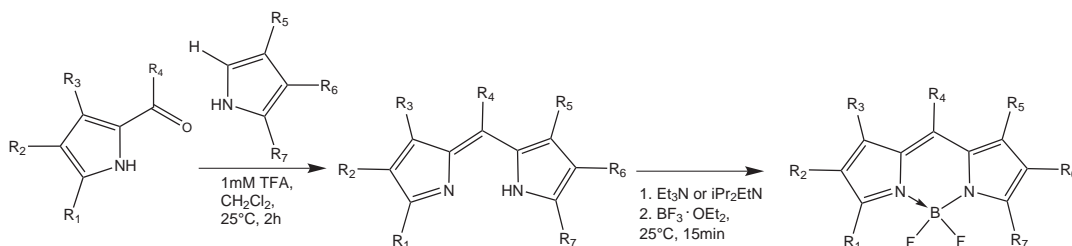


Fig. 2.7: Synthesis of asymmetric BODIPY dyes from carbonyl-pyrroles and pyrroles

BODIPY core molecules and BODIPYs with different core substituents were synthesized via the asymmetric preparation route (Figure 2.8). Common problems lie in the proper choice of the pyrrole components and the aldehyde components. A highly electrophilic aldehyde compound is needed in order to form the methene bridge between the two pyrroles. The pyrroles themselves tend to polymerize or form porphyrins, which can be avoided by choosing pyrroles with substituents in a position adjacent to the nitrogen atoms (pos. 3 and 5). Otherwise an excess of non-substituted pyrrole is needed to obtain the corresponding dye. By complexation with boron tri-

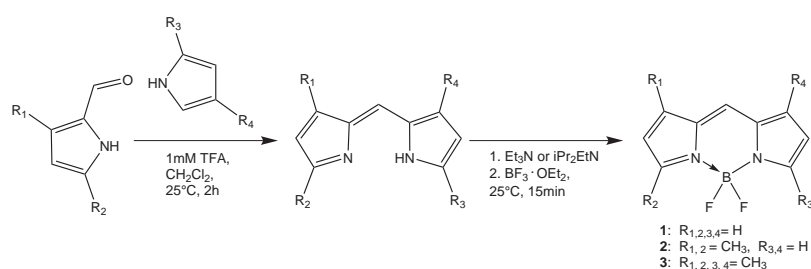


Fig. 2.8: Performed synthesis of BODIPY core compounds via the asymmetric route

fluoride, the desired dye is generally willingly formed. A huge problem in both synthesis paths lies in the purification of the wanted products. Numerous purification steps are needed in order to get rid of salts, excesses of base and boron trifluoride and polymerized by-products and built-up porphyrins. A fine tuning of reaction conditions and purification means, like e.g. optimized solvent mixtures for chromatography, aqueous reprocessing, etc., is necessary to increase the yields of the synthesis.

The symmetric synthesis strategy allows the connection of selective groups directly onto the fluorophore without a distinct change of their transition energies, since the geometry and electron density of the BODIPY fluorophore are not gravely disturbed. Important to mention, although, is that the choice of pyrrole units with substituents in the 3-position of the pyrroles inhibits rotation of aromatic groups in the 8-position. In an excited state, this rotation leads to a faster energy loss compared to a functional group with inhibited rotation and leads to a shortening of fluorescence lifetime and decrease of fluorescence quantum yield. This effect is known as the “loose bolt” mechanism [Lew39]. The effect can, on the other hand, also be used to the development of many chemical sensors. This wide field of applications made the symmetric synthesis route the most popular of the available routes.

The asymmetric route can often be used to extend the chromophore to tune the maximum absorption and emission wavelengths. By the right choice of the carbonyl pyrrole compound substituents in *meso* position can also be inserted, but it is limited to the availability of ketone pyrroles that are reactive enough to react with a non-carbonyl

pyrrole moiety. More common are variations of the substituents in 1-,3-,5- and 7-positions. The possibility to insert different functional groups allow to form potent BODIPY label dyes. Due to the lack of an additional oxidation step the asymmetric method is often used to produce greater amounts of dye. This is to result from the yield reduction of the usage of oxidizing agents. These have to be separated fast and thorough to avoid further oxidation and destruction of the fluorophore.

During this work several BODIPY compounds with substitutions to expand the chromophore were investigated, departing from dye **2** (Figure 2.9) [Sat94]. The applied synthesis follows a Knoevenagel-like reaction pathway [Kol99, Mar01]. The fluorescence colour of

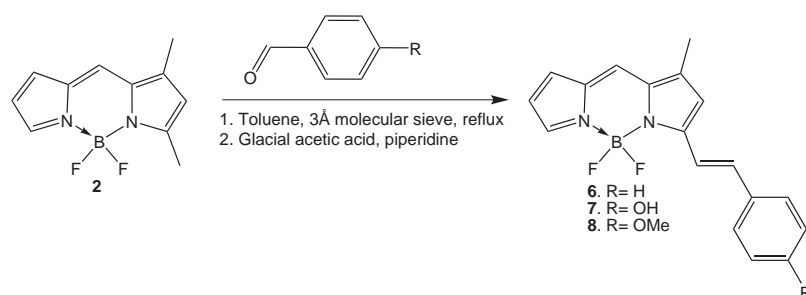


Fig. 2.9: Applied synthesis of BODIPY dyes with expanded chromophoric system derived from the BODIPY core compound **2**

these compounds **6-8** varies from orange to red, depending on the substitution pattern. Donor groups like dimethylamino- or methoxy-

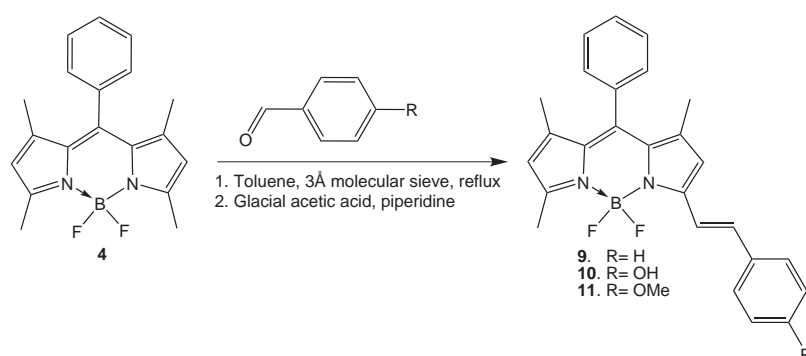


Fig. 2.10: Applied synthesis of BODIPY dyes with expanded chromophoric system derived from the *meso*-substituted BODIPY core compound **4**

groups in *p*-position of the styryl moiety lead to a larger redshift of

the fluorescence compared to an unsubstituted styryl unit. In addition analogically substituted BODIPY dyes with a phenyl moiety in *meso*-position were prepared. The syntheses followed the symmetrical preparation route, starting from dye **4** (Figure 2.10).

### 2.2.5 BODIPYs for fluorescent model systems

A key attribute common to all our research approaches is the usage of the Bodipy dye class. For different photophysical, technical and practical reasons this dye class seemed most suitable for those studies. A first problem occurring during the theoretical planning of the research simply was the right choice of an appropriate dye which would allow us to analyze the desired changes of fluorescence colour during a chemical reaction. The educt and the product of the reaction should therefore both emit fluorescence in the visible range at the reaction conditions. Thus it would be most convenient if the chosen chromophore is least affected by these conditions. Disturbing influences of the chromophore itself should be minimized, so that changes in photophysical properties could be traced back to structural changes during a reaction.

Nowadays various and well researched fluorescent dyes are commercially and synthetically available. And many different dyes provide many advantages and disadvantages concerning their chemical and photophysical properties.

As an example and competitor to the chosen BODIPY dye class we mention the Rhodamine dye class. Here we pose the question if our projects could also be realized with such dyes as Rhodamines.

Chemically, Rhodamines are derived from triphenylmethane dyes and are similar in structure to Xanthene dyes as e.g. fluorescein. Their usual applications are as dyes for papers and textiles, as markers in fluorescence microscopy and as active media in dye lasers. Rhodamines have high fluorescence quantum yields (mostly close to 100%) and have a sparse tendency to be excited to a triplet state. Their emission spectra range from green-yellow to orange-red [Hau02]. All these properties make them also suitable for the application in single-molecule research.

So far these properties resemble close to the mentioned properties of BODIPY dyes. But in contrary to BODIPY dyes Rhodamine dyes have a variety of different reactive functional groups in their molecular structures. Two usable Rhodamine dyes concerning their different emission spectra and structural similarity in comparison to the used BODIPY system are shown in Figure 2.11. A suitable

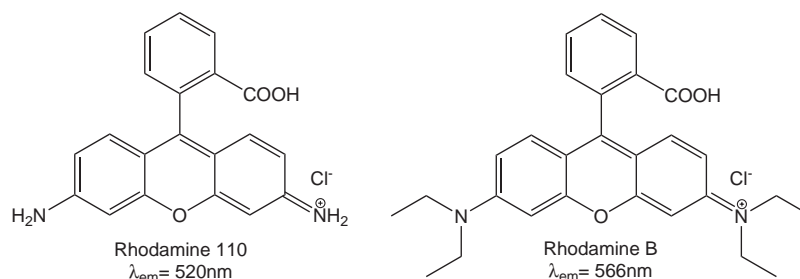


Fig. 2.11: Green-yellow fluorescent Rhodamine 110 and orange-red fluorescent Rhodamine B as competitor dyes to the applied BODIPY dye system

chemical reaction would not be easy to find to convert these dyes one into another without provoking further changes to the chromophore. And due to the fact that the Rhodamines carry charges they are also sensitive to reaction conditions like pH variations or solvent influences. The BODIPY dyes on the other hand are not affected by these influences. In addition the fluorophore and therefore the range of fluorescence emission maxima can be quite easily expanded by synthetic means. Also a conversion of the “expansions” can far more easily be achieved than with the e.g. Rhodamines by disturbing the conjugated system at a chosen point by a reactive species attacking a in-built functional group which can act as a “predetermined breaking point” for the fluorophore.

Because of the independence and stability of the BODIPY chromophore one can concentrate on the modifications that can be made on the molecule to expand the emission range and the incorporated targets for active reaction agents. After a chemical reaction the molecule will end up either as a fluorescent core structure similar to compound **1** (Figure 2.8) or a compound with a non-fluorescent and therefore destroyed fluorophore. Luckily the BODIPY structure provides many possibilities of variations because electrophilic and nucleophilic sites on the core molecule exist. By carefully choosing

the substitution pattern, a wide range of chemical reactions, like e.g. oxidations/reductions, metal catalysis or the establishing of carbon-carbon bonds, can be exerted with the new dyes.

In addition to the synthetic accessibility and the chemical and physical aspects of the BODIPY dye, it proves to be valuable to use only one dye family with one similar core structure for the different experiments. The advantage lies in the always (mostly) similar photophysical properties of the core chromophore which makes the results easier to analyse and to compare.

Finally BODIPY dyes are well suited for single-molecule methods. BODIPY dyes are also highly photostable and the photostability correlates with structural variations which could have been shown by comparative FCS studies with fluorescein dyes. Even the “classical” Förster dye HPTS (Fig. 2.15) does not show a higher photostability than that of BODIPYs.

The sum of all these properties and advantages convinced us that the BODIPY dye family would be the most promising dye system for a success in the located research fields.

Therefore, each of the isolated dyes **1** to **8** were prepared for a distinguished usage in our projects.

Firstly we investigated promising, well explored textbook chemical reactions as a starting point. In assumption of the product generation starting from our prepared educts, we synthesized BODIPY dyes possessing similar structures (like the assumed products) in order to compare their photophysical properties with those of the products yielded by the chosen reactions.

One of our first experimental interests focused on the overall question what makes a dye photostable and if there is a connection to its structure. This is a quite important question, since a high photostability is required for almost all applications and experiments involving dyes. In general photostability can be defined as the number of photocycles a molecule undergoes before it suffers photobleaching. Many attempts to understand the dependencies and requirements of photostability have been made [Egg98, End05, Egg05]. Generally they can be divided into two classes: ensemble and single-molecule studies.

Once again BODIPY dyes seemed to be a grateful research subject. And again we used a well researched fluorescent dye system for comparative studies with our used BODIPY dyes, the fluorescein dyes. The FCS studies involved four different substituted fluorescein (Figure 2.12) and BODIPY dyes (Figure 2.13). The following

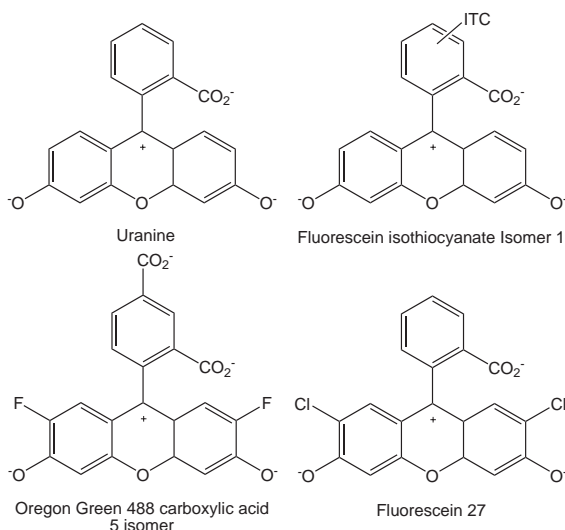


Fig. 2.12: Structures of the used fluorescein dyes

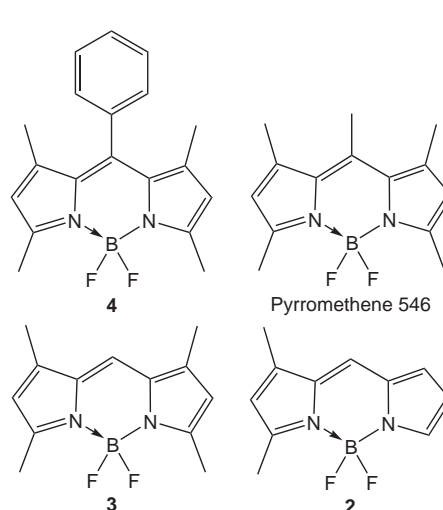


Fig. 2.13: Structures of the used BODIPY dyes

analysis of both dye families investigated the state of origin of photobleaching which was assumed to happen from the excited triplet state [Wid95]. The investigation involved single-molecule approaches like fluorescence correlation spectroscopy (FCS) to observe diffusion behaviour of the dyes. To guarantee that changes in diffusion time  $\tau_D$  can be exclusively traced back to photobleaching, (due to the loss of a fluorescence signal of a bleached dye in the observed excitation volume) several modifications to a "classical" FCS setup had to be made. Paying attention to this, a comparative study of the photostability of structurally related fluorescent dyes was possible.

A known reaction occurring with some fluorescent dyes is the photoinduced electron transfer, PeT [Gab04]. This photochemical reaction was previously made responsible for fluorescence quenching in fluorescent dyes. We used this circumstance as a read-out mechanism if PeT has occurred or not. Excited dyes are redoxamphoteric

and can act as electron donor, i.e. reductant, or as electron-acceptor, i.e. oxidant. In the majority of the mentioned cases the latter is realized (Figure 2.14). With an oxidable counterpart in close vicinity, i.e. the substituent in *meso*-position, electron transfer to the excited dye occurs faster than fluorescence emission. This leads to fluorescence quenching and thus to a loss of fluorescence. Our approach was to inhibit this reaction by “blocking” the phenyl group in *meso*-position of a BODIPY dye (**5**), with phosphate esters [Kab99, Sil96, Laz92]. This suppression of PeT could be observed

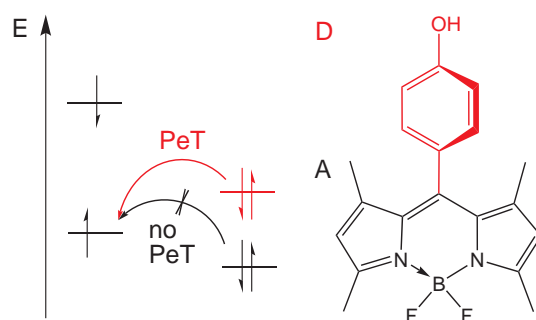


Fig. 2.14: Disabling PeT in BODIPY **5**. By lowering the energy of the highest occupied molecular orbital in the donor moiety (D), i.e. raising the oxidation potential, electron transfer to the singly occupied molecular orbital of the accepting moiety (A) is disabled

by the increase of fluorescence lifetime  $\tau_{Fl}$ . Future applications for this proof-of-principle system could be a single-molecule detection capable sensor-molecule for phosphate cleavage in bioanalytical research. Application could be e.g. the development of sensor molecules for phosphatase in biological environments.

In addition to PeT we investigated the behaviour of BODIPY dyes in a similar reaction also originating from the excited state, the Excited State Proton Transfer (ESPT) [För49, För50, Moh05]. To draw conclusions for prediction of ESPT behaviour of BODIPY dyes, we reinvestigated the solvatochromism, i.e. the dependance of photophysical properties to the used solvent, of 8-hydroxypyrene-1,3,6-trisulfonate (HPTS, pyranine), its methoxylated analogon 8-methoxypyrene-1,3,6-trisulfonate (MPTS) and 1-hydroxypyrene (PyOH, pyrenol) (Figure 2.15) in comparison with hydroxylated and methoxylated BODIPY dyes (**10**, **11**). Solvatochromism was

## 2.2 The BODIPY dye system

## 2.2.5. BODIPYs for model systems

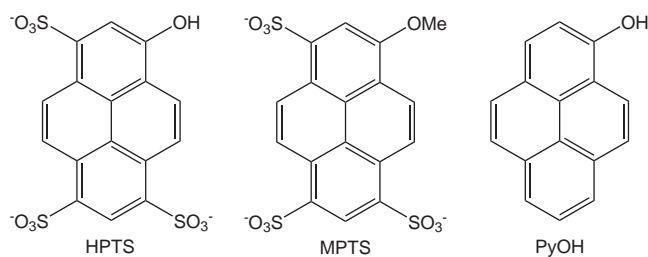


Fig. 2.15: Pyranines used for reinvestigation of their solvatochromism

surveyed with 25 different solvents, giving indications to the driving force behind photoacidity of the examined fluorescent aromatic alcohols.

Apart from these experiments we attempted to create such a model system involved oxidation reactions of a double bond. This field of chemical reactions is well researched beyond textbook examples and is established in university lectures. For the sake of this knowledge and of technical and chemical simplicity we chose dihydroxylation chemistry starting on the one hand with *syn*- dihydroxylation by the usage of metallate oxides like potassium permanganate ( $\text{KMnO}_4$ ) and osmiumtetroxide ( $\text{OsO}_4$ ), and on the other hand with *anti*- dihydroxylation by the usage of hydrogenperoxide ( $\text{H}_2\text{O}_2$ ) [Mar01]. Our idea was to create a fluorophore which would be susceptible to

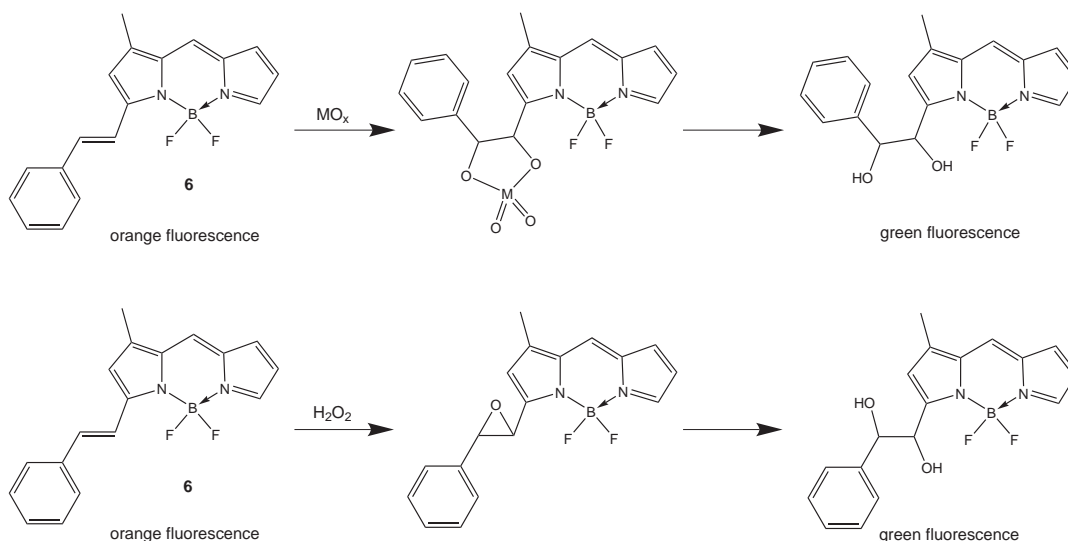


Fig. 2.16: Dihydroxylation chemistry of compound **6**

oxidation chemistry without the presence of perturbing functional

groups [Dru02]. For this purpose BODIPY dye **6** was synthesized. In the presence of an oxidizing agent the double bond of the styryl moiety would be attacked and the conjugation would be lost. The resulting dye exhibits a fluorescence colour similar to dye **2** (Figure 2.16).

Our final proposition, which is still *research in progress* and therefore *not published*, for a dye system allowing single-molecule observations of chemical reactions based on the BODIPY dye family, dealt with the metathesis reaction. Our projection involved a BODIPY dye containing functional groups that allows the molecule to undergo a metathesis reaction in presence of a metathesis catalyst, i.e. a Grubbs catalyst. Similar to the approach with the oxidation of dye **6**, the originally orange fluorescent BODIPY dye should experience a hypsochromic fluorescence shift during the reaction and yield a green fluorescent product (Figure 2.17).

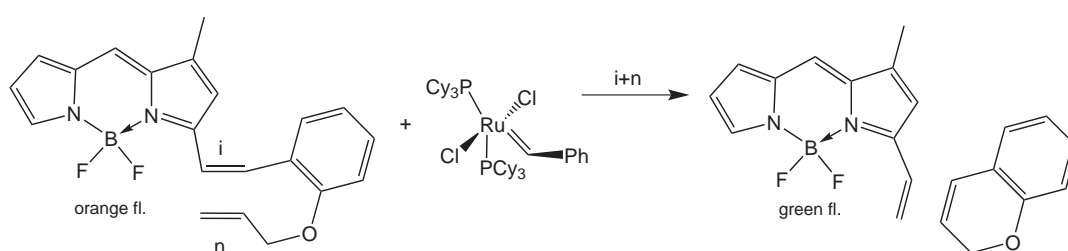


Fig. 2.17: Assumed product generation of a reaction between a metathesis capable BODIPY dye and a Grubbs catalyst (i stands for the intrinsic double bond and n for the terminal double bond which react with one another)

## 2.3 Fluorescence spectroscopic investigations

### 2.3.1 Interactions of light and matter

Since antiquity, humans are fascinated by light and colour. 4000 years ago the Egyptians learned to dye with indigo and the Phoenicians collected purple from the purple murex. Still, thousands of years later, in the medieval era that dye still was extremely expensive and rare due to its highly elaborate production. The ability to produce coloured objects, like clothes, or the gathering of coloured natural products, like gems and minerals, was popular through all times of human history. And for a long time, human understanding of the physical or chemical causes of these phenomena remained, literally, in the dark. Chemicals that were used as dyes were invariably accumulated from natural sources. The first documented synthesis of a dye in a laboratory was achieved by Perkin in 1856. He obtained the violet mauveine while trying to synthesize quinine out of aniline. It was followed by an avalanche of new colourful synthetic discoveries [Gar01].

Even then the true nature of light and its interaction with matter were still unknown. At the end of the 19th century famous scientists like Lorentz, Rayleigh and Einstein uncovered the nature of electromagnetic radiation, its wave/particle duality and the effects of different wavelengths and frequencies to different kinds of matter [Atk98]. Scattering and refraction could be explained and the fact that electromagnetic radiation moves with a finite velocity changed our view of the world and the universe fundamentally.

The discovery of the quantum world of light and its related radiation opened new pathways to numerous new techniques that allowed us to see things that we could not see with our own eyes. Starting from there new spectroscopic and microscopic imaging techniques evolved [Lak99].

Here we focus first on the classical optical methods that were established with the understanding of light and that allowed use to finally understand and use dyes and colours.

## 2.3.2 Classical optical spectroscopy:

### Absorption

The colours of objects that we perceive result from the removal of certain wavelengths of light from the spectrum of white light by absorption (gas, liquids) or dispersion (solid matter). The leftover wavelength spectrum that is reflected from the objects surface is the colour apprehended by the human eye. The amount of the absorbed or dispersed photons is a function of the extinction coefficient and the thickness of the absorbing material. This function is represented by the Beer-Lambert law (Equation 2.1).

$$E = -lg \frac{I}{I_0} = \epsilon \cdot c \cdot d \quad (2.1)$$

$E$  is the optical density,  $\epsilon$  is the molar extinction coefficient,  $c$  the concentration of an absorbing liquid and  $d$  the layer thickness of the material. The Beer-Lambert law is the base of absorption spectroscopy or UV/Vis spectroscopy (because it covers the range of UV radiation and visible light). This analytical tool to determine extinction coefficients or concentrations of absorbing substances, depending on which of both is already known, is long established and widely applied [Atk98]. It is applied in almost every scientific and commercial field where analytics of dissolved or gaseous (e.g. in astronomy) species are needed and a base principle that is learned by science students. A schematic set-up of the absorption spectrometer Perkin-Elmer Lambda 5 that was used in this work is shown in figure 2.18.

### Excitation/Emission

The question deriving from absorption of electromagnetic radiation by a molecule is: What happens with the absorbed energy and what does it do to the molecules? In the case of absorbed light the reception of the energy contained in it leads to an excitation of the molecules. If a molecule is excited electrons move from the the HOMO to the LUMO. This transfers the molecule from an unexcited ground state  $S_0$  to the vibrational state of an excited state

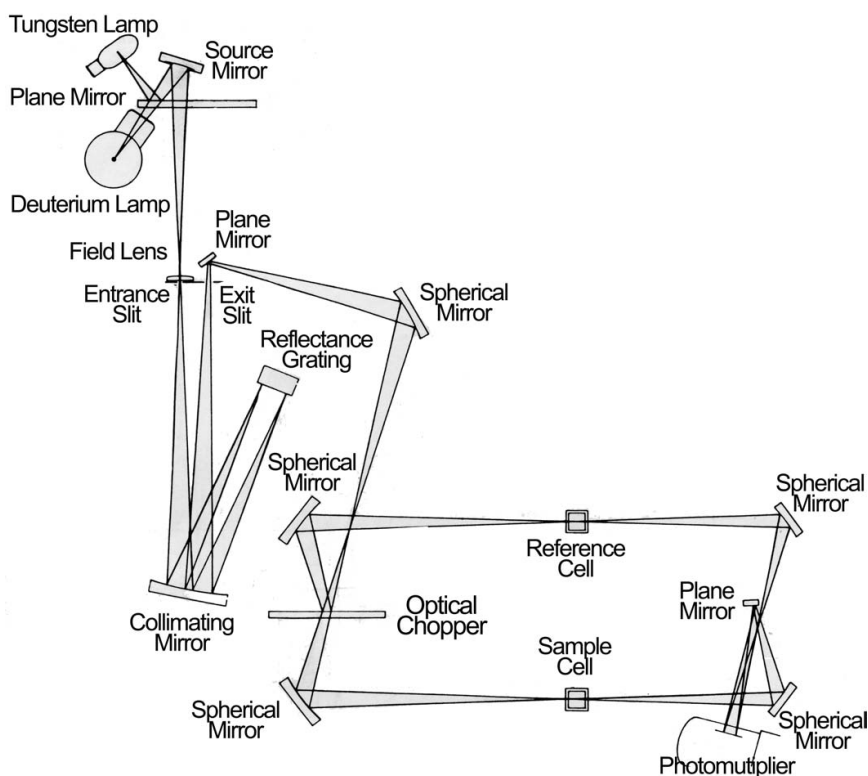


Fig. 2.18: Schematic setup of the absorption (UV/Vis) spectrometer Perkin Elmer Lambda 5

$S_1$  to  $S_n$  (figure 2.19) [Lak99]. First a relaxation from the vibrational excited state to the appropriate vibrational ground state of the excited electronic state occurs. There the molecule has different possibilities to leave this state. Then a further relaxation to a lower energetic state follows. By most molecules this relaxation happens radiationless to the unexcited ground state  $S_0$  by means of Intersystem Crossing or transitions to dark states ( $k_{IC}$ ). Luminescent dye molecules additionally have the possibility to either move to a spin forbidden triplet state ( $k_{23}$ ) and then relax under emission of radiation to  $S_0$  ( $k_{31}$ , phosphorescence). Or they can relax directly to the unexcited ground state by emission of fluorescence ( $k_{rad}$ ).

Typical lifetimes of the excited state  $S_1$  of fluorescent dyes range from 1 to 10ns. This corresponds to rate constants of the fluorescence decay  $k_{Fl}$  from  $10^8$  to  $10^9\text{s}^{-1}$ . This rate constant is composed of radiating contributions ( $k_{rad}$ ), radiationless contributions (Intersystem transitions,  $k_{IC}$ ) and triplet transitions ( $k_{23}$ ) as shown

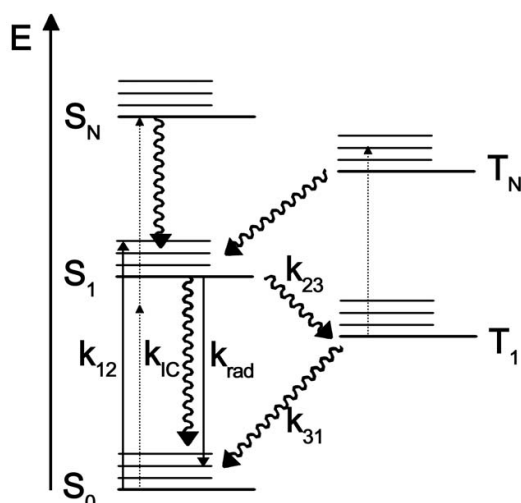


Fig. 2.19: Simplified Jablonski diagram showing the most important transitions and their rate constants. The electronic states are supplemented with vibrational states.

in equation 2.2

$$k_{Fl} = (k_{rad} + k_{IC}) + k_{23} = k_{21} + k_{23} \quad (2.2)$$

Rate constant  $k_{21}$  is the fluorescent rate or excitation saturation rate constant ( $k_S$ ) representing the limit of excitation cycles a molecule can undergo in a given time [Jun01]. A fluorescence emission rate constant of a fluorophore, can be defined (2.3) in combination with the fluorescence quantum yield ( $\Phi_{Fl}$ ).  $\Phi_{Fl}$  is defined as the ratio of the number of photons emitted to the number of photons absorbed.

$$k_{Em} = \frac{k_{12} \cdot \Phi_{Fl}}{1 + \frac{k_{12}}{k_S}} ; k_S = k_{21} + k_{23} \quad (2.3)$$

With this knowledge a whole new area of scientific research emerged with many scientific and technological breakthroughs. For further theoretical information we refer to literature [Lak99, För51].

On the technological side fluorescence and excitation spectroscopy became mighty analytical tools that added up to the complementary absorption spectroscopy. Usually absorption and excitation spectroscopy generate identical spectra in the case of luminescent material, but the difference between the methods should be noted. An emission spectrum is the spectrum of energies emitted (fluorescence)

by a material after an exposure to radiation, while the absorption spectrum is the spectrum of energies absorbed by the material. In absorption measurements the substance is exposed to large wavelength range of radiation (UV/white light) and the radiation that goes through the material unabsorbed is detected and put in ratio to the incident radiation.

To obtain an excitation spectrum, on the other hand, the material is exposed to a very narrow range of wavelengths, at best monochromatic radiation. The wavelength of the detected emission radiation should be bathochromically shifted to the maximum emission wavelength of the material. Then the excitation of fluorescence over a wide wavelength range is recorded. The spectral region where fluorescence can be generated is therefore the range where the material absorbs the excitation light. This leads to a spectrum similar to an absorption spectrum. The advantage of excitation spectroscopy over absorption spectroscopy is that only fluorescent species are detected, but non-fluorescent, absorbing impurities are not.

Excitation and emission spectra were recorded on the same experimental setup shown in figure 2.20.

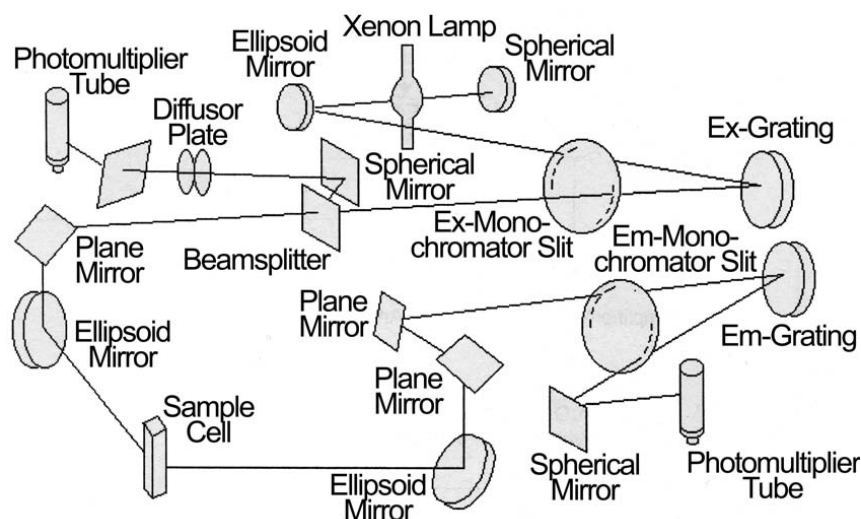


Fig. 2.20: Schematic representation of the configuration of the fluorescence spectrometer used in this work, Jasco FP-6500

### 2.3.3 Modern optical spectroscopy:

#### Fluorescence Correlation Spectroscopy (FCS)

Fluorescence correlation spectroscopy (FCS), which was first introduced in 1972 by Madge, Elson and Webb, [Mag72, Mag74, Ehr74] can be regarded as a special case of relaxation analysis. Where classical methods observed disturbances of, e.g. temperature or pressure in a reaction system, which are induced externally, the new concept of FCS observed fluctuations of physical parameters that correlate with the fluorescence emission of the molecules in the equilibrium. A molecule diffuses through an excitation focus of the beam and is only fluorescent while it is inside the irradiated volume. The fluorescence fluctuations of the individual diffusing molecule can only be observed if they are not disturbed or hidden by the fluorescence of the ensemble of molecules in solution. Therefore only a few (at best one) molecules should be observed at the same instant. A typical experimental setup is shown in figure 2.21. The basic principle of

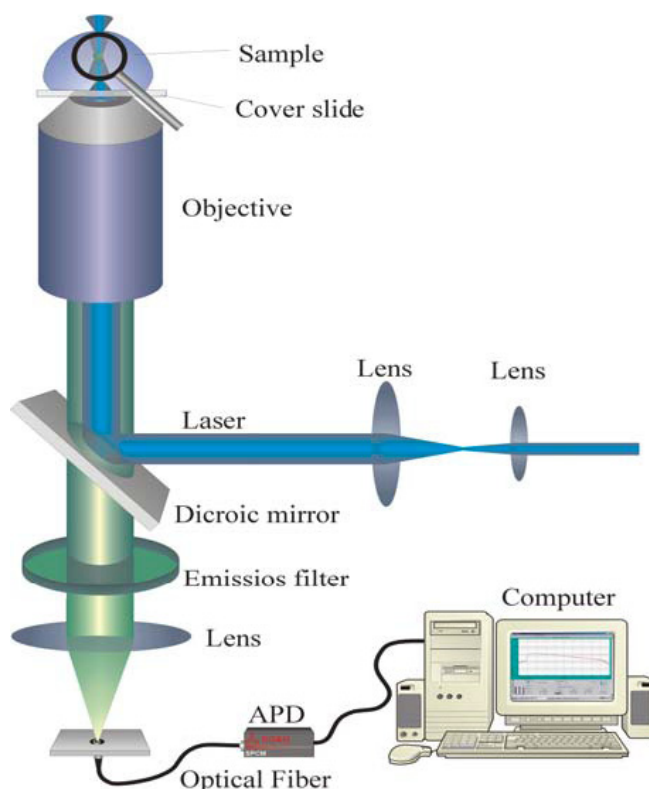


Fig. 2.21: Typical experimental FCS setup

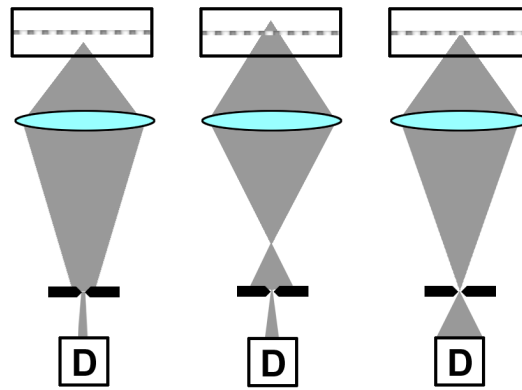


Fig. 2.22: Schematic representation of the confocal principle

confocal FCS consists of the epi-illumination of a diffraction limited volume by a laser beam. Adding to that, working in a highly diluted probe solution (nanomolar to subnanomolar concentrations) under an objective lens with a high numeric aperture, generally water immersion objectives, and a short focal length, results in the generation of a focal spot with only about a several 100 nm in diameter that forms the open volume of measurement of the fluorescence analysis. Only in this confined space of the probe solution the presence of fluorescent molecules can be detected and their dynamics analysed. The emitted radiation of a laser is guided into the microscope objective by a dichroic mirror and focused on the probe. The fluorescence of the probe is collected by the same objective and passes the dichroic mirror and emission filter that cuts out the unwanted excitation light of the laser. In addition a pinhole is used to suppress fluorescence light that does not originate from the focal region and increases the axial resolution by enhancing the signal/background-ratio. This is called “the confocal principle” [Dap95] and is pointed up schematically in Figure 2.22. It permits that out-focal emission is not detected while fluorescence from the focal region is detected up to 83%. After passing the pinhole the emission light is focused on a highly sensitive detector, preferably an avalanche photodiode. In our setup, a beamsplitter and two photodiodes were applied to minimize the effects of the dead time of the diodes and other artefacts. A computer equipped with a hardware correlator then produces the

typical FCS curves.

At a given temperature these fluorescence fluctuations can be noticed as noise patterns in the measured fluorescence signal. By the mathematical procedure of temporal autocorrelation these noise patterns can be quantified in strength and duration. The obtained temporal pattern, representing the rise and decay of fluorescence, contains information about the molecular dynamics of the diffusing molecules in the observed volume (Equation 2.4).

$$g^2(\tau) = \frac{[S(0)S(0 + \tau)]}{[S(t)]^2} = 1 + \frac{[\delta S(0)\delta S(0 + \tau)]}{[S(t)]^2} \quad (2.4)$$

with

|                        |  |              |
|------------------------|--|--------------|
| $g^2(\tau)$            | Correlation function   | [-]          |
| $S(0/0 + \tau)$        | Signal at time 0/0 + $\tau$                                  | [ $s^{-1}$ ] |
| $[S(t)]$               | Signal average value   | [ $s^{-1}$ ] |
| $\delta S(0/0 + \tau)$ | Signal fluctuation around average value at time 0/0 + $\tau$ | [ $s^{-1}$ ] |
| $\tau$                 | Time lag   | [s]          |
| 0                      | Starting time (arbitrary)                                    | [s]          |

Derived from this theoretical starting point, experimental data can be linked with parameters such as rate constants like  $k_{23}^{eff}$ , the effective rate constant for the transition from a singlet to a triplet state,  $k_{31}$ , the rate constant of relaxation from the triplet state and  $\tau_D$ , the diffusion time of the molecule in the observed volume (Equation 2.5).

$$G(\tau) = 1 + \frac{1}{N} \left( \frac{1}{1 + \frac{\tau}{\tau_D}} \right) \left( 1 + \frac{k_{23}^{eff}}{k_{31}} \exp \left[ - \left( k_{23}^{eff} + k_{31} \right) \tau \right] \right) \quad (2.5)$$

For a more detailed description of the theory and the derivations of its equations we refer to the technical literature [Els74, Sch96b, Jun01].

The obtained autocorrelation curve originating from equation 2.5

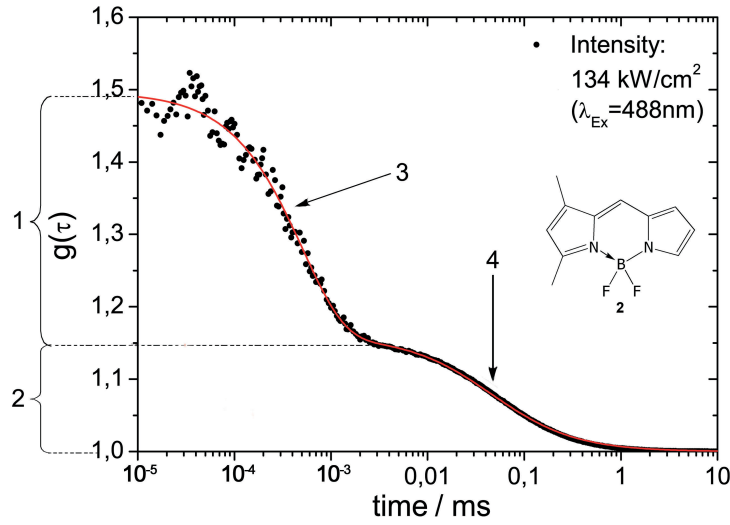


Fig. 2.23: Recorded FCS spectrum of BODIPY **2** at two different excitation intensities.

can be analyzed as shown on the example of FCS experiments performed with BODIPY dye **2** (figure 2.8). Figure 2.23 shows the autocorrelation curves of BODIPY **2** recorded at an excitation intensity of  $134 \frac{kW}{cm^2}$  ( $\lambda_{ex}=488nm$ ). The red coloured lines shows the data fitted according to equation 2.5. There are four sections in an autocorrelation curve containing vital information. The section marked as 1 delivers the amount of excited molecules in the triplet state  $\frac{T}{1-T}$ . Section 2, is called the contrast and shows the inverted average number of molecules passing the irradiated volume during a measurement,  $\frac{1}{N}$  in a normalized FCS curve. The section 3 of the exponential decay  $e^{-\lambda\tau}$  ( $\lambda = k_{23}^{eff} + k_{31}$ ) of the higher step of the graph at  $\frac{1}{\lambda} = \frac{\tau}{e}$  contains the rate constant  $\tau^{-1} = k_{23}^{eff} + k_{31}$ . From the turning point 4 the diffusion time  $\tau_D = \frac{\omega^2}{4D}$  can be determined, which delivers the diffusion coefficient  $D$ . The recording at different intensities shows changes in rate constants of state population and especially in triplet population, resulting in variations of section 3. The graph then shows the tendency of a fluorescent dye to populate the triplet state stronger induced by the higher excitation intensity.

### Time Correlated Single Photon Counting (TCSPC)

TCSPC is a technique where photons are counted correlated to the instant an excitation pulse is applied [Lak99]. The most important device in the method is the time-to-amplitude converter (TAC), which can be regarded as an ultrafast stopwatch. By using a pulse light source, e.g. a pulsed laser, a probe sample is repetitively excited. Each pulse is optically monitored by, e.g. a photomultiplier, to produce a start signal used by the TAC. It is stopped when the first photon from the sample is detected. The TAC then outputs a voltage signal that is proportional to the time between the start and stop signals. A multichannel analyzer (MCA), usually part of a computer system, converts the voltage into a digital signal. The schematic experimental setup used in this work is shown in Figure 2.24. Many pulses form a histogram of counts versus time. In a plot

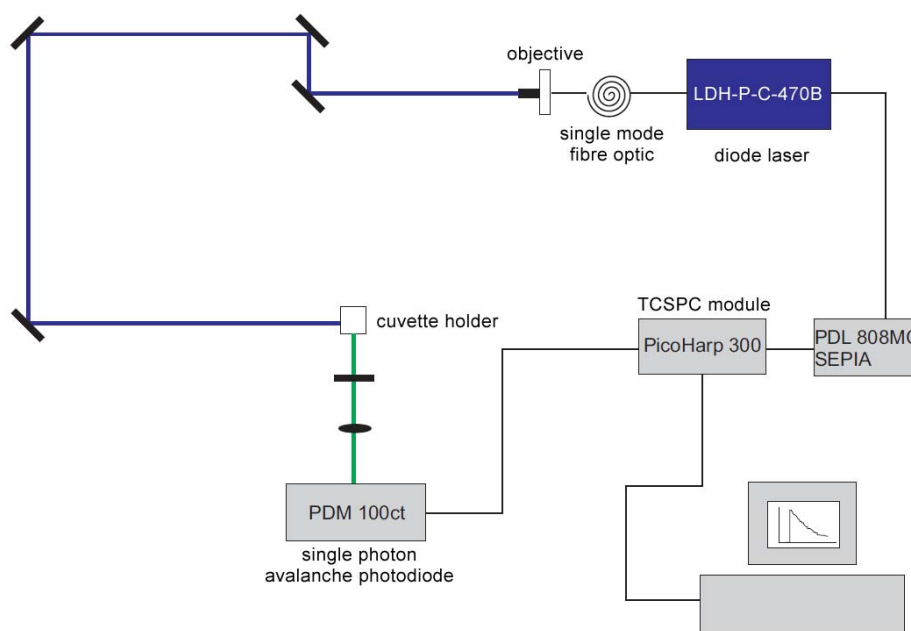


Fig. 2.24: Schematic setup of an TCSPC experiment

with a logarithmic scale of fluorescence intensity (counts/s) versus the time scale a linear decay of counts is visible. This linear decay is related to the fluorescence lifetime  $\tau_D$ . Monoexponential decay (straight line in semi-logarithmic plot) indicates one single decay

time, following the law shown in equation 2.6.

$$N(t) = N_0 \cdot \exp\left(-\frac{t}{\tau_{Fl}}\right) \quad (2.6)$$

where  $N(t)$  is the number of excited molecules at time  $t$ . The fluorescence intensity  $F$  at time  $t$  is proportional to  $N(t)$  and equation 2.6 can be rearranged to equation 2.7.

$$F(t) = F_0 \cdot \exp\left(-\frac{t}{\tau_{Fl}}\right) \quad (2.7)$$

The value of the fluorescence lifetime  $\tau_{Fl}$  can therefore be determined by a linear regression of the linear decay segment in the recorded fluorescence decay histograms delivered by the experiment. Figure 2.25 shows typical recorded decay curves of BODIPY dyes.

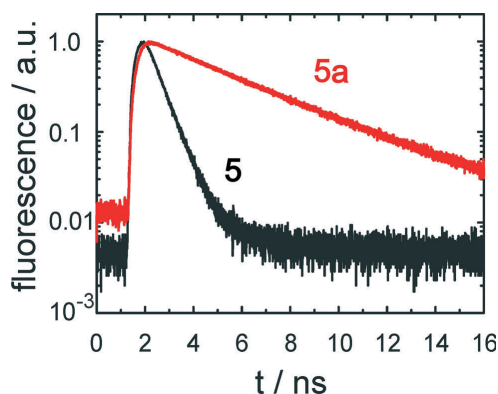


Fig. 2.25: Recorded TCSPC spectrum of BODIPY **5** and its phosphorylated analogon **5a**. The lowered donor energy level by phosphorisation explains the prolongation of the fluorescence lifetime from **5** ( $\tau_{Fl}=0,7\text{ns}$ ) to **5a** ( $\tau_{Fl}=3,7\text{ns}$ )

### 2.3.4 Ratiometric Methods

Generally a ratio is defined as a relation in degree or number between two similar things or the numerical comparison of one class of objects with another.

In science, especially in the life sciences, the ratio imaging procedure is used to pursuit changing conditions around a sensitive probe. Benefits of this detection method compared to other

methods (anisotropy, FRET, lifetime measurements, etc.) to factors like, e.g. the insensitivity to the concentration of the sensor molecules, to uncontrolled quenching and to instrumental factors. Also photobleaching of the fluorophores that decreases the concentration of the sensor molecules will not influence the result if the photobleaching products are non-fluorescent [Dem08]. The sensor molecules are usually fluorescent dyes that are exposed to biological environments or tagged to various biomolecules. With this method the effectiveness of different substrates or catalysts to various fluorescent compounds can be screened at high quantities. The highly sensitive fluorescence imaging methods, that are applied in biochemistry, can detect the slightest changes in fluorescence emission and also be employed in technical screenings on well plates where reactive species react with fluorescent probe dyes. Many different probe dyes that

are sensitive to other ions like, e.g. potassium, sodium, calcium, magnesium, chloride and other bioactive ions are commercially available. The choice of a probe dye depends on the analyte. Fluorescence spectra (or changes in a distinct fluorescence wavelength) are collected at different times, wavelengths, polarities, pH ranges, etc., depending on the sensitivity of the probe dye. Figure 2.26 shows the commercially available pH sensitive dye, carboxy SNARF-1, a long wavelength fluorescent pH indicator that was developed by *Molecular Probes* [Hau02]. The dye undergoes a bathochromic shift in emission wavelength maximum with increasing pH value at a constant excitation wavelength. Thus a ratiometric analysis of the fluorescence intensities at two emission wavelengths can be used for accurate determination of pH values in

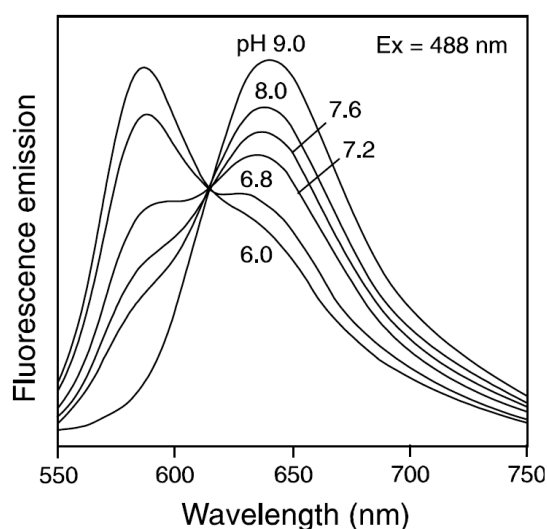


Fig. 2.26: Emission spectra of carboxy SNARF-1 in 50 mM potassium phosphate buffers at various pH values. Samples were excited at 488 nm.

intracellular environments.

With a given suitable sensor ratiometric analysis gives insight to intracellular processes by the distribution of fluorophores and their cellular environments [Gro94, Bur03]. Grynkiewicz, Tsien *et al.* developed a family of fluorescent indicators to unveil the physiological role of calcium ions in cytosols [Gry85]. Ratiometric intracellular calcium imaging has been continuously evolving and even been applied to cells of a beating rat heart [Eer04].

But ratiometric methods are not limited to biochemical applications [Lee05, Cho06]. Ratiometric proceedings can also be applied in combinatoric applications or be implemented in screening techniques. The ratiometric analysis of two different fluorescent species can be used in combinatoric chemistry or chemical engineering as well. Ratiometric analysis, in combination with the kinetics of fluorescence changes give valuable information about affinity and effectiveness of the used reactive species. Attempts to evaluate a methodology have been made with e.g. fluorescent lipid peroxidation probes to detect reactive oxygen species in egg vesicles [Dru02].

In this work ratiometric analysis is applied to a fluorescence dye changing its fluorescence colour upon oxidation. After optimization of the system an employment as probe dye for reactive oxidizing species in screening or in biochemical environments (*in vitro* or *in vivo*) is a realistic research goal.

### 2.3.5 Excited state reactivity (ESPT)

In 1950 Theodor Förster postulated that, due to the thermodynamics of excited and ground states of molecules containing protons and their conjugated bases, the excited state acid is stronger than the ground state acid (with exceptions). This happens when the absorption or emission spectrum of the conjugated base exhibits a bathochromic shift relative to the absorption/emission spectrum of the conjugated acid [För49, För50, För51]. This definition became known as the “Förster cycle” (Figure 2.27). In the case of hydroxyarenes the proton transfer is a process occurring in competition to the decay of excited states. Deprotonated hydroxyarenes

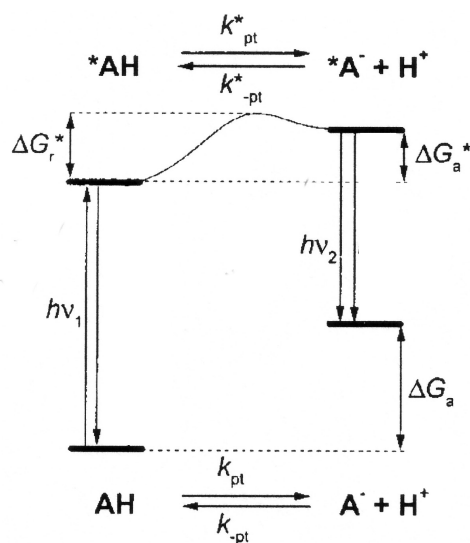


Fig. 2.27: Diagram of the Förster-cycle [Tol02]

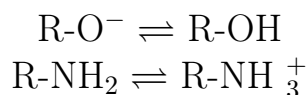
with

$k_{pt}^*, k_{-pt}^*$  Rate constants for forward/backward reaction of excited state proton transfer

$pK_a^*$   $pK_a^* = -\log_{10} \cdot \frac{k_{pt}^*}{k_{-pt}^*}$ ,  $pK_a$  of the excited state derived from the Förster equation, known as Förster acidity

are fluorescent bases with non-binding, oxygen centered, molecular orbitals. In these orbitals the charge distribution appears distal to the oxygen atom. This reduces the basicity of the excited anion. Therefore the acidity of the conjugated acid increases. In addition to fluorescence and proton transfer, hydroxyarenes succumb to a number of additional processes, like proton induced fluorescence quenching and homolytical bond cleavage leading to radicals. These processes have been well researched on 1-Naphtol and phenol derivatives. Förster himself studied these processes on HPTS (Figure 2.15) and its nitrogen analogon 3-Aminopyrene-5,8,10-trisulfonate (APTS) [För50, Pet49]. In these compounds, the sulfonyl groups strongly increase the water solubility and are dissociated over a wide pH range, but they also exert some influence to absorption and emission spectra due to hydrogen bonding to the solvent molecules [Spr07]. Spectroscopic measurements can be carried

out at different pH values to examine the behaviour of the molecules. HPTS and APTS only differ in the presence of a hydroxyl group on one compound and an amino group on the other. Each is subject to a protonation/deprotonation equilibrium:



The spectral transitions for these processes and pH values where they occur are shown in Figure 2.28. If  $\Delta\nu = h\nu_1 - h\nu_2$  is calculated and

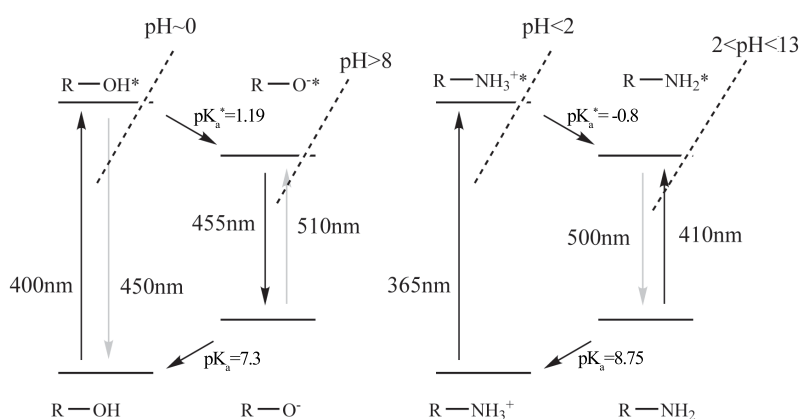


Fig. 2.28: Spectral transitions of the pyrenes used by Förster, and the pH range where they occur

using equation 2.8. The  $pK_a$  of the excited state  $pK_a^*$  is determined, the values of  $pK_a=7.3$  and  $pK_a^*=1.19$  are received for HPTS [För50].

$$pK_a^* = pK_a - \frac{(h\nu_1 - h\nu_2)}{\ln 10 RT} \quad (2.8)$$

This means that the compound is significantly more acidic in the excited state. Therefore HPTS exists in a pH range from 1 to 8 only in a dissociated, excited state  $\text{R-O}^{-*}$ . It prefers to switch over to this energetically more advantageous state than to remain in the excited, undissociated state  $\text{R-OH}^*$ . These processes are similar with protonated APTS in a pH range lower than 2. Calculations yield  $pK_a=8.75$  and  $pK_a^*=-0.8$ . This elucidates that the initial acidity of the amino group increases the acidity of APTS relative to HPTS.

In short donor substitution provokes a redshift of the fluorescence spectra and thus a raise of the acidity.

According to Förster's pyrene similar calculations and behaviours should be achievable for other fluorescent dyes like BODIPYs. This would make the examination of ESPT on a single-molecule level possible. BODIPY dyes like **10** and **11** (figure 2.9) seemed to be a promising system to examine their ESPT capability. Unfortunately limitations arise due to the poor water solubility of the compounds relative to the excellent solubility of HPTS. If, however, ESPT can be observed in a given, calculated pH range on these compounds, FCS and other single-molecule techniques like TCSPC would be mighty tools to unveil the dynamics, rate and consequently the mechanism of the fast process ESPT.

### 2.3.6 The Solvatochromic Comparison Method

The solvatochromic comparison method was used to evaluate a scale of solvent hydrogen-bond acceptor (HBA) capabilities (the  $\beta$ -scale), a scale of solvent hydrogen-bond donor (HBD) capabilities (the  $\alpha$ -scale), and a scale of solvent dipolarity/polarizability (the  $\pi^*$ -scale) using UV/Vis spectral data of solvatochromic compounds. This system was employed and developed by Kamlet, Taft *et. al.* in 1976 [Taf76, Kam76, Kam77, Kam83]. The  $\alpha$  scale describes the ability of the solvent to donate a proton in a solvent-to-solute hydrogen bond. The  $\beta$  scale provides a measure of the solvent's ability to accept a proton (donate an electron pair) in a solute-to-solvent hydrogen bond and to evaluate hydrogen-bond-acceptor strengths of solid HBA bases dissolved in non-HBA solvents. The  $\pi^*$  scale is an index for the ability of the solvent to stabilize a charge or a dipole via its dielectric effect.

The parameters for different solvents were determined by measuring the magnitudes of solvatochromic shifts,  $\Delta\Delta\tilde{\nu}$  for distinct compounds relative to a single fixed reference points for the different scales. Starting from that the  $\alpha$ ,  $\beta$  and  $\pi^*$  values for more than 70 solvents have been determined. The  $\pi^*$  scale ranges from 0.00 (for cyclohexane) to 1.00 (for dimethylsulfoxide). The  $\alpha$  and  $\beta$  scales also

range from 0.00 to 1.00 (with exceptions like e.g. Trifluorethanol and Hexafluorisopropanol). The solvatochromic parameters have been used in one, two and three parameter correlations involving different combinations of these parameters, called *linear solvation energy relationships* (LSER's). But it has to be mentioned that this empirical analysis is simply an attempt to quantify solute properties. Some generalisations have been made by neglecting specific solute-solvent interactions, which can not be grasped by solvatochromism. Therefore all values are containing errors. However, the method is well suited for an estimation of general tendencies. More than 40 articles dealing with LSER's have been published until today. The system has been continuously enhanced and enlarged, also with the help of other workgroups. Only elemental aspects of the system shall be discussed in this chapter.

### The Kamlet-Taft-equation

The most common multiparameter equation in LSER's, known as Kamlet-Taft equation (equation 2.9) [Rei03], can be considered as a linear three parameter regression of the spectral shifts of an OH-species,  $\nu_i$ , gathered from spectral data like absorption and emission maxima and the tabulated solvatochromic parameters of the different used solvents [Lau94, Agm05].

$$\nu_i = \nu_{i0} + p_i\pi^* + b_i\beta + a_i\alpha \quad (2.9)$$

with

|                        |   |
|------------------------|---|
| $\nu_i$                | spectral transition frequency   |
| $\nu_{i0}$             | reference spectral transition frequency                               |
| $\alpha, \beta, \pi^*$ | Kamlet and Taft solvatochromic parameters<br>(solvent properties)     |
| $a_i, b_i, p_i$        | parameters of the molecule under investigation<br>(solute properties) |

The coefficients  $a_i, b_i$  and  $p_i$  are characteristic properties of the solutes in the i-th electronic state.  $p_i$  is related to the transition dipole moment of the substance,  $b_i$  is a measurement for its basicity

and  $a_i$  describes its acidity. The index  $i$  describes either the properties of the ground state ( $i=0$ , excitation) or the excited state ( $i=1$ , emission). Hence solvatochromism,  $\nu_i - \nu_{i0}$ , of the solute in dependence of the solvent can be used to gather information of the stabilization of the excited state relative to the ground state.

### Differential solvatochromism

Different dyes that are known to be good photo acids have been examined for their solvatochromic parameters  $a_i$ ,  $b_i$  and  $p_i$ , like the naphthols 5-cyano-2-naphthol (5CN) and 2-naphthol (2OH) by Agmon *et al.* in 1998 [Sol98a, Sol98b, Sol99]. The comparison between solvatochromic shifts of a hydroxysubstituted dye (ROH) and the shifts of a homomorph methoxysubstituted dye (ROMe) shows that the difference between the shifts only relates to the loss of the ROH $\cdots$ S hydrogen bridge bond between the oxygen atom of the hydroxyl group and the hydrogen of a protic solvent. The dipolar effects of ROH and ROMe are considered to be similar. This means that by the subtraction of the maximal frequencies of the given transitions of both species (Equation 2.10)

$$\Delta\nu = \nu(ROMe) - \nu(ROH) \approx b_i\beta \quad (2.10)$$

only the influence of the effect of the ROH $\cdots$ S-bond, between the hydrogen atom of the hydroxyl group and a hydrogen bridge bond accepting atom (e.g. nitrogen, oxygen) of a solvent S, remains. This approach is called “differential solvatochromism”. The result is a correlation between spectral shifts in relation to the empirical solvatochromic parameters of different solvents. The solute dependent parameters  $a_i$ ,  $b_i$  and  $p_i$  correspond to the slopes of the resulting linear fits of the graphs.

**Determination of  $b_i$ :** Figure 2.29 shows the differential solvatochromism of 5CN relative to its methoxyderivative [Agm05]. The higher the ability of a solvent to accept hydrogen bridge bonds, the higher gets the relative stabilization of the excited state R\*OH and

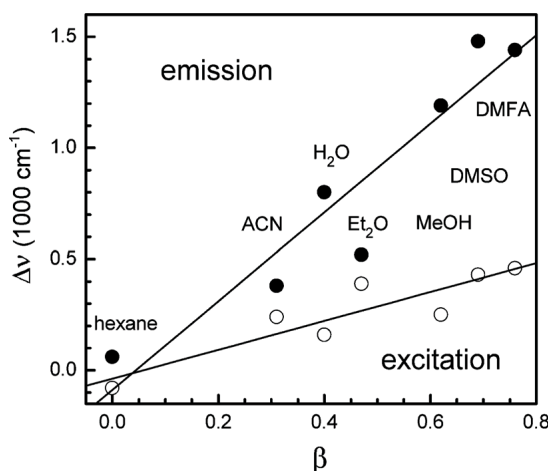


Fig. 2.29: Differential solvatochromism of 5CN relative to its methoxyderivative in different solvents. Emission is represented by circles and excitation by filled circles.

the greater becomes  $\Delta\nu$ . The slopes of the two straight lines ( $b_0$  for the ground state and  $b_1$  for the excited state) show a higher slope for the fluorescence case than for the absorption/excitation case. This can be explained by a relaxation of the solvent occurring after excitation but before emission. These rearrangements, also partly responsible for the Stoke's shift, strengthen the ROH $\cdots$ S- bond, which causes the solute to react more sensitive to changes in solvent properties [Agm05].

**Determination of  $p_i$ :** After the parameter  $b_i$  was determined, the Kamlet-Taft equation can be rearranged to determine the parameter  $p_i$ . By the choice of solvents with a HBD acidity of  $\alpha=0$ ,  $a_i\alpha$  drops out of the equation 2.11.

$$\nu_i - \nu_{i0} - b_i\beta = p_i\pi^* \quad (2.11)$$

If a solvent, whose solvatochromic parameters  $\alpha$ ,  $\beta$  and  $\pi^*$  are zero, (e.g. cyclohexane) is used  $\nu_{i0}$  can be calculated to equation 2.11, by entering the appropriate values for absorption and emission,  $\nu_i$ . A graphic data analysis analogue to figure 2.29, by plotting the calculated values against the empirical values of  $\pi^*$ , yield straight lines with slopes corresponding to  $p_i$ .

**Determination of  $a_i$ :** If the solute parameters  $b_i$  and  $p_i$  have been determined, the Kamlet-Taft equation can be resolved into  $a_i\alpha$  (equa-

tion 2.12):

$$\nu_i - \nu_{i0} - b_i\beta - p_i\pi^* = a_i\alpha \quad (2.12)$$

Graphical data analysis analogue to the previous point yield  $a_i$  from the slopes of the gained straight lines.

If the parameters  $a_i$ ,  $b_i$  and  $p_i$  have been determined, they can be compared to published solvatochromic data of other dyes in order to assess the suitability of a dye as photoacid.

### The Ooshika-Lippert-Mataga-Equation

As an alternative to the thermodynamic proposals for prediction of solute-to-solvent behaviours (like e.g. Förster's ESPT model), Lippert described in 1957 a consideration derived from a quantum mechanic point-of-view [Lip57]. Here the solvent sensitivity of a fluorophore can be estimated from a Lippert plot. The more sensitive a fluorophore reacts to a new solvent, the larger are its changes in dipole moment upon excitation. The polarizability of a molecule is a result of both the mobility of electrons in the solvent and the dipole moment of the solvent molecules. Both effects show different time dependencies. Reorientation of electrons happens instantaneously, whereas the dielectric constant also determines the polarisability of the solvent and therefore includes the effects of molecular orientation of solvent molecules. This molecular orientation (low frequency polarisability) shows a slower timescale than electron orientation (high frequency polarizability). The orientation polarisability  $\Delta f$  is defined as the difference between the high-frequency polarisability  $f(n)$ , which is a function of the refractive index, and the low-frequency polarisability that is given as a function of the dielectric constant (equation 2.13).

$$\Delta f = \frac{\varepsilon - 1}{2\varepsilon + 1} - \frac{n^2 - 1}{2n^2 + 1} \quad (2.13)$$

Lippert represented this in a plot where the difference between the wavenumbers of absorption and emission  $\nu_A - \nu_E$  is plotted against the orientation polarisability,  $\Delta f$ . Linearity of these plots can be regarded as evidence for a dominance of solvent effects in spectral shifts (although specific solvent effects may lead to a non-linear plot). The higher the slope of linear fit lines in the plot, the more sensitive the fluorophore reacts to changes in solvent properties.

It can be shown that the difference of absorption and emission maxima as a function of the dielectrical constant of a solvent is proportional to the difference of absorption and emission maxima as a function of the solvatochromic Kamlet-Taft parameter  $\pi^*$  of the solvent. A plot of the differences of absorption and emission maxima as a function of the  $\Delta f$  should result in the case of proportionality to the solvatochromic parameter  $\pi^*$ , in a straight line. This line should be similar to the line in a plot of the differences between absorption and emission maxima as a function of  $\pi^*$  of the respective solvent. This can be achieved by putting equation 2.13 in a form where it considers collected spectroscopic data. For this equation 2.13 has to be combined with an equation showing the correlation between wavenumber differences and changes in dipole moments (2.14).

$$\Delta\nu = \frac{2\Delta f}{a^3hc}(\vec{\mu}_e - \vec{\mu}_g)^2 \quad (2.14)$$

$\Delta\nu$  is the wavenumber difference of the 00-transitions of absorption and emission.  $\mu_G$  and  $\mu_E$  are the dipole moments of the ground and excited states.  $a$  is the Onsager radius. The term  $(\vec{\mu}_e - \vec{\mu}_g)^2$  describes a molecular characteristic. This equation is called the Ooshika-Lippert-Mataga equation [Bün87], giving credit to Ooshika and Mataga who were helping Lippert in deducing the quantum mechanical relationships. The result of the combination of the equations 2.13 and 2.14 is shown in equation 2.15:

$$\Delta\nu = \nu_{abs} - \nu_{em} = \frac{2}{a^3hc} \Delta\vec{\mu}^2 \left[ \frac{\epsilon_r - 1}{2\epsilon_r + 1} - \frac{n^2 - 1}{2n^2 + 1} \right] \quad (2.15)$$

The advantage of the application of the Ooshika-Lippert-Mataga equation lies in the possibility to determine a molecular property, like the change of the dipole moment of a compound during the transition from the ground state to an excited state, if other influences on solvation can be disregarded.

The described solvatochromic approaches can be used as an alternative to the prediction of ESPT effects, if the Förster method can not be applied. This approach is not limited to water soluble probe molecules. By observation of the influence of solvent effects (acidity and basicity) on excitation and emission spectra a tendency of a molecule to undergo ESPT in a protic solvent can be qualitatively pre-estimated.

### 3 Publications of the results

1. *Comparative Photostability Studies of BODIPY and Fluorescein Dyes by Using Fluorescence Correlation Spectroscopy*; Babette Hinkeldey, Alexander Schmitt, Gregor Jung\*; *ChemPhysChem* **2008**, 9, 2019-2027
2. *Synthesis of the Core Compound of the BODIPY Dye Class: 4,4-Difluoro-4-bora-(3a,4a)-diazas-indacene*; Alexander Schmitt, Babette Hinkeldey, Mandy Wild, Gregor Jung\*; *J. Fluoresc.* **2009**, 19, 755-758
3. *Disabling Photoinduced Electron Transfer in 4,4-Difluoro-8(-4'-hydroxyphenyl)-1,3,5,7-tetramethyl-4-bora-3a,4a-diazas-indacene by Phosphorylation*; Michaela Jacob, Alexander Schmitt, Gregor Jung\*; *J. Fluoresc.* **2008**, 18, 639-644
4. *Solvent-dependent steady-state fluorescence spectroscopy for searching ESPT-dyes: Solvatochromism of HPTS revisited*; Gregor Jung\*, Stephan Gerharz, Alexander Schmitt; *Phys. Chem. Chem. Phys.* **2009**, 11, 1416- 1426
5. *Fluorescent Probes for Chemical Transformations on the Single-Molecule Level*; Gregor Jung\*, Alexander Schmitt, Michaela Jacob, Babette Hinkeldey; *Ann. N. Y. Acad. Sci.* **2008**, 1130, 131-137
6. *A ratiometric fluorescent substrate for mechanistic studies of oxidation reactions*; Alexander Schmitt, Babette Hinkeldey, Benjamin Hötzer, Gregor Jung\*; *J. Phys. Org. Chem.* **2009**, accepted 27-Jun-2009

**Comparative photostability studies of BODIPY and Fluoresceine dyes using Fluorescence Correlation Spectroscopy**

*B. Hinkeldey, A. Schmitt, G. Jung\**

*University of Saarbruecken, Biophysical Chemistry,  
Campus B2.2, 66123 Saarbruecken, Germany*

*\* corresponding author: [g.jung@mx.uni-saarland.de](mailto:g.jung@mx.uni-saarland.de)*

**Abstract**

In single-molecule applications, photostability of fluorescent molecules is a key parameter. We applied Fluorescence Correlation Spectroscopy (FCS) to compare the photostability of four Fluoresceine and four BODIPY dyes of similar structure but different triplet yields. The latter dye class turned out to be more stable. In the kinetic analysis which we developed, diffusion and photobleaching were treated as competitive processes. Corrections, which accounted for saturation and for experimental artefacts were achieved by solely using experimental data. Photobleaching is found to occur mainly via the first excited singlet state  $S_1$  in contrast to previous findings.

**Keywords**

Fluorescence correlation spectroscopy

Photostability

Single-molecule studies

Bodipy, Fluoresceine

## **Introduction**

In recent years, ultrasensitive fluorescence microscopy has become a widely applied method for studying biological processes or interactions between molecules [1-13]. In general, fluorescent labelling of different proteins, cell parts or metabolites is used to observe their molecular behaviour by microscopic means. Also time resolved methods are applied for following active movements, diffusion of intracellular and membrane bound molecules. Ensemble averaging methods like Fluorescence Loss in Photobleaching (FLIP) [1] and Fluorescence Recovery After Photobleaching (FRAP)[12] are available and FCS on the single-molecule level is applied to gain information about chemical reaction rates, flow rates, diffusion coefficients, molecular weights or molecular aggregates [7,8,11-18].

All these examples share the photostability of the chosen dyes as key parameter. The time resolution in FLIP and FRAP depends directly on the maximum of photocycles a molecule undergoes before it becomes photobleached, whereas a high photostability of the employed dyes is recommended for most other applications. In principle, a molecule is considered photobleached if it is in a non-fluorescing state after excitation, either irreversibly or in a long-living dark state [11]. Several attempts to understand photobleaching processes have been made before [14-23]. They can be divided in at least two classes; i.e. ensemble and single-molecule approaches.

At the ensemble level, cuvette experiments have been performed [14,24]. However, the typical excitation intensity is in the range of  $W/cm^2$ , which leads to only weak photobleaching and long time constants of the fluorescence loss. Moreover, typical excitation intensities in single-molecule microscopy are in the range of  $kW/cm^2$  where also higher order processes can occur, so that the values obtained by cuvette experiments are not transferable to these conditions.

Methods like FRAP and FLIP are used to investigate the photostability of fluorescent dyes at higher intensities [1,12]. Photostability is also explored on the single-molecule level by immobilizing single molecules on a surface or in a polymer matrix and monitoring the off-rate of their fluorescence signal [19,20,22,25]. But due to the different environment in a matrix compared to the liquid phase, the access of oxygen to the dyes is altered. Also the probability for ionisation changes [26]. Furthermore, most biological applications take place in an aqueous environment; therefore photostability properties of fluorescent dyes in such solution are more significant. In

order to combine high excitation intensities as well as observation of freely diffusing molecules, FCS is a convenient method since it also allows the access to photophysical parameters.

As FCS is nowadays a well established and theoretically understood method, analysis of photostability should be possible by regarding the diffusional behaviour [12-18, 27-38]. Here, a molecule diffuses through the excitation focus and is only fluorescing while it is inside the irradiated volume. As the collection efficiency function (CEF) is described by the excitation volume convolved with the pinhole function, the size of the detection pinhole hence determines the volume from which the fluorescence photons are collected. This is called the detection volume. The observation time corresponds to the time which a molecule needs in average to diffuse through the detection volume [18,21,28]. With increasing excitation intensities the apparent diffusion time decreases as molecules become photobleached while diffusing through the detection volume [23,27]. This implies that the decrease of the diffusion time with increasing excitation intensity correlates to photobleaching. But still the origin of the bleaching processes is not exactly known. Higher excited states, which are extremely energetic, are regarded as highly reactive, so that degradation can occur more easily [39,40].

Also, the triplet state is often considered as the origin of decomposition due to its relatively long lifetime of microseconds compared to the singlet lifetime in the range of nanoseconds [39-41]. The triplet state thus is regarded as energy storage with a higher probability to undergo excited state reactions.

Recently, Eggeling et al. [36] showed an approach to circumvent photobleaching by pulsed laser excitation. The pulse separation was above the typical lifetime of a triplet state, ensuring that transient molecular dark states with lifetimes  $< 1\mu\text{s}$  can relax between two absorption events and thus avoiding higher order processes out of the triplet state. A 5 to 25 times fold increase in total fluorescence yield was observed.

Chemical attempts like polyfluorination [42,43], insertion of a cyano-group [24] or addition of triplet quenchers and antioxidants are reported [44-46] to result in a higher photostability. But most of the photostability studies focused on solely the triplet state as origin of bleaching processes. Therefore, bleaching via the singlet state is neglected.

In contrast to photobleaching studies which investigated only the triplet state, the purpose of this work is to correlate the bleaching behaviour with the populations of

both singlet and triplet state. As both states are considered, the outcome should be the amount of contribution of the singlet and triplet state to photobleaching. We studied two dye classes. Fluoresceine dyes are chosen as a reference substance class. Dyes of this family are prototypes in photostability research and studies on the photodegradation processes are reported [41,47]. In addition, we use BODIPY (Bordipyromethene) dyes, which exhibit high fluorescence quantum yields [48,49]. They are used in photostability research and FCS applications [25,28,44,49-51]. The chosen members of one dye family are structurally nearly identical with very similar excited state lifetimes, but different intersystem crossing yields. Thus, the only variation within one dye family lies in their intensity dependent triplet population. We perform intensity dependent FCS measurements and correlate the obtained decrease of the diffusion time with the photophysical parameters of the dyes. The developed approach consists in treating the apparent diffusion time as the sum of the rate constants for bleaching and diffusion, which leads to a Stern-Volmer analogue analysis. We also circumvent previously described optical artefacts by a careful experimental design [34,38]. Simplifications of our approach are discussed and the outcome is compared to previous published results.

## **Experimental section**

### **Materials**

BODIPY dyes **1–3** (purity > 90%) are synthesized according to standard methods [52,53] and identified by NMR. Details will be described elsewhere. BODIPY **4** and Fluoresceine **4** (Fluoresceine 27) are purchased from Radiant dyes (Germany) (laser grade purity), Fluoresceine **2** (Fluoresceine isothiocyanate isomer I) from Fluka (Germany) (purity > 97.5%), Fluoresceine **3** (Oregon Green 488 carboxylic acid 5 isomer) from Molecular Probes (Invitrogen, Germany) (laser grade purity) and Fluoresceine **1** (Uranin) is obtained from Merck (Germany) (purity > 95%).

### **UV/Vis and Fluorescence Spectra**

Absorption spectra are recorded with an UV/Vis Spectrophotometer (Lambda 5, Perkin Elmer, USA), emission spectra are taken by a fibre coupled spectrometer (SD

2000, Ocean Optics, USA). The concentration of the used aqueous solutions is in the micromolar range. Fluoresceine dyes are measured at pH 10 by adding buffer solution (HPCE-grade, Fluka, Germany).

## TCSPC

Fluorescence lifetime measurements are performed by using a custom-built setup. It consists of a pulsed diode laser ( $\lambda_{\text{exc}} = 470$  nm, pulse width = 60 -120 ps), a diode laser driver unit (PDL 808 MC SEPIA, PicoQuant, Germany), followed by a single photon avalanche detector (PDM 100ct SPAD, Micro Photon Devices, Italy) and a photon counting device (PicoQuant Microtime, Germany). The overall instrumental response function is between 200-300 ps. Data are analyzed by commercial software (SymPhoTime, PicoQuant, Germany).

## FCS

FCS measurements are also performed with a custom-built confocal setup. The laser source basically consists of a frequency doubled diode laser (Picarro, Soliton) operating at  $\lambda = 488$  nm and a beam diameter of 0.7 mm. For beam extension, the laser beam is coupled into a fibre and led through a 10 x objective, yielding finally a beam with a diameter of 4 mm. The laser is directed into an inverted microscope (Axiovert 200, Zeiss) and reflected by a dichroic mirror (495 DRLP, Omega) onto a water immersion objective (PlanApo 63x, NA 1.2 WI, Zeiss). The objective focuses the laser into a diffraction limited spot above thickness corrected cover slides (0.17 +/- 0.01 mm, Assistent). As sample, a drop of nanomolar solution is put on the coverslide on top of the microscope. Fluorescence is collected by the same objective, passes the dichroic mirror and is focused by the tube lens onto a 50 or 75 $\mu$ m pinhole. Afterwards, light is filtered by a band pass filter (HQ 525/50, AHF Analysentechnik) and is splitted into two beams by a 50:50 beamsplitter. Two Avalanche photo diodes (SPCM-14-AQR, Perkin Elmer Optoelectronics) detect the photons and the output of the modules is cross-correlated by a hardware correlator (FLEX 02 D, Correlator.com). Fluorescence correlation curves are taken with excitation powers varying between 10 $\mu$ W and 5 mW corresponding to intensities of 0.68 and 335 kW/cm<sup>2</sup> at the sample, respectively.

This is a pre-peer reviewed version of the following article: *ChemPhysChem*, 2008, 9, 2019-2027; DOI: 10.1002/cphc.200800299; Reproduced by permission of the *ChemPhysChem* owner societies;

Correlation data is analysed according to the 2D-model [Eq. (1)] which is sufficient to describe  $g(\tau)$  for the here used pinhole diameter [54]

$$g(\tau) = \frac{1}{N} \cdot \left( \frac{1}{1 + \frac{\tau}{\tau_{diff}(I)}} \right) \cdot \left( 1 + \frac{k_{23}^{eff}}{k_{31}} \exp\left(-\left(k_{23}^{eff} + k_{31}\right)\tau\right) \right) \quad (1)$$

$g(\tau)$  is the obtained correlation function of the fluorescence fluctuations,  $N$  the particle number and  $\tau_{diff}(I)$  represents the apparent diffusion time. The parameters  $k_{23}^{eff}$  and  $k_{31}$  correspond to the effective ISC rate constant and the inverse of the triplet lifetime  $\tau_T$ , respectively. For global fitting,  $k_{31}$  is kept constant for all correlation curves of one dye. The intersystem crossing rate constant  $k_{23}$  can be extracted using Equation (2) according to [27] by

$$k_{23}^{eff} = k_{23} \cdot \frac{k_{12}}{k_{12} + k_{21}} \quad (2)$$

with  $k_{21}$  as the inverse of fluorescent lifetime  $\tau_{fl}$

$$k_{21} = \frac{1}{\tau_{fl}} \quad (3)$$

and  $k_{12}$  as the excitation rate constant

$$k_{12} = \frac{\sigma \cdot I}{\nu \cdot h} \quad (4)$$

$\sigma$  is the absorption cross section,  $I$  the applied excitation intensity,  $\nu$  the laser frequency and  $h$  the Planck constant. For the sake of comparability, all shown FCS data are normalized to  $N = 1$ .

The contrast  $C$  and its maximum value,  $C_{max}$ , are expressed by

$$C = \frac{k_{23}}{k_{31}} \cdot \frac{k_{12}}{k_{12} + k_{21}} = C_{max} \cdot \frac{k_{12}}{k_{12} + k_{21}} \quad (5)$$

and are connected to the triplet population  $T$  by

$$T = \frac{C}{C+1} \quad (6)$$

## Results

**Electronic spectra and determination of photophysical parameters:**

We use eight different fluorescent dyes, four BODIPY and four Fluoresceine dyes. Their chemical structures are depicted in scheme 1 and 2. Within the BODIPY family, BODIPY 2, 3 and 4 differ only in their number of methyl groups. BODIPY 1 is structurally equivalent to 2 except the additional phenyl group in the *meso*-position. Among the Fluoresceines, Fluoresceine 4 is the chlorinated analogue to Fluoresceine 1 which is expected to lead to an increased intersystem crossing rate constant [55]. Fluoresceine 3 carries fluor atoms in order to amplify photostability [56]. Fluoresceine 2 is substituted by an isothiocyanate group in the phenyl moiety, but except this, identical to Fluoresceine 1. Both dyes are expected to have nearly identical photobleaching properties since the phenyl moiety is perpendicular to the chromophoric system.

All eight dyes were investigated by UV/Vis spectroscopy as well as fluorescence lifetime measurements. Because of their similar absorption maxima  $\lambda_{\text{abs}}$  (around 490nm) and emission maxima  $\lambda_{\text{em}}$  (around 520 nm) FCS is possible and comparable data should be obtained with an excitation wavelength of 488 nm. All four Fluoresceine dyes exhibit a fluorescence lifetime  $\tau_{\text{fl}}$  of about 4 ns. The lifetime of the BODIPY dyes is about 6 ns except BODIPY 1, of which the lifetime is shortened to 3.6 ns. This reduction is attributed to the freely rotating phenyl moiety of which rotational movements represent an alternative pathway to loose the received excitation energy ("loose bolt mechanism" [57]).

The ISC rate constants  $k_{23}$  of BODIPY 3 and 4 as well as  $k_{23}$  of the Fluoresceine dyes are all in the range of  $3 - 5 \times 10^6 \text{ s}^{-1}$ , indicating a high triplet quantum yield. Fluoresceine 2 has an even larger ISC rate constant of  $8 \times 10^6 \text{ s}^{-1}$ . Only BODIPY 1 and 2 have a relatively low ISC rate constant below  $10^6 \text{ s}^{-1}$ . Except Fluoresceine 3, of which  $\tau_{\text{T}}$  is comparatively long (2.4  $\mu\text{s}$ ), all other dyes exhibit triplet lifetimes between 1.3 and 1.6  $\mu\text{s}$  which indicate diffusion controlled triplet quenching by molecular oxygen [39].

All spectroscopic parameters are listed in table 1.

**FCS as a valuable tool for analysing photobleaching**

### 3.1 *ChemPhysChem* 2008, 9, 2019-2027

FCS measurements are performed with the setup described above. BODIPY **3** is measured at even lower excitation intensities, beginning at  $0.68 \text{ kW cm}^{-2}$  (see Supporting Information). Figure (1) shows FCS data of three different dyes at three different excitation intensities. Figure (1 a) depicts the data obtained from BODIPY **2**, Figure (1 b) of BODIPY **3** and Figure (1 c) corresponds to Fluoresceine **3**.

Comparison of the three data sets in the sub-microsecond time range gives information about the triplet population. The contrast  $C$  which is related to the triplet population increases from Figure (1 a to c) at the same intensity. This means, that BODIPY **2** is rarely in triplet state ( $C_{\text{max}} \sim 2$ ) whereas Fluoresceine **3** ( $C_{\text{max}} \sim 8$ ) is nearly exclusively in triplet state upon high excitation intensities. All Fluoresceines and BODIPY **3** and **4** reveal high ISC rate constants, whereas BODIPY **1** and **2** show relatively low triplet population.

Upon increasing intensities the diffusion times of all dyes (except BODIPY **3**) exhibit a distinct decrease in  $\tau_{\text{diff}}$ .

Figure (2) summarizes the dependence of the diffusion time  $\tau_{\text{diff}}$  on the excitation intensity  $I$  for three examples. The decrease is nonlinear and at higher intensities  $\tau_{\text{diff}}$  levels off. There, while increasing the excitation intensity the excitation rate remains constant, because the rate-limiting step is the decay of the excited states.

The degree of change in  $\tau_{\text{diff}}$  in the case of BODIPY dyes seems to be anticorrelated to the triplet population. The lower the contrast, the more distinct the decrease of diffusion time appears. In contrast, all four Fluoresceine dyes exhibit high triplet populations and a decrease of  $\tau_{\text{diff}}$  at the same time.

### **Analysis of photobleaching in analogy to Stern - Volmer**

Several attempts were made to describe the observed photobleaching behaviour phenomenologically. [17,27,40]

Our alternative approach is to treat photobleaching as a competitive process to diffusion (see supporting information). In a kinetic description, this results in a sum of two rate constants for the observed "disappearance rate constant"  $k_{\text{diss}}$ :

$$k_{\text{diss}} = \frac{1}{\tau_{\text{diff}}(I)} = \frac{1}{\tau_{\text{diff}}(0)} + k_{\text{bl}} \quad (7)$$

$\tau_{\text{diff}}(0)$  is the unbiased diffusion time if no photobleaching occurs and  $k_{\text{bl}}$  is the intensity dependent rate constant for all bleaching processes. It is a

phenomenological rate constant, which also includes transitions from higher singlet ( $S_n$ ) or triplet ( $T_n$ ) states. This perception strongly resembles the Stern-Volmer interpretation of fluorescent quenching [58]. There, the higher the concentration of the quencher the less fluorescence is emitted. This relation is expressed by Equation (8)

$$\frac{\tau_{fl,0}}{\tau_{fl}([Q])} = \frac{\Phi_0}{\Phi([Q])} = 1 + k_q \tau_0 [Q] \quad (8)$$

with  $\Phi_0$  denoting the fluorescence in absence of quencher,  $\Phi$  the fluorescence in presence of quencher,  $\tau_0$  the fluorescence lifetime in absence of quencher and  $[Q]$  the quencher concentration. We used in Equation (8) the proportionality of  $\tau_0$  and  $\Phi_0$  [59]. The product  $\tau_0 k_q$  is called the Stern – Volmer quenching constant.

In our case, the analogy to Equation (8) is represented by Equation (9)

$$\frac{\tau_{diff}(0)}{\tau_{diff}(I)} = 1 + k_{bl} \cdot \tau_{diff}(0) \cdot I \quad (9)$$

$\tau_{diff}(0)$  can be extrapolated from Figure (2). However, its value is of minor importance. Figure (3a) depicts our analysed data. At least at low intensities a straight line behaviour with an ordinate intercept of 1 results from treating the diffusion time in analogy to fluorescence quenching. But at higher intensities, the data levels off from the linear behaviour. At these intensities, we have to consider saturation effects, leading to the fraction term in brackets [60].

$$\frac{\tau_{diff}(0)}{\tau_{diff}(I)} = 1 + k_{bl} \cdot \tau_{diff}(0) \cdot I \cdot \left( \frac{1}{1 + \frac{I}{I_{sat}}} \right) = 1 + k_{bl} \cdot \tau_{diff}(0) \cdot \frac{I \cdot I_{sat}}{I_{sat} + I} \quad (10)$$

Photobleaching as well as saturation follow the excitation profile; i.e.  $k_{bl}(r)$  and  $C(r)$  are affected in the same manner. Due to this inhomogeneity, photobleaching in FCS cannot be solved analytically [23]. We correct for these non-linearities by the intensity dependent contrast  $C(I)$  as will be described in the next section.

### Correction of the intensity inhomogeneity

As mentioned before, saturation effects lead to an inhomogeneity of the intensity dependent diffusion time. By using the experimental contrast  $C$  **instead** of the

intensity, these saturation effects can be experimentally accounted for, since the contrast also saturates [38]. Equation (5) can be rewritten as

$$C = C_{\max} \cdot \frac{I}{I + I_{\text{sat}}} \quad (11)$$

with

$$I_{\text{sat}} = \frac{k_{21} \cdot \sigma}{h\nu} \quad (12)$$

As the experimental contrast  $C$  is a position dependent parameter, it is a measure of the averaged actual intensity in the detection volume. ISC and photobleaching are linked together via the intensity conditions in the monitored area. Therefore, saturation should affect  $C$  as well as  $\tau_{\text{diff}}$  in a similar manner. By introducing the experimental contrast as internal reference of the actual intensity, this “first order” correction recompenses also imperfect alignment of the detection pinhole. Introducing the experimental contrast in Equation (10) leads to

$$\frac{\tau_{\text{diff}}(0)}{\tau_{\text{diff}}(I)} = 1 + k_{\text{bl}} \cdot \tau_{\text{diff}}(0) \cdot \frac{C(I)}{C_{\max}} \cdot I_{\text{sat}} \quad (13)$$

$\tau_{\text{diff}}(0)$  occurs on both sides of the equation and can be cancelled. We keep it in the figures for the sake of clearness to stress the analogy to Stern – Volmer analysis.

The slope of the Stern – Volmer plot becomes

$$\frac{\partial \left( \frac{1}{\tau_{\text{diff}}(I)} \right)}{\partial C} = \frac{k_{\text{bl}} \cdot I_{\text{sat}}}{C_{\max}} \quad (14)$$

Therefore, a correlation between the diffusion based parameter  $\tau_{\text{diff}}(0) / \tau_{\text{diff}}(I)$  with the contrast  $C$  (Fig. (3 b)) is obtained. Both BODIPY **2** (black squares) and **3** (dark grey triangles) exhibit almost a linear relation between the diffusion time and the contrast. Fluoresceine **3** (light grey squares) still levels off originating from a still increasing contrast while no change in  $\tau_{\text{diff}}(I)$  is observed. One reason could be that our correction with the experimental contrast is not sufficient at very high contrast build up.

As  $C_{\max}$  is proportional to the triplet population [Eq. (6)], our analysis correlates bleaching behaviour with the populations of the photophysical states.

### Correlation with photophysical parameters

The next step in our analysis is to eliminate  $C_{\max}$  in Equation (14), as  $C_{\max}$  is the parameter by which the dyes Fluoresceine **1 - 4** and BODIPY **1 - 4** differ. A convenient way is a Lineweaver-Burke-plot, described by Equation (15). It can alternatively be used to extract  $k_{23}$ . The outcome does not differ from the value obtained by the correlation data listed in Table (1).

$$\frac{1}{C} = \frac{k_{31}}{k_{23}} + \frac{k_{21}}{k_{12}} \cdot \frac{k_{31}}{k_{23}} \quad (15)$$

However, the advantage of plotting  $1/C$  versus the  $1/I$  [Fig. (4)] is that this plot gives information about the triplet population without further conversion of the experimental data. It is connected to the triplet population as

$$\frac{\partial \frac{1}{C}}{\partial \frac{1}{I}} = \frac{k_{31}}{k_{23}} \cdot \frac{h \cdot \nu \cdot k_{21}}{\sigma} = \frac{1}{C_{\max}} \cdot I_{\text{sat}} = \frac{\partial \frac{1}{T}}{\partial \frac{1}{I}} \quad (16)$$

Figure 5 shows the dependence of the contrast build up of  $C$  on the excitation intensity for BODIPY **2** (black dots), BODIPY **3** (dark grey triangles) and Fluoresceine **3** (light grey squares). All three substances exhibit a nearly linear correlation between the inverse contrast and the inverse intensity. The steeper the slope the lower is the triplet yield.

### Correlation of triplet population and photobleaching behaviour

As Equation (14) and Equation (16) both contain the parameters  $C_{\max}$  and  $I_{\text{sat}}$ , combination leads to the master Equation (17):

$$\frac{\partial \left( \frac{1}{\tau_{\text{diff}}(I)} \right)}{\partial C} / \frac{\partial \frac{1}{C}}{\partial \frac{1}{I}} = \frac{k_{bl} \cdot I_{\text{sat}}}{C_{\max}} = \frac{1}{C_{\max}} \cdot I_{\text{sat}} = k_{bl} \quad (17)$$

This means that by plotting the slope of the Stern – Volmer plot [Fig. (3b)] against the slope of the inverse of the contrast versus the inverse of intensity [Fig. (4)], the resulting slope should represent the bleaching rate  $k_{bl}$  for a given molecular structure [Fig. (5)].

### **Photobleaching out of the singlet state**

Figure (5) shows the plot obtained by use of Equation (17). In this plot, the ordinate displays the magnitude of photobleaching. The lower the data points the less photobleaching occurs, i.e. indication of a higher photostability. The abscissa describes the triplet yield. Both dye families exhibit similar tendencies, i.e. a linear correlation between photobleaching and singlet population which is expected from Equation (17). We conclude from the depicted linear correlation that one dye class exhibits a constant photobleaching yield.

Although both dye families have a similar slope, their bleaching rate constants are not the same. The Fluoresceine dyes are parallel shifted upwards, as shown by comparison of BODIPY **3** and Fluoresceine **1**. Both dyes exhibit a similar triplet population but while BODIPY **3** is rather stable, Fluoresceine **1** bleaches obviously. Therefore, the photostability of BODIPY dyes seems to be superior to the Fluoresceines. One has to consider that the more time a molecule spends in its triplet state, the less bleaching occurs. A dye which is in this long-living bottleneck state for the most time undergoes less photocycles than a molecule which is almost exclusively in its singlet state. This kind of dead time leads to an error in applying the Stern-Volmer analogous analysis versus the uncorrected excitation intensity. In the master plot, however, we accounted for the number of excitation cycles. Moreover, it turns out that a molecule in the triplet state  $T_1$  is not as susceptible for bleaching processes as in the singlet state  $S_1$ . Otherwise we would expect an anticorrelation in Figure (5).

The most efficient single-molecule dyes should be located in the lower right corner in Figure (5), resulting from a low bleaching rate and a low triplet population. Again, this supports the result that Fluoresceine dyes are less photostable than BODIPY dyes.

We introduced several simplifications (see discussion) and therefore cannot expect that we can extract exclusively  $k_{bl}$  from the slope. However, at least a qualitative correlation should be possible within a class of dyes.

### **Discussion**

In order to analyse photostability by FCS we carefully redesigned our experimental setup. The main sources of optical artefacts, i.e. beam astigmatism, varying cover

slide thickness, out-of-focus fluorescence and diffractive index mismatch, are minimized [see Supporting Information]. By this, the changes in the apparent diffusion time in FCS data can be traced back to photobleaching. As a bleached molecule becomes non fluorescing, the observation time is shortened relatively to the dwell time, which an intact molecule needs to diffuse through the whole detection area. Consequently, photobleaching and diffusion are treated as competitive processes. This is the foundation of our analysis by a Stern-Volmer analogue approach.

Saturation, which occurs at high intensities, leads to a limited maximum number of photocycles [60]. These effects are corrected for in the master plot [Fig. (5)]. As saturation effects are predominantly present in the centre of the focus, the exact position of the detection volume is of high importance. As a first-order approximation, the bleaching rate  $k_{bl}(r)$  follows the excitation profile  $I_{fl}(r)$  in the same way as the ISC rate constant,  $k_{isc}(r)$ . Therefore, the experimental contrast is used as an internal reference to the excitation intensity at the monitored position. As a result, we correct for a feasible misalignment as well as saturation.

We investigated two families of structurally similar fluorescent dyes, and in both families a correlation between the extent of singlet state population and photobleaching is found [Fig. (5)]. Since this is a rather unexpected result, possible error sources have to be considered.

As the experimental setup is optimized, changes in  $\tau_{diff}$  solely originate from photobleaching. This is verified by measurements of BODIPY **3**, which hardly undergoes any bleaching (see supporting information). The obtained diffusion time varies below 10%, which implies that experimental error sources are evidently minimized. A fully correct treatment of diffusion and photobleaching must obey Fick's equations, but so far, only approximations are developed for this treatment [18,28,54].

Our derived method also simplifies the treatment of competitive processes, at the expense of accuracy and quantitative results. We thus extract only relative relations. This is possible since the investigated dyes are approximately of the same size; measurements are taken at the same temperature with the use of a 50 $\mu$ m pinhole. Therefore, diffusion properties should be similar for all dyes.

In analogy to Stern-Volmer analysis, bleaching processes are assumed to relate linearly to the excitation intensity. This means, that higher order processes are

neglected in our model. This is reasonable for higher triplet states, as BODIPY **3** and Fluoresceine **3** show a high triplet population but low photobleaching yield. But higher singlet states could be involved. In the case that the  $S_0$ - $S_1$ -excitation is the rate-limiting step and subsequent  $S_1$ - $S_n$  excitation leads directly to e.g. ionisation, no kinetic information about such processes can be obtained. Therefore, bleaching via higher excited singlet states cannot be excluded. Furthermore, bleaching out of triplet states can not be excluded entirely. Under different experimental conditions than described in this work, i.e. different  $\lambda_{max}$ , triplet-triplet absorption could become more relevant.

As our investigated dyes show similar photophysical parameters, it is reasonable to figure out the effect which a variation of these parameters would have on our analysis. The absorption cross section cancels out in Figure (5) and Equation (17), therefore differences concerning this parameter can be neglected. If the triplet yield of the investigated dyes strongly differs, the dyes with a low triplet yield would also exhibit a low triplet population. In the master plot [Fig. (5)] this would lead to a shift to the right, because a low triplet population induces a small contrast. Furthermore, a molecule which is more in its singlet state exhibits more photobleaching according to our findings, leading to an upward movement of the data point. As a result, a difference in triplet yields results in a shift of data points to the right and upwards, so that the linear behaviour is maintained. Indeed, this behaviour is observed for the BODIPY dye class.

The effect of  $\tau_{fl}$  is visualized by another example of the BODIPY family. Within these dyes, only BODIPY **1** deviates downwards from the linear behaviour. BODIPY **1** has only a lifetime  $\tau_{fl}$  of 3.6 ns compared to lifetimes around 6 ns of the other BODIPY dyes. As a result, BODIPY **1** spends roughly half the time in its excited singlet state relative to the other BODIPY dyes, so that its probability to become photobleached out of some singlet state is also correspondingly reduced. This would explain the downward shift. If the fluorescence lifetimes were similar, all four BODIPY dyes should exhibit one linear relation.

In fact, all four Fluoresceine dyes also correlate linearly, indicating a similar kind of bleaching behaviour. The lower photostability could originate out of the negative charge of the Fluoresceine dyes, which might facilitate autoionisation at high intensities. Another possibility is that Fluoresceine dyes possess a resonant  $S_1$ - $S_n$  transition which is not prominent for the BODIPY families at our experimental

wavelength. Pump-probe experiments could reveal information about excited state absorption [61].

The presented analysis of both dye families leads to the assumption, that photobleaching occurs out of the excited singlet state. Until now, solely the triplet state was held responsible for bleaching processes due to its long lifetime. Song et al [41,62] investigated the photobleaching of Fluoresceine and its suppression by use of mercaptoethylamine. This latter agent can act both as triplet quencher and as one electron reductant which hampers the distinction between both modes of action. In addition, they found that the bleaching kinetics is not a single-exponential process indicating different possible bleaching pathways [62]. This means that bleaching can occur via several possible pathways including e.g. excitation into higher excited states, which is considered in [23, 45].

We explain bleaching out of the singlet state as follows: the reduction potentials of the used dyes lie in the range of -1.2 V vs. SCE (standard calomel electrode) which is roughly the energy of the singly occupied LUMO after excitation [64,65]. The triplet state is lowered by approximately 0.5 V if we transfer the red-shift of phosphorescence compared to fluorescence to the model of photon induced electron transfer. Its thermodynamics are quantified by consideration of the Rehm-Weller equation (18)

$$\Delta G_{PeT} = E_{ox} - E_{red} - \Delta E_{00} - w_P \quad (18)$$

where  $E_{ox}$  and  $E_{red}$  represent the oxidation and reduction potentials of the electron donor and acceptor,  $\Delta E_{00}$  is the transition energy for fluorescence or phosphorescence, respectively, and  $w_P$  is the work term for charge separation.

Hence, photobleaching is interpreted as single-electron-transfer (SET) to an oxygen molecule, which has a reduction potential of -0.57 V vs SCE [66]. This would explain the favourable effect of reducing agents which often also act as triplet quenchers [67]. According to Marcus theory the reaction between the excited singlet state and oxygen is accelerated compared to the triplet reaction due to the larger potential difference [68]. Moreover, the given interpretation would also support a higher photostability for red shifted fluorophores due to the smaller energy gap. The rate constant for bleaching reactions with oxygen is  $1.4 \cdot 10^8 \text{ M}^{-1}\text{s}^{-1}$  [41]; combined with an oxygen concentration of about 0.3 mmol in water, the reaction rate is  $4.2 \cdot 10^4 \text{ s}^{-1}$ . The product of this effective bleaching rate with the lifetime of Fluoresceine **1**

3.1 *ChemPhysChem* **2008**, 9, 2019-2027

represents the quantum yield for bleaching out of the excited singlet state  $\Phi_{bl} = 1.6 \cdot 10^{-4}$ . This is in the common order of magnitude for bleaching processes of Fluoresceine. Therefore, bleaching out of the singlet state is important, although  $\tau_{fl}$  is much shorter than  $\tau_T$ , as long as the excitation rate is high enough. In contrast to ensemble experiments, which operate at low excitation intensities, our measurements take place at high intensities, so that bleaching out of the singlet state becomes more dominant. Moreover, in single-molecule experiments the concentration of the dyes which might act as triplet sensibilisators is very small (~nM range). Therefore, the amount of generated  $^1O_2$  is negligible in contrast to ensemble experiments with at least 1000 times higher sensibilisator concentrations.

### **Conclusion**

We investigated the capabilities of FCS study photobleaching of fluorescent dyes. By using a carefully modified setup and correction for saturation, changes in diffusion time are exclusively traced back to photobleaching. Hence, a comparative analysis of photostability of structurally similar fluorescent dyes is possible. Although only relative values are obtained, we conclude that BODIPY dyes are more photostable than Fluoresceine dyes. Furthermore, photobleaching seems to originate out of the excited singlet state, opposite to previous results. We explain the bleaching by a single electron oxidation by molecular oxygen.

In order to quantify our conclusions, the approximation in the treatment of the diffusion has to be analysed. Brownian motion simulations are currently performed.

### **Acknowledgements**

This work was supported by the German Science Foundation (DFG, JU 650/1-1).

We also thank Anna Jacob for help with the HPTS measurements (see S.I.).

### **References**

- [1] P. James, C. Hennessy, T. Berge, R. Jones, *J. Cell. Sci.*, **2004**, 117, 6485.
- [2] M. Leake, J. Chandler, G. Wadhams, F. Bai, R. Berry, J. Armitage, *Nature*, **2006**, 443, 355 .

This is a pre-peer reviewed version of the following article: *ChemPhysChem*, 2008, 9, 2019-2027; DOI: 10.1002/cphc.200800299; Reproduced by permission of the *ChemPhysChem* owner societies;

- [3] M. Sotomayor, K. Schulten, *Science*, **2007**, 316, 1144.
- [4] J. Yu, J. Xiao, X. Ren, K. Lao, S. Xie, *Science*, **2006**, 311, 1600.
- [5] X. Xie, J. Yu, W. Yang, *Science*, **2006**, 312, 228.
- [6] R. Deidel, C. Dekker, *Curr. Op. Struc. Biol.*, **2007**, 80.
- [7] E. Van Craenenbroeck, Y. Engelborghs, *Biochemistry*, **1999**, 38, 5082.
- [8] J. Politz, E. Browne, D. Wolf, T. Pederson, *Proc. Nat. Acad. Soc.*, **1998**, 95, 6043.
- [9] T. Schmidt, G. Schütz, W. Baumgartner, H. Gruber, H. Schindler, *Proc. Nat. Acad. Soc.*, **1996**, 93, 2926.
- [10] G. Harms, L. Cognet, P. Lommerse, G. Blab, H. Kahr, R. Gamsjäger, H. Spaink, N. Soldatov, C. Romanin, T. Schmidt, *Biophys. J.*, **2001**, 81, 2639.
- [11] G. Jung, J. Wiehler, W. Göhde, J. Tittel, T. Basché, B. Steipe, C. Bräuchle, *Bioimaging*, **1998**, 6, 54.
- [12] J. Schüler, J. Frank, U. Trier, M. Schäfer-Korting M., W. Saenger, *Biochemistry*, **1999**, 38, 8402.
- [13] K. Häsler, O. Pänke, W. Junge, *Biochemistry*, **1999**, 38, 13759.
- [14] P. Schwille, F. Oehlenschläger, N. Walter, *Biochemistry*, **1996**, 35, 10182.
- [15] U. Kettling, A. Koltermann, P. Schwille, M. Eigen, *Proc. Nat. Acad. Soc.*, **1998**, 95, 1416.
- [16] A. Koltermann, U. Kettling, J. Bieschke, T. Winkler, M. Eigen, *Proc. Nat. Acad. Soc.*, **1998**, 95, 1421.
- [17] S. Hess, S. Huang, A. Heikal, W. W. Webb, *Biochemistry*, **2002**, 41, 697.
- [18] J. Enderlein, I. Gregor, D. Patra, T. Dertinger, U. Kaupp, *ChemPhysChem.*, **2005**, 6, 2324.
- [19] R. Zondervan, F. Kulzer, M. Kol'chenko, M. Orrit, *J. Phys. Chem. A*, **2004**, 108, 1657.
- [20] C. Carbonaro, A. Anedda, S. Grandi, A. Magistris, *J. Phys. Chem. B*, **2006**, 110, 12932.
- [21] C. Eggeling, A. Volkmer, C. Seidel, *ChemPhysChem*. **2005**, 6, 791.

3.1 *ChemPhysChem* **2008**, *9*, 2019-2027

- [22] C. Jung, B. Müller, D. Lamb, F. Nolde, K. Müllen, C. Bräuchle, *J. Am. Chem. Soc.*, **2006**, *128*, 5283.
- [23] C. Eggeling, J. Widengren, R. Rigler, C. Seidel, *Anal. Chem.*, **1998**, *70*, 2651.
- [24] A. Toutchkine, D. Nguyen, K. Hahn, *Org. Lett.*, **2007**, *9*, 2775.
- [25] K. Kang, W. Sisk, M. Raja, F. Farahi, *Photochem. Photobiol. A*, **1999**, *121*, 133.
- [26] J. Schuster, F. Cichos, C. von Borczyskowski, *Optics and Spectroscopy*, **2005**, *98*, 712
- [27] J. Widengren, R. Rigler, *Bioimaging* , **1996**, *4*, 149.
- [28] M. Kinjo, R. Rigler, *Nucl. Ac. Res.*, **1995**, *23*, 1795.
- [29] D. Magde, E. Elson, W. W. Webb, *Phys. Rev. Lett.*, **1972**, 705.
- [30] D. Magde, W. W. Webb, E. Elson, *Biopolymers*, **1974**, *17*, 6512.
- [31] J. Dix, E. Hom, A. Verkman, *J. Phys. B*, **2006**, *110*, 1896.
- [32] H. Qian, *Biophys. Chem.*, **1990**, *38*, 49.
- [33] T. Wohland, R. Rigler, H. Vogel, *Biophys. J.*, **2001**, *80*, 2987.
- [34] S. Hess, W. W. Webb, *Biophys. J.*, **2002**, *83*, 2300.
- [35] D. Koppel, *Phys. Rev. A*, **1974**, *10*, 1938.
- [36] G. Donnert, C. Eggeling, S. Hell, *Nature Methods*, **2007**, *4*, 81.
- [37] J. Bieschke, P. Schwille, *Fluorescence Microscopy and Fluorescent Probes (J. Slavik, Ed.)*, Vol 2, Plenum Press, New York **1988**.
- [38] J. Enderlein, I. Gregor, D. Patra, J. Fitter, *Curr. Pharm. Biotech.*, **2004**, 155.
- [39] J. Widengren, Ü. Mets, R. Rigler, *J. Phys. Chem.*, **1995**, *99*, 13368.
- [40] M. Talhavini, W. Corradini, T. Atvars, *J. Photochem. Photobiol. A*, **2001**, *139*, 187.
- [41] L. Song, C. Varma, J. Verhoeven, H. Tanke, *Biophys. J.*, **1996**, *70*, 2959.

This is a pre-peer reviewed version of the following article: *ChemPhysChem*,2008, *9*, 2019-2027;  
DOI: 10.1002/cphc.200800299; Reproduced by permission of the *ChemPhysChem* owner societies;

- [42] B. Renikuntla, H. Rose, J. Eldo, A. Waggoner, B. Armitage., *Org. Lett.*, **2004**, 6, 909.
- [43] W. Sun, K. Gee, R. Haughland, *Bioorg. Med. Chem. Lett.*, **1998**, 8, 3107.
- [44] V. Buschmann, K. Weston, M. Sauer, *Bioconj. Chem.*, **2003**, 14, 195.
- [45] J. Widengren, A. Chmyrov, C. Eggeling, P. Löfdahl, C. Seidel, *J. Phys. Chem. A*, **2007**, 111, 429.
- [46] P. Dittrich, P. Schwille, *Appl. Phys. B*, **2001**, 73, 829.
- [47] A. Gaigalas, L. Wang, R. Vogt, *Photochem. Photobiol.*, **2002**, 76, 22.
- [48] a) R. Hermes, T. Allik, S. Chendra, J. Hutchinson, *Appl. Phys. Lett.*, **1993**, 63, 877 b) A. Costela, I. Garcia-Moreno, J. Barroso, R. Sastre, *Appl. Phys. B*, **2000**, 70, 367.
- [49] W. Sisk, N. Ono, T. Yano, M. Wada, *Dyes and Pigments*, **2002**, 55, 143.
- [50] M. Ahmad, T. King, D. Ko, B. Cha, J. Lee, *Opt. Comm.*, **2002**, 203, 327.
- [51] B. Wittmershaus, J. Skibicki, J. McLafferty, Y. Zhang, S. Swan, *J. Fluor.*, **2001**, 11, 119.
- [52] J. Chen, A. Burghart, C. Wan, L. Tahj, C. Ortiz, J. Reibenspies, K. Burgess, *Tetrahedron Letters*, **2000**, 41, 2303.
- [53] A. Burghart, H. Kim, M. Welch, L. Thoresen, J. Reibenspies, K. Burgess, *J. Org. Chem.*, **1999**, 64, 7813.
- [54] R. Rigler, Ü. Mets, J. Widengren, P. Kask, *Eur. Biophys. J.*, **1993**, 22, 169.
- [55] D. McClure, *J. Chem. Phys.*, **1949**, 17, 905.
- [56] W. Sun, K. Gee, R. Haughland, *Bioorg. Med. Chem. Lett.*, **1998**, 8, 3107.
- [57] G. Lewis, M. Calvin, *Chem. Rev.*, **1939**, 273.
- [58] O. Stern, M. Volmer, *Physikalische Zeitschrift*, **1919**, 183.

This is a pre-peer reviewed version of the following article: *ChemPhysChem*, 2008, 9, 2019-2027;  
DOI: 10.1002/cphc.200800299; Reproduced by permission of the *ChemPhysChem* owner societies;

3.1 *ChemPhysChem* **2008**, *9*, 2019-2027

- [59] J. R. Lakowicz, *Principles of Fluorescence Spectroscopy*, 2nd ed, **1999**, Kluwer Academic/Premium Press, New York.
- [60] W. Moerner, *J. Lum.*, **1994**, *60&61*, 997.
- [61] E. van Dijk, J. Hernando, J. Garcia-Lopez, M. Garcia-Parajo, N. Van Hulst, *Phys. Rev. Lett.*, **2005**, *94*, 078302.
- [62] L. Song, E. Hennink, T. Young, H. Tanke, *Biophys. J.*, **1995**, *68*, 2588.
- [63] S. Strickler, R. Berg, *J. Chem. Phys.*, **1962**, *37*, 814.
- [64] Y. Urano, M. Kamiya, K. Kanda, T. Ueno, K. Hirose, T. Nagano, *J. Am. Chem. Soc.*, **2005**, *127*, 2888.
- [65] Y. Gabe, Y. Urano, K. Kikuchi, H. Kojima, T. Nagano, *J. Am. Chem. Soc.*, **2004**, *126*, 3357.
- [66] Hollemann, Wiberg, *Lehrbuch der Anorganischen Chemie*, 101 ed, New York **1995**.
- [67] J. Vogelsang, R. Kaspar, C. Steinhauer, B. Person, M. Heilemann, M. Sauer, P. Tinnefeld, *Angew. Chem.*, in press
- [68] R. Marcus, *J. Chem. Phys.*, **1956**, *24*, 966.

### **Captions**

#### Scheme 1

Structures of the four used BODIPY dyes

#### Scheme 2

Structures of the four used Fluoresceines

#### Table 1

Fluorescent properties (maximum wavelength of absorption  $\lambda_{\text{abs}}$  and emission  $\lambda_{\text{em}}$ , fluorescence lifetime  $\tau_{\text{fl}}$ , intersystem crossing  $k_{23}$  and triplet decay rate  $k_{31}$  as well as absorption cross section  $\sigma$ ) of all used fluorescent dyes.  $k_{23}$  was calculated according to Equations (1) and (2),  $k_{31}$  was extracted as global fitting parameter out of the FCS measurements by use of Equation (1). Fluoresceine dyes were measured in pH 10 buffer solution, BODIPY dyes in water.

Figure 1

FCS data of BODIPY **2**, **3** and Fluoresceine **3**.

- a) BODIPY **2**: with increasing intensity, the diffusion time shifts to shorter values with a concomitant slight rise of the triplet population.
- b) BODIPY **3**: increasing the excitation intensity results in a high triplet population, but no change in diffusion behaviour can be observed.
- c) Fluoresceine **3**: increase of the excitation intensity affects both a high triplet population and a decrease in diffusion time.

Figure 2

Diffusion times  $\tau_{\text{diff}}(I)$  at different excitation intensities  $I$  for BODIPY **2** (black dots), **3** (dark grey triangles) and Fluoresceine **3** (light grey squares).

Figure 3

- a) Stern-Volmer analogue parameter  $\tau_{\text{diff}}(0)/\tau_{\text{diff}}(I)$  versus intensity  $I$ . At high intensities the values of BODIPY **2** (black dots) and Fluoresceine **3** (light grey squares) level off while BODIPY **3** (dark grey triangles) remains nearly constant within an error of 7%.
- b) Stern-Volmer analogue parameter  $\tau_{\text{diff}}(0)/\tau_{\text{diff}}(I)$  versus the experimental contrast  $C$  instead of the intensity  $I$ . According to Equation (10), the y-axis intercept equals 1. The value of the derivatives goes linear with the amount of photobleaching. BODIPY **3** (dark grey triangles) is photostable, Fluoresceine **3** (light grey squares) shows slight degradation in diffusion times and BODIPY **2** (black dots) bleaches obviously.

Figure 4

Dependence of the contrast on excitation intensity according to Equation (16). A linear relation is obtained meaning the stronger the rise the lower the triplet fraction. This plot results from the FCS data denoting that BODIPY **2** (black dots) has the least triplet population, followed by BODIPY **3** (dark grey triangles) and Fluoresceine **3**.

Figure 5

Correlation between the triplet population and the magnitude of photobleaching. This plot is the visualisation of Equation (17). The lower the value on the x axis the higher is the triplet population. Vice versa, a higher value on the x axis results out of a higher singlet population with stronger rise in the slope of Figure (5). Furthermore the lower the ordinate value the less the change of diffusion time which is associated with a higher photostability, respectively the higher the ordinate value the more photobleaching occurs.

This means that the Fluoresceines (black dots) exhibit low photobleaching but a high triplet population which limits the number of photocycles.

The BODIPY dyes (grey triangles) behave more sophisticatedly. **3** and **4** exhibit a similar photobleaching rate like the Fluoresceines with a lower population of the bottleneck state. BODIPY **1** and **2** perform more photocycles which enables photobleaching during the transit through the detection volume.

Table 1

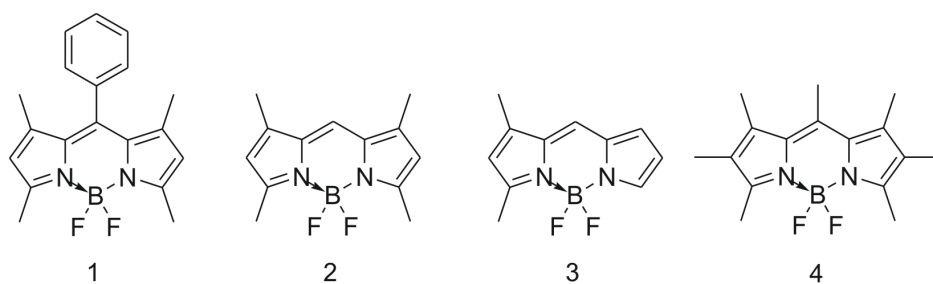
| BODIPY         | $\lambda_{\text{abs}}$ / nm | $\lambda_{\text{em}}$ / nm | $\tau_{\text{fl}}$ / ns<br>(+/- 0.1 ns) | $k_{23}/10^6 \text{ s}^{-1}$<br>(+/-30%) | $k_{31}/10^5 \text{ s}^{-1}$<br>(+/-10%) | $\sigma$ (488nm) / $10^{-16} \text{ cm}^2$ |
|----------------|-----------------------------|----------------------------|---|--|--|--|
| <b>1</b>       | 496                         | 506                        | 3.6                                     | 0.84                                     | 7.04                                     | 2.39                                       |
| <b>2</b>       | 500                         | 506                        | 5.7                                     | 0.86                                     | 7.50                                     | 2.62                                       |
| <b>3</b>       | 491                         | 502                        | 6.0                                     | 3.97                                     | 6.09                                     | 2.25                                       |
| <b>4</b>       | 494                         | 519                        | 5.8                                     | 3.52                                     | 6.75                                     | 3.28                                       |
| Fluoresceine   | $\lambda_{\text{abs}}$ / nm | $\lambda_{\text{em}}$ / nm | $\tau_{\text{fl}}$ / ns<br>(+/- 0.1 ns) | $k_{23}/10^6 \text{ s}^{-1}$<br>(+/-30%) | $k_{31}/10^5 \text{ s}^{-1}$<br>(+/-10%) | $\sigma$ / $10^{-16} \text{ cm}^2$         |
| <b>1(FL)</b>   | 490                         | 514                        | 3.9                                     | 3.74                                     | 6.30                                     | 3.78                                       |
| <b>2(ITC)</b>  | 494                         | 519                        | 3.8                                     | 8.06                                     | 6.71                                     | 2.60                                       |
| <b>3(OG)</b>   | 492                         | 517                        | 4.0                                     | 2.70                                     | 4.24                                     | 2.90                                       |
| <b>4(FL27)</b> | 502                         | 523                        | 3.5                                     | 5.32                                     | 6.16                                     | 2.56                                       |

### **Text for table of contents**

#### Fluorescence Correlation Spectroscopy and Photostability

The diffusion time in FCS measurements decreases with increasing intensity. This is analysed similar to the Stern-Volmer treatment of fluorescence quenching. It turns out that BODIPY dyes are more photostable than Fluoresceines. Photobleaching originates out of the excited singlet state via one electron oxidation by molecular oxygen.

Scheme 1)



Scheme 2)

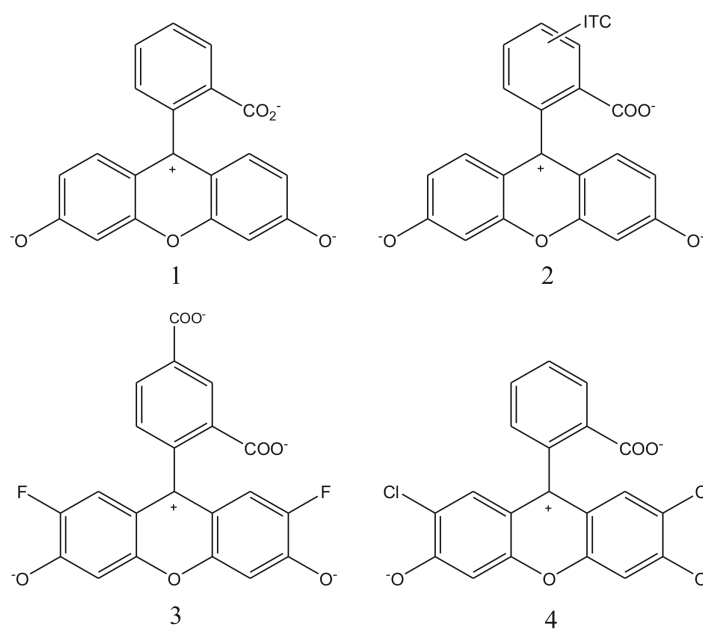


Figure 1a)

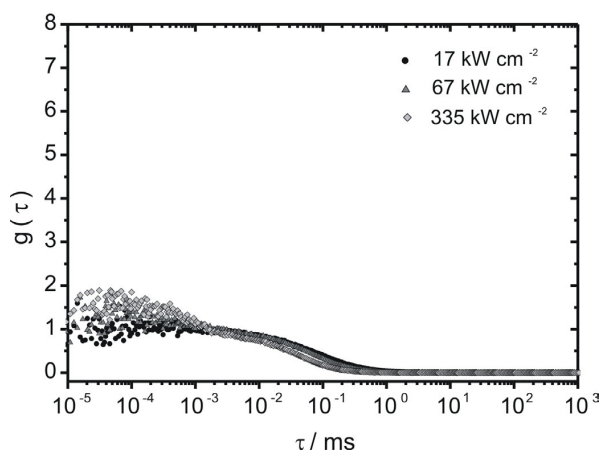


Figure 1b)

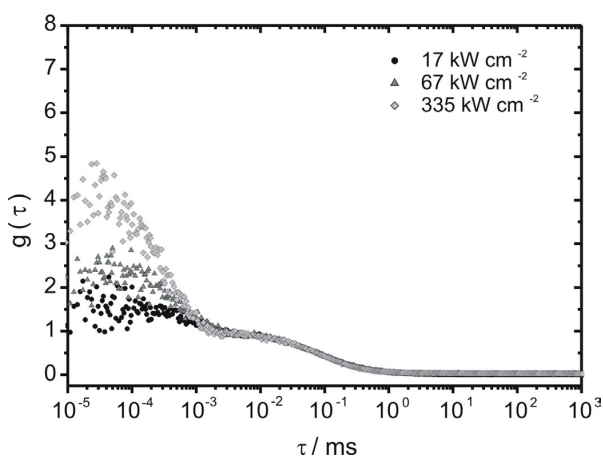


Figure 1c)

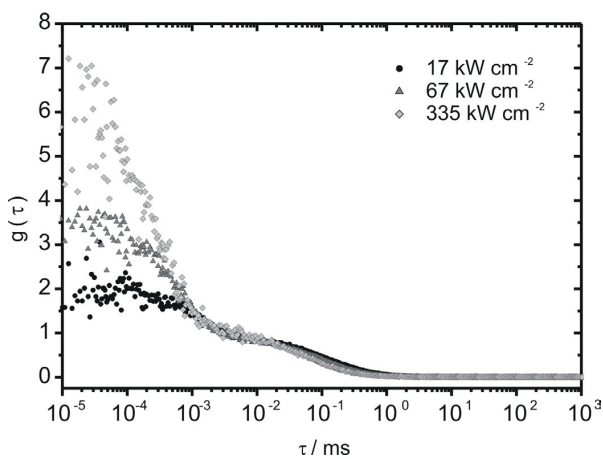


Figure 2)

Figure 3a)

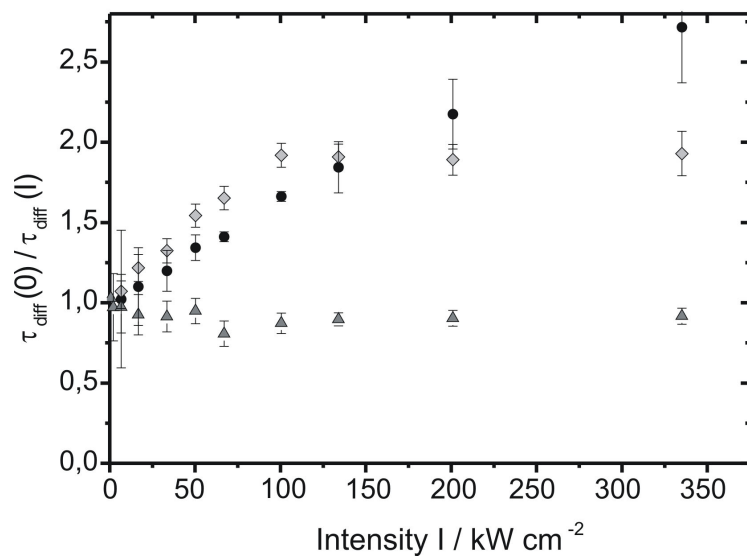


Figure 3b)

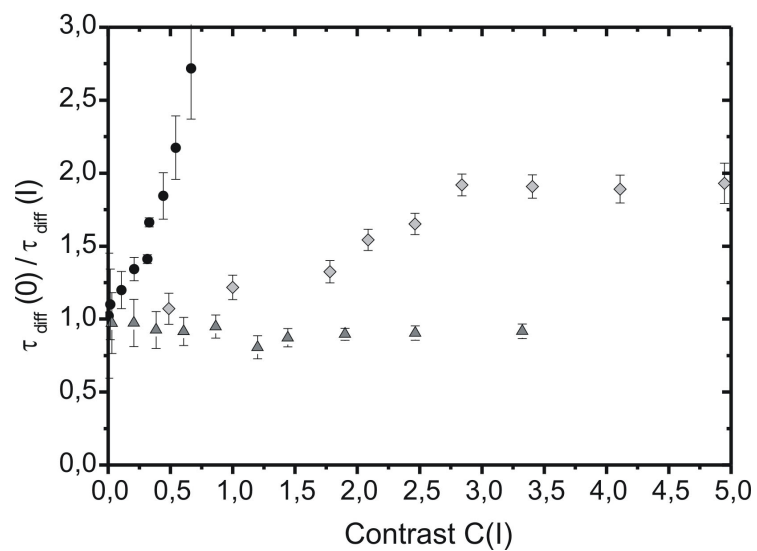


Figure 4)

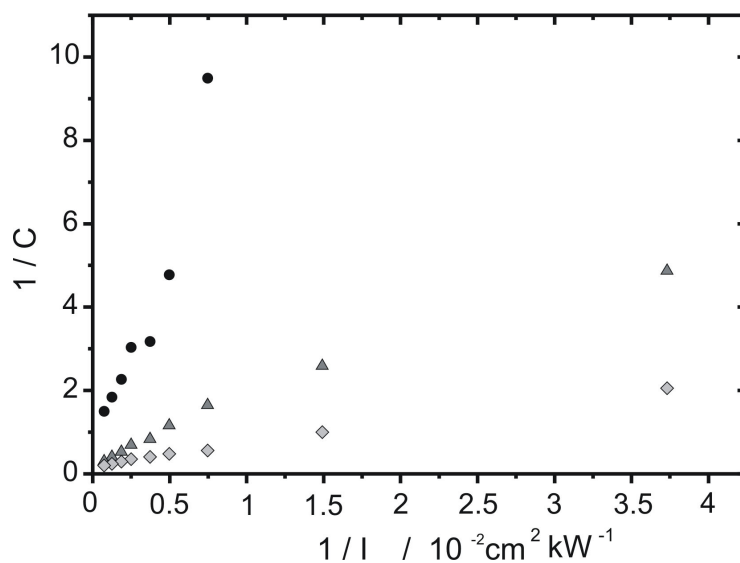
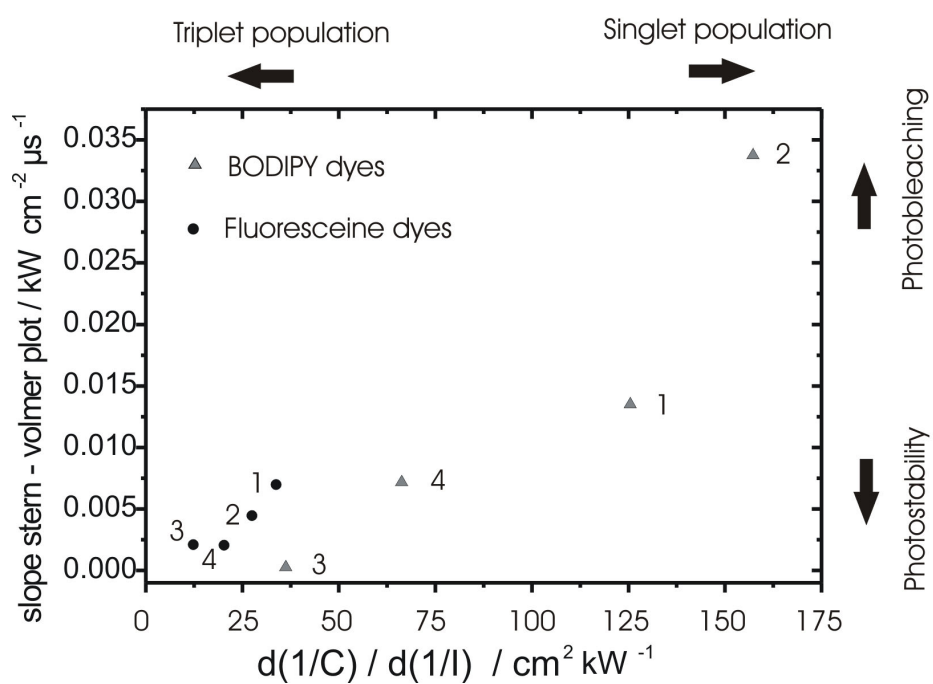


Figure 5)



**Supporting information (1) to Comparative photostability studies of BODIPY and Fluorescein dyes by Fluorescence Correlation Spectroscopy by B. Hinkeldey et al.****Minimizing optical artefacts in FCS**

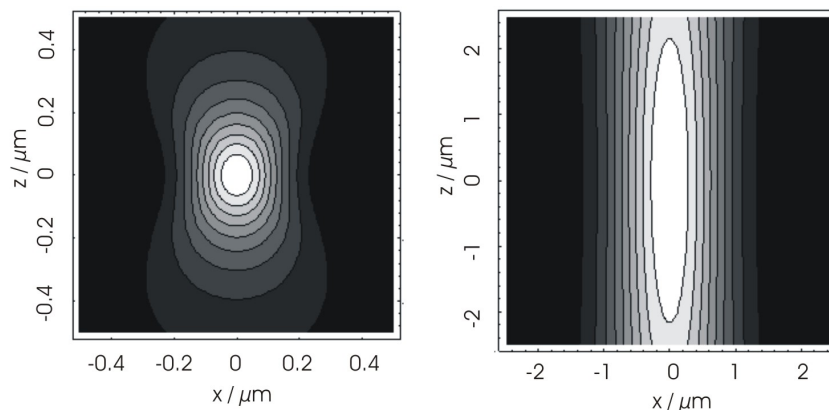
FCS is a valuable method for gaining information about several parameters, such as the ISC rate constant  $k_{23}$ , the depopulation rate of the triplet state  $k_{31}$  and moreover the so-called diffusion time  $\tau_{\text{diff}}$  (l). The latter is the key parameter in the analysis of photobleaching by FCS. It describes the time which a molecule spends in the detection volume. As a molecule can only be seen in FCS measurements while it is fluorescing, the diffusion time also corresponds to the time a molecule spends in the detection area until it becomes non fluorescing, i.e. photobleached. The higher the excitation intensity the earlier molecules are photobleached. That means that photobleaching should occur as a decrease of diffusion time upon increasing excitation power.

But before we can obtain reliable results, we have to exclude optical artefacts in our setup in order to ensure that the decrease in diffusion time only originates from photobleaching. Four main problems were identified [38,34]: varying cover slide thickness, astigmatism of the laser beam, out-of-focus contribution at high intensities and refractive index mismatch.

As we verified a circular laser beam profile, which is not distorted by passing any lenses or other optical devices before being directed into the microscope objective (without beam extension), astigmatism of the entering laser beam is minimized. Also the second point is avoided by the use of thickness corrected cover slides.

Operating with a relatively large diameter of the laser beam results in an overfilled objective, which leads to a waisted form of the focus and an increased optical resolution (Scheme SI1) [34].

3.1 *ChemPhysChem* 2008, 9, 2019-2027



Scheme S11: Calculated intensity profiles of the focus resulting from a large laser beam diameter (left) and from a small laser beam diameter (right) in lateral (x) and axial (z) direction

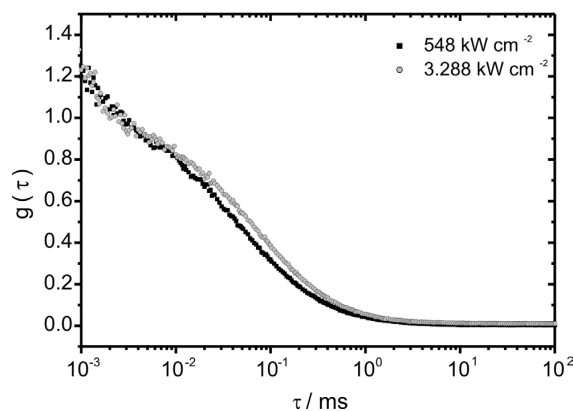
This tailored shape, however, is detrimental to the performance of FCS for investigating photobleaching. At high intensities saturation in the centre of the focus occurs, so that the fluorescence of peripheral regions, especially in axial direction, contributes to the detected autocorrelation signal to a greater extent; this leads to a broadened detection profile. This means that the detection volume appears magnified resulting in an apparent higher diffusion time.

FCS measurements of BODIPY **3** are shown in Figure (S11) under different optical conditions. We will show later that BODIPY **3** hardly undergoes any photobleaching and is therefore an ideal candidate to monitor optical artefacts. A laser beam is magnified to a diameter of 4 mm. The apparent diffusion time increases about 25% from 44  $\mu\text{s}$  at 548  $\text{kW}/\text{cm}^2$  up to 59  $\mu\text{s}$  at 3.288  $\text{kW}/\text{cm}^2$  due to the described saturation effect. At higher intensities the maximal factor even goes up to 29%. This means that due to a too large beam diameter the obtained diffusion times at different excitation intensities correspond to different focal geometries and are therefore no longer comparable with each other.

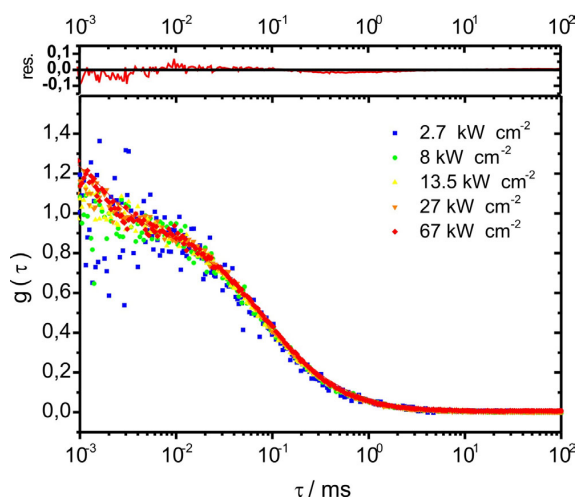
In order to circumvent this geometric problem, we decided to abandon the high optical resolution and reduced the beam diameter to 0.7 mm, i.e. the output of the laser on the backside aperture of the objective. The use of a smaller beam diameter leads to a less waisted, nearly cylindrical focus (Scheme S11)[34]; therefore broadening of the focus at higher intensities should be less distinct.

Figure S11)

FCS data of BODIPY 3 at different excitation intensities



- 1) Measurements using a large beam diameter of 4 mm at low (black dots) and high (grey triangles) intensities. The high excitation intensities result out of the strongly focussed laserbeam.



- 2) Measurement at five different intensities (blue, green, yellow, orange, red; increasing from blue to red) with a laser beam diameter of 0.7 mm.

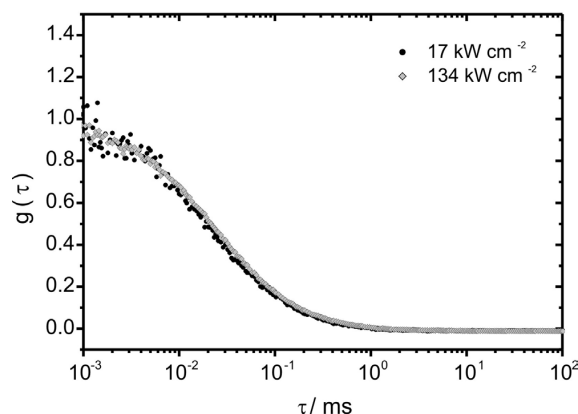
3) Measurements in acetonitrile ( $n_o = 1.34$ )

Figure (SI1 b) shows FCS data of BODIPY 3 using this small beam diameter. Even at  $335 \text{ kW cm}^{-2}$  there is no change in diffusion time. Although the optical resolution should be considerably lower than in the previous case (Fig. (SI1a)) and thus,  $\tau_{\text{diff}}$  should be higher,  $\tau_{\text{diff}}$  is hardly affected and varies only about 7% around  $70 \mu\text{s}$ . This variation lies in the range of the typical statistical error and indicates, that strong saturation effects like those displayed in Figure (SI1a) are minimized. Therefore, a beam diameter of  $0.7 \text{ mm}$  is sufficiently small to establish an intensity independent shape of the detection volume. Moreover, showing at every intensity the same diffusion time ( $\sim 70 \mu\text{s}$ ) means that the molecules always need the same time to get through the focus. If there is no shortening of the diffusion time, then this property indicates that BODIPY 3 hardly undergoes photobleaching under these conditions.

The last error source lies in refractive index mismatch between the objective and the solvent. Figure (SI1b) verifies already the careful optical design. However, we performed a control with a small difference in refractive index. If the used solvent's refraction index differs from the correction parameter of the objective, this mismatch again leads to unreliable results in FCS. Figure (SI1c) shows data of BODIPY 3 in acetonitrile ( $n = 1.34$ ) measured with the water immersion objective. Comparison with the data in Figure (SI1b) reveals that the increase of the diffusion time arises out of the mismatch between the immersion liquid and the solvent.

**Supporting information (2) to Comparative photostability studies of BODIPY and Fluorescein dyes by Fluorescence Correlation Spectroscopy by B. Hinkeldey et al.**

**Photobleaching of 1-Hydroxypyren-3,6,8-trisulfonate (HPTS, Pyranine), investigated by means of Fluorescence correlation spectroscopy**

**Experimental:**

In the beginning, we investigated the photophysics and photostability of 1-Hydroxypyren-3,6,8-trisulfonate (HPTS) at pH 10. HPTS is a well known photoacid with a  $pK_A$ -value  $\sim 7.5$  which exhibits green fluorescence ( $\lambda_{\text{max}} = 510 \text{ nm}$ ) above pH 3 [S1]. The strong basic condition was chosen since at this pH-value only the anionic, deprotonated chromophore is stable and its protonation is not detectable by FCS [S2]. Excitation was performed by  $\lambda_{\text{exc}} = 457 \text{ nm}$  of an Ar-ion laser. After guiding the laser through a single-mode fiber, the beam was outcoupled by a 10x objective or a 50x objective finally yielding beam diameters of 4 mm and 0.8 mm, respectively. These two conditions are termed in the following large (= 4 mm) and small (= 0.8 mm) beam diameter. Except from the altered excitation wavelength, the same setup, which is described in the experimental section of the main manuscript, was used for the experiments. FCS traces were recorded for different excitation intensities (see Fig. (SI2)). Due to the low photostability and despite the high fluorescence quantum yield of HPTS, a measurement time up to two hours for one trace was required.

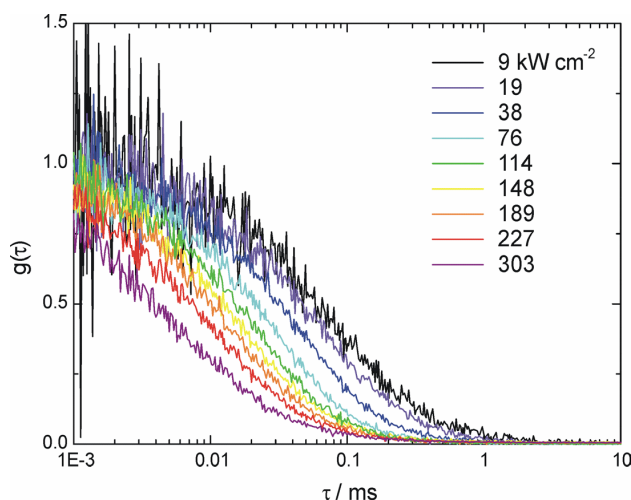


Figure SI2: FCS traces of HPTS at pH 10. The depicted curves were recorded with the small beam diameter

**Analysis of the FCS data:**

FCS traces were fitted using eq. (1) of the main manuscript. Where possible, we renounced the terms implying triplet kinetics although its inclusion considerably improved the fits. We partially trace this improvement back to an overlap of the triplet dynamics and photobleaching dynamics which both occur on a similar time scale at high intensities. It is also obvious that an additional exponential decay would also minimize the deviations between a two-dimensional diffusion model for fitting and the actual convolution of diffusion and photobleaching in the experiment. Figure (SI3) shows a plot of the computed diffusional time  $\tau_{\text{diff}}$  versus the applied excitation intensity for both laser beam diameters.

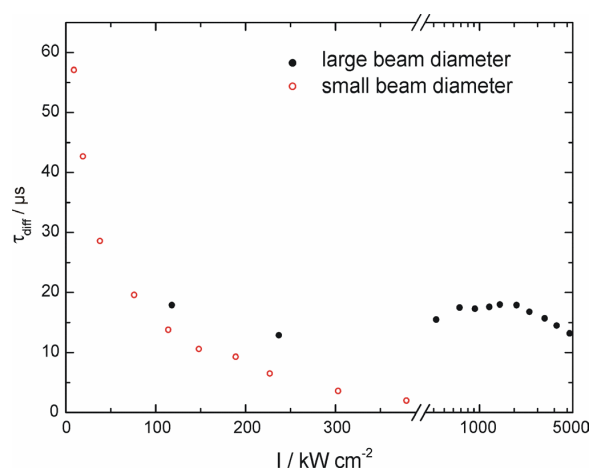


Fig. SI3: The intensity dependent diffusional time for both laser diameters.

Whereas  $\tau_{\text{diff}}$  exhibits a distinct, almost hyperbolic decrease for the small beam diameter, the large beam diameter generated FCS-curves with an almost constant  $\tau_{\text{diff}}$ . Two reasons can be found for this unexpected behaviour of a highly photolabile dye, i.e. saturation broadening described in ref. S3, and the above mentioned fit improvements where a noticeable triplet population is detected. We were not able to unambiguously separate the photobleaching and the triplet dynamics.

We further analysed the data for the small beam diameter according to the Stern-Volmer like approach described in the main manuscript (Fig. (SI4)). For HPTS,  $\tau_0$  was set to 58  $\mu\text{s}$ .

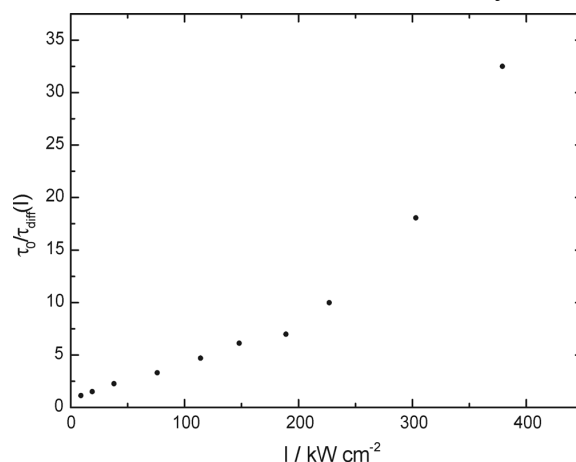
Fig. S14: Stern-Volmer like plot of  $\tau_{\text{diff}}$ .

Figure (S14) shows a linear increase of the disappearance rate constant  $k_{\text{diss}}$  up to an intensity of  $\sim 200 \text{ kW cm}^{-2}$ . This is in agreement with the proposed model in the main manuscript for low intensities. In contrast to the photobleaching in Fluorescein or BODIPY dyes, the photobleaching does not saturate but apparently increases in a nonlinear way at high intensities. This might be an indication of dominant photobleaching out of the triplet state.

#### Comparison with the model of ref. S3:

As BODIPY **3** is an excellent compound to test the excellent reliability of our setup, HPTS is a prototype dye for comparing different analytical models for photobleaching. It was reported several times that the convolution of photobleaching and diffusion cannot be described by an analytical expression. Most successfully, so far, is the model of Eggeling et al. [S3]. In this model, the whole population of molecules is formally split into two fractions. Fraction *A*, which is according to the reference  $\sim 0.75$  to  $0.8$ , is the population which undergoes photobleaching with some effective photobleaching rate constant  $k_{z,\text{av}}$  whereas the rest,  $1-A$ , is the photostable fraction with an unaltered  $\tau_{\text{diff}}$ . We applied this model to our curves where the triplet population term in the fitting function is obsolete (Fig. (S15)).

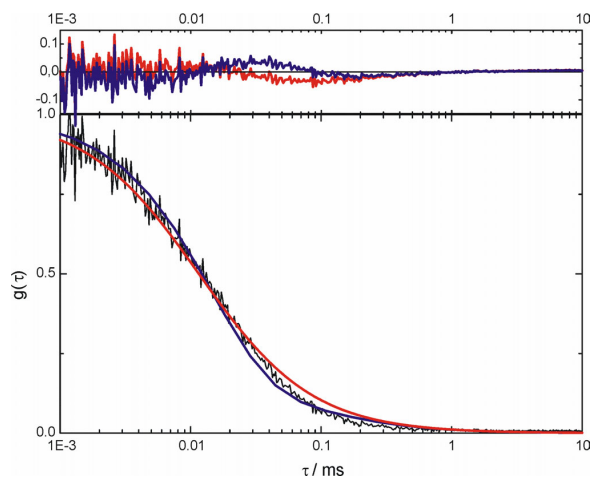


Fig. SI5: Analysis of the FCS trace, recorded with  $148 \text{ kW cm}^{-2}$ , with our Stern-Volmer-like model (red trace) and the model of Eggeling et al. (blue curve). In the upper plot, the fit residuals are plotted for both models.

Our model which is developed in the main manuscript requires only one fit parameter for these curves which is  $\tau_{\text{diff}}$ . Of course, the simplifications of our model cannot fully cover photobleaching. The fit residuals indicate that our model hardly describes  $g(\tau)$  at longer times. Nevertheless, plot of  $\tau_{\text{diff}}$  vs.  $I$  reveals a linear dependence (Fig. (SI4)).

The model of Eggeling et al. is based on three fit parameters, i.e.  $\tau_0$ ,  $k_{z,\text{av}}$  and  $A$ . Boundary conditions, however, set limits to the parameter space.  $A$  should be close to the theoretical value of 0.8, although under our experimental conditions, this value might be different. We investigated both cases.  $\tau_0$  should be constant among all FCS curves and therefore close to the value of  $58 \mu\text{s}$ . Only  $k_{z,\text{av}}$  should vary with the excitation intensity. The blue curve in Figure (SI5) is a fit with  $k_{z,\text{av}} = 55 \text{ ms}^{-1}$ .

In none of the investigated curves of HPTS, the fit was improved with respect to our simple model although more degrees of freedom were at disposal. We identified in simulations that the presence of a photostable fraction,  $1-A$ , enforces an additional decay of  $g(\tau)$  at long correlation times. The deviation between fit and experimental curve were even more pronounced at higher intensities than depicted in Figure (SI5). We conclude that the model of Eggeling et al. fails under conditions of very strong photobleaching. Therefore, we continued with our own model.

[S1] see e.g. N. Agmon, J. Phys. Chem. A, 2005, 109, 13

[S2] J. Widengren, B. Terry, R. Rigler, Chem. Phys, 1999, 249, 259

[S3] C. Eggeling, J. Widengren, R. Rigler, C.A.M. Seidel, Anal. Chem, 1998, 70, 2651

**Synthesis of the core compound of the BODIPY dye class: 4,4-Difluoro-4-bora-(3a,4a)-diazas-indacene**

*Alexander Schmitt,<sup>a</sup> Babette Hinkeldey<sup>a</sup>, Mandy Wild<sup>a</sup> and Gregor Jung<sup>a</sup>*

a: Biophysical Chemistry, Saarland University, D-66123 Saarbrücken, Germany

**Keywords:** Bodipy, fluorescence spectroscopy, fluorescent probes, single molecule studies

**Abstract:** We report the synthesis and characterization of the missing reference core compound 4,4-Difluoro-4-bora-(3a,4a)-diazas-indacene **1** of the BODIPY fluorescent dye class. The compound exhibits a fluorescence lifetime of 7.2ns and has a high photostability.

### 3.2 *J. Fluoresc.* **2009**, 19, 755-758

The development of emissive dyes for applications in personal diagnostics and organic fluorescent devices is steadily growing in recent years. The BODIPY (BORon-DIPYrromethene) dye class earned increasing interest in biomedical and bioanalytical applications in the last two decades. The first synthesis of a BODIPY dye was accidentally achieved in 1968 by Treibs and Kreuzer<sup>[1]</sup>. BODIPY dyes are nowadays used as active media in dye lasers<sup>[2-6]</sup> due to their high extinction coefficients, high fluorescence quantum yields, high photostability and a convenient excitation with Ar- ion Lasers (~500nm). Owing to these fluorescence properties, various BODIPY dyes are also commercially available for protein labelling, modification of nucleotides and dextrans, as well as fluorescent substrates for enzymes and compounds with longwave excitation maxima<sup>[5]</sup>. Even more applications in biological systems, as fluorescent switches<sup>[7]</sup> or as system for light harvesting<sup>[8]</sup>, photodynamic therapy<sup>[9]</sup> or sensor molecule<sup>[10]</sup> are reported. Several reviews were recently published summarizing most of the actual knowledge about BODIPY dyes<sup>[11, 12]</sup>. As the name of the dye class suggests, the BODIPY chromophore is composed of two units of pyrrole which are connected by a methene bridge in the 2-position and a boron atom which is coordinated by the heteroatoms. The frame of carbon atoms of the molecule is planar and due to the heteroatoms slightly polarized, which provides nucleophilic and electrophilic reaction sites at different positions of the molecule. These reaction sites enable substitutions directly on the carbon frame of the BODIPY chromophore and were made responsible for the low stability of the core compound described here in this work<sup>[12]</sup>. Hence, the synthesis of the core compound of the BODIPY dye class, the 4,4-Difluoro-4-bora-(3a,4a)-diazas-indacene **1**, has not been reported yet. The synthesis of BODIPY dyes can be achieved by different reaction paths<sup>[13-16]</sup>, which are all based on pyrrole condensation with aldehydes. The differences in these paths originate from the desired symmetric or asymmetric substitution patterns of the obtained product. Our strategy here follows the asymmetric synthesis. By that we could avoid an extra oxidation step from the dipyrromethane to the dipyrromethene, which is required in the symmetric preparation routes<sup>[11, 12]</sup>. The one pot synthesis involves the trifluoroacetic acid-catalyzed direct condensation of 2-formylpyrrole **2** and 1H-pyrrole **3**. This is followed by deprotonation with diethyl-diisopropylamine and subsequent complexation of the intermediate dipyrromethene with borontrifluoroetherate (Scheme 1).

The appearance of many side products like polymers or porphyrins demanded repeated purification steps by fast filtration and column chromatography over silica gel and aluminum oxide. The yield of the product was low (<10%). In addition, the compound is temperature-sensitive. Elevated temperatures (>50°C) lead to rapid loss of fluorescence which we trace

This is a pre-peer reviewed version of the following article: *J Fluoresc* (2008), 19, 755-758; DOI: 10.1007/s10895-008-0446-7; Reproduced with kind permission of Springer Science and Business Media

back to the lack of stabilizing substituents like methyl groups. However, once purified, no further condensation to porphyrins is noticed. The purified product was characterized via ESI<sup>-</sup> and ESI<sup>+</sup> (Electro Spray Ionization) mass spectroscopy. Assignment of the signals of the structure was achieved by one and two dimensional <sup>1</sup>H- and <sup>13</sup>C- NMR spectroscopy (Fig. 1a). All available data are in agreement with the proposed structure, which was verified by x-ray crystallography (Fig. 1b).

We further characterized **1** by absorption ( $\lambda_{\text{max}} = 503\text{nm}$ ) and emission ( $\lambda_{\text{max}} = 512\text{nm}$ ) spectroscopy which revealed the typical pattern for green fluorescent BODIPY dyes (Fig. 2) (Table 1), with a strong vibronic shoulder. The energy spacing between 0-0 transition and the shoulder is about  $740\text{ cm}^{-1}$ , which can be tentatively assigned to a C-H out-of-plane vibration. The fluorescence lifetime  $\tau_{\text{F1}}$  via TCSPC (Time-Correlated-Single-Photon-Counting)<sup>[17]</sup> and fluorescence quantum yield  $\Phi_{\text{F1}}$ <sup>[18]</sup> were determined (Table 1). It turned out that the fluorescence quantum yield of the fluorescent dye is even superior to other BODIPY dyes<sup>[11,12]</sup> and comparable to dyes like rhodamine or fluoresceine.

The comparison of the photophysical properties of **1** with the commercially available Borondipyromethene PM 546 (Lambdachrome Laser Dyes)<sup>[19]</sup>, allows by a rough assessment an explanation of the high fluorescence lifetime of **1**. The molar absorptivity of the latter is reported to be about  $80.000\text{ M cm}^{-1}$ <sup>[20]</sup> and its fluorescence quantum yield is about 1<sup>[20]</sup>. The oscillator strength *f* which we calculated for PM546 and compound **1** are 0.42 and 0.32, respectively. This reduction of *f* coincides with a prolongation of the radiative lifetime from 5.8 ns to 7.2 ns, for the here described compound **1**<sup>[21]</sup>.

In addition, fluorescence correlation spectroscopy was used to determine the rate constant for intersystem crossing (ISC)  $k_{23}$ .  $k_{23}$  and  $\tau_{\text{F1}}$  are used to calculate the intersystem crossing quantum yield  $\Phi_{\text{ISC}}$  ( $\Phi_{\text{ISC}} = k_{23} \cdot \tau_{\text{F1}}$ ). The calculated  $\Phi_{\text{ISC}} = 1.1\%$  for **1** is high for a dye of this structure as it is lacking heavy atoms or ketogroups. We synthesized a partially deuterated compound **1** by using perdeuterated pyrrole for comparison. No significant change of  $k_{23}$  or  $\tau_{\text{F1}}$  could be detected. This excludes overtones of C-H vibrations as accepting modes according to the energy gap law<sup>[22]</sup>. The value of the quenching rate constant  $k_{31}$ , is in agreement with an diffusion controlled quenching of the triplet state by molecular oxygen<sup>[23]</sup>. Moreover, from the FCS- experiments, the photostability as a key parameter for single- molecule experiments can be estimated by measuring the diffusional time  $\tau_{\text{D}}$ <sup>[24]</sup>.  $\tau_{\text{D}}$  is the dwell time which a molecule needs in average to pass the observation volume. Photobleaching is detected as a shortening of this time. Most remarkably, despite the distinct population of the triplet state no change of

$\tau_D$  upon increasing excitation intensity is detected. Reversely, the fact that  $\tau_D$  is not affected by higher excitation intensities, indicates that no photobleaching occurs during the residence time of the dye in the excitation area. From comparison to fluoresceine, we conclude that the photostability of **1** is superior to fluoresceine, in agreement with our previous findings<sup>[24]</sup>.

In conclusion, we reported the synthesis of the core compound of the BODIPY dye class, 4,4-Difluoro-4-bora-(3a,4a)-diazas-indacene. This compound is suitable for single-molecule experiments, and exhibits a high photochemical but low thermal stability. Although the synthesis itself is straightforward, the purification of the product is quite extensive. Currently, work is in progress to elucidate the subtle effects of methylation on the photophysical properties in the BODIPY dye family. As unsubstituted reference molecule of the dye class, compound **1** may prove to be helpful in fundamental research of photostability and photochemistry of fluorescent dyes, which was the motivation of this work

### **Acknowledgement**

We thank the German Science Foundation (DFG) for financial support (JU650-1) and Benjamin Hötzer for recording fluorescence lifetimes and Volker Huch for performing x-ray crystallography.

### **Experimental Section**

*General instrumentation.* Mass spectra (MS) were measured with a Waters LCMS-system consisting of a HPLC- system coupled with a single quadrupole mass spectrometer for ESI. NMR spectra were recorded on an Bruker BioSpin GmbH Avance 500 instrument.

*Optical spectroscopy (UV/Vis).* Absorbtion spectra were measured on a Perkin-Elmer Lambda 5 two-beam spectrophotometer. Fluorescence and emission spectra were recorded on different (Fluorolog 3, Jobin-Yvon, FP-6500, Jasco and SD2000 Fibre Optic Spectrometer, Ocean Optics). The latter was fibre-coupled which allowed us to take fluorescence spectra directly from the TLC-foils.

*Fluorescence correlation spectroscopy.* Experiments were performed with a home-built confocal setup based on an inverted microscope<sup>[24]</sup>. A frequency-doubled diode laser ( $\lambda_{ex} = 488$  nm) was directed to the microscope body and deflected by a dichroic mirror (495DCLP). The laser was focused by a water immersion objective lens into a drop of dye solution on top of a cover slide. Fluorescence was collected by the same objective and was focussed by the tube lens to a pinhole with a diameter of 50  $\mu\text{m}$ . After additional filtering with a bandpass filter (HQ525/50), fluorescence was split by semitransparent mirror and detected by two

avalanche photodiode modules. TTL-signals, each corresponding to a detected photon, were cross-correlated by a hardware correlator finally yielding the autocorrelation function  $g^2(\tau)$ . Analysis of all curves was done by fitting with

$$g^2(\tau) = \frac{1}{N} \left( \frac{1}{1 + \left( \frac{\tau}{\tau_d} \right)} \right) \left( 1 + \frac{k_{23}^{eff}}{k_{31}} \cdot \exp\left(-\left(k_{23}^{eff} + k_{31}\right)\tau\right) \right) + \text{Offset}$$

$\tau_d$  and  $1/k_{31}$  are the diffusional time and the triplet lifetime, respectively. From the intensity dependent  $k_{23}^{eff}$ , the intersystem crossing rate constant  $k_{23}$  can be computed as described previously<sup>[23,24]</sup>. The depicted curves were normalized to  $N=1$ .

*Fluorescence lifetime measurements.*  $\tau_f$  were determined by time-correlated single photon counting under magic-angle conditions. A picosecond excitation laser (LDH-P-C-470B, Picoquant;  $\lambda_{ex} = 470$  nm, pulse width  $\sim 70$  ps, repetition rate 20 MHz) was focused into a cuvette. Fluorescence was collected in  $90^\circ$  geometry and detected after spectral filtering with the same filter as in FCS by an avalanche-photodiode (DM 100ct, MPD). The instrumental response function was  $\sim 200$  ps and electronic signals were recorded on a stand-alone TCSPC-module (PicoHarp 300, Picoquant). The fluorescence lifetime was determined by monoexponential reconvolution-fit using commercial software (SymPhoTime, Picoquant).

*Synthesis of 4,4'-Difluoro-bora-3a-4a-diaza-(s)-indacene (1).*

A solution of pyrrole (2mmol) and a drop of trifluoroacetic acid in 50mL dichloromethane is stirred at room temperature. Then 2-formylpyrrole (2.3mmol), dissolved in 25ml dichloromethane, is added dropwise. The reaction mixture is stirred until reaction control by thin layer chromatography shows complete consumption of the aldehyde. 7ml of N-ethyl-diisopropylamine in 20ml dichloromethane and 10ml borontrifluoride-etherate in 20 ml dichloromethane are consecutively and slowly added. Ice cooling was applied during these additions. Purification is achieved by column chromatography with silica gel and alumoxan (solvent:  $\text{CH}_2\text{Cl}_2$ ). Several cycles of column chromatography were needed to completely purify the product from the starting materials. A stable fluorescent solution of **1** could only be achieved by completely purifying the product. The overall yield was about 8%.

Data of mass spectroscopy: ( $m/z_{theo} = 192\text{g/mol}$ ;  $\text{ES}^+$ :  $m/z_{exp} = 210$  [ $\text{M}+\text{NH}_4^+$ ], 211 [ $\text{M}+\text{H}_3\text{O}^+$ ];  $\text{ES}^-$ :  $m/z_{exp} = 192$  [ $\text{M}$ ], 191 [ $\text{M}-\text{H}$ ]), Thin Layer Chromatography:  $R_f = 0.6$ .

$^1\text{H-NMR}$  (400 MHz,  $\text{CDCl}_3$ )  $\delta/\text{ppm}$  6.53 (d,  $J = 4.0\text{Hz}$ , 2H, 3/5) 7.13 (d,  $J = 4.0\text{Hz}$ , 2H, 2/6) 7.39 (s, 1H, 8) 7.88 (s, 2H, 1/7)

3.2 *J. Fluoresc.* **2009**, 19, 755-758

<sup>13</sup>C-NMR (125 MHz, CDCl<sub>3</sub>) δ/ppm 118.53 (sec. C, 3/5) 131.00 (sec. C 8) 131.06 (sec. C, 2/6) 134.93 (quart. C, 8a/8b) 144.81 (sec. C, 1/7)

Crystallographic data: "CCDC 702859 contains the supplementary crystallographic data for this paper. These data can be obtained free of charge from The Cambridge Crystallographic Data Centre via [www.ccdc.cam.ac.uk/data\\_request/cif](http://www.ccdc.cam.ac.uk/data_request/cif)."

## References

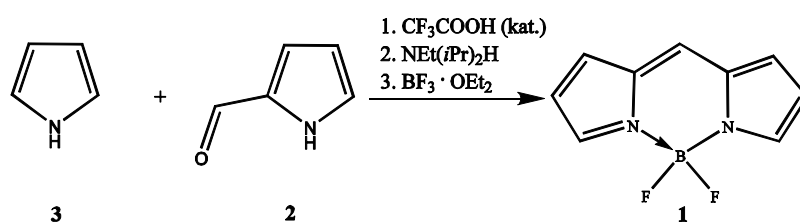
- 1 A. Treibs, F.-H. Kreuzer, *Justus Liebigs Ann. Chem.* **1968**, 718, 208-223.
- 2 H. Falk, O. Hofer, H. Lehner, *Monatsh. Chem.* **1974**, 105, 169 - 178  
E. VosdeWael, J. A. Pardoën, J. A. Vankoeveringe, J. Lugtenburg, *Recl. Trav. Chim. Pays-Bas* **1977**, 96, 306 – 309.
- 3 H. J. Worries, J. H. Koek, G. Lodder, J. Lugtenburg, R. Fokkens, O. Driessen, G. R. Mohn, *Recl. Trav. Chim. Pays-Bas* **1985**, 104, 288 – 291.
- 4 R. P. Haughland, H. C. Kang, US Patent US4774339, **1988**; F. J. Monsma, A. C. Barton, H. C. Kang, D. L. Brassard, R. P. Haughland, D. R. Sibley, *J. Neurochem.* **1989**, 52, 1641 – 1644.
- 5 R. P. Haughland, *The Handbook, A Guide to Fluorescent Probes and Labeling Technologies*, 10th edn, **2005**, Invitrogen Corp, Eugene.  
<http://probes.invitrogen.com>.
- 6 M. Shah, K. Thangraj, M. L. Soong, L. Wolford, J. H. Boyer, I. R. Politzer, T. G. Pavlopoulos, *Heteroat. Chem.* **1990**, 1, 389 – 399.
- 7 A. Coskun, E. Deniz, E. U. Akkaya, *Org. Lett.* **2005**, Vol. 7, 23, 5187 - 5189
- 8 A. Burghart, L. H. Thoresen, J. Chen, K. Burgess, F. Bergstrom, L. B. A. Johansson, *Chem. Comm.* **2000**, 2203 - 2204
- 9 T. Yogo, Y. Urano, Y. Ishitsuka, F. Maniwa, T. Nagano, *J. Am. Chem. Soc.* **2005**, 127, 12162 - 12163
- 10 M. Kollmannsberger, U. Resch- Genger, J. Daub, *J. Am. Chem. Soc.* **2000**, 122, 968-969
- 11 G. Ulrich, R. Ziessel, A. Harriman, *Angew. Chem. Int. Ed.* **2008**, 47, 1184 - 1201
- 12 A. Loudet, K. Burgess, *Chem. Rev.* **2007**, 107, 4891-4932
- 13 A. Burghart, H. Kim, M. B. Welch, L.H. Thorensen, J. Reibenspies, K. Burgess, *J. Org. Chem.* **1999**, 64, 7813 – 7819.
- 14 H. C. Kang, R. P. Haughland, US Patent 5187288, **1993**

This is a pre-peer reviewed version of the following article: *J. Fluoresc.* (2008), 19, 755-758; DOI: 10.1007/s10895-008-0446-7; Reproduced with kind permission of Springer Science and Business Media

- 15 G. Ulrich, R. Ziessel, *J. Org. Chem.* **2004**, 69, 2070 - 2083
- 16 L. R. Morgan, J. H. Boyer, US Patent 5446157, **1993**
- 17 J. R. Lakowicz, *Principles of Fluorescence Spectroscopy*, 2nd edn, **1999**, Kluwer Academic/ Plenum Publishers, New York
- 18 Horiba Jobin Yvon, *A Guide to Recording Fluorescence Quantum Yields*, <http://www.jobinyvon.com/SiteResources/Data/MediaArchive/files/Fluorescence/applications/quantumyieldstrad.pdf>
- 19 Lambda Physik, *Lambdachrome Laser dyes*, [http://bcp.phys.strath.ac.uk/ultrafast/Blue\\_book/Lamdachrome-laser-dyes.pdf](http://bcp.phys.strath.ac.uk/ultrafast/Blue_book/Lamdachrome-laser-dyes.pdf)
- 20 M. Shah, K. Thangaraj, M.-L. Soong, L.T. Wolford, J. H. Boyer, *Heteroatom Chem.* **1990**, 1(5), 389
- 21 S. J. Strickler, R.A. Berg, *J. Chem. Phys.* **1962**, 37, 814-822.
- 22 W. Siebrand, D.F. Williams, *J. Chem. Phys.* **1967**, 49, 403-404.
- 23 J. Widengren, Ü. Mets, R. Rigler, *J. Phys. Chem.* **1995**, 99, 13368 - 13379
- 24 B. Hinkeldey, A. Schmitt, G. Jung, *ChemPhysChem.* **2008**, 9, in press

**Table 1:** Spectroscopic data of **1**. <sup>1</sup>Measurement taken in Dichloromethane; <sup>2</sup>Measurement taken in Acetonitrile <sup>3</sup>Measurement taken in Water

| $\lambda_{\max}(\text{abs.})$<br>[nm] | $\lambda_{\max}(\text{em.})$<br>[nm] | $\Phi_{\text{Fl}}$<br>[%] $\pm$ 5% | $\Phi_{\text{ISC}}$<br>[%] | $\epsilon$<br>Mcm <sup>-1</sup> | $\tau_{\text{Fl}}$<br>[ns] | $k_{23}$<br>[ $\mu\text{s}^{-1}$ ] | $k_{31}$<br>[ $\mu\text{s}^{-1}$ ] |
|---------------------------------------|--------------------------------------|------------------------------------|----------------------------|---------------------------------|----------------------------|------------------------------------|------------------------------------|
| 503 <sup>1</sup>                      | 512 <sup>1</sup>                     | 90 <sup>2</sup>                    | 1.1                        | $5 \times 10^4$                 | 7.2 <sup>1</sup>           | 1.52 <sup>3</sup>                  | 0.58 <sup>3</sup>                  |

**Scheme 1.** Synthesis of 4,4-Difluoro-4-bora-(3a,4a)-diazas-indacene **1**

### Figure captions

#### Figure 1:

- a) H,H-Cosy-NMR spectrum of **1** in Deuteriochloroform. Integrations of the signals are (from low to high ppm) 2, 2, 1, 2. Strong coupling is visible at signals of vicinal atoms (e.g. 1-2, 7-6), weaker constants for the  $^3J$ -couplings (e.g. 1-3, 5-7). The H-atom in *meso*- position (8) exhibits weak coupling to H(1, 7).
- b) X-Ray crystallographic structure of **1**.

**Figure 2:** Normalized absorption (solid line) and fluorescence emission (dashed line) of **1** in dichloromethane.

**Figure 3:** Normalized fluorescence correlation function  $g(\tau)$  of the molecule at two different excitation intensities. The solubility of **1** in water is high enough to record FCS. The increase of the correlation function at short times ( $<10^{-2}$ ms) shows that the molecule is strongly transferred into the triplet state with increasing excitation intensity. The good overlapping of both correlation functions at longer timescales ( $>10^{-2}$ ms) indicates good photostability of the molecule<sup>[24]</sup>.

**Figure 1a**

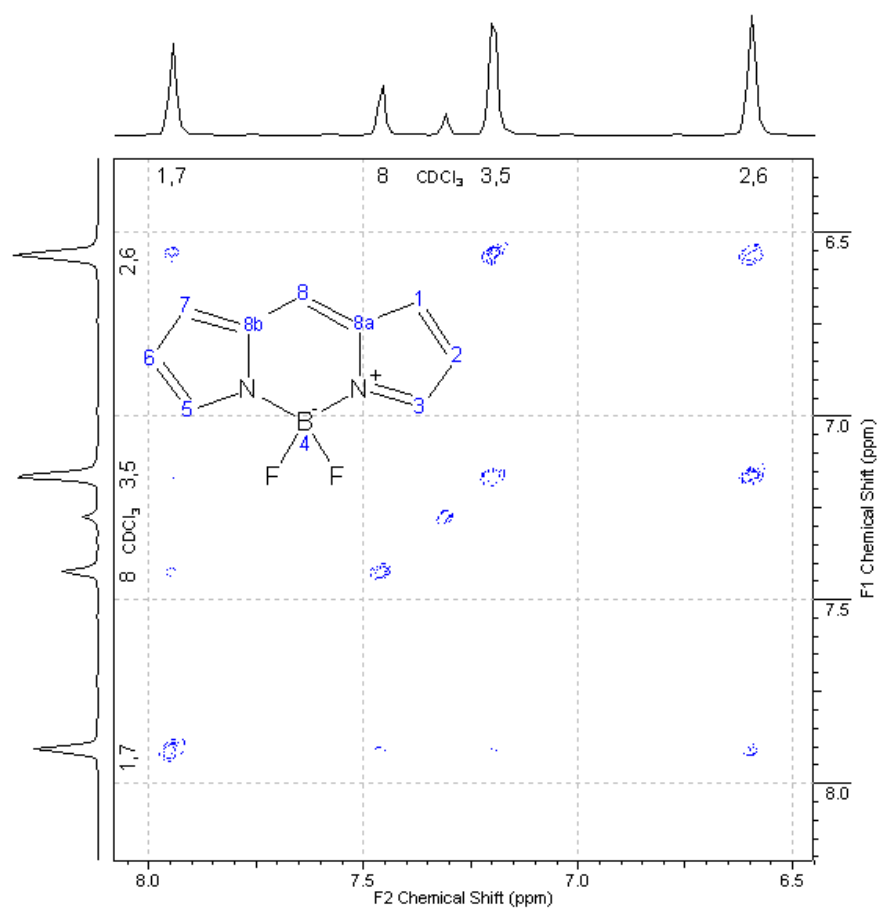
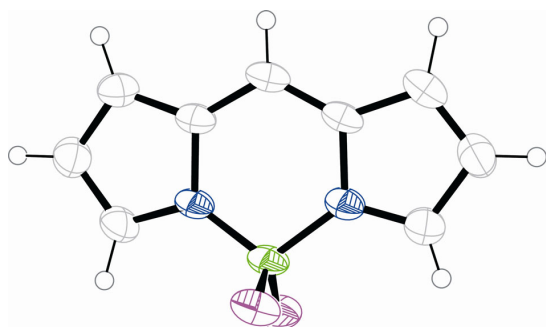


**Figure 1b**



This is a pre-peer reviewed version of the following article: *J Fluoresc* (2008), 19, 755-758; DOI: 10.1007/s10895-008-0446-7; Reproduced with kind permission of Springer Science and Business Media

Figure 2

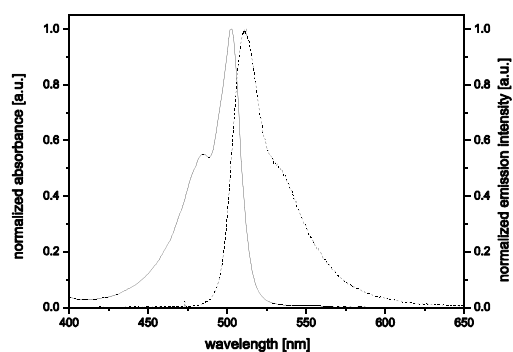
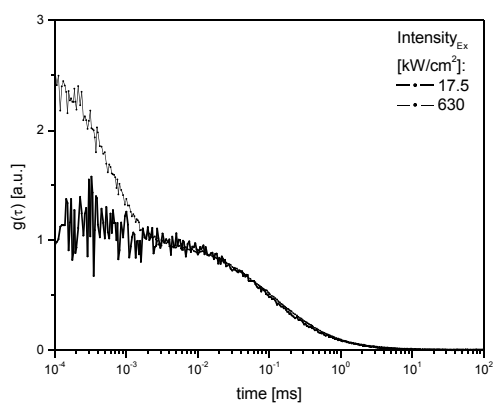


Figure 3



3.3 *J. Fluoresc.* 2008, 18, 639-644

## **Disabling Photoinduced Electron Transfer in 4,4-Difluoro-8-(4'-hydroxyphenyl)-1,3,5,7-tetramethyl-4-bora-3a,4a-diaza-s-indacene by Phosphorylation**

Michaela Jacob, Alexander Schmitt, Gregor Jung\*

Biophysical Chemistry, Saarland University, D-66041 Saarbruecken, Germany

\* Corresponding author: Gregor Jung, Biophysical Chemistry, Saarland University, Building B2 2, Campus, D-66123 Saarbruecken, Tel.: +49-681-302-64848, Fax: +49-681-302-64846, E-Mail: g.jung@mx.uni-saarland.de

**RUNNING HEAD:** Phosphoryl-Bodipy

### **ABSTRACT:**

The synthesis and photophysical characterization of the phosphorylated Bodipy dye **5** are reported and compared to those of its hydroxyphenyl counterpart **1**. Conversion of the latter by three methods of phosphorylation yields the strongly fluorescent dye **5** which exhibits similar steady-state spectra like **1** but an approximately 5 times prolonged fluorescence lifetime  $\tau_{\text{Fl}}$ . We attribute this distinct change from  $\tau_{\text{Fl}} = 0.7$  ns for **1** to  $\tau_{\text{Fl}} = 3.7$  ns for **5** to the suppression of photoinduced electron transfer in **5**. This photochemical reaction was previously held responsible for fluorescence quenching in **1**. Fluorescence correlation spectroscopy reveals that **5** can be detected by single-molecule methods and that uncaging of phosphate in **5** is a minor problem.

**KEYWORDS:** Phosphorylation; Fluorescence correlation spectroscopy; Bodipy; photoinduced electron transfer; single-molecule; phenol.

This is a pre-peer reviewed version of the following article: *J Fluoresc* (2008) 18:639–644; DOI:10.1007/s10895-008-0373-7; Reproduced with kind permission of Springer Science and Business Media

## INTRODUCTION

Dyes with a 4,4-Difluoro-4-bora-3a,4a-diaza-s-indacene core, the so-called BODIPY (Bodipyromethene) dyes, find widespread application as fluorescent labels in bioanalytics or as laser dyes [1, 2]. The fluorescence properties of the alkyl-substituted representatives are comparable to those of Xanthene-dyes like Fluorescein or Rhodamine dyes, but in contrast to these, Bodipy dyes are uncharged. Their synthesis is established and lead to the development of sensors for numerous ions [3-10]. Most often, the unit which binds the analyte is connected to the fluorescing core via the *meso*-position of the latter. Ion sensing then is achieved by suppression of fluorescence quenching mechanisms, notably photoinduced electron transfer (PeT) [2, 3]. Excited dyes are redoxamphoteric and can act as electron-donor, i.e. reductant, or as electron-acceptor, i.e. oxidant. In the majority of the mentioned cases, the latter is realized (scheme 1) [2]. With an oxidizable counterpart in close vicinity, i.e. the substituent in *meso*-position, electron transfer to the excited dye occurs faster than fluorescence emission. If ligand binding or a chemical transformation now increases the oxidation potential of the donor, then fluorescence quenching is suppressed. For enhancing the analytical ability, one can match their redox potential by fine-tuning the donor or the acceptor [3, 11].

In the present work, we demonstrate that the electron-donor properties of a hydroxyphenyl-moiety in *meso*-position can be removed by phosphorylation. Different methods for obtaining phosphomonoesters of a weakly fluorescent p-hydroxyphenyl-Bodipy dye are employed which lead to a highly water-soluble and strongly fluorescent product [12-14]. IR, UV/Vis, fluorescence emission, lifetime (TCSPC) and correlation spectroscopy (FCS) are performed for characterization. We finally discuss the suitability of the product as substrate for studying the activity of phosphatases on the single-molecule level where both the substrate and its product should be detectable but distinguishable by their photophysical properties.

## MATERIALS AND METHODS

### *Reagents*

4,4-Difluoro-8-(4'-hydroxyphenyl)-1,3,5,7-tetramethyl-4-bora-3a,4a-diaza-s-indacene **1** as educt was obtained following the literature [16]. The successful synthesis was verified by <sup>1</sup>H-NMR spectroscopy. Reagents for the syntheses were used at least in *purum* quality; solvents for spectroscopic measurements were in Chromasolv or comparable quality.

### *Phosphorylation methods [12-14] (scheme 2)*

a) Phosphorylchloride POCl<sub>3</sub> [12]

This is a pre-peer reviewed version of the following article: *J Fluoresc* (2008) 18:639–644; DOI:10.1007/s10895-008-0373-7; Reproduced with kind permission of Springer Science and Business Media

3.3 *J. Fluoresc.* **2008**, 18, 639-644

20 mg (0.06 mmol) **1** were dissolved in 15 ml CH<sub>2</sub>Cl<sub>2</sub> as solvent and cooled to 0° C. 17 µl POCl<sub>3</sub> (0.18 mmol) and 21 µl NEt<sub>3</sub> (0.15 mmol) in 2 ml CH<sub>2</sub>Cl<sub>2</sub> were consecutively added. After two hours, the reaction was stopped by pouring the solution on ice. The strongly fluorescent organic phase was separated from the colorless aqueous phase and dried over MgSO<sub>4</sub>. Thin-layer chromatography (TLC) indicated the coexistence of the educt and a more polar product species. Hydrolysis of the latter was achieved by mixing the fluorescent CH<sub>2</sub>Cl<sub>2</sub> solution with an equal amount of a saturated K<sub>2</sub>CO<sub>3</sub> solution. The immediately green fluorescent aqueous solution was separated from the organic phase and neutralized with diluted HCl.

b) Dibenzylphosphite (DBP) [13]

180 mg (0.53 mmol) **1** were dissolved in 20 ml MeCN and cooled to -10° C. Successively, 256 µl CCl<sub>4</sub> (2.65 mmol), 194 µl Diisopropylethylamin (DIPEA) (1.11 mmol), 6.5 mg Dimethylaminopyridine (DMAP) (0.05 mmol) and finally 174 µl DBP (0.77 mmol) were added and stirred for one hour under a N<sub>2</sub>-atmosphere. Afterwards, a mixture of MeCN and 0.5 M KH<sub>2</sub>PO<sub>4</sub>-solution (1:3) was used for terminating the reaction. After eluting three times with 20 ml Ethylacetate, the combined organic phases were washed with water and saturated NaCl solution, and dried over MgSO<sub>4</sub>. After evaporation of the solvent, the remainder was dissolved in CH<sub>2</sub>Cl<sub>2</sub> and subjected to column chromatography. Two fractions, which were more polar than the educt, could be eluted by increasing solvent polarity (mixture CH<sub>2</sub>Cl<sub>2</sub>/Tetrahydrofuran ranging from 1:0 to 1:1; finally methanol). Both fractions could be converted to a water-soluble, highly fluorescent product by stirring with diluted NaOH (0.1 M). The aqueous solutions were neutralized with diluted HCl.

c) Diethylchlorophosphonate on magnesia [14]

85 mg (0.25 mmol) **1** were mixed with 44 µl Diethylchlorophosphonate (0.3 mmol) and 15 mg MgO and heated for one hour at 60°C. After cooling down, the remainder was eluted with CH<sub>2</sub>Cl<sub>2</sub>. Treatment with diluted NaOH (0.1 M) again yielded a yellowish, strongly fluorescent solution. The aqueous solutions were neutralized with diluted HCl.

*UV/Vis, Fluorescence and IR spectroscopy*

Absorption and fluorescence emission spectra were recorded with a double-beam spectrometer (Lambda 5, Perkin Elmer) and a fibre coupled array spectrometer (SD 2000, Ocean Optics), respectively. IR spectra were recorded in ATR geometry (attenuated total reflection; Spectrum 1000, Perkin Elmer). For that purpose, the dye solutions were put on the ZnSe prism and evaporated under N<sub>2</sub>-atmosphere.

This is a pre-peer reviewed version of the following article: *J Fluoresc* (2008) 18:639–644; DOI:10.1007/s10895-008-0373-7; Reproduced with kind permission of Springer Science and Business Media

*Lifetime measurements*

We performed lifetime measurements of **1** and **5** in water. For that purpose, **1** was diluted in MeCN to  $\sim 10^{-5}$  M and then added to water. The content of MeCN during the measurement was below 1%. Aqueous solutions of **5** were directly diluted to the appropriate concentration range ( $OD_{\max} < 0.1$ ).

Fluorescence lifetimes were determined by a home-built time-correlated single photon counting system (TCSPC) in right-angle geometry. We used a picosecond-diode laser (LDH-P-C-470B, Picoquant) with a pulse width of  $\sim 70$  ps at 40 MHz as excitation source, and detected the fluorescence photons under the magic angle and after filtering (HQ 500/35, AHF Analysentechnik) by a single-photon counting module (PD1CTC, Molecular Photon Device). The overall instrumental response function was about  $\sim 200$  ps (FWHM). Data registration and analysis was performed using commercial software (SymPhoTime, Picoquant).

*Fluorescence correlation spectroscopy (FCS)*

Experiments were performed with a home-built confocal setup based on an inverted microscope (Axiovert 200, Zeiss). A frequency-doubled diode laser (Picarro, Soliton), operating at  $\lambda_{\text{exc}} = 488$  nm, with a diameter of 0.7 mm was used as excitation source. The laser beam was directed to the microscope body and there deflected by a dichroic mirror (495 DRLP, Omega). The laser was focussed by a water immersion objective lens (63x NA 1.2 WI, Zeiss) into an aqueous solution of the dyes **1** and **5** at a concentration of  $\sim 10^{-8}$  M. Fluorescence was collected by the same objective and was focussed by the tube lens to a pinhole with a diameter of 50  $\mu\text{m}$ . After additional filtering (HQ 525/50, AHF Analysentechnik), fluorescence was split by a semitransparent mirror and detected by two avalanche photodiode modules (SPCM-14-AQR, PerkinElmer Optoelectronics). The electronic outputs of these devices were cross-correlated by a hardware correlator (FLEX 02 D, Correlator.com). The autocorrelation curves  $g(\tau)$  were fitted using eq. 1 by means of commercial software (Origin 7.5, Wolfram Scientific).

$$(1) \quad g(\tau) = 1 + \frac{1}{N} \cdot \frac{1}{1 + \frac{\tau}{\tau_{\text{diff}}}} \cdot (1 + C \exp(-k\tau)) = 1 + \frac{1}{N} \cdot \frac{1}{1 + \frac{\tau}{\tau_{\text{diff}}}} \cdot \left( 1 + \frac{k_{23}^{\text{eff}}}{k_{31}} \exp\left(-\left(k_{23}^{\text{eff}} + k_{31}\right)\tau\right) \right)$$

$N$  is the number of molecules in the detection volume,  $\tau_{\text{diff}}$  is the diffusional time,  $C$  is the amplitude for the flickering dynamics, which is characterized by the overall rate constant  $k$ .

C and k are given by the reciprocal of the triplet lifetime,  $k_{31}$ , and the effective intersystem rate constant  $k_{23}^{\text{eff}}$ . The latter is determined by the intersystem rate constant  $k_{23}$ , the intensity I, the reciprocal of the excited state lifetime,  $k_{21}$ , and the absorption cross section  $\sigma$  (eq. 2)

$$(2) \quad k_{23}^{\text{eff}} = k_{23} \frac{\sigma \cdot I}{\sigma \cdot I + k_{21} \cdot h\nu}$$

From a saturation plot, i.e. plot of  $k_{23}^{\text{eff}}$  vs. I,  $k_{23}$  can be computed as the limit for high intensities without explicit need of the absorption coefficient  $\sigma$  [15].

## RESULTS AND DISCUSSION

### *Selection of educt*

Bodipy dyes with hydroxyaryl substituents in *meso*-position were described several times [16-18]. Ionization of phenolic or naphtholic moieties with  $\text{pK}_a$  values between 7.5 and 10.5 was employed for pH measurements. Higher fluorescence quantum yields  $\Phi_{\text{Fl}}$  up to 12% were detected for the neutral forms [18]. As pointed out in the introduction, we are interested in systems where both educt and product of a chemical reaction are appropriate for single-molecule spectroscopy. In this future application, the labelled phenol should be the reaction product and exhibit a higher  $\Phi_{\text{Fl}}$  than the so far published compounds. Comparison of  $\Phi_{\text{Fl}}$  of some of the mentioned dyes in aqueous solution has suggested that  $\Phi_{\text{Fl}}$  could be increased further if more alkyl-substituents were attached to the Bodipy core [18]. In scheme 1, this corresponds to raising the energetic level of the acceptor. We therefore synthesized **1**, which was described previously [16], as starting point for the phosphorylation.

### *Phosphorylation*

Monoesters of **1** are preferred as any ester cleavage should be detectable by changes in the fluorescence properties. We applied three different procedures for the synthesis of phosphoesters and combined them with subsequent hydrolyzation (scheme 2) [12-14]. In all cases, the conversion of **1** to the products **2** – **4** as the first reaction step in scheme 2 was not quantitative, and TLC indicated a mixture of at least two compounds with the educt being one of these. The putative intermediates **2** and **3** were isolated but not further characterized. As expected, none of the fractions was water soluble. Hydrolyzing the double and triple esters by trimethylbromsilane was not successful and led to a complete loss of fluorescence [19]. However, hydrolyzing the esters by diluted basic solutions yielded green fluorescent aqueous solutions (fig. 1). Despite the different access routes, hydrolyzation led to the same *one* final product according to optical spectroscopy and, more significant, its migration behaviour in

TLC with different solvents. Further hydrolysis of the water soluble compound, however, led again to the educt which could subsequently be extracted by  $\text{CH}_2\text{Cl}_2$ . From the mentioned solvation behaviour, we conclude that the water soluble fraction is the wanted phosphomonoester **5**. In agreement with these findings, hydrolysis of the phosphodi- and triesters **2** - **4** by means of highly concentrated NaOH solutions (1M) directly led back to the educt.

#### *IR-Spectroscopy*

Due to the low yields of the phosphomonoester and the experimental observation that complete removal of the solvent partially cleaved the ester, we performed IR-spectroscopy of the water soluble product under ATR-geometry for further support of our interpretation (fig. 2). Comparison of the educt and the product revealed significant differences in the range between  $1000\text{ cm}^{-1}$  and  $1600\text{ cm}^{-1}$ . First of all, the different bands of the product species appear much broader than those of **1**. No coinciding absorbances between both spectra are detectable in this range. Furthermore, experimental FTIR-spectra of  $\text{HPO}_4^{2-}$  or  $\text{H}_2\text{PO}_4^-$  showed no agreement with our spectra [20]. Most significant for the existence of a phosphoester is the product band at  $\sim 1230\text{ cm}^{-1}$ , which is assigned to the P=O stretch vibration as in other aromatic phosphoesters [12].

#### *Photophysical characterization*

Fig. 3 shows the comparison of TCSPC data of **1** and **5**. Excited **1** exhibits a very rapid fluorescence decay with a single lifetime  $\tau_{\text{F1}} = 0.7$  (+/- 0.1) ns. By contrast, the excited state lifetime of its phosphorylated counterpart **5** is prolonged by roughly a factor of 5 ( $\tau_{\text{F1}} = 3.7$  (+/- 0.1) ns). This latter value is close to the value obtained for 4,4-Difluoro-8-phenyl-1,3,5,7-tetramethyl-4-bora-3a,4a-diaza-s-indacen ( $\tau_{\text{F1}} = 3.6$  ns; B. Hinkeldey, G. Jung, unpublished results) which bears a phenyl-group in the *meso*-position. No pH-dependence of  $\tau_{\text{F1}}$  of **5** was detected.

The low  $\Phi_{\text{F1}}$  of different hydroxyaryl-substituted Bodipy-dyes was explained by fluorescence quenching due to PeT [18, 21]. The phenol acts as electron donor and the excited Bodipy core as electron acceptor. Probably, this also holds for **1** since its  $\tau_{\text{F1}}$  is considerably smaller than that of the phenyl-derivative. Thus, our interpretation of the prolonged  $\tau_{\text{F1}}$  of **5** compared to that of **1** is that phosphorylation of the hydroxyaryl-group cancels its donor properties and, consequently, PeT.

We finally performed FCS of **1** and **5** to judge their suitability for single-molecule experiments (fig. 4). Only a few autocorrelation traces of **1** were recorded since this was very time consuming due to its low  $\Phi_{\text{Fl}}$ , whereas acquisition of intensity dependent FCS data of **5** were quickly obtained. Comparison of curves at the same intensity (grey and black curves) shows a higher amplitude  $C$  for **1** than for **5**. This corresponds to a higher  $k_{23}$  for **1** than for **5** (eq. 1), if one assumes that both dyes possess similar  $\sigma$ . On the basis of the available fluorescence lifetimes  $\tau_{\text{Fl}}$ , i.e. the reciprocal values of  $k_{21}$ , we can estimate that the intersystem crossing quantum yield,  $\Phi_{\text{isc}} = k_{23}/k_{21}$  is larger for **1** than for **5** by a factor of  $\sim 10$ . From the determined values for **5** (fig. 4), we calculate  $\Phi_{\text{isc}} = 0.007$ .

The fact that FCS curves could be obtained for dyes **1** and **5** evidences their suitability for single-molecule research. The decrease of the diffusional time  $\tau_{\text{diff}}$  of **5**, which is normally interpreted as photobleaching, also sets an upper limit for other imaginable photochemical reactions. Most relevant for future applications of **5** would be the cleavage of the here synthesized ester. Indeed, fluorescently labelled phosphoesters are employed for this so-called uncaging of phosphate, and such a reaction would exclude the use of **5** for measuring e.g. phosphatase activity [22]. However, it can be concluded from the curves that the light-induced release of phosphate in **5** occurs, if observable at all, with a very low quantum yield since otherwise the quality of the curves would drop considerably.

## CONCLUSION

We have shown that the donor ability of phenol in PeT can be switched off by phosphorylation. This proof-of-principle sketches how phosphoester cleavage can be studied with dyes which are also appropriate for single-molecule detection. Different methods of obtaining **5** were tested, but there is still demand for improving its synthesis. The purification is the most challenging procedure and appears critical due to the decomposition of **5** upon drying. As the proposed concept is not restricted to Bodipy dyes, we will turn to correspondingly modified Xanthene-dyes which are inherently more water soluble than Bodipy dyes. The enhanced water solubility favors these dyes for bioanalytical applications.

**ACKNOWLEDGEMENT** Financial support is provided by the German Science Foundation (DFG, JU-650/2-2). We are indebted to Benjamin Hötzer, Babette Hinkeldey, Michael Schmitt and Rolf Hempelmann for assistance and support.

## REFERENCES

- [1] R. Ziessel, G. Ulrich, A. Harriman, (2007), The chemistry of Bodipy: A new *El Dorado* for fluorescence tools, *New J. Chem.* **31**, 496-501.
- [2] A. Loudet, K. Burgess, (2007), BODIPY dyes and their derivatives: Syntheses and spectroscopic properties, *Chem. Rev.*, in press.
- [3] Y. Gabe, Y. Urano, K. Kikuchi, H. Kojima, T. Nagano, (2004), Highly sensitive fluorescence probes for nitric oxide based on Boron dipyrromethene chromophore-Rational design of potentially useful bioimaging fluorescence probe, *J. Am. Chem. Soc.* **126**, 3357-3367.
- [4] N. Basaric, M. Baruah, W. Qin, B. Metten, M. Smet, W. Dehaen, N. Boens, (2005), Synthesis and spectroscopic characterisation of BODIPY based fluorescent off-on indicators with low affinity for calcium, *Org. Biomol. Chem.* **3**, 2755-2761.
- [5] M. Kollmannsberger, K. Rurack, U. Resch-Genger, J. Daub, (1998), Ultrafast charge transfer in amino-substituted Boron dipyrromethene dyes and its inhibition by cation complexation: A new design concept for highly sensitive fluorescent probes, *J. Phys. Chem. A* **102**, 10211-10220.
- [6] K. Rurack, M. Kollmannsberger, U. Resch-Genger, J. Daub, (2000), A selective and sensitive fluoroionophore for HgII, AgI and CuII with virtually decoupled fluorophore and receptor, *J. Am. Chem. Soc.* **122**, 968-969.
- [7] X. Qi, E. Jun, S. Kim, J. Hong, Y. Yoon, J. Yoon, (2006), New BODIPY derivatives as off-on fluorescent chemosensors and fluorescent chemodosimeter for Cu<sup>2+</sup>: Cooperative selectivity enhancement toward Cu<sup>2+</sup>, *J. Org. Chem.* **71**, 2881-2884.
- [8] M. Li, H. Wang, X. Zhang, H.-S. Zhang, (2004), Development of a new fluorescent probe: 1,3,5,7-tetramethyl-8-(4'-aminophenyl)-4,4-difluoro-4-bora-3a,4a-diaza-s-indacene for the determination of trace nitrite, *Spectrochim. Acta A* **60**, 987-993.
- [9] T. Kalai, K. Hideg, (2006), Synthesis of new, BODIPY-based sensors and labels, *Tetrahedron* **62** (2006), 10352-10360.
- [10] H. Koutaka, J. Kosuge, N. Fukasaku, T. Hirano, K. Kikuchi, Y. Urano, H. Kojima, T. Nagano, (2004), A novel fluorescent probe for Zinc ion based on Boron dipyrromethene (BODIPY) chromophore, *Chem. Pharm. Bull.* **52**, 700-703.
- [11] Y. Urano, M. Kamiya, K. Kanda, T. Ueno, K. Hirose, T. Nagano, (2005), Evolution of fluorescein as a platform for finely tunable fluorescence probe, *J. Am. Chem. Soc.* **127**, 4888-4894.
- [12] L. Tietze, T. Eicher, (1991), *Reaktionen und Synthesen im organisch-chemischen Praktikum und Forschungslaboratorium*, Georg Thieme, Stuttgart.
- [13] L. Silverberg, J. Dillon, P. Vemishetti, (1996), A simple, rapid and efficient protocol for the selective phosphorylation of phenols with dibenzylphosphite, *Tetrahedron Lett.* **37**, 771-774.
- [14] B. Kaboudin, (1999), Phosphorylation of phenols with diethylchlorophosphonate on the surface of magnesia, *J. Chem. Res.* 402-403.
- [15] J. Widengren, Ü. Mets, R. Rigler, (1995), Fluorescence correlation spectroscopy of triplet states in solution: A theoretical and experimental study, *J. Phys. Chem.* **99**, 13368-13379.
- [16] A. Coskun, E. Deniz, E. Akkaya, (2005), Effective PET and ICT switching of boradiazaindacene emission: A unimolecular, emission mode molecular half-subtractor with reconfigurable logic gates, *Org. Lett.* **7**, 5187-5189.
- [17] T. Gareis, C. Huber, O. Wolfbeis, J. Daub, (1996), Phenol/phenolate-dependent on/off switching of the luminescence of 4,4-difluoro-4-bora-3a,4a-diaza-s-indacenes, *Chem. Comm.* 1717-1718.

3.3 *J. Fluoresc.* **2008**, 18, 639-644

- [18] M. Baruah, W. Qin, N. Basaric, W. DeBorgraeve, N. Boens, (2005), Bodipy-based hydroxyaryl derivatives as fluorescent pH-probes, *J. Org. Chem.* **70**, 4152-4157.
- [19] S. Lazar, G. Guillaumet, (1992), A selective removal of benzyl protecting groups in arylphosphate esters with bromotrimethylsilane, *Synth. Comm.* **22**, 923-931.
- [20] M. Klähn, G. Mathias, C. Kötting, M. Nonella, J. Schlitter, K. Gerwert, P. Tavan, (2004), IR spectra of phosphate ions in aqueous solution: Predictions of a DFT/MM approach compared with observations, *J. Phys. Chem.* **108**, 6186-6194.
- [21] W. Qin, M. Baruah, A. Stefan, M. Van der Auweraer, N. Boens, (2005), Photophysical properties of BODIPY-derived hydroxyaryl fluorescent pH probes in solution, *ChemPhysChem* **6**, 2343-2351.
- [22] M. Goeldner, R. Givens, (2005), *Dynamic Studies in Biology*, Wiley-VCh, Weinheim.

**FIGURE CAPTIONS**

**Scheme 1:** Disabling PeT in **1**. Upon lowering the energy of the highest occupied molecular orbital in the donor moiety (D), i.e. raising the oxidation potential, electron transfer to the singly occupied molecular orbital of the acceptor (A) is disabled.

**Scheme 2:** Three syntheses of **5** starting from **1** using Phosphorylchloride POCl<sub>3</sub> [12], Dibenzylphosphite (DBP, (PhO)<sub>2</sub>HP=O) [13] or Diethylchlorophosphonate (EtO)<sub>2</sub>POCl on magnesia MgO [14]. See text for details.

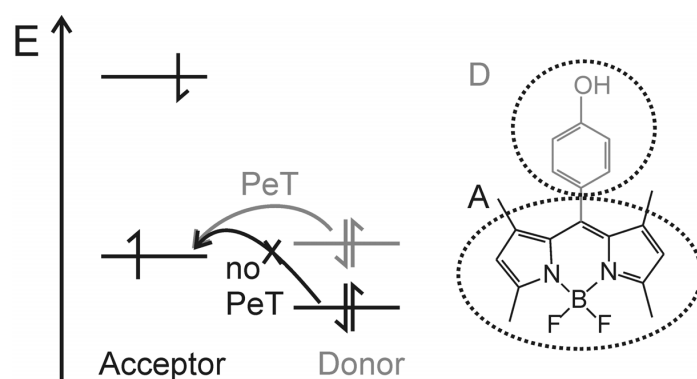
**Figure 1:** Normalized absorption (left) and fluorescence emission spectra (right) of **1** in CH<sub>2</sub>Cl<sub>2</sub> (black) and **5** at pH 7 (grey). The blue shift from **1** to **5** in absorption ( $\lambda_{\max}(\mathbf{1}) = 501$  nm,  $\lambda_{\max}(\mathbf{5}) = 495$  nm) and emission ( $\lambda_{\max}(\mathbf{1}) = 515$  nm,  $\lambda_{\max}(\mathbf{5}) = 510$  nm) is not significant as solvent dependent changes of the spectra of hydroxyaryl-Bodipy's in different solvents were noticed [20].

**Figure 2:** ATR-IR spectra of **1** (black) and **5** (grey) in solid form.

**Figure 3:** Fluorescence lifetime measurement of **1** and **5** in water by time-correlated single photon counting. The prolongation of  $\tau_{\text{Fl}}$  from **1** ( $\tau_{\text{Fl}} = 0.7$  ns) to **5** ( $\tau_{\text{Fl}} = 3.7$  ns) is explained by lowering the donor energy level in scheme 1 by phosphorylation.

**Figure 4:** Fluorescence correlation curves of **1** (left) and **5** (right) in water at different intensities (dotted: 67 kWcm<sup>-2</sup>, grey: 0.27 MWcm<sup>-2</sup>, black: 0.80 MWcm<sup>-2</sup>). The offset 1 in eq. 1 was subtracted from the curves; subsequently the curves were normalized to N = 1. The amplitude C of the decay on the (sub) $\mu$ s time scale is a measure for the triplet population, and shows a stronger intersystem crossing for **1** than for **5** at the same intensities [15].  $k_{31}(\mathbf{5}) = 7.3 \cdot 10^5$  s<sup>-1</sup> (+/- 20%) and, from the intensity dependent  $k_{23}^{\text{eff}}$ ,  $k_{23}(\mathbf{5}) = 1.8 \cdot 10^6$  s<sup>-1</sup> (+/-25%; inset) can be determined. Photobleaching which appears in a reduction of the diffusional time  $\tau_{\text{diff}}$  is more eminent for **5** than for **1** and might indicate phosphate uncaging.

Scheme 1)



Scheme 2)

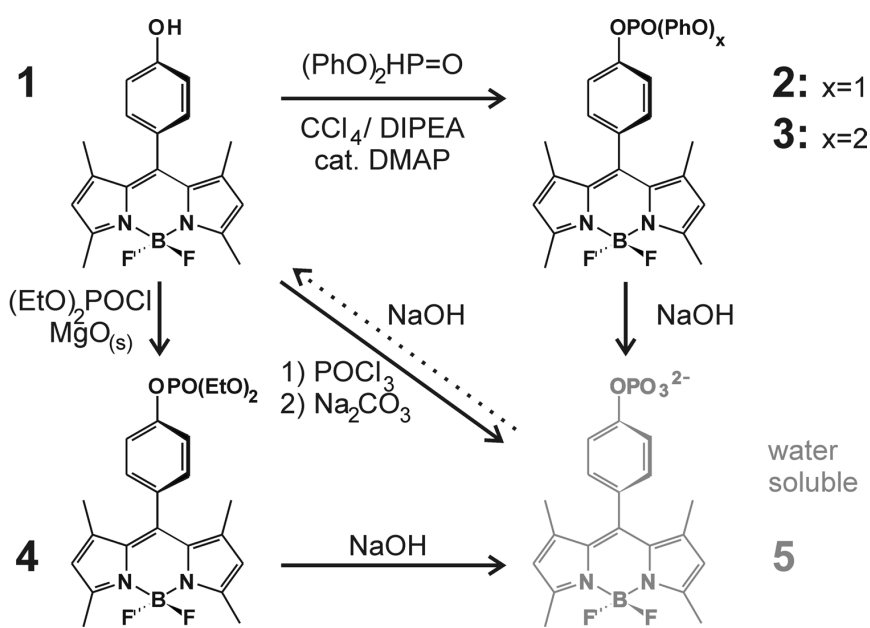


Figure 1)

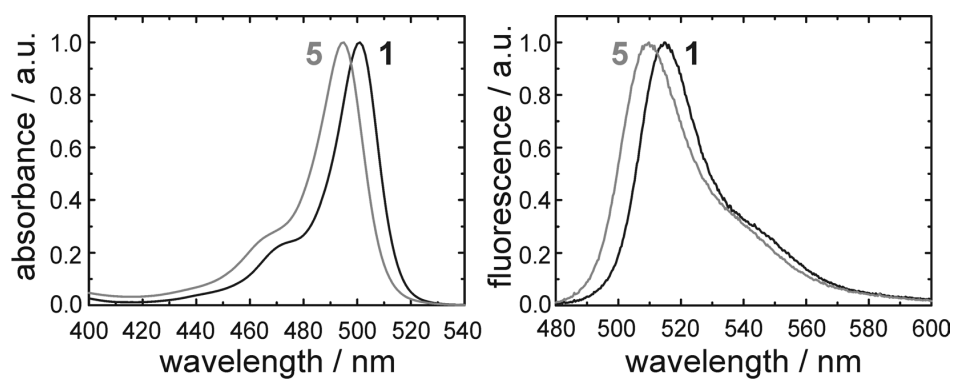


Figure 2)

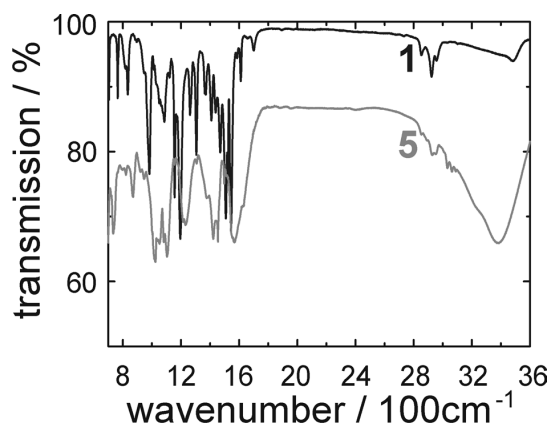


Figure 3)

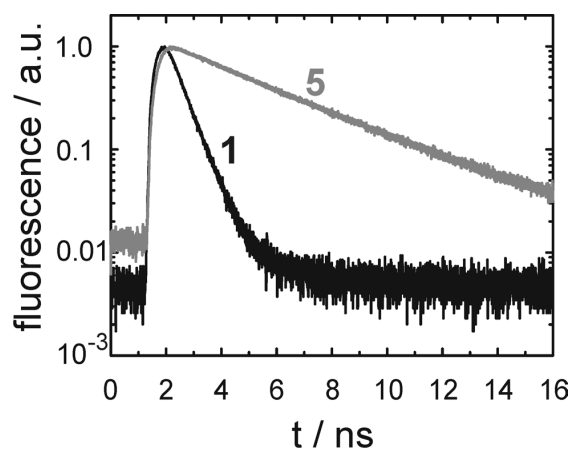
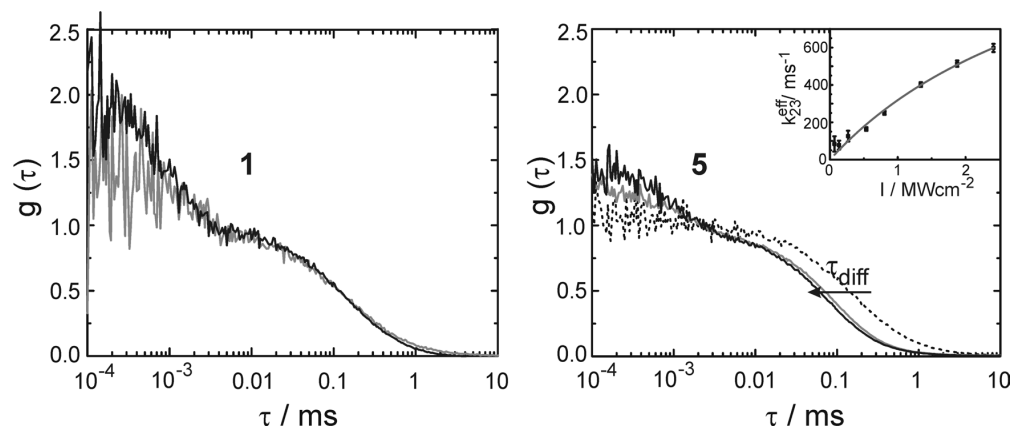


Figure 4)



## **Solvent-dependent steady-state fluorescence spectroscopy for searching ESPT-dyes: Solvatochromism of HPTS revisited**

**Gregor Jung\*, Stephan Gerharz, Alexander Schmitt**

Biophysical Chemistry, Saarland University, D-66123 Saarbruecken, Germany

\* Corresponding author: Biophysical Chemistry, Saarland University, Campus, Building B2 2, D-66123 Saarbruecken, Germany. phone: +49-681-302-64848, fax: +49-681-302-64846, email: [g.jung@mx.uni-saarland.de](mailto:g.jung@mx.uni-saarland.de)

### **Summary:**

We reinvestigated the solvatochromism of 8-hydroxypyrene-1,3,6-trisulfonate (pyranine) in conjunction with that of 8-methoxypyrene-1,3,6-trisulfonate and of 1-hydroxypyrene (pyrenol) by use of 25 different solvents. Conclusions for the prediction of ESPT behaviour of synthetic dyes were drawn by comparison with the solvatochromism of p-hydroxystyryl-Bodipy-dyes. Solvents were chosen according to their Kamlet-Taft parameters  $\alpha$  and  $\beta$  for elucidating the acidity of the dyes and the basicity of their conjugated bases in the ground and excited state.

Comparison of the spectra of pyranine and pyrenol in solvents with varying  $\beta$ -values revealed that the acidity of both dyes is similar therein. The well-known ESPT behaviour of pyranine in water is assigned to a change of the electronic state at  $\alpha$ -values  $\sim 0.7$  to  $0.8$ . The high acidity of this excited state also appears in the vanishing solvatochromism of the photoproduct fluorescence. However, prediction of an ESPT tendency of synthetic dyes might fail when only fluorescence emission data are considered. We propose to refer instead to the energetic difference of the 0-0 transition *in absorption* together with the solvatochromism of the acidic form in aprotic solvents of similar polarity.

## 1. Introduction

Excited state proton transfer (ESPT) of 8-hydroxypyrene-1,3,6-trisulfonate (HPTS; pyranine) to water was first described by Förster [1,2] more than 50 years ago and is still in the focus of scientific research [3]. This photochemical reaction exemplifies the more general case of various aromatic alcohols which undergo an increase of their acidity upon excitation (for reviews, see [4-6]). Especially naphthol and pyrene derivatives were thoroughly investigated in the past, but ESPT reactions were also detected in stilbene-derivatives, fluorescent dyes and proteins [7-11]. ESPT is not limited to water as final acceptor but protonation of other solvents can be observed in super-photoacids [5, 12,13]. One reason for the ongoing interest is that proton transfer reactions are the most basic chemical reactions with an overwhelming importance in many areas of chemistry. Especially helpful are ESPT-systems where both substrate and product are fluorescent. Thus, triggering of these reactions with short excitation pulses allows for studies of the underlying photophysical mechanisms which precede the protolysis with time-resolved fluorescence spectroscopy [3, 10-18]. Additionally, the fluorescent product states are long-living (~ ns), and the kinetics of diffusion-controlled recombination processes also can be monitored by the same techniques [6, 18-20].

In most of the cited systems, excitation has to be performed in the UV or near-UV range. Ubiquitously excited background fluorescence, enhanced Raman scattering and the energy content of the absorbed photons make an observation of ESPT in ultrasensitive spectroscopy challenging. Even in cases, where ESPT could be initiated by near UV light, photodestruction and photoconversion counteract these experiments [21, 22]. This deficiency of known molecules provokes our search for dye molecules which exhibit ESPT and strong visible fluorescence in both states. Though, straightforward and systematic synthetic work relies on a tool with which the synthetic direction can be confined and, finally, the ability of ESPT can be predicted. Steady-state fluorescence and UV-Vis spectroscopic signatures are most convenient in this approach as they can be applied to screening techniques.

The increase of acidity of a dye upon excitation can roughly be estimated by thermodynamics applied to optical spectroscopy. A red-shift in the lowest electronic transition of the conjugate base compared to the acidic form results in a change of the acidity constant  $pK_A$  according to

$$\Delta pK_A \approx \frac{(h\nu_A - h\nu_B)}{kT \ln 10} \quad (1)$$

where  $\nu_A$  and  $\nu_B$  are the frequencies of 0-0 optical transitions of the acid and the base, respectively [5, 6]. Time constants for proton transfer to solvent ought to be faster than the

radiation emission, otherwise ESPT remains hidden. Therefore, kinetic parameters have to be converted to spectroscopic data to be useful in screening applications.

Such more kinetic approach is based on the analysis of spectroscopic data of aromatic alcohols, recorded in different solvents with varying hydrogen-bonding capability [23-26]. Most often, the Kamlet-Taft parameters  $\alpha$  and  $\beta$  are used to describe the ability of a solvent to donate ( $\alpha$ ) or accept ( $\beta$ ) a hydrogen-bond (HB) [24-29]. Solvatochromism of a solute, i.e. the difference of the transition frequency  $\nu_i$  to a reference transition frequency  $\nu_{i0}$  in dependence of the solvent, then provides a tool to quantify the stabilization of the excited state with respect to the ground state. The index  $i$  describes whether properties of the ground state ( $i = \text{exc}$ ) or the excited state ( $i = \text{em}$ ) of the probe molecule are investigated [6]. This classification results from the different time scales of the instantaneous absorption/emission process and the subsequent rearrangement of nuclei. Equation 2 comprehends solvatochromism in a mathematical way with  $\pi^*$  as a measure of the dipolarity of the solvent.

$$\nu_i = \nu_{i0} + p_i \pi^* + b_i \beta + a_i \alpha \quad (2)$$

$a_i$ ,  $b_i$  and  $p_i$  are parameters of the molecule under investigation. The latter value is related to the change of charge distribution within the molecule whereas the first two parameters characterize therein the acidity ( $a_i$ ) and basicity ( $b_i$ ) in the considered electronic state. Applied to HPTS, specific interactions like the HBs depicted in scheme 1 can be probed in the respective electronic state if reference molecules like 1-hydroxypyrene (pyrenol, PyOH) and the methoxy-derivative of HPTS, 8-methoxypyrene-1,3,6-trisulfonate (MPTS), are at disposal.

Nonspecific dipolar solvation, which contributes to the Stokes-shift in systems with a considerable change of the static dipole moment, can be eliminated by comparison of the spectra of hydroxyl-arenes and their methoxy-derivatives (“differential solvatochromism”) [6, 26, 27]. Only a few ESPT systems were investigated so far, but the known examples share a dependence of solvatochromic shifts on the solvents’  $\beta$ -values. These shifts are more pronounced in fluorescence than in absorption and are explained by a stronger HB from the solute to the solvent in the excited state. This is not unexpected because proton release occurs along this coordinate.

ESPT can also be investigated from the product side, i.e. by inspecting solvatochromism of the conjugated base. All studied examples of naphtholate bases show that the excitation spectra are more affected by the solvent acidity than the emission spectra [6]. Again, this is

reasonable as the basicity of the ESPT products is reduced compared to the ground state since the acidity of the photoacid is increased in the excited state.

The contribution of HB donating, protic solvents to the stabilization of the excited state before ESPT is ambiguous [24, 26]. In HPTS, a strong dependence of the red-shift in fluorescence on parameter  $\alpha$  is observed, whereas in naphthol and its derivatives, only the spectral position of the excitation maximum is sensitive to  $\alpha$  [6]. A meanwhile accepted explanation resolves this discrepancy by ascribing the impact of  $\alpha$  to charge stabilization at the sulfonate groups of HPTS in protic solvents [24]. Recent experiments with derivatives of HPTS show that strongly withdrawing substituents are necessary to enable charge transfer in the excited state [13, 14]. As a consequence, HBs directly from solvent to the hydroxyl-moiety ( $\alpha_1$  in scheme 1) therefore appear less important or even detrimental for the initial stages of ESPT. In conclusion, solvatochromism of fluorescent acids in solvents of varying  $\beta$ -values as well as solvatochromism of the conjugated base in solvents of varying  $\alpha$ -values is promising in search of new ESPT dyes.

In our contribution, we reinvestigate the solvent dependence of spectra of paradigmatic HPTS and compare it to solvatochromism of its sulfonato-deficient derivative PyOH and its methoxy-derivative MPTS. To date, solvent variation of MPTS and HPTS mainly was performed with polar and protic solvents, of which the H-bond donating capability exerted a stronger effect on spectroscopic band position and shape of the solute than their HB accepting power [16, 23, 30, 31]. Multiparameter fitting according to eq. 2 was used to extract the values of  $a_i$  and  $b_i$  [24]. However, when the assumed linearity in the energetics is no longer maintained, such analyses are misleading. Our strategy separates both contributions: in the first part, we focus on the dependence of fluorescence excitation and emission spectra on the Kamlet-Taft parameter  $\beta$  of the solvent which aims at finding reliable values for  $b_i$ . Next, we analyse the influence of solvents on the spectra of MPTS. The reduced basicity of the photoproduct 8-oxypyrene-1,3,6-trisulfonate (OPTS) is characterized by the impact of HB-donating solvents on its spectra. Solubility problems are overcome by the usage of crown ether. The presented results are discussed with respect to our ongoing synthetic work of borondipyromethene (Bodipy, BDP)-dyes [22, 32].

## 2. Experimental Section

**Materials and synthesis.** HPTS (Aldrich, 97%), MPTS (Fluka, 98%), Pyrenol (Aldrich, 98%) and 18-Crown-6 (Aldrich, 99%) were used without further purification. The solvents used in this study were of highest available purity (Spectranal, Chromasolv, Uvasol or HPLC-grade) and –if not– tested for fluorescent impurities. All solvents were used as received.

The p-hydroxystyryl- and p-methoxystyryl-Bodipy-Dyes (HO-BDP, MeO-BDP; scheme 2) were synthesized by the Knoevenagel condensation in boiling toluene of methylated, green fluorescent Bodipy-dyes [22, 32-34] and p-hydroxybenzaldehyde (Aldrich, 98%) or p-methoxybenzaldehyde (Aldrich, 98%), respectively [35]. The raw product was purified twice by column chromatography to finally yield the desired product. Details will be described elsewhere. The solubilities of HO-BDP and MeO-BDP were high enough to record spectra in all solvents; however, due to the vanishingly small fluorescence quantum yield of deprotonated HO-BDP (O-BDP), we synthesized for these measurement HO-BDP lacking the phenyl moiety in the *meso*-position [33, 34].

**Sample preparation - spectra of acidic forms in apolar solvents.** PyOH, MPTS and HPTS were dissolved in methanol (MeOH) or ethanol (EtOH), and an aliquot was taken for each sample which ensured that the optical density in the final experiments was low enough in each case to avoid spectral distortion due to innerfilter effects and emission reabsorption. After complete evaporation of EtOH, the final solvent was added. Visual inspection of the fluorescence by means of blacklight illumination showed us whether enough dye was dissolved for recording reliable fluorescence and excitation spectra. In the cases where no fluorescence could be detected, 10 – 25 mg of crown ether was added in order to improve the solubility of the multiple charged dye anions by complexation of sodium counter ions. The final concentration of the crown ether (< 20mM) resulted in an ionic strength far below those which were reported to influence the spectra of HPTS [36]. Please note also, that the actual concentration of sodium ions is still considerably smaller than millimolarity as the only source of these counter ions was the dye. However, we cross-checked our procedure with solvents where fluorescence was sufficient without addition of the helper molecule (table 1).

Only in a few cases (chloroform (CHCl<sub>3</sub>), methylene chloride (CH<sub>2</sub>Cl<sub>2</sub>) and bromobenzene (BrB)), saturated solutions of the crown ether were able to dissolve some amount of the charged dyes. We were not able to record fluorescence excitation or emission spectra of HPTS and MPTS in cyclohexane, toluene, acetophenone, ethyltrichloroacetate and of HPTS in BrB.

This is a pre-peer reviewed version of the following article: *Phys. Chem. Chem. Phys.*, 2009, *11*, 1416–1426; DOI: 10.1039/b816695a; Reproduced by permission of the PCCP owner societies; <http://www.rsc.org/>

**Sample preparation – spectra of 8-oxypyrene-1,3,6-trisulfonate (OPTS).** An aliquot of HPTS was taken as described above, and the organic solvent was added after complete dryness. Except from water, the solutions showed typical blue fluorescence of HPTS. Therefore, 10 – 25 mg crown ether and additional, solid NaOH (~ 5 – 10 mg) was added. Greenish fluorescence indicated successful deprotonation. Spectra of OPTS could be detected only in a few, highly polar solvents, in which HPTS itself was already analysed. The solubility in protic solvents was higher; only in HFIP, no reliable excitation spectra and a very weak fluorescence spectrum of OPTS was detectable.

**Fluorimetry.** Depicted fluorescence excitation and emission spectra of the blue-green emitting dyes were recorded with a fluorescence spectrophotometer (Fluoromax-3, Jobin-Yvon and FP 6500, Jasco) with 1 nm resolution. Afterwards, spectra were converted to the wavenumber range with the necessary corrections [37]. As far as comparison to reported values is possible, the evaluated maxima of our study lie within  $< 100 \text{ cm}^{-1}$  of ref [24]. Slight deviation ( $< 200 \text{ cm}^{-1}$ ) to the fluorescence values of ref. [30] are noticed.

### 3. Results and Discussion

#### 3.1 Correlation of spectroscopic maxima and $\beta$ -values of the solvents

All used solvent in this section share the property that they are aprotic, i.e.  $\alpha = 0$ . Excitation and emission spectra of PyOH and HPTS in several solvents with similar polarity, i.e. similar values of Kamlet-Taft parameter  $\pi^*$ , are displayed in fig. 1 and 2, respectively. Table 2 summarizes the found spectroscopic maxima. Both dyes exhibit red-shifts of the maxima upon increasing  $\beta$  values of the solvents. These dependencies are displayed in fig. 1c and 2c. The regression lines represent single parameter fits according to eq. 2, of which the slope is  $b_1$  and the intercept at the ordinate is an extrapolation to the transition energy  $\nu_{i0}$  of a non-interacting solvent.  $b_1$  is a property of the solute's electronic state and describes its tendency to release the proton. The results of these one-parameter fits are summarized in table 4.

Solvents with similar  $\pi^*$  values are evenly distributed around the regression lines. PyOH was reported to exhibit only a small change of its static dipole moment [24]. MPTS, which is taken as analogue to HPTS, does not show a clear dependence in a Lippert-Ooshika-Mataga plot (data not shown). This is compatible with a minor change of the static dipole moment upon excitation, which is predicted by theoretical calculations [30]. It is therefore justified to

neglect the dependency of the energy gap on  $\pi^*$  while applying eq. 2 to solvatochromism of HPTS and PyOH.

The obtained  $b_i$  values are close for HPTS and PyOH ( $-320\text{ cm}^{-1}$  vs.  $-390\text{ cm}^{-1}$  for  $b_{\text{exc}}$ ;  $-560\text{ cm}^{-1}$  vs.  $-530\text{ cm}^{-1}$  for  $b_{\text{em}}$ ). The hydroxyl-moieties are more strongly interacting with the solvent in the excited than in the ground state as indicated by  $|b_{\text{em}}| > |b_{\text{exc}}|$ . This is in agreement with a higher acidity in the excited state and resembles the behaviour of naphthol derivatives [6, 26].

For comparison, we also investigated the solvatochromism of MPTS. The  $b_i$ -values for MPTS are close to 0 within their error limits (fig. 2d). This is expected due to lack of an acidic proton. The data also verify that other acidic hydrogen atoms in the core structure are missing. Specific and reliable assignment of spectroscopic changes to an altered local environment can be found out by differential solvatochromism [6, 26]. Here, the frequency values  $\nu_i$  of HPTS are subtracted from those of MPTS and, subsequently, the spectroscopic differences can be traced back to HB differences among different solvents. It is assumed that other solvent-solute interactions are cancelled. Taking the differences between the excitation and emission maxima yields  $b'_{\text{exc}} = -360$  ( $\pm 90$ )  $\text{cm}^{-1}$  and  $b'_{\text{em}} = -630$  ( $\pm 170$ )  $\text{cm}^{-1}$ , and thus, similar values as above are obtained within the error limits (table 4). Bathochromic shifts in HPTS with increasing HB-accepting power of the solvent, therefore, reflect solely the increased HB-strength in the excited state of the solute compared to its ground state.

We conclude that the acidity of HPTS upon excitation is rather similar to the increased acidity of PyOH. However, even a small discrepancy might not explain the differences in the ESPT behaviour: HPTS easily releases a proton to water whereas PyOH requires “catalysis” by hydrogenphosphate [31].

### 3.2 Influence of HB-donating solvents on the spectra of MPTS

The missing differences of spectroscopic behaviour between PyOH and HPTS encouraged us to investigate the influence of increasing  $\alpha$ -values of the solvent. Previously, HPTS was examined in a variety of solvents, and multiparameter fitting of the spectroscopic maxima was performed [24]. While  $b_{\text{exc}}$  reported in this reference is close to our value,  $b_{\text{em}}$  deviates strongly. As redoing the same measurements presumably would not lead to different results, we performed fluorescence spectroscopy of MPTS in different solvents (fig. 3 and table 3). MPTS can substitute HPTS due its spectroscopic, chemical and electronic similarity [16, 30]. The extrapolated values of  $\nu_{i0}$  in fig. 2c and 2d coincide within the error limits (table 4) and, thus, verify this similarity. MPTS, however, is convenient as it does not exhibit a

spectroscopic dependence on the HB-accepting power of the solvent. As shown in section 3.1,  $p_i$  and  $b_i$  of MPTS are approximately 0. Hence, solvatochromism can be analysed on the basis of varying  $\alpha$ -values independent of the solvent's  $\beta$ -value and multiparameter fits can be avoided. This is helpful in screening applications where elaborate computations should be avoided. Figure 3a shows the excitation and figure 3b the emission spectra of MPTS in several solvents with differing  $\alpha$ -values. Increasing  $\alpha$ -values are accompanied by bathochromic shifts both in excitation and emission. This behaviour is different to what has been described for naphthol-derivatives and PyOH [24, 26]. A blue-shift of the electronic spectra, which corresponds to positive  $a_i$  values, is explained by a HB between the oxygen atoms of the aromatic alcohols and the solvent (e.g.  $\alpha_1$  in scheme 1) which is weakened upon excitation. In terms of the molecular electronics of the probe molecule, electron density is transferred from the donor to the aromatic core upon excitation.

A plot of the spectroscopic maxima against  $\alpha$  can return  $a_{exc}$  and  $a_{em}$  of MPTS after fitting, which is a measure of the HB-accepting character of the respective electronic state (fig. 3c). The extracted value for  $a_{exc}$ ,  $-350$  ( $\pm 70$ )  $\text{cm}^{-1}$ , is of the same order as the value given by ref. [24] for HPTS. A negative value (in HPTS) was traced back to the increasing electron withdrawing power of sulfonate groups in conjunction with the donor ability of a hydroxyl-group. The sulfonamide derivative of HPTS, in which the electron-withdrawing strength of the substituents is further enhanced, also exhibit red-shifted spectra compared to HPTS [13, 15]. The same argumentation also holds for MPTS. It is worth to mention that the observed red-shift is likely reduced due to the blue-shift due to HB directly at the methoxy-position.

The influence of  $\alpha$  on the fluorescence maxima is more complex. While at low HB-donating ability, the fluorescence is (more or less linearly) bathochromically shifted by a higher solvent acidity. The observed Stokes-shifts ( $\nu_{exc} - \nu_{em}$ ) are in the range of the extrapolated values of HPTS and MPTS in the  $\beta$ -dependence plot (fig. 2c, d;  $\nu_{exc,0} - \nu_{em,0}$ ). In contrast, the fluorescence emission maxima are nearly constant at high  $\alpha$  values. A change of behaviour appears around a  $\alpha$ -value of 0.7 - 0.8. Both sections are separated by a step of  $\sim 1000$   $\text{cm}^{-1}$ . Also the line shape changes [38]. In HPTS under highly acidic conditions, this change of behaviour was attributed to charge redistribution, but was explicitly excluded for MPTS [14]. We, however, argue by means of a rough estimate that, indeed, MPTS and HPTS are identical in the occurrence of the charge transfer state:  $\nu_{em}$  of MPTS in water is  $\sim 22900$   $\text{cm}^{-1}$  which is larger by  $\sim 300$   $\text{cm}^{-1}$  than the value of  $\nu_{em}$  of HPTS [24]. If we add the bathochromic shift due to HB between the base  $\text{H}_2\text{O}$  and the photoacid HPTS, then we further reduced the transition

energy by  $b_{em} \cdot \beta$  (the  $\beta$ -value of H<sub>2</sub>O is  $\sim 0.5$ ) which is in the range of the missing 300 cm<sup>-1</sup>. The mentioned change of spectroscopic behaviour, although not further quantified, has impact on previous solvatochromic investigations: it indicates that multiparameter fitting procedures are misleading when a linear dependence is not given. This might especially be important in the investigation of chemical reactions.

### 3.3 Influence of HB-donating solvents on the spectra of OPTS

The deprotonated OPTS is the photoproduct after ESPT of HPTS. The idea behind the investigation of its solvatochromism in  $\alpha$ -solvents is that we now explore ESPT dyes from the photoproduct side. We would like to find out whether this approach is appropriate to find target structures. First of all, the response of the OPTS-spectra to stronger HB from the solvent allows for verifying whether the basicity of the excited state is reduced compared to the ground state. For very strong photoacids,  $|a_{em}| < |a_{exc}|$  was found in agreement with a higher excited state acidity and opposite to the effect of HB-donating solvents at the reactant side. The values are positive indicating spectral blueshifts with increasing solvent acidity (fig. 4a). For the search of ESPT dye, the  $a_{em}$  values, which are specific for the properties of the excited state, are more important.

Fluorescence emission spectra of OPTS in different solvents are depicted in fig. 4b, and the spectral maxima positions versus the solvents  $\alpha$ -value are shown in fig. 4c. The spectra in highly protic solvents are broader than in aprotic solvents; however the centre is hardly affected by the  $\alpha$ -value:  $a_{em}$ , obtained as +240 (+/- 60) cm<sup>-1</sup> from the linear fit in fig. 4c, indeed is comparably small with respect to other deprotonated ESPT dyes [6]. The peak positions of fluorescence in purely aprotic solvents ( $\alpha = 0$ ) cover a spectral range which is as large as the whole energetic variation due to HB. Thus, these non-HB interactions are equally important for the spectral position, and might be the reason for the low correlation value of  $a_{em}$  and  $a_{exc}$  ( $R = 0.75$ ) in our one-parameter correlation. However, a correlation with polarity ( $\pi^*$  or the dielectric constant  $\epsilon_{rel}$ ) was not found. In contrast to the excited state, the ground state is more sensitive to HB as expected for a base ( $a_{exc} = + 780 (+/- 210)$  cm<sup>-1</sup>). The acidity of HFiP ( $pK_A = 9.3$ ), which shifts the equilibrium to HPTS, might therefore be the reason, why only rather poor spectra of OPTS could be obtained in this solvent.

It is interesting to compare the effect of solvents with high  $\alpha$ -values on the emission spectra of MPTS, which is similar to HPTS shortly before ESPT, and OPTS, which is HPTS after the

3.4 *Phys. Chem. Chem. Phys.* **2009**, *11*, 1416- 1426

ESPT. Although the HB at the electron-donor moiety (methoxy-group vs. oxy-group) is different in both species, the HB at the sulfonate-groups is nearly identical.  $a_{em}$  of MPTS, although not further determined (fig. 3c), and  $a_{em}$  of OPTS are in a similar range. This comparison shows that, once charge redistribution occurred at a  $\alpha$ -value of  $\sim 0.8$ , excited HPTS becomes more acidic than before and only then the proton can be transferred to the solvent without the need of catalysts. This is also reflected by the equilibrium constant of  $HPTS + H_2O/OPTS + H_3O^+$  which is shifted to the neutral chromophore state on a time scale before charge redistribution occurs [18]. It is vain to discuss whether  ${}^1L_a/{}^1L_b$  state reversal or not occurs along the ESPT-coordinate on the basis of our experiments [16, 24, 38]. Nevertheless, we adhere to the mentioned acidity change in the excited state of HPTS as the difference to PyOH.

### 3.4 Discussion of solvent effects with respect to HO-BDP

According to the revisited solvatochromism of HPTS, the wealth of available dyes can be narrowed down during the search of ESPT-dyes by the investigation of solvatochromism. In this last section, we would like to discuss the example where an acidity increase of an aromatic alcohol is not observed although fluorescence emission data misled us to assume its ESPT-capability. This is the case of HO-BDP (scheme 2).

We applied the solvatochromic method to HO-BDP in order to find out whether this compound might be a target structure for an ESPT-dye in the visible range. Bodipy-dyes exhibit high fluorescence quantum yields, are superior to fluoresceine dyes in terms of photostability and are therefore appropriate for our long-term goal of ESPT-dyes in the visible range [22, 32-34]. The dye in the focus of this section has in its neutral form  $\lambda_{exc} = 569$  nm,  $\lambda_{em} = 581$  nm and in its anionic form  $\lambda_{exc} = 573$  nm,  $\lambda_{em} \sim 710$  nm (fig. 5a). According to eq. 1, one calculates  $\Delta pK_a = 0.25$  on the basis of the excitation data and  $\Delta pK_a = 6.55$  on the basis of the emission data. Even if we take the average, as suggested by ref. [5], then a distinct increase of the acidity by more than 3 orders of magnitude could be expected.

Other dyes with styryl-moieties were shown to exhibit ESPT [7]. However, we were led by the spectroscopic similarity of ammonium-group and hydroxyl-groups and their deprotonated counterparts, i.e. amino-groups and oxy-substituents. The comparability is e.g. manifested in substituted xanthene dyes, i.e. rhodamine vs. fluoresceine dyes. With respect to ESPT, the similarity was already noticed by Förster [1, 2] and, quite recently, by time-resolved spectroscopy [14]. Differences between isoelectronic  $NH_3^+$  and OH-groups concern the  $pK_a$ -values of the considered dyes.

This is a pre-peer reviewed version of the following article: *Phys. Chem. Chem. Phys.*, 2009, *11*, 1416–1426; DOI: 10.1039/b816695a; Reproduced by permission of the PCCP owner societies; <http://www.rsc.org/>

The synthesis and spectroscopic properties of p-dimethylaminostyryl-Bodipy dyes (NMe<sub>2</sub>-BDP) were published in the last years [35, 39], and recently, we performed theoretical calculations to elucidate its ESPT-behaviour [40]. Whereas the protonated dye exhibits only small Stokes-shifts upon excitation, the neutral chromophore undergoes charge-transfer with a large change of the static dipole moment. The reported spectroscopic values of excitation and emission maxima for NMe<sub>2</sub>-BDP and its conjugated acid NMe<sub>2</sub>H<sup>+</sup>-BDP are close to our values of the pair HO-BDP/O-BDP. We therefore assume that all conclusions drawn for NMe<sub>2</sub>-BDP/NMe<sub>2</sub>H<sup>+</sup>-BDP pair also hold for HO-BDP/O-BDP although we did not perform such elaborate solvatochromic studies as in ref. [39]. We summarize that if ESPT occurs then charge-transfer as the thermodynamic driving force would act only *after* ESPT.

We studied the solvatochromism of HO-BDP in β-solvents (fig. 5b-d). We renounced the aromatic solvents benzonitrile (3), bromobenzene (4) and toluene (23) which showed systematic deviations in the spectra of PyOH and HPTS. We assign this to putative π-π interactions between the solvent and the aromatic solute. The b<sub>i</sub>-values, b<sub>exc</sub> and b<sub>em</sub>, are close to the values of PyOH and HPTS (table 4). However, the uncritical interpretation as an increased acidity in the excited state like in the case of PyOH and HPTS fails: the β-dependence of the spectra of the methoxy-derivative MeO-BDP as well as differential solvatochromism provide evidence that the acidity of the OH-group is not substantially raised and that some other slightly acidic proton exists within the molecule (table 4). Very acidic solvents like hexafluoro-2-propanol shift both excitation and emission spectra of MeO-BDP in equal measure to the blue (fig. 5e, f). The blue-shift is in agreement with a reduction of the donor properties of the methoxy-moiety; the likewise blue-shift in the ground state as well as in the excited state imply, however, that a<sub>exc</sub> ~ a<sub>em</sub> and that no additional electron density is shifted from the electron donor toward the aromatic system in the excited state.

We also performed excitation and emission spectra of O-BDP, the conjugated base of HO-BDP, in dependence of the α-value of some protic solvents (solvents 12, 14, 15, 18, 19, 24, 25; fig. 5a). They share as common property a similar Lippert solvation parameters Δf ~ 0.3

$$\Delta f = \frac{\epsilon_{rel} - 1}{2\epsilon_{rel} + 1} - \frac{n^2 - 1}{2n^2 + 1} \quad (3)$$

where ε<sub>rel</sub> is the dimensionless dielectric constant and n the refractive index of the solvent. This should ensure that the contribution of unspecific dipolar solvation is cancelled. A slight blue-shift of the excitation spectra was found for O-BDP, a<sub>exc</sub> = + 190 cm<sup>-1</sup>, which is unexpectedly small for a base on the basis of naphtholate or OPTS data [6]. One has to consider the noticed solvatochromism of MeO-BDP in the sense that here also the β-values of

the solvents have impact on the spectral position. For  $a_{em}$ , however, we could not find a clear dependence. All fluorescence maxima lie within a range of 705 to 710 nm. The fact that all recorded emission data are broad in combination with very weak fluorescence aggravates here the analysis and a proper assignment of the emission maxima is hardly achievable. Moreover, it is questionable whether one-parameter fitting can fully describe the solvatochromism of a charge-transfer dye, even if solvents with similar  $\Delta f$ -values but differing  $\alpha$ -values are used. Nevertheless, our data are in good agreement with the behaviour of NMe<sub>2</sub>-BDP where vanishingly small  $a_{exc}$  and  $a_{em}$  were found by multiparameter fitting [39].

In summary, the situations for HPTS (at early times), PyOH and HO-BDP are not so different: whenever a suitable proton acceptor is so close that proton transfer can occur, this will happen in the excited state [31, 41]. For example, ultrafast ESPT to acetate was observed for HPTS on a time scale before charge redistribution occurs [36]. However, differences among the investigated dyes concern the time scales of proton transfer. The rate constants for proton transfer are related to the free energy release  $\Delta G$  during the reaction [42]. This is also exemplified in the protonation kinetics of pyrene-1-carboxylate by various acids [20]. While the acidity increase of HPTS (at early times) and PyOH, which is probed by the variation of the solvent  $\beta$ -value, consequently enables proton transfer during the excited state lifetime, ESPT is rather unlikely to proceed in HO-BDP. If, however, ESPT accidentally occurs in HO-BDP, then the energy release due to solvation in the anionic state would lock the thermodynamics.

We therefore conclude that the spectroscopic signature which points to the ESPT propensity is likely the difference of the excitation maxima of acid and conjugated base, i.e. the transition energy difference  $\Delta v_{exc0}$  before solvent relaxation occurs.  $\Delta v_{exc0}$  be regarded as a measure for the gradient of ESPT although subtleties of the potential energy surface are ignored. In the case of HO-BDP,  $\Delta v_{exc0}$  is 100-150 cm<sup>-1</sup> which is in contrast to a roughly ten times larger value of PyOH [31].

#### 4. Conclusion

In our contribution, we investigated the solvatochromism of several dyes with the aim to predict the ESPT behaviour of freshly synthesized dyes. The dyes HPTS, PyOH and HO-BDP are all aromatic alcohols but decreasingly tend to undergo ESPT. The strong photoacidity of HPTS presumably results from charge redistribution in succession of solvent rearrangement, i.e. the formation of strong electron withdrawing substituents by HB from solvent to HPTS

[14, 24]. PyOH, HO-BDP and many naphtholes have in common that acidic solvents do not accelerate ESPT. We therefore propose the following criteria to distinguish potential ESPT dyes like PyOH from slower reacting dyes like HO-BDP. Firstly, differences in  $\Delta v_{\text{exc0}}$  are related to the thermodynamics and should hint at the overall ESPT driving force. The best procedure would be to compare the spectra in a solvent of low polarity; solubility problems can be overcome by use of crown ether. Secondly, spectra of the acid in solvents with varying  $\beta$ -values should explore their kinetic tendency of ESPT. Differential solvatochromism ensures to assign observed effects to a certain proton. In the case where methoxy-derivatives are not available, solvents of similar polarity are preferential. A set of 5 solvents (butyrolactone, dimethylformamide, hexamethylphosphoric triamide, propylene carbonate and tetramethylurea) covers a large range of  $\beta$ -values and should provide already insight into the ESPT behaviour. Finally, we do not recommend judging the ESPT tendency on the basis of  $a_{\text{em}}$  since dipolar relaxation might mask subtle effects of the solvent acidity.

**Acknowledgement:** The authors thank M. Wild for assistance in the synthetic work and I. Bernhardt for generous support. The work was supported by the German Science Foundation (DFG JU650/1).

## References:

- [1] Th. Förster, *Naturwissen.* **36** (1949), 186.
- [2] Th. Förster, *Z. Elektrochem.* **54** (1950), 42.
- [3] O. Mohammed, D. Pines, J. Dreyer, E. Pines, E. Nibbering, *Science* **310** (2005), 83.
- [4] P. Wan, D. Shukla, *Chem. Rev.* **93** (1993), 571.
- [5] L. Tolbert, K. Solntsev, *Acc. Chem. Res.* **35** (2003), 19.
- [6] N. Agmon, *J. Phys. Chem. A* **109** (2005), 13.
- [7] F. Lewis, L. Sinks, W. Weigel, M. Sajimon, E. Crompton, *J. Phys. Chem. A* **109** (2005), 2443.
- [8] B. Cohen, D. Huppert, *J. Phys. Chem. A* **105** (2001), 7157.
- [9] A. Orte, L. Crovetto, E. Talavera, N. Boens, J. Alvarez-Pez, *J. Phys. Chem. A* **109** (2005), 734.
- [10] M. Chattoraj, B. King, G. Bublitz, S. Boxer, *Proc. Natl. Acad. Sci. USA* **93** (1996), 8362.
- [11] H. Lossau, A. Kummer, R. Heinecke, F. Pöllinger-Dammer, C. Kompa, G. Bieser, T. Jonsson, C. Silva, M. Yang, D. Youvan, M. Michel-Beyerle, *Chem. Phys.* **213** (1996), 1.
- [12] B. Cohen, J. Segal, D. Huppert, *J. Phys. Chem. A* **106** (2002), 7462.
- [13] D. Spry, M. Fayer, *J. Chem. Phys.* **127** (2007), 204501.
- [14] D. Spry, M. Fayer, *J. Chem. Phys.* **128** (2008), 084508.
- [15] E. Pines, D. Pines, Y.-Z. Ma, G. Fleming, *ChemPhysChem* **5** (2004), 1315.
- [16] O. Mohammed, J. Dreyer, B. Magnes, E. Pines, E. Nibbering, *ChemPhysChem* **6** (2005), 625.
- [17] T. Tran-Thi, T. Gustavsson, C. Prayer, S. Pommeret, J. Hynes, *Chem. Phys. Lett.* **329** (2000), 421.
- [18] P. Leiderman, L. Genosar, D. Huppert, *J. Phys. Chem. A* **109** (2005), 5965.
- [19] K. Solntsev, D. Huppert, N. Agmon, *Phys. Rev. Lett.* **86** (2001), 3427.
- [20] B. Zelent, J. Vanderkooi, R. Coleman, I. Gryczynski, Z. Gryczynski, *Biophys. J.* **91** (2006), 3864.
- [21] A. Kotlyar, N. Borovok, S. Raviv, L. Zimanyi, M. Gutman, *Photochem. Photobiol.* **63** (1996), 448.
- [22] B. Hinkeldey, A. Schmitt, G. Jung, *ChemPhysChem* **9** (2008), 2019.
- [23] N. Barrash-Shiftan, B. Brauer, E. Pines, *J. Phys. Org. Chem.* **11** (1998), 743.
- [24] T.-H. Tran-Thi, C. Prayer, Ph. Millié, P. Uznanski, J. Hynes, *J. Phys. Chem. A* **106** (2002), 2244.
- [25] K. Solntsev, D. Huppert, L. Tolbert, N. Agmon, *J. Am. Chem. Soc.* **120** (1998), 7981.
- [26] K. Solntsev, D. Huppert, N. Agmon, *J. Phys. Chem. A* **102** (1998), 9599.
- [27] K. Solntsev, D. Huppert, N. Agmon, *J. Phys. Chem. A* **103** (1999), 6984.
- [28] M. Kamlet, J. Abboud, M. Abraham, R. Taft, *J. Org. Chem.* **48** (1983), 2877.
- [29] C. Reichardt, *Solvent and Solvent Effects in Organic Chemistry*, 2<sup>nd</sup> Ed. 1988, VCh (Weinheim).
- [30] R. Jimenez, D. Case, F. Romesberg, *J. Phys. Chem. B* **106** (2002), 1090.
- [31] B. Milosavljevic, J. Thomas, *Photochem. Photobiol. Sci.* **1** (2002), 100.
- [32] A. Schmitt, B. Hinkeldey, M. Wild, G. Jung, *J. Fluoresc.*, in press; DOI 10.1007/s10895-008-0446-7.
- [33] G. Ulrich, R. Ziessel, A. Harriman, *Angew. Chem.* **120** (2008), 1202; *Angew. Chem. Int. Ed.* **47** (2008), 1184.
- [34] A. Loudet, K. Burgess, *Chem. Rev.* **107** (2007), 4891.
- [35] K. Rurack, M. Kollmannsberger, J. Daub, *Angew. Chem.* **113** (2001), 396.
- [36] L. Genosar, D. Cohen, D. Huppert, *J. Phys. Chem. A* **104** (2000), 6689
- [37] J. Lakowicz, *Principles of Fluorescence Spectroscopy*, 2<sup>nd</sup> ed., 2000.

This is a pre-peer reviewed version of the following article: Phys. Chem. Chem. Phys., 2009, 11, 1416–1426; DOI: 10.1039/b816695a; Reproduced by permission of the PCCP owner societies; <http://www.rsc.org/>

- [38] D. Spry, A. Goun, C. Bell, M. Fayer, *J. Chem. Phys.* **125** (2006), 144514.
- [39] M. Baruah, W. Qin, C. Flors, J. Hofkens, R. Vallée, D. Beljonne, M. Van der Auweraer, W. Borggraeve, N. Boens, *J. Phys. Chem. A* **110** (2006), 5998.
- [40] O. Clemens, M. Basters, M. Wild, S. Wilbrand, C. Reichert, M. Bauer, M. Springborg, G. Jung, *J. Mol. Struct.: THEOCHEM* **866** (2008), 15.
- [41] T. Thun, *J. Fluoresc.* **13** (2003), 323.
- [42] E. Pines, G. Fleming, *J. Phys. Chem.* **95** (1991), 10448.
- [43] I. Renge, *J. Phys. Chem. A* **104** (2000), 7452.

**Tables:**Table 1: Used solvents in this study and their physical (refractive index  $n_0$ , dielectric constant  $\epsilon_{rel}$ ) and solvatochromic parameters ( $\alpha$ ,  $\beta$ ,  $\pi^*$ ) [24, 28, 43].

| #  | Solvent                        | $\alpha$ | $\beta$ | $\pi^*$ | $\epsilon_{rel}$ | $n_0$ | PyOH | HPTS | MPTS | OPTS |
|----|--------------------------------|----------|---------|---------|------------------|-------|------|------|------|------|
| 1  | Acetone                        | 0.08     | 0.48    | 0.71    | 20.56            | 1.359 | -    | -    | +    | --   |
| 2  | Acetonitrile                   | 0.19     | 0.31    | 0.75    | 35.94            | 1.344 | -    | -    | +    | 0    |
| 3  | Benzonitrile                   | 0        | 0.41    | 0.90    | 25.20            | 1.528 | --   | +    | +    | -    |
| 4  | Bromobenzene                   | 0        | 0.07    | 0.71    | 5.40             | 1.557 | +    | --   | --   | -    |
| 5  | Butyrolactone                  | 0        | 0.49    | 0.87    | 40.96            | 1.437 | +    | +    | +    | --   |
| 6  | Chloroform                     | 0.44     | 0       | 0.58    | 4.81             | 1.446 | -    | -    | 0    | --   |
| 7  | Cyclohexane                    | 0        | 0       | 0       | 2.02             | 1.426 | +    | --   | --   | -    |
| 8  | Dichloromethane                | 0.30     | 0       | 0.82    | 8.93             | 1.424 | -    | -    | 0    | --   |
| 9  | Dimethyl-formamide             | 0        | 0.69    | 0.88    | 36.71            | 1.431 | +    | +    | +    | 0    |
| 10 | Dimethyl sulfoxide             | 0        | 0.76    | 1.00    | 46.45            | 1.479 | +    | +    | +    | +    |
| 11 | Dioxane                        | 0        | 0.37    | 0.55    | 2.21             | 1.422 | +    | +    | +    | --   |
| 12 | Ethanol                        | 0.83     | 0.77    | 0.54    | 24.55            | 1.361 | -    | -    | +    | +    |
| 13 | Ethyl acetate                  | 0        | 0.45    | 0.55    | 6.02             | 1.372 | +    | 0    | 0    | -    |
| 14 | Ethylene glycol                | 0.90     | 0.52    | 0.92    | 37.7             | 1.432 | -    | -    | +    | +    |
| 15 | Formamide                      | 0.71     | 0.48    | 0.97    | 111.0            | 1.448 | -    | -    | +    | +    |
| 16 | Hexafluoro-2-propanol          | 1.96     | 0       | 0.65    | 16.70            | 1.275 | -    | -    | +    | 0    |
| 17 | Hexamethyl-phosphoric triamide | 0        | 1.05    | 0.87    | 29.6             | 1.459 | +    | +    | +    | 0    |
| 18 | Methanol                       | 0.93     | 0.62    | 0.60    | 32.66            | 1.328 | -    | -    | +    | +    |
| 19 | 2-Propanol                     | 0.76     | 0.95    | 0.48    | 19.92            | 1.377 | -    | -    | +    | +    |
| 20 | Propylene carbonate            | 0        | 0.40    | 0.83    | 64.92            | 1.422 | +    | +    | +    | +    |
| 21 | Tetrahydrofuran                | 0        | 0.55    | 0.58    | 7.58             | 1.407 | +    | +    | +    | --   |
| 22 | Tetramethylurea                | 0        | 0.80    | 0.83    | 23.60            | 1.449 | +    | +    | +    | 0    |
| 23 | Toluene                        | 0        | 0.11    | 0.54    | 2.38             | 1.497 | +    | --   | --   | -    |
| 24 | Trifluoroethanol               | 1.51     | 0       | 0.73    | 26.53            | 1.30  | -    | -    | +    | +    |
| 25 | Water                          | 1.17     | 0.47    | 1.09    | 78.30            | 1.333 | -    | -    | +    | +    |

Definition of symbols: +: good spectra; 0: noisy spectra or spectra under extreme conditions recorded; --: no spectra obtained; -: no spectra recorded.

Table 2: Fluorescence excitation and emission maxima of PyOH, HPTS and MPTS in  $\beta$ -solvents ( $\alpha = 0$ ) (+/- 30  $\text{cm}^{-1}$ ).

| #  | solvent                       | Excitation maximum / $\text{cm}^{-1}$ |       |       | Emission maximum / $\text{cm}^{-1}$ |       |       |
|----|-------------------------------|---------------------------------------|-------|-------|-------------------------------------|-------|-------|
|    |                               | PyOH                                  | HPTS  | MPTS  | PyOH                                | HPTS  | MPTS  |
| 3  | Benzonitrile                  | -                                     | 24913 | 25106 | -                                   | 24308 | 24613 |
| 4  | Bromobenzene                  | 26010                                 | -     | -     | 25820                               | -     | -     |
| 5  | Butyrolactone                 | 25963                                 | 25120 | 25222 | 25775                               | 24675 | 24827 |
| 7  | Cyclohexane                   | 26167                                 | -     | -     | 26071                               | -     | -     |
| 9  | Dimethylformamide             | 25881                                 | 25111 | 25274 | 25638                               | 24671 | 24926 |
| 10 | Dimethyl sulfoxide            | 25793                                 | 24951 | 25155 | 25569                               | 24373 | 24694 |
| 11 | Dioxane                       | 26001                                 | 25099 | 25218 | 25834                               | 24665 | 24848 |
| 13 | Ethyl acetate                 | 26040                                 | 25093 | 25285 | 25884                               | 24581 | 24902 |
| 17 | Hexamethylphosphoric triamide | 25751                                 | 24890 | 25299 | 25507                               | 24271 | 24943 |
| 20 | Propylene carbonate           | 26016                                 | 25150 | 25182 | 25824                               | 24722 | 24706 |
| 21 | Tetrahydrofuran               | 25957                                 | 25075 | 25271 | 25783                               | 24615 | 24888 |
| 22 | Tetramethylurea               | 25863                                 | 25066 | 25283 | 25632                               | 24570 | 24921 |
| 23 | Toluene                       | 26060                                 | -     | -     | 25916                               | -     | -     |

Table 3: Fluorescence excitation and emission maxima of MPTS and OPTS in  $\alpha$ -solvents (+/- 30  $\text{cm}^{-1}$ ).

| #  | solvent               | Excitation maximum / $\text{cm}^{-1}$ |       | Emission maximum / $\text{cm}^{-1}$ |       |
|----|-----------------------|---------------------------------------|-------|-------------------------------------|-------|
|    |                       | MPTS                                  | OPTS  | MPTS                                | OPTS  |
| 1  | Acetone               | 25370                                 | -     | 25035                               | -     |
| 2  | Acetonitrile          | 25297                                 | 20619 | 24886                               | 19493 |
| 6  | Chloroform            | 25056                                 | -     | 24563                               | -     |
| 8  | Dichloromethane       | 25076                                 | -     | 24592                               | -     |
| 12 | Ethanol               | 25076                                 | 21459 | 24450                               | 19608 |
| 14 | Ethylene glycol       | 24862                                 | 21645 | 23753                               | 19531 |
| 15 | Formamide             | 24788                                 | 21142 | 23474                               | 19268 |
| 16 | Hexafluoro-2-propanol | 24629                                 | -     | 23310                               | 19763 |
| 18 | Methanol              | 25049                                 | 21838 | 24213                               | 19646 |
| 19 | 2-Propanol            | 25136                                 | 21097 | 24691                               | 19569 |
| 24 | Trifluoroethanol      | 24779                                 | 23095 | 23419                               | 19685 |
| 25 | Water                 | 24797                                 | 21692 | 22936                               | 19569 |

Table 4: Fitting results of solvatochromism experiments. All data are obtained using linear fits according to equation 2. R denotes the correlation coefficient.

| Spectra : solvent dependence |                             | fig. | ordinate intercept / $\text{cm}^{-1}$ | slope $a_i, b_i / \text{cm}^{-1}$  | R    |
|------------------------------|-----------------------------|------|---------------------------------------|------------------------------------|------|
| exc.                         | PyOH: $\beta$               | 1a,c | $v_{\text{exc}0}$ : 26150 (+/- 20)    | $b_{\text{exc}}$ : - 390 (+/- 40)  | 0.96 |
|                              | HPTS: $\beta$               | 2a,c | $v_{\text{exc}0}$ : 25260 (+/- 50)    | $b_{\text{exc}}$ : - 320 (+/- 80)  | 0.84 |
|                              | MPTS: $\beta$               | 2d   | $v_{\text{exc}0}$ : 25190 (+/- 50)    | $b_{\text{exc}}$ : + 90 (+/- 80)   | 0.38 |
|                              | Diff. solvato-chrom. HPTS   | -    | 30 (+/- 60)                           | $b'_{\text{exc}}$ : -360 (+/- 90)  | 0.82 |
|                              | HO-BDP                      | 5b,d | $v_{\text{exc}0}$ : 17635 (+/- 40)    | $b_{\text{exc}}$ : - 350 (+/- 70)  | 0.87 |
|                              | MeO-BDP                     | 5e   | $v_{\text{exc}0}$ : 17620 (+/- 50)    | $b_{\text{exc}}$ : - 160 (+/- 80)  | 0.58 |
|                              | Diff. solvato-chrom. HO-BDP |      | 10 (+/- 20)                           | $b'_{\text{exc}}$ : -190 (+/- 30)  | 0.91 |
|                              | MPTS: $\alpha$              | 3a   | $v_{\text{exc}0}$ : 25280 (+/- 60)    | $a_{\text{exc}}$ : - 350 (+/- 70)  | 0.86 |
|                              | OPTS: $\alpha$              | 4a   | $v_{\text{exc}0}$ : 20830 (+/- 160)   | $a_{\text{exc}}$ : + 780 (+/- 210) | 0.75 |
|                              | O-BDP: $\alpha$             | 5a   | $v_{\text{exc}0}$ : 17190 (+/- 80)    | $a_{\text{exc}}$ : + 190 (+/- 80)  | 0.74 |
| em.                          | PyOH: $\beta$               | 1b,c | $v_{\text{em}0}$ : 26040 (+/- 30)     | $b_{\text{em}}$ : - 530 (+/- 50)   | 0.96 |
|                              | HPTS: $\beta$               | 2b,c | $v_{\text{em}0}$ : 24920 (+/- 90)     | $b_{\text{em}}$ : - 560 (+/- 140)  | 0.83 |
|                              | MPTS: $\beta$               | 2d   | $v_{\text{em}0}$ : 24760 (+/- 100)    | $b_{\text{em}}$ : + 150 (+/- 150)  | 0.36 |
|                              | Diff. solvato-chrom. HPTS   | -    | 100 (+/- 110)                         | $b'_{\text{em}}$ : - 630 (+/- 170) | 0.80 |
|                              | HO-BDP                      | 5c,d | $v_{\text{em}0}$ : 17340 (+/- 50)     | $b_{\text{em}}$ : - 525 (+/- 90)   | 0.91 |
|                              | MeO-BDP                     | 5f   | $v_{\text{em}0}$ : 17320 (+/- 50)     | $b_{\text{em}}$ : - 310 (+/- 80)   | 0.81 |
|                              | Diff. solvato-chrom. HO-BDP | -    | 10 (+/- 30)                           | $b'_{\text{em}}$ : - 220 (+/- 40)  | 0.87 |
|                              | MPTS: $\alpha$              | 3b   | not determined                        | not determined                     | -    |
|                              | OPTS: $\alpha$              | 5    | $v_{\text{em}0}$ : 19330 (+/- 50)     | $a_{\text{em}}$ : + 240 (+/- 60)   | 0.75 |
|                              | O-BDP: $\alpha$             | 5a   | not determined                        | not determined                     | -    |

**Scheme captions:**

**Scheme 1:** Structure of HPTS, its anionic form OPTS and the reference dyes MPTS and PyOH. HB between protic solvents (HS) and basic solvents (S) are probed by varying  $\alpha$ - and  $\beta$ -values of the solvent. The effect of HB at the donor and the sulfonate-groups differs as indicated by the subscript.

**Scheme 2:** Structures of the synthesized Bodipy-dyes. HO-BDP ( $R_1 = \text{HO-}$ ) and MeO-BDP ( $R_1 = \text{HO-}$ ) were carrying a phenyl-group in the meso-position ( $R_2 = \text{Phenyl-}$ ). Only for the measurements of the spectra of O-BDP (fig. 5a), we used a better soluble and more fluorescent HO-BDP ( $R_1 = \text{HO-}$ ,  $R_2 = \text{H-}$ ).

**Figure captions:**

**Figure 1:** Solvatochromism of PyOH in solvents with varying  $\beta$ -values ( $\alpha = 0$ ). Depicted numbers correspond to the solvent numbers in table 1.

a) Fluorescence excitation spectra ( $\lambda_{\text{det}} = 380 - 420 \text{ nm}$ ). b) Fluorescence emission spectra ( $\lambda_{\text{exc}} = 365 - 375 \text{ nm}$ ). c) Plot of all spectroscopic maxima versus the solvent's  $\beta$ -value. The grey lines represent linear fits to the excitation maxima (open circles) and emission maxima (filled triangles), respectively. For PyOH,  $b_{\text{exc}} = -390 (+/- 40) \text{ cm}^{-1}$  and  $b_{\text{em}} = -530 (+/- 50) \text{ cm}^{-1}$ . The data of bromobenzene (4) were not considered for the fit.

**Figure 2:** Solvatochromism of HPTS in solvents with varying  $\beta$ -values ( $\alpha = 0$ ). Depicted numbers correspond to the solvent numbers in table 1.

a) Fluorescence excitation spectra ( $\lambda_{\text{det}} = 400 - 450 \text{ nm}$ ). b) Fluorescence emission spectra ( $\lambda_{\text{exc}} = 380 - 390 \text{ nm}$ ). c) Plot of all spectroscopic maxima versus the solvent's  $\beta$ -value. The grey lines represent linear fits to the excitation maxima (open circles) and emission maxima (filled triangles), respectively. For HPTS,  $b_{\text{exc}} = -320 (+/- 80) \text{ cm}^{-1}$  and  $b_{\text{em}} = -560 (+/- 140) \text{ cm}^{-1}$ . The data of benzonitrile (3) were not considered for the fit. Differential solvatochromism verifies these values. d) For comparison: Plot of the excitation and emission maxima of MPTS vs. the solvent's  $\beta$ -value. The slopes are close to 0 within the error margins.

**Figure 3:** Solvatochromism of MPTS in solvents with varying  $\alpha$ -values. Depicted numbers correspond to the solvent numbers in table 1.

3.4 *Phys. Chem. Chem. Phys.* **2009**, *11*, 1416- 1426

a) Fluorescence excitation spectra ( $\lambda_{\text{det}} = 450$  nm). b) Fluorescence emission spectra ( $\lambda_{\text{exc}} = 380 - 390$  nm). c) Plot of all fitted spectroscopic maxima versus the solvent's  $\alpha$ -value. The grey line represents a linear fit to the excitation maxima (open circles) and yields for MPTS,  $a_{\text{exc}} = -350$  (+/-70)  $\text{cm}^{-1}$ . The value of  $a_{\text{em}}$  was not determined by a fit to the emission maxima (filled triangles), see text for further details.

**Figure 4:** Solvatochromism of OPTS in solvents with varying  $\alpha$ -values. Depicted numbers correspond to the solvent numbers in table 1.

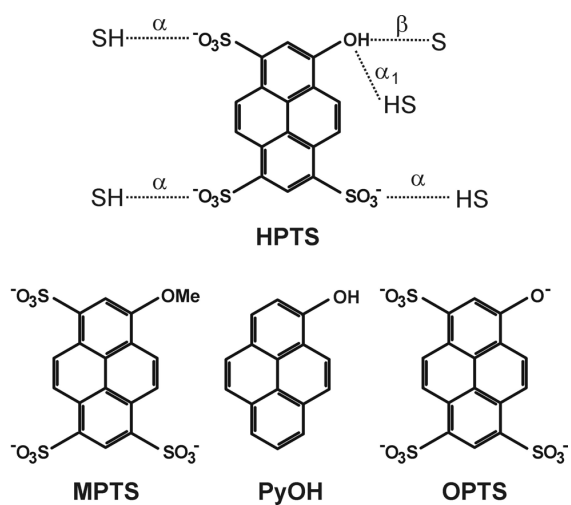
a) Fluorescence excitation spectra ( $\lambda_{\text{det}} = 530$  nm). b) Fluorescence emission spectra ( $\lambda_{\text{exc}} = 420 - 460$  nm). c) Plot of all fitted spectroscopic maxima versus the solvent's  $\alpha$ -value. The grey lines represent linear fits to the excitation maxima (open circles) and emission maxima (filled triangles), respectively. For OPTS,  $a_{\text{exc}} = +780$  (+/- 210)  $\text{cm}^{-1}$  and  $a_{\text{em}} = +240$  (+/-60)  $\text{cm}^{-1}$ . For the fit of the excitation maxima, not the maximum in trifluoroethanol (24) but the shoulder at  $\lambda = 452$  nm (see a) was used. An excitation maximum in hexafluoro-2-propanol (16) was not found.

**Figure 5:** Solvatochromism of Bodipy-dyes. Depicted numbers correspond to the solvent numbers in table 1.

a) Fluorescence excitation (full lines) of HO-BDP (grey,  $\lambda_{\text{det}} = 590$  nm) and its conjugated base O-BDP (black,  $\lambda_{\text{det}} = 710$  nm) and fluorescence emission spectrum of O-BDP (black-dotted,  $\lambda_{\text{exc}} = 585$  nm) in water. The large Stokes-shift of the anionic form was considered as an indication of ESPT. Note also the very uncommon line shape of the excitation spectrum of O-BDP. b) Fluorescence excitation spectra ( $\lambda_{\text{det}} = 600 - 635$  nm) of HO-BDP in solvent with varying  $\beta$ -values. c) Fluorescence emission spectra ( $\lambda_{\text{exc}} = 520 - 550$  nm) of HO-BDP in solvent with varying  $\beta$ -values. d) Plot of all spectroscopic maxima of HO-BDP versus the solvent's  $\beta$ -value. The grey lines represent linear fits to the excitation maxima (open circles) and emission maxima (filled triangles), respectively. For HO-BDP,  $b_{\text{exc}} = -350$  (+/- 70)  $\text{cm}^{-1}$  and  $b_{\text{em}} = -525$  (+/- 90)  $\text{cm}^{-1}$ . However, differential solvatochromism yields  $b'_{\text{exc}} = -190$  (+/- 30)  $\text{cm}^{-1}$  and  $b'_{\text{em}} = -220$  (+/- 40)  $\text{cm}^{-1}$ . e) Fluorescence excitation spectra ( $\lambda_{\text{det}} = 600 - 615$  nm) of MeO-BDP in different solvents. Note the spectral shifts of MeO-BDP in highly basic solvent (17). f) Fluorescence emission spectra ( $\lambda_{\text{exc}} = 525 - 550$  nm) of MeO-BDP in solvent with varying  $\beta$ -values. Note the spectral shifts of MeO-BDP in highly basic solvent (17).

This is a pre-peer reviewed version of the following article: *Phys. Chem. Chem. Phys.*, 2009, *11*, 1416–1426; DOI: 10.1039/b816695a; Reproduced by permission of the PCCP owner societies; <http://www.rsc.org/>

Scheme 1



Scheme 2

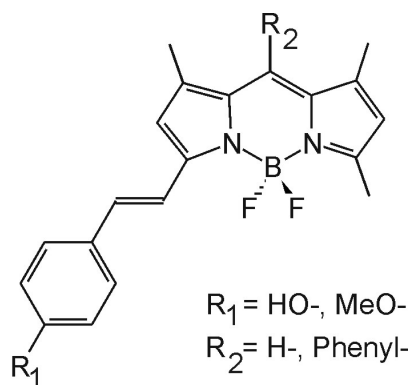


Figure 1a)

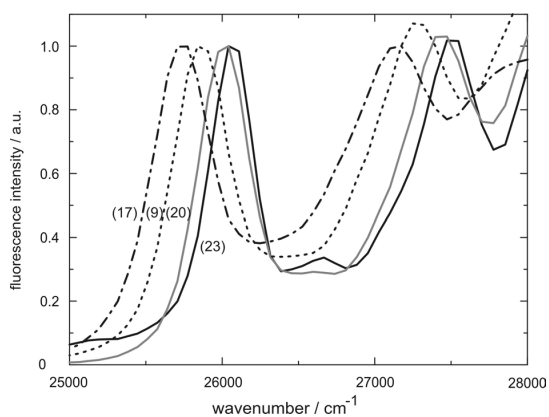


Figure 1b)

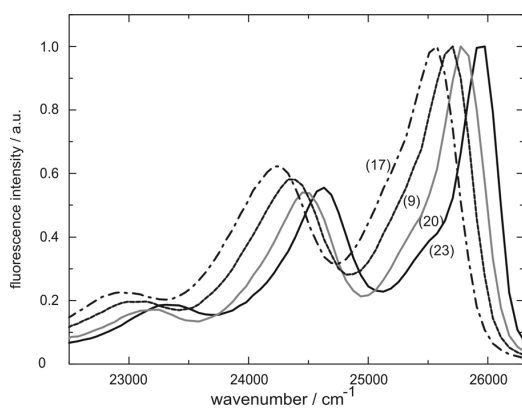


Figure 1c)

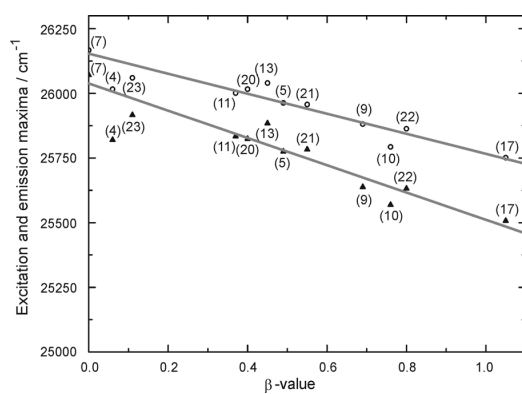


Figure 2a)

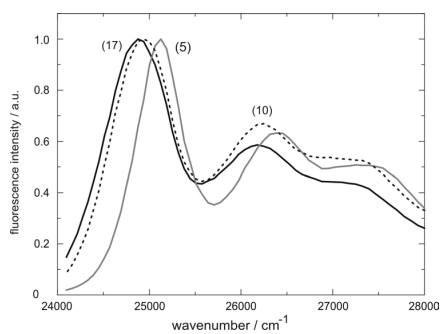


Figure 2b)

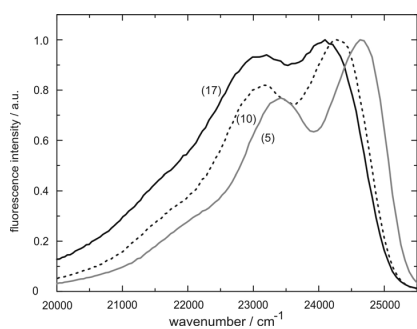


Figure 2c)

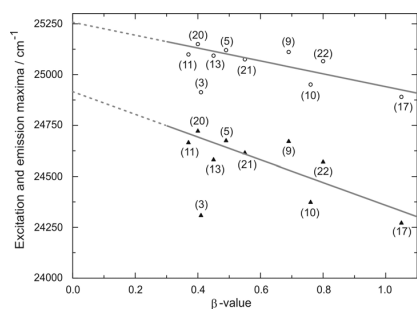
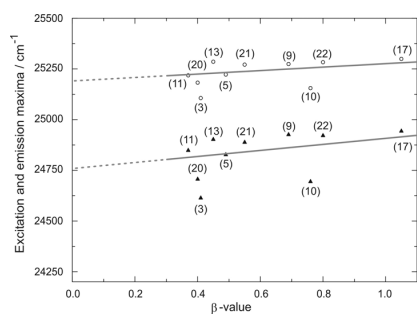


Figure 2d)



This is a pre-peer reviewed version of the following article: *Phys. Chem. Chem. Phys.*, 2009, 11, 1416–1426; DOI: 10.1039/b816695a; Reproduced by permission of the PCCP owner societies; <http://www.rsc.org/>

Figure 3a)

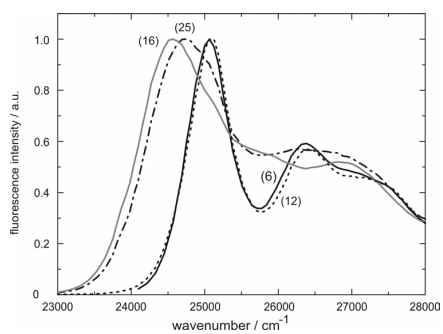


Figure 3b)

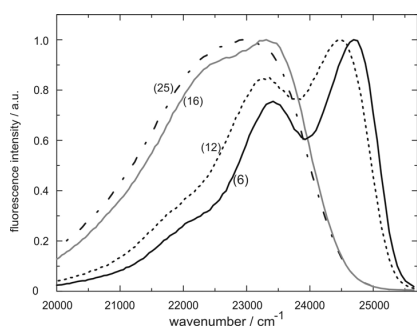


Figure 3c)

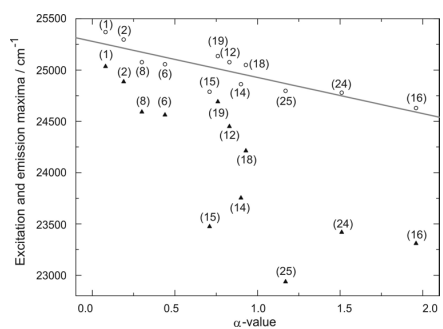


Figure 4a)

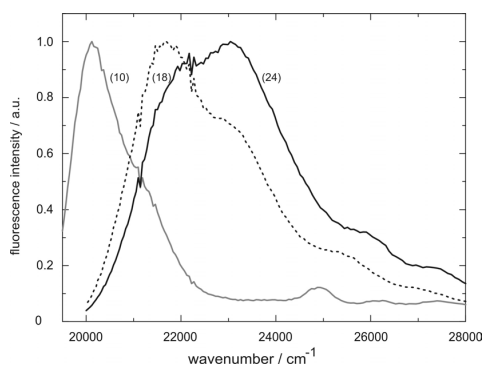


Figure 4b)

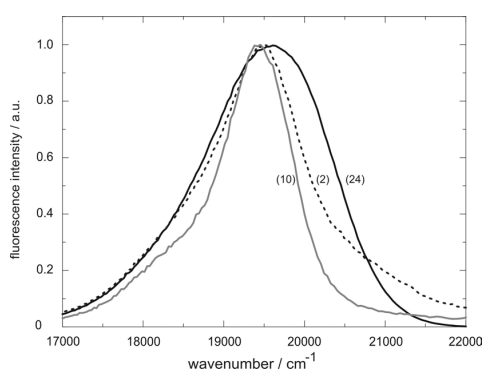
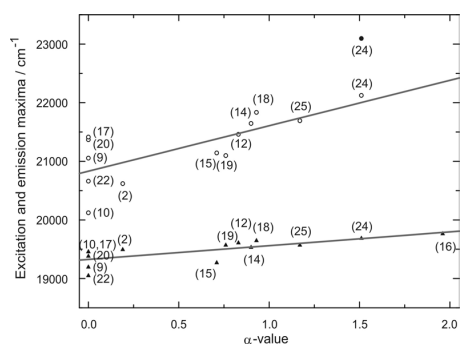
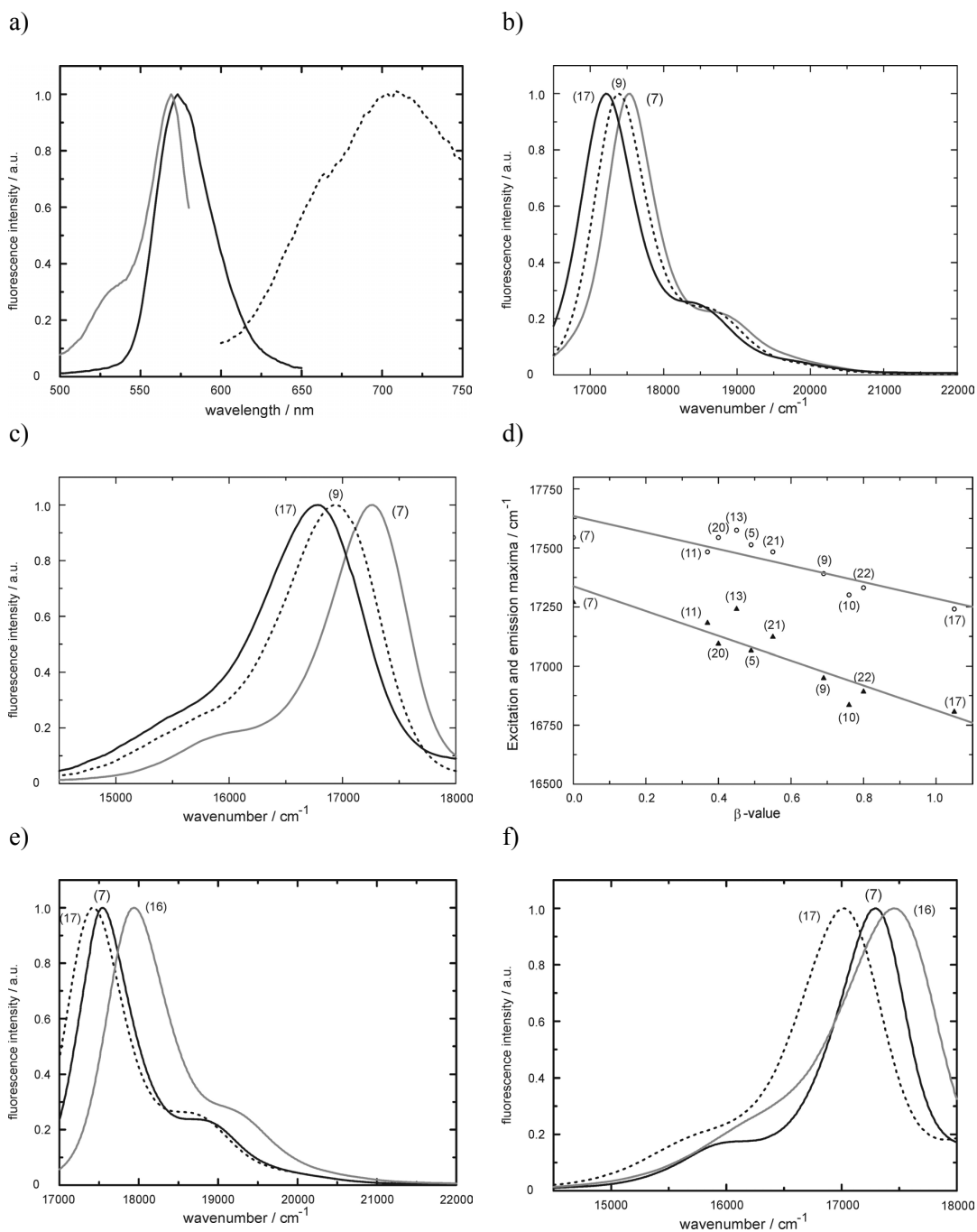


Figure 4c)



This is a pre-peer reviewed version of the following article: Phys. Chem. Chem. Phys., 2009, 11, 1416–1426; DOI: 10.1039/b816695a; Reproduced by permission of the PCCP owner societies; <http://www.rsc.org/>

Figure 5)



This is a pre-peer reviewed version of the following article: *Phys. Chem. Chem. Phys.*, 2009, 11, 1416–1426; DOI: 10.1039/b816695a; Reproduced by permission of the PCCP owner societies; <http://www.rsc.org/>

## **Fluorescent Probes for Chemical Transformations on the Single-Molecule Level**

*Gregor Jung\**, Alexander Schmitt, Michaela Jacob, and Babette Hinkeldey  
Saarland University, Biophysical Chemistry,  
Saarbruecken, Germany

\* corresponding author: [g.jung@mx.uni-saarland.de](mailto:g.jung@mx.uni-saarland.de)

### **Abstract**

We highlight our recent achievements in the design of fluorescent dyes for the investigation of chemical reactions on the single-molecule level. These fluorophores are tailored to undergo changes in their photophysical properties upon chemical transformations. Three examples are presented: electrophilic aromatic substitution, phosphoester cleavage, and oxidation of double-bonds. Thinlayer chromatography and fluorescence correlation spectroscopy are used to separate and characterize the different reaction products, respectively. We are planning to develop more fluorescent synthons which enable us to perform single-molecule chemistry of various reactions.

### **Keywords**

single-molecule

fluorescence correlation spectroscopy

alkaline phosphatase

Bodipy

self-calibrating

high-throughput screening

dihydroxylation

### **Introduction**

Synthetic chemical products have entered everyday life worldwide. Their industrial production with an annual conversion of hundreds of tons is founded on highly selective chemical reactions. For these efficiencies to have become realized, mechanistic descriptions were elaborated in research laboratories by numerous stereochemical, thermodynamic and kinetic investigations. The essence of those efforts is a reaction mechanism in which a standard substrate molecule undergoes the transformation to the product molecule. Hence, chemists are destined to think on the level of single molecules although the experiments they carry out are typically done with a huge number of molecules. Evidently, there is a concentration gap between perception and performance of chemistry which we would like to overcome.

In the past three decades, researchers have made the observation of single molecules feasible. Scanning probe microscopies, patch-clamp techniques and fluorescence-based techniques are widespread methods to follow the behaviour and fate of individual molecules. Most versatile for the transfer to “real” chemistry might be fluorescence based detection schemes in combination with confocal microscopy. In this article, we present our efforts towards the visualization of chemical reactions on the single-molecule level by initially designing fluorescent probes for that purpose.

Beyond its aesthetics (“seeing is believing”), studying reactions of individual molecules is expected to help in understanding side reactions. While bimolecular reaction sequences are hardly synchronizable and, hence, reactive and short-living intermediates are often hidden in ensemble investigations, such transient structures appear as fluorescing or dark species in single-molecule spectroscopy. The gain of such studies in biocatalysis, i.e. reactions mediated by macromolecules, is even more far-reaching since memory-effects, the way of dieing or the putatively altering selectivity of an individual enzyme can be addressed.

Imagine the addition of bromine to double-bonds (fig. 1) which is taught in first-semester courses in organic chemistry and an example of a basic organic transformation. Little is known about the stability of bromonium ions and the reversibility of their generation. Although the backside attack by a bromide is the commonly accepted second reaction step, exceptions of this anti-addition are known [1]. The intermediate where branching takes place might be discovered by single-molecule methods and specifically designed fluorescent probes.

### **Conceptual approaches**

This is a pre-peer reviewed version of the following article: *Ann. N.Y. Acad. Sci.* 1130: 131–137 (2008); DOI: 10.1196/annals.1430.006; Reproduced with kind permission of the New York Academy of Sciences/ Wiley-Blackwell

The reversible binding of two reaction partners which often initiates a chemical reaction is studied by fluorescence correlation spectroscopy (FCS) or single-molecule spectroscopy [2, 3]. Stochastic fluorescence fluctuations which are a signature of reversible single-molecule processes are averaged by taking the autocorrelation function  $g(\tau)$  of these fluctuations. Thus, the typical rate constants for binding and unbinding can be extracted. By contrast, our interest is aimed at the understanding of (irreversible) organic reactions beyond bimolecular association and dissociation and which we refer to as *chemical transformations*. We make no difference between stoichiometric and catalytic reaction steps; a catalyst is just reformed by another reaction sequence. We are aware of the fact that an individual activity of a chemical species can only be assessed when it performs repeated reaction cycles. However, different isomers of small molecules equilibrate within a time window below the time resolution of conventional single-molecule experiments so that conformational heterogeneities before the reaction are blurred; moreover, it is a signature of most organic reactions that every molecule can react only once.

So far, most examples to date have been done with leuco-dyes which become fluorescent during the investigated reaction [4-10] (fig. 2a). From a practical point of view these experiments are convenient as a large excess of the fluorogenic substrate can be provided to the active species and, additionally, a large variety of substances is commercially available. In the majority of these cases, catalytic species like enzymes are detected as spots which generate fluorescent molecules. Heterogeneity in the activity and selectivity of individual reaction centers can be discerned. It is obvious that the reverse effect, i.e. disappearance of fluorescence, might only be practicable in very special cases. A strongly fluorescent background and ambiguity about the fluorescence loss are hindering.

In a few examples, the course of reactions was followed by changes of fluorescence properties of a probe dye (fig. 2b). Repeated on-off dynamics revealed the catalytic cycles of an enzyme [11]. Blue shifting of fluorescence spectra in Terrylene and red shifting of fluorescence spectra in Green Fluorescent Protein were used to track individual and irreversible oxidation reactions [12, 13]. Determination of the transition-dipole polarization demonstrated single-molecule tautomerism in porphycene [14]. It is noteworthy that some further promising systems like e.g. Ethylresorufin/Resorufin exist; the limited number of such systems however might explain why only a few studies have tackled the visualisation of individual chemical reactions so far.

Further fluorescence properties can be exploited for monitoring a chemical reaction [15].

Changes of the fluorescence lifetime  $\tau_{\text{Fl}}$  and of the intersystem crossing quantum yield  $\Phi_{\text{isc}}$

3.5 *Ann. N. Y. Acad. Sci.* **2008**, 1130, 131-137

also appear appropriate. Fig. 3 shows the example of the pair Fluorescein/Dichlorofluorescein in which the first dye can be converted to the latter by electrophilic aromatic substitution. Due to the heavy-atom effect, both fluorophores can be distinguished on the single-molecule level by their  $\Phi_{isc}$ . Too high values of  $\Phi_{isc}$ , however, are limiting the single-molecule detection.

Another example is depicted in fig. 4, where we make use of switching fluorescence quenching on and off by photoinduced electron transfer (PeT). We exploit the redoxamphoteric character of an excited dye which can cause intramolecular electron transfer [16, 17]. Here, the chromophoric unit of a Bodipy-dye acts as oxidizing agent and the phenolic moiety in the *meso*-position as electron-donor. In contrast, a phosphorylated phenol is less susceptible to oxidation thereby disabling PeT. For this pair to become a valuable substrate for e.g. alkaline phosphatase, both dyes have to be detectable and to differ in  $\tau_{fl}$ . Whereas the 4-Phosphophenyl derivative is highly fluorescent, the radiative decay of the excited, hydrolyzed product competes with PeT. Fine tuning of the redox potentials by substitutions at the electron-donor or the electron-acceptor allows for shifting the rate constant for PeT close to that for fluorescence so that both relaxation mechanisms operate simultaneously. Consequently, the fluorescence lifetimes of starting material and product differ by a factor of  $\sim 5$ .

Instead of using PeT as quenching mechanism, which acts over sub-nm distances, one could think about using Förster resonance energy transfer (FRET) to manipulate  $\tau_{fl}$ . Typical Förster-radii, i.e. the donor-acceptor distance where the fluorescence decay rate constant equals the FRET rate constant, are in the range of 3 – 7 nm. The conformational flexibility of most spacers, attached to a small probe molecule, might aggravate measuring a constant  $\tau_{fl}$ . This approach is more useful with macromolecules of defined, rigid architecture like enzymes. Consequently, changes of the oxidation state of proteins were measured using FRET [18, 19].

### Technical constraints

The understanding of nucleophilic substitutions following the  $S_N2$  mechanism wouldn't be deepened if such a reaction is studied on the single-molecule level. The chemical transformation, for which single-molecule investigation might provide insight into its mechanism, has to meet several requirements. So far, most single-molecule experiments –if not with immobilized molecules within a polymer- have been performed in aqueous solution. Therefore, our first choices are reactions which also proceed in such an environment. This, however, is more for the sake of convenience; due to the availability of multiimmersion objectives, other solvents with a refractive index  $n_0$  between 1.3 to 1.5 can be used. Secondly,

This is a pre-peer reviewed version of the following article: *Ann. N.Y. Acad. Sci.* 1130: 131–137 (2008); DOI: 10.1196/annals.1430.006; Reproduced with kind permission of the New York Academy of Sciences/ Wiley-Blackwell

the reaction should be observable at room temperature. Expensive objectives with high numerical apertures, which are indispensable due to their higher collection efficiency, hardly withstand temperatures far below or above room temperature. Thirdly, the reaction should exhibit some selectivity. Radical substitutions with e.g. the highly reactive OH\* might result in a wealth of products with similar fluorescence properties.

The fluorescent moieties, if they are not reactive themselves like the substances in fig. 3, are used to tag the reactive moiety. Such fluorophors should display the photophysical properties which are believed to be common to all dyes for single-molecule applications: high absorption cross sections, high fluorescence quantum yield, low intersystem crossing, high photostability and emission in the visible or near-infrared part of the electromagnetic spectrum. The less reactive functionalities like amino groups are present in the marker, the less likely is the interference with the chemical transformation under examination. The synthetic challenge consists in combining chemical reactivity, selectivity and maintenance of fluorescence during the reaction. Changes in the fluorescence properties upon reaction are expected to be more distinct with smaller chromophores. This, however, is not a general rule and exception can probably be found. Currently, we generate Bordipyrromethene (Bodipy) dyes as prototypes for “fluorescing synthons” since this dye class fulfils the mentioned needs and is easy to synthesize although other dyes are believed to be superior with regard to photostability [20].

#### **An elaborated example**

We have achieved most progress so far with double-bonds labelled with a Bodipy core (fig. 5a). Extension of the chromophoric system shifts the fluorescence color from green for unsubstituted Bodipy dyes to orange. Fluorescence correlation spectroscopy (FCS) is used to judge the suitability of the substrate for single-molecule experiments. Exocyclic double-bonds experience a versatile chemistry: oxidation by peroxide (Prilezhaev reaction) ( $\rightarrow$  anti diol), attack by OsO<sub>4</sub> or MnO<sub>4</sub><sup>-</sup> ( $\rightarrow$  syn diol), electrophilic addition, metathesis, polymerisation etc. As a proof of concept, selective oxidation of the double-bond shortens the chromophoric system which can be detected by a decrease of the orange fluorescence and increase of the green fluorescence (fig. 5b). Thin-layer chromatography (TLC) of the reaction mixture in acetonitrile, performed at different reaction times, is used to follow the course of the reaction (fig. 5c). Separation due to different polarities reveals at least two different fluorescent products of the oxidation reaction, i.e. the yellow fluorescent product P<sub>1</sub> and the green fluorescent product P<sub>2</sub>. Astonishingly, both products always show up together immediately after initializing the reaction. This observation suggests that both dyes emerge in parallel and

3.5 *Ann. N. Y. Acad. Sci.* **2008**, 1130, 131-137

are not coupled by a consecutive reaction. Both spots were scratched off the TLC-foil, dissolved in acetone and immediately characterized by fluorescence spectroscopy (fig. 5d). Unfortunately, the thermal stability of the isolated fluorescent products is rather low which has prevented us from collecting more material for a further chemical analysis. Although the reaction is assumed to yield primarily one adduct, i.e. the syn diol, the existence of a second product with similar brightness on the chromatogram does not match our present view of this reaction. By comparison with the products of the oxidation by hydrogen peroxide which gives a different green fluorescent product, we interpret the green fluorescent  $P_2$  as the syn diol. The chemical nature of the yellow fluorescent  $P_1$  is not identified yet. We could imagine that further oxidation of the diol occurs, although preliminary IR-spectroscopic characterizations give no evidence for carbonyl- or carboxyl functionalities. Single-molecule chemistry might help us to identify the individual reaction pathways. With this approach, we should be able to distinguish, unambiguously, whether side products like  $P_2$  are formed in one step or rapidly from the diol. We also would like to approve or disprove the existence of the cyclic manganate-ester which is still under debate. This putative intermediate of the reaction is expected to be a dark state before one of the products shows up, as depicted in fig. 2b. It is noteworthy that our dye has two stereocenters which makes our substrate also applicable to asymmetric oxidation reactions.

The success of the proposed experiments is strongly coupled to the suitability of the products for single-molecule detection. We therefore performed FCS for addressing this issue (fig. 5e). FCS at different excitation intensities is a convenient method to assess  $\Phi_{isc}$  and, more important, the photostability. Our data show a strongly intensity-dependent decay on the sub- $\mu$ s-time scale in agreement with a high  $\Phi_{isc}$  for  $P_1$ . The time constant of the second decay on the sub-ms time scale is related to diffusion and sets an upper limit of a typical molecule being detectable in the detection volume. Here, this time is not affected by the applied intensity. We conclude that photobleaching is not competing with the diffusion of the molecules in and out of the detection volume, being therefore a minor problem for the single-molecule detectability of  $P_1$ .

### **Benefits for other applications**

Even if our planned experiments on the single-molecule level ask for further developments like a way of immobilizing the substrate or are not as informative as expected, the demonstrated achievements already show that other areas besides single-molecule spectroscopy can gain from this approach. Synthesis can be improved with the aim of

This is a pre-peer reviewed version of the following article: *Ann. N.Y. Acad. Sci.* 1130: 131–137 (2008); DOI: 10.1196/annals.1430.006; Reproduced with kind permission of the New York Academy of Sciences/ Wiley-Blackwell

reducing side products as they are easily detectable. Dyes which follow the proposed concepts are self-calibrating (ratiometric readout or lifetime measurements) and can accordingly be used in biosamples, other challenging environments like turbid media or in miniaturized assays [21, 22]. In each case, expansion to high throughput screening is feasible since microplate readers based on fluorescence methods are nowadays standard technology.

### **Outlook**

While standing at the very beginning of the proposed experiments, we can dream of (yet) utopian experiments with individual molecules: molecules, diffusing in only two dimensions, encounter in a stochastic manner and react occasionally. Temperature dependent experiments allow for accessing the kinetic parameters of these reactions including those of the involved intermediates. All reaction partners have to be fluorescently tagged like in fig. 2c, and all involved intermediates ought to be distinguishable. Several fluorescence properties can be exploited for their discrimination, but the challenge is to synthesize dyes which are tailored to undoubtedly report the transformation. For a large variety of reactions to be studied, fluorescing and synthetically active units (fluorescing synthons) are prerequisite which subsequently can be combined. Although the proposed experiments might be performed finally with other dyes, we keep on synthesizing Bodipy-dyes for fathoming the opportunities of this concept.

**Acknowledgement:** Financial support is provided by the German Science Foundation (DFG, JU 650/2-2).

## References

- [1] Ruasse M. 1993. Electrophilic Bromination of Carbon-Carbon Double-Bonds – Structure, Solvent and Mechanism. *Adv. Phys. Org. Chem.* **28**: 207-291.
- [2] Widengren, J., B. Terry, R. Rigler. 1999. Protonation Kinetics of GFP and FITC Investigated by FCS – Aspects of the Use of Fluorescent Indicators for Measuring pH. *Chem. Phys.* **249**: 259-271.
- [3] Kiel, A., J. Kovacs, A. Mokhir, R. Krämer, D. Hertel. 2007. Direct Monitoring of Formation and Dissociation of Individual Metal Complexes by Single-Molecule Fluorescence Spectroscopy. *Angew. Chem. Int. Ed.* **46**: 3363-3366.
- [4] Craig, D., E. Arriaga, J. Wong, H. Lu, N. Dovichi. 1996. Studies on Single Alkaline Phosphatase Molecules: Reaction Rate and Activation Energy of a Reaction Catalyzed by a Single Molecule and the Effect of Thermal Denaturation – The Death of an Enzyme. *J. Am. Chem. Soc.* **118**: 5245-5253.
- [5] La Clair, J. 1997. Analysis of Highly Disfavoured Processes through Pathway-Specific Correlated Fluorescence. *Proc. Natl. Acad. Sci. USA* **94**: 1623-1628.
- [6] Uhl, V., G. Pilarczyk, K. Greulich. 1998. Fluorescence Microscopic Observation of Catalysis by Single or few LDH-1 Enzyme Molecules. *Biol. Chem.* **379**: 1175-1180.
- [7] Ha, T., A. Ting, J. Liang, B. Caldwell et al. 1999. Single-Molecule Fluorescence Spectroscopy of Enzyme Conformational Dynamics and Cleavage Mechanism. *Proc. Natl. Acad. Sci. USA* **96**: 893-898.
- [8] Edman, L., R. Rigler. 2000. Memory Landscapes of Single-enzyme Molecules. *Proc. Natl. Acad. Sci. USA* **97**: 8266-8271.
- [9] Velonia, K., O. Flomenbom, D. Loos, S. Masuo et al. 2005. Single-Enzyme Kinetics of CALB-Catalyzed Hydrolysis. *Angew. Chem. Int. Ed.* **44**: 560-564.
- [10] Roeffaers, M., B. Sels, H. Uji, F. De Schryver et al. 2006. Spatially Resolved Observation of Crystal-Face-Dependent Catalysis by Single Turnover Counting. *Nature* **439**: 572-575.
- [11] Lu, H., L. Xun, X. Xie. 1998. Single-Molecule Enzymatic Dynamics. *Science* **282**: 1877-1882.
- [12] Christ, T., F. Kulzer, P. Bordat, T. Basché. 2001. Watching the Photo-Oxidation of a Single Aromatic Hydrocarbon Molecule. *Angew. Chem. Int. Ed.* **40**: 4192-4195.
- [13] Blum, C., A. Meixner, V. Subramaniam. 2004. Room Temperature Spectrally Resolved Single-Molecule Spectroscopy Reveals New Spectral Forms and Photophysical Versatility of Aequorea Green Fluorescent Protein Variants. *Biophys. J.* **87**: 4172-4179.
- [14] Piwonski, H., C. Stupperich, A. Hartschuh, J. Sepiol et al. 2005. Imaging of Tautomerism in a Single Molecule. *J. Am. Chem. Soc.* **127**: 5302-5303.

- [15] Widengren, J. V. Kudryavtsev, M. Antonik, S. Berger et al. 2006. Single-Molecule Detection and Identification of Multiple Species by Multiparameter Fluorescence Detection. *Anal. Chem.* **78**: 2039-2050.
- [16] Gabe, Y., Y. Urano, K. Kikuchi, H. Kojima, T. Nagano. 2004. Highly Sensitive Probes for Nitric Oxide Based on Boron Dipyrromethene Chromophore – Rational Design of Potentially Useful Bioimaging Fluorescence Probe. *J. Am. Chem. Soc.* **126**: 3357-3367.
- [17] Urano, Y., M. Kamiya, K. Kanda, T. Ueno et al. 2005. Evolution of Fluorescein as a Platform for Finely Tunable Fluorescence Probes. *J. Am. Chem. Soc.* **127**: 4888-4894.
- [18] Schmauder, R., F. Librizzi, G. Canters, T. Schmidt, T. Aartsma. 2005. The Oxidation State of a Protein Observed Molecule-by-Molecule. *ChemBioChem* **6**: 1381-1386.
- [19] Erker, W., S. Sdorra, T. Basché. 2005. Detection of Single Oxygen Molecules with Fluorescence-Labeled Hemocyanins. *J. Am. Chem. Soc.* **127**: 14532-14533.
- [20] Jung, C., B. Müller, D. Lamb, F. Nolde et al. 2006. A New Photostable Terrylene Diimide Dye for Applications in Single Molecule Studies and Membrane Labeling. *J. Am. Chem. Soc.* **128**: 5283-5291.
- [21] Demchenko, A. 2005. The Problem of Self-Calibration of Fluorescence Signal in Microscale Sensor Systems. *Lab-on-a chip* **5**: 1210-1223.
- [22] Shynkar, V., A. Klymchenko, C. Kunzelmann, G. Duportail et al.. 2007. Fluorescent Biomembrane Probe for Ratiometric Detection of Apoptosis. *J. Am. Chem. Soc.* **129**: 2187-2193.

### Figure captions

**Figure 1:** Electrophilic addition of Bromine to double-bonds. Even this rather basic chemical reaction proceeds via several intermediates ( $\pi$ -complex, bromonium-ion). The anti-addition of  $\text{Br}_2$  is explained by the backside attack of bromide. In the case of stabilized carbocations, also syn-adducts can be detected.

**Figure 2:** Different ideas of studying single-molecule chemistry by fluorescence spectroscopy. The size and the shape of the icons symbolize different structures which are distinguishable by their fluorescence colors. The filling denotes strong (black), weak (grey), lacking (white) or intermitting (dotted) fluorescence. Intermitting fluorescence specifies the strongly fluctuating emission of dyes with e.g. high intersystem crossing yields. In this case, the fluctuations are the result of frequent transitions into short-living dark states. So far, most experiments were conducted with fluorogenic substrates by which the activity of catalysts can be analyzed (a). More insight into reaction mechanisms, branching and the kinetics of individual reaction steps is gained when the different states along the reaction path can be distinguished (b). Not all states need to be fluorescent. Their nature can be interpreted, if fluorescence is subsequently restored. [11]. Different kinetics in enantioselective or diastereoselective reactions can be visualized if both reagents are fluorescently labelled (c). For this purpose, fluorescent synthons are required.

**Figure 3:** Effect of chlorination on the photophysical properties of Fluorescein. The combination of a higher quantum yield for intersystem crossing ( $\Phi_{\text{isc}}$ ), a slightly lower fluorescence lifetime ( $\tau_{\text{fl}}$ ) and a red shift of the electronic spectra lead to reduction of the brightness of 2,7-Dichlorofluorescein compared to the parent compound when excited at  $\lambda_{\text{exc}} = 488 \text{ nm}$ . Practically, one would try to register all depicted fluorescence parameters simultaneously to make a clear decision whether a reaction has occurred [15].

**Figure 4:** Detection of phosphoester cleavage by photoinduced electron transfer (PeT). The p-hydroxyphenyl-moiety acts as donor (D) in PeT (grey), the acceptor (A) is the excited Bodipy-dye. Upon dephosphorylation, the energy of the donor HOMO is raised thereby enabling PeT. Since PeT competes in the product with the radiative electron recombination of the excited Bodipy-dye, phosphatase activity can be detected by the reduction of the

fluorescence lifetime  $\tau_n$ . The methyl-groups at the Bodipy-core are required for shifting the redox-potential of the acceptor close to that of the donor.

**Figure 5:** Studying the oxidation of a double-bond by fluorescence spectroscopy. Double-bonds can be dihydroxylated by  $\text{OsO}_4$ ,  $\text{MnO}_4^-$  (syn) or peroxides (anti) and subsequent hydrolysis (a). Further substituents at the chromophore core are omitted for the sake of clearness. Asterisks denote the stereocenters created by this reaction. Oxidation of the double-bond by  $\text{OsO}_4$  leads to a decrease of orange fluorescence at  $\lambda_{\text{det}} = 568$  nm (dotted; before addition of  $\text{OsO}_4$ ) and increase of green fluorescence at  $\lambda_{\text{det}} = 520$  nm (full line; final spectrum) (b). Some green fluorescent impurities from the synthesis are seen at the beginning. The mixture of different products of the oxidation by  $\text{MnO}_4^-$  can be separated by thin-layer chromatography (TLC) (c). Beside the starting material S, two transiently appearing fluorescent spots ( $\text{P}_1$ ) and ( $\text{P}_2$ ) can be detected in the course of the reaction. These products (here the orange, yellowish fluorescing product  $\text{P}_1$ ) were characterized by absorption and fluorescence spectroscopy. Emission spectra were taken directly on the TLC-foil and after collection in a cuvette (d). The spectra show some differences and might indicate the decomposition of an intermediate. Finally, the (sufficiently) stable products were characterized by FCS with respect to their single-molecule detectability (e). The autocorrelation functions  $g(\tau)$  of  $\text{P}_1$  at different intensities are characterized by two decays. Their time constants reflect the typical duration of occurring fluorescence fluctuations. The distinct, intensity dependent build-up on the sub- $\mu\text{s}$  time scale indicates a high probability of intersystem crossing. The decay on the longer time scale is associated with the typical residence time of the molecule in the detection volume which is determined by the molecule's diffusion constant and the optical resolution of our confocal microscope.

Figure 1)

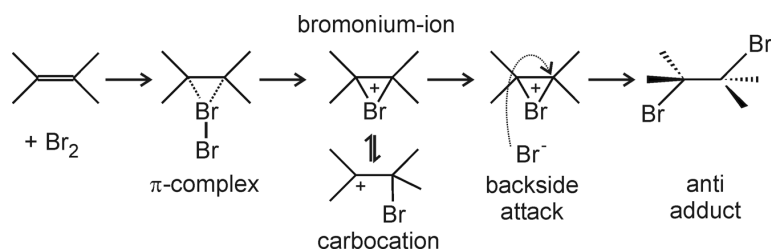


Figure 2)

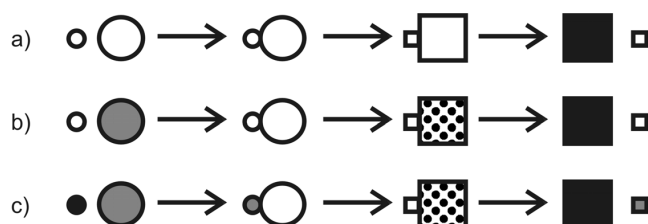


Figure 3)

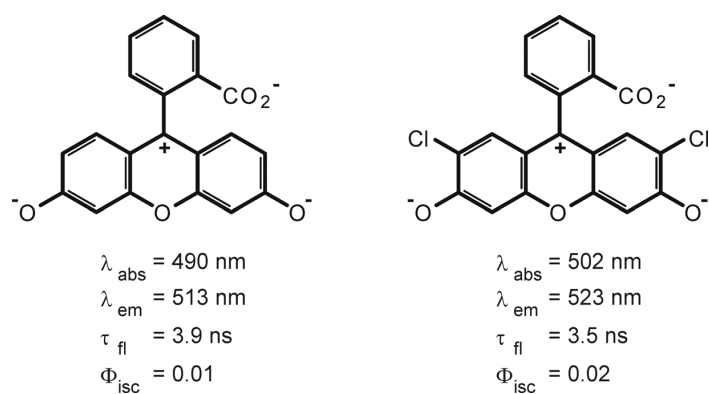


Figure 4)

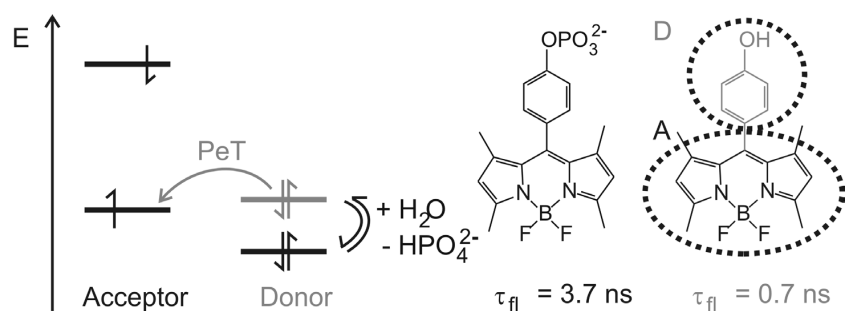
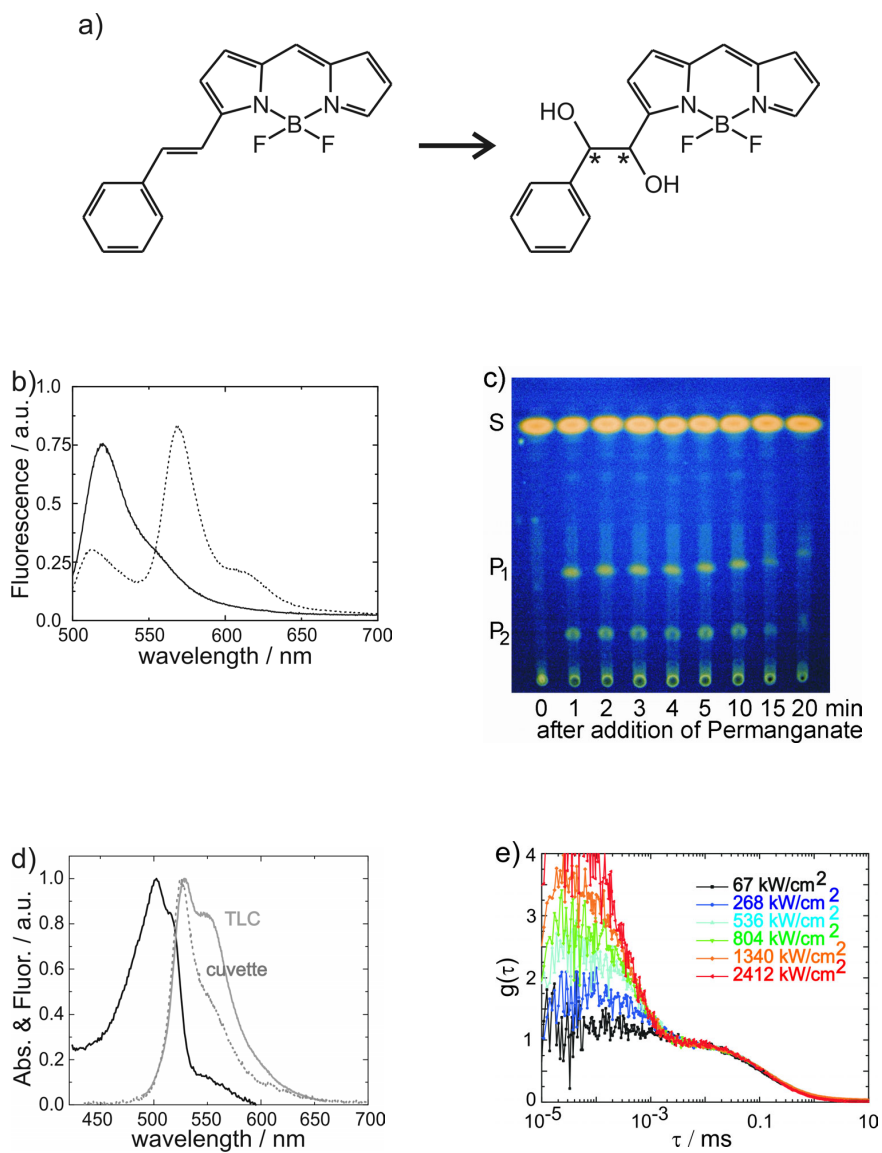


Figure 5)



This is a pre-peer reviewed version of the following article: *Ann. N.Y. Acad. Sci.* 1130: 131-137 (2008); DOI: 10.1196/annals.1430.006; Reproduced with kind permission of the New York Academy of Sciences/ Wiley-Blackwell

## **Mechanistic studies of oxidation reactions by fluorescence spectroscopy: A critical assessment**

*Alexander Schmitt*<sup>[a]</sup>, *Babette Hinkeldey*<sup>[a]</sup>, *Benjamin Hötzer*<sup>[a]</sup>, *Gregor Jung*<sup>\*,[a]</sup>

[a] Biophysical Chemistry, Saarland University, Campus B2.2,

D-66123 –Saarbrücken, Germany,

Fax: +49 681 302-64846, E-mail: g.jung@mx.uni-saarland.de

**Keywords:** Bodipy, dihydroxylation, fluorescence correlation spectroscopy, fluorescent probes, fluorescence spectroscopy, epoxidation

**Abstract:** The synthesis and properties of a ratiometric fluorescent dye system as a probe for the detection of oxidizing species are described. The dye consists of a strongly fluorescent Bodipy label attached to a styryl moiety. The oxidation by agents for *syn*- and *anti*- dihydroxylation of the exocyclic double bond leads to a visible change in fluorescence colour from orange to green. IR-spectroscopy provides evidence for the generation of the epoxide in the reaction with peroxides whereas a ketone and a product of unknown structure are produced in the reaction with osmiumtetroxide, each in contrast to the expected hydroxylations. Based on these first attempts, we discuss the significance of fluorescence spectroscopy to track chemical reactions at low concentrations and give a perspective how present shortcomings can be overcome.

## Introduction

Fluorescence spectroscopy became very valuable especially in the life sciences. Fluorophores for the detection of ions and small molecules are nowadays commercially available. Due to technology improvements, fluorescence spectroscopy provides the capability to detect minute amounts of analytes down to the level of single molecules [1, 2]. Very recently, studies of oxidation reactions using a fluorescent probe as substrate have been published [3]. In most applications, however, the fluorescence intensity depends on the concentration of the analyte as well as the concentration of the probe molecule. Therefore, scientists are interested in finding self-referencing probes, i.e. probe molecules where the signal, which is used for quantification, is independent of the probe concentration. Among these, ratiometric detection is most widespread [4]. We focus here on dyes where the ratio of two specific fluorescence intensities is related to the concentration of an analyte. This approach, however, is sparsely applied to monitor chemical kinetics or to determine the concentration of reactive species [5]. We are currently synthesizing such ratiometric fluorophores. Our long-term aim is to use ultrasensitive spectroscopy to get deeper mechanistic insight into reaction mechanisms of organic and biochemical reactions [6]. Here, we present a fluorescently tagged double-bond which is amenable to a wealth of oxidation reactions. The label of the functional group is a Bordipyromethene (BDP) dye [7]. The attack of oxidants on the double-bond results in the shortening of the chromophoric system and a change of fluorescence colour. In contrast to the preparative designation of the oxidants [8], we do not detect the expected products. This finding is discussed with respect to our long-term aim.

## Results and Discussion

Styryl-BDP **1** was synthesized from a condensation of doubly methylated Bodipy with benzaldehyde (fig. 1) [9]. Optical spectra show that the chromophoric system of the BDP core is extended (see table 1 for all spectroscopic data). Excitation intensity dependent fluorescence correlation spectroscopy (FCS) curves of a highly diluted aqueous solution of **1** reveal a slight increase of the amplitude *C* of the fast process indicating weak intersystem crossing. The maximum molecular brightness, which is the normalized count rate per molecule, is of the same order like that of the reference dye Rhodamine B (68,000 vs. 70,000 counts per second) which was recently used as reporter of a single-molecule reaction [2a]. The combination of the crystallographic structure, the lacking observation of cis-trans isomerization in FCS [10] and the <sup>3</sup>J-coupling constant in proton magnetic resonance (<sup>1</sup>H-

NMR) spectroscopy for the exocyclic protons provide evidence that **1** is locked in its trans-(*E*)-configuration.

Selective anti dihydroxylation is achieved by reaction with 3-chloroperbenzoic acid (MCPBA) via the epoxide whereas osmiumtetroxide ( $\text{OsO}_4$ ) is the preferred reagent for syn hydroxylation (Scheme 1) [8]. We renounced a cooxidant for the sake of simplicity and used  $\text{OsO}_4$  in excess. Both reactions were followed in cuvette experiments (fig.2).

The decrease of the orange substrate fluorescence and increase of green product fluorescence centered at  $\lambda_{\text{em}} \sim 510$  nm were analyzed for the reaction with MCPBA according to pseudo-first-order kinetics, from which a second-order rate constant  $k_{\text{ox}} \sim 1 \cdot 10^4 \text{ M}^{-1} \text{ s}^{-1}$  was deduced. The overall trend in the reaction of  $\text{OsO}_4$  is similar to that of MCPBA on a  $\sim 100$ x expanded time scale and with the simultaneous appearance of two fluorescent products centered at  $\lambda_{\text{em}} \sim 510$  nm and at  $\lambda_{\text{em}} \sim 530$  nm (figure 2b). This unexpected finding provoked our ambition to isolate the different products by thin-layer chromatography (TLC) for further characterization (fig. 2c). We used highly reactive permanganate ( $\text{MnO}_4^-$ ), which is known to perform syn-hydroxylation like  $\text{OsO}_4$ , instead of the latter because of its low solubility in organic solvents [11, 12].  $\text{MnO}_4^-$  and its decomposition product manganese(IV)oxide  $\text{MnO}_2$  are left at the starting line of the chromatogram. Apart from the unconsumed substrate **1**, two further fluorescent products **P**<sub>1</sub> and **P**<sub>2</sub> became visible by their fluorescence upon UV-excitation ( $\lambda_{\text{ex}} = 365$  nm). Both products displayed different colors already on the TLC-foil. Whereas **P**<sub>1</sub> appeared orange colored with yellow fluorescence, **P**<sub>2</sub> was faintly yellow with green fluorescence. The stability of **P**<sub>1</sub> and **P**<sub>2</sub> turned out to be critical and excluded large scale time-consuming synthetic approaches so far. Therefore, the amounts, by which the TLC-foils were charged, were scaled up in a “preparative” approach. Subsequently, **P**<sub>1</sub> and **P**<sub>2</sub> were scratched off the foil, dissolved in acetone and immediately characterized by optical spectroscopy (fig. 3a-3d).

The emission spectrum of **P**<sub>2</sub> ( $\lambda_{\text{em}} = 513$  nm) was similar to unsubstituted BDP (fig. 3a) [7]. This finding is interpreted as the destruction of the extended chromophoric system. The yellow fluorescent product **P**<sub>1</sub> exhibits a fluorescence maximum at  $\lambda_{\text{em}} = 530$  nm, with a shoulder at 550 nm. The fluorescence maxima of **P**<sub>1</sub> and **P**<sub>2</sub> also coincide with those of the  $\text{OsO}_4$  oxidation (fig. 2b).

The fluorescence of **P**<sub>1</sub> and **P**<sub>2</sub>, both species, decayed each with a single lifetime  $\tau_{\text{F1}} \sim 5.3$  ns and 5.9 ns, respectively. Analysis of the intensity dependent FCS curves revealed triplet quantum yields  $\Phi_{\text{isc}}$  which are in the range of Fluoresceine dyes (fig. 3b,c) [13]. **P**<sub>1</sub> and **P**<sub>2</sub> also differ in their bleaching behaviour, i.e. the intensity dependent reduction of the diffusional

This is a pre-peer reviewed version of the following article: *J Phys. Org. Chem.* (2009), accepted 27-Jun-2009, DOI: 10.1002/poc.1604

time  $\tau_d$  [13]. For comparison, we isolated the green fluorescent product **P**<sub>3</sub> of the reaction of **1** with hydrogen peroxide (H<sub>2</sub>O<sub>2</sub>) in the same manner [8]. Its electronic spectra are almost identical to those of **P**<sub>2</sub>. FCS experiments, where we carefully established the same experimental conditions for **P**<sub>2</sub> and **P**<sub>3</sub>, yielded almost identical autocorrelation traces under identical excitation conditions [8]. A fluorescence spectroscopic distinction between **P**<sub>2</sub> and **P**<sub>3</sub>, however, can be realized by lifetime measurements (fig. 3d).

In order to unravel the chemical nature of **P**<sub>1</sub> to **P**<sub>3</sub>, we performed Infrared (IR) spectroscopy of the isolated compounds (fig. 3e). Here, we carefully renounced the usage of acetone in the isolation and exclusively employed CH<sub>2</sub>Cl<sub>2</sub> as solvent. Surprisingly, none of the spectra **P**<sub>1</sub> to **P**<sub>3</sub> exhibited strong absorption at  $\nu > 3000\text{ cm}^{-1}$  which would be indicative of mono- or dihydroxylation [14]. Comparison of the spectra with those of the doubly methylated, green BDP, which was used for the synthesis of **1**, as well as of the substrate **1** showed some interpretable changes. All product spectra as well as the green BDP are lacking the bands at  $1520\text{ cm}^{-1}$  and  $1590\text{ cm}^{-1}$  of **1**. This is a typical range where conjugated double bonds absorb IR light [14]. Therefore, these spectroscopic observations support our interpretation that the exocyclic double bond has been attacked by the oxidizing agents. Other significant changes include the exclusive appearance of a band at  $1670\text{ cm}^{-1}$  in **P**<sub>1</sub>. This is a typical value of a carbonyl-function connected to double bonds which could be the BDP-chromophore.. A second band close to  $1730\text{ cm}^{-1}$  is found in all products but, interestingly, also in the doubly methylated BDP core and does therefore not allow for a reliable interpretation. A putative chemical assignment of **P**<sub>3</sub> as the epoxide could be achieved by identification of a broad band at  $\sim 1270\text{ cm}^{-1}$ . This band, however, is superimposed by two sharp bands which are ubiquitous in the spectra of BDP dyes.

The nature of **P**<sub>2</sub> is yet unknown. We exclude metallate esters which are expected to be non-fluorescent and unstable. Its properties can be summarized: (i) the chromophoric system is, highly likely, shortened with respect to **1** as indicated by the blue-shift of the fluorescence. (ii) The reaction which leads to **P**<sub>2</sub> occurs not for peroxides. (iii) The available kinetic data do not support yet the generation of **P**<sub>1</sub> from **P**<sub>2</sub>, or vice versa, in a slow consecutive reaction. (iv) No specific IR absorptions could be detected.

Before sequences of elementary reactions on the level of single molecules can be followed by a change of the fluorescence properties [6], several pitfalls have to be considered:

The first difference between the preparative use of the reagents MCPBA, OsO<sub>4</sub> and the investigations here is the excessive, non-stoichiometric amount of oxidant which was applied.

This is a pre-peer reviewed version of the following article: *J Phys. Org. Chem.* (2009), accepted 27-Jun-2009, DOI: 10.1002/poc.1604

Concentrations of **1** hardly passed  $10^{-4}$  M for the isolation of the products and were even lower by 1-2 orders of magnitude for the kinetic experiments. The established concentration ratios result from the experimental boundary conditions. On the one hand, higher concentrations of the substrate **1** are not easily compatible with fluorescence spectroscopy whereas on the other hand lower concentration of the oxidant would tremendously decelerate the reactions. Therefore, **1** can be regarded as an “impurity” in the reaction mixture and also unexpected reactions might be observed. This also might explain why we observed the ketone **P<sub>1</sub>**: the (yet undetected) dihydroxylated product is formed as the first product and likely undergoes further, rapid oxidation [15]. In addition, the generation of transient, highly reactive species, e.g. Os(VI) or Mn(V) with much higher oxidation potentials and likely diffusion-controlled reaction kinetics, is detrimental to the performance under the mentioned conditions. This might be the reason for the disappearance of the fluorescent species in fig. 2c after 15 min despite the abundance of **1** and the oxidant. Thus, further attempts have to avoid the accumulation of such species.

The second and yet more challenging demand for the proposed experiments is the univocal assignment of the products by fluorescence spectroscopy. In the here reported experiments, the expected dihydroxylation likely turns the substrate also into a green fluorescent product. A full chemical characterization of the reaction products is essential as the fluorescence colour is *a priori* not significant enough. Whether OsO<sub>4</sub> or MnO<sub>4</sub><sup>-</sup> yield the identical products **P<sub>1</sub>** and **P<sub>2</sub>** [8] has still to be answered. The distinction between the yet detected and the expected products might require modifications of the substrate for establishing detectable spectroscopic differences. Also selection of reaction mechanisms based on textbook knowledge, which guided us to the presented experiments, is not sufficient due to the altered concentration conditions. Extended chemical analyses have to be performed.

## Conclusion

We established a ratiometric system for studying chemical reactions by means of fluorescence spectroscopy instead of absorption based techniques. Both the substrate and all products, which we detected so far, could be analyzed by FCS. This feature indicates their suitability for ultrasensitive analytics. However, fluorescence detection has the character to rely on smaller concentration of the probe molecules. The large excess of the co-substrate, which is indicated for the sake of operability, can activate side and consecutive reactions which are hardly documented. Therefore, conventional bulk chemistry is indispensable to characterize

the fluorescent products. Alternative large scale approaches to the expected and detected products are currently under the way.

### Experimental Section

*General instrumentation.* Mass spectra (MS) were measured with a Waters liquid chromatography- mass spectroscopy (LCMS) system consisting of a high performance liquid chromatography (HPLC) system coupled with a single quadrupole mass spectrometer for electron spray ionization (ESI). NMR spectra were recorded on an Bruker BioSpin GmbH Avance 500 instrument.

*Synthesis of 1-Methyl-3-styryl-4,4'-difluoro-bora-3a-4a-diaza-(s)-indacene (1).* A solution of 1.3-Dimethyl-4,4'-difluoro-bora-3a-4a-diaza-(s)-indacene [9] (2mmol) and benzaldehyde (2.3mmol) in 60mL toluene with some 3Å molecular sieve is stirred and heated until reflux. Then 1.5mL of glacial acetic acid is added, followed by 1.8mL of piperidine and stirring under reflux for 2 hours. Purification is achieved by column chromatography (solvent: dichloromethane (CH<sub>2</sub>Cl<sub>2</sub>)). Several cycles of column chromatography were needed to completely purify the product from the starting material. The overall yield was 60%.

<sup>1</sup>H NMR (500MHz, CDCl<sub>3</sub>, 25°C, TMS): δ= 2.20 (s, 3H), 6.37 (s, 1H), 6.65 (s, 1H), 6.84 (d, 1H, J=2,25Hz), 7.06(s, 1H), 7.26-7.32 (m, 4H, <sup>3</sup>J<sub>trans</sub>=16,5Hz), 7.52 (d, 2H, J=6,94Hz), 7.55 (d, 1H, <sup>3</sup>J<sub>trans</sub>=16,5Hz), 7.56 (s, 1H). <sup>13</sup>C NMR (125MHz, CDCl<sub>3</sub>, 25°C, TMS): δ= 11.42 (CH<sub>3</sub>), 116.43 (CH), 117.16 (CH), 118.54 (CH<sub>trans</sub>), 123.24 (CH), 126.09 (CH), 127.90 (2C, CH), 128.88 (CH), 129.83 (2C, CH), 133.16 (C), 135.77 (C), 137.79 (C), 139.02 (CH), 139.89 (CH<sub>trans</sub>), 144.54 (C), 158.68 (C). LCMS (ES<sup>+</sup>): m/z (%), [M+H<sup>+</sup>], 309 (100).

*Sample preparations.* For all experiments, **1** was dissolved in acetonitrile (Chromasolv-grade, Fluka) to give a 10<sup>-4</sup> M stock solution. Experiments which were aimed at isolating the fluorescent products were done with this original solution. For the kinetic studies and time correlated single photon counting (TCSPC) experiments in cuvettes, samples were 100x diluted. Solutions for FCS experiments were obtained by a further dilution with water (Chromasolv-grade, Fluka).

*Reaction with oxidants.* To the described samples, oxidants were added in amount of less than 1/10 of the cuvette volume. For TLC, the concentration of the oxidants MnO<sub>4</sub><sup>-</sup> and H<sub>2</sub>O<sub>2</sub> was adjusted so that the reaction could proceed on an hour time scale. After the indicated times, 20 μl were taken, put equidistantly at the start line and air dried. CH<sub>2</sub>Cl<sub>2</sub> was found to be the best solvent for separating fluorescent spots in TLC.

This is a pre-peer reviewed version of the following article: *J Phys. Org. Chem.* (2009), accepted 27-Jun-2009, DOI: 10.1002/poc.1604

*Optical spectroscopy: Absorption spectroscopy (UV/Vis).* Absorption spectra were measured on a Perkin-Elmer Lambda 5 two-beam spectrophotometer. Fluorescence and emission spectra were recorded on different devices (Fluorolog 3, Jobin-Yvon, FP-6500, Jasco and SD2000 Fibre Optic Spectrometer, Ocean Optics). The latter was fibre-coupled which allowed us to take fluorescence spectra directly from the TLC-foils.

*Infrared spectroscopy (IR).* IR spectra were recorded in ATR geometry (attenuated total reflection; Spectrum 1000, Perkin Elmer). For that purpose, the dye solutions were put on the ZnSe prism and evaporated under N<sub>2</sub>-atmosphere.

*Fluorescence correlation spectroscopy (FCS).* Experiments were performed with a home-built confocal setup based on an inverted microscope [10c]. An Erbium-doped fibre laser ( $\lambda_{\text{ex}} = 544$  nm) and a frequency-doubled diode laser ( $\lambda_{\text{ex}} = 488$  nm) were directed to the microscope body and there deflected by appropriate dichroic mirrors. The respective laser was focused by a water immersion objective lens into a drop of dye solution on top of a cover slide. Fluorescence was collected by the same objective and was focussed by the tube lens to a pinhole with a diameter of 50  $\mu\text{m}$ . After additional filtering with appropriate bandpass filters, fluorescence was split by semitransparent mirror and detected by two avalanche photodiode modules. TTL-signals, each corresponding to a detected photon, were cross-correlated by a hardware correlator finally yielding the autocorrelation function  $g^2(\tau)$ . Analysis of all curves was done by fitting with

$$g^2(\tau) = \frac{1}{N} \left( \frac{1}{1 + \left(\frac{\tau}{\tau_d}\right)} \right) \left( 1 + \frac{k_{23}^{\text{eff}}}{k_{31}} \cdot \exp\left(-\left(k_{23}^{\text{eff}} + k_{31}\right)\tau\right) \right) + \text{Offset}$$

$\tau_d$  and  $1/k_{31}$  are the diffusional time and the triplet lifetime, respectively. From the intensity dependent  $k_{23}^{\text{eff}}$ , the intersystem crossing rate constant  $k_{23}$  can be computed as described previously [9, 13a]. Photobleaching can be analysed as a decrease of  $\tau_d$ . [9c, 13b]. All depicted curves were normalized to  $N=1$ .

*Fluorescence lifetime measurements.*  $\tau_{\text{fl}}$  were determined by time-correlated single photon counting under magic-angle conditions. A picosecond excitation laser (LDH-P-C-470B, Picoquant;  $\lambda_{\text{ex}} = 470$  nm, pulse width  $\sim 70$  ps, repetition rate 20 MHz) was focused into a cuvette. Fluorescence was collected in 90° geometry and detected after spectral filtering with the same filters as in FCS by an avalanche-photodiode (SPQM-14, Perkin Elmer). The instrumental response function (FWHM) was  $\sim 700$  ps and electronic signals were recorded on a stand-alone TCSPC-module (PicoHarp 300, Picoquant). Fluorescence lifetimes were

3.6 *J. Phys. Org. Chem.* **2009**, accepted  
determined by monoexponential reconvolution-fits using commercial software (SymPhoTime,  
Picoquant). For all measurements  $\chi^2$  was lower than 1.1.

### **Acknowledgments**

Financial support was provided by the Saarland University and the German Science foundation (DFG grant JU-650/1-2 and 2-2). We are also indebted to J. Lenz, M. Wild and Volker Huch for assistance.

## References

- [1] a) W. E. Moerner, D. P. Fromm, *Rev. Sci. Instrum.* **2003**, 74, 3597-3619.  
b) E. Haustein, P. Schwille, *Annu. Rev. Biophys. Biomol. Struct.* **2007**, 36, 151-169.
- [2] a) A. Kiel, J. Kovacs, A. Mokhir, R. Krämer, D. Hertzen, *Angew. Chem. Int. Ed.* **2007**, 46, 3363-3366.  
b) J. La Clair, *Proc. Natl. Acad. Sci. USA* **1997**, 94, 1623-1628.  
c) Th. Christ, F. Kulzer, P. Bordat, Th. Basché, *Angew. Chem. Int. Ed.* **2001**, 40, 4192-4195.
- [3] A.C. Benniston, G. Copley, K. J. Elliot, R.W. Harrington, W. Clegg, *Eur. J. Org. Chem.* **2008**, 2705- 2713.
- [4] a) A.A. Deniz, T.A. Laurence, M. Dahan, D.S. Chemla, P.G. Schultz, S. Weiss, *Annu. Rev. Phys. Chem.* **2001**, 52, 233-253. b) Y. Zhang, X. Guo, W. Si, L. Jia, X. Qian, *Org. Lett.* **2008**, 10, 473-476. c) Y. Xiang, A. Tong, *J. Lumin.* **2008**, 23, 28-31. d) W.W. Qin, M. Baruah, M. Sliwa, M. Van der Auweraer, W.M. De Borggraeve, D. Beljonne, B. Van Averbeke, N. Boens, *J. Phys. Chem. A* **2008**, 112, 6104-6114 .e) F. Bergstrom, I. Mikhalyov, P. Hagglof, R. Wortmann, T. Ny, L.B.A. Johansson, *J. Am. Chem. Soc.* **2002**, 124, 196- 204.
- [5] a) E.H.W. Pap, G.P.C. Drummen, V.J. Winter, T.W.A. Kooij, P. Rijken, K.W.A. Wirtz, J.A.F Op den Kamp, W.J. Hage, J.A. Post , *FEBS Letters* **1999**, 453, 278-282.  
b) Martínez-Urreaga J., Larena A, *Monatsh. Chem.* **1991**, 122, 697- 704.
- [6] G. Jung, A. Schmitt, M. Jacob, B. Hinkeldey, *Ann. N.Y. Acad. Sci.* **2008**, 1130, 131-137.
- [7] a) A. Loudet, K. Burgess, *Chem. Rev.* **2007**, 107, 4891- 4932. b) G. Ulrich, R. Ziessel, A. Harriman, *Angew. Chem. Int. Ed.* **2008**, 47, 1184- 1201. c) A. Schmitt, B. Hinkeldey, M. Wild, G. Jung, *J. Fluoresc.*, **2009**, 19, 755- 758 .
- [8] M. B. Smith, J. March in *Advanced organic chemistry*, Wiley- Interscience, New York, **2001**, 5th ed.

- [9] a) K. Rurack, M. Kollmannsberger, J. Daub, *Angew. Chem. Int. Ed.* **2001**, *40*, 385-387. b) M. Baruah, W.W. Qin, C. Flors, J. Hofkens, R.A.L. Vallee, D. Beljonne, M. Van der Auweraer, W.M. De Borggraeve, N. Boens, *J. Phys. Chem. A* **2006**, *110*, 5998-6009.
- [10] a) J. Widengren, P. Schwille, *J. Phys. Chem. A* **2000**, *104*, 6416-6428. b) G. Jung, A. Zumbusch, *Micros. Res. Techn.* **2006**, *69*, 175-185. c) S. Veettil, N. Budisa, G. Jung, *Biophys. Chem.* **2008**, *136*, 38-43.
- [11] This is the reason for the destruction of the fluorescent products in TLC while using MCPBA and OsO<sub>4</sub>. Both oxidants are soluble in organic solvents and can continuously react during the migration process. This was also observed for other green BDPs.
- [12] The high reactivity of MnO<sub>4</sub><sup>-</sup> becomes visible in the generation of a byproduct with an absorption maximum at  $\lambda_{\text{max}} = 565 \text{ nm}$  in the fraction of **P**<sub>2</sub> (fig. 3a). Its spectra are even red-shifted compared to **1**. From comparison with unpublished data, we attribute it to a BDP with a hydroxylated phenyl-moiety.
- [13] a) J. Widengren, Ü. Mets, R. Rigler, *J. Phys. Chem.* **1995**, *99*, 13368- 13379. b) B. Hinkeldey, A. Schmitt, G. Jung, *ChemPhysChem.* **2008**, *9*, 2019-2027.
- [14] a) M. Hesse, H. Meier, B. Zeeh in *Spektroskopische Methoden in der organischen Chemie*, Georg Thieme, Stuttgart, **2005**, 7th ed.  
b) J. Weidlein, U. Müller, K. Dehnike, in *Schwingungsfrequenzen Band I & II*, Georg Thieme, Stuttgart, New York, **1981**
- [15] V. VanRheenen, R. C. Kelly, D. Y. Cha, *Tetrahedron Letters*, **1976**, *17*, 1973- 1976.
- [16]  $k_{31}$  of **P**<sub>1</sub> – **P**<sub>3</sub> is only slightly increased compared to  $k_{31}$  of **1** which agrees with diffusion controlled quenching by O<sub>2</sub> [13a].

**Table 1: Spectroscopic Data of all compounds.**  $\Phi_{\text{isc}}$  can be determined as the product of  $k_{23}$  and  $\tau_{\text{fl}}$ . Solvent for all measurements is acetone, except FCS where water (Chromasolv Grade) is used. Excitation spectra are not depicted (n.d.: not determined).

| compound             | $\lambda_{\text{ex}}$ [nm] | $\lambda_{\text{em}}$ [nm] | $\tau_{\text{fl}}$ [ns]<br>(+/- 0.1) | $k_{23}$ [ $\text{s}^{-1}$ ]<br>(+/- 20%) | $k_{31}$ [ $\text{s}^{-1}$ ]<br>(+/- 20%)<br><sup>[16]</sup> |
|----------------------|----------------------------|----------------------------|--------------------------------------|---|--|
| <b>1</b>             | 549                        | 557                        | 6.3                                  | $2.7 \cdot 10^5$                          | $4.5 \cdot 10^5$   |
| <b>P<sub>1</sub></b> | 519                        | 528                        | 5.3                                  | $4.2 \cdot 10^6$                          | $5.3 \cdot 10^5$   |
| <b>P<sub>2</sub></b> | 504                        | 513                        | 5.9                                  | $3.4 \cdot 10^6$                          | $4.9 \cdot 10^5$   |
| <b>P<sub>3</sub></b> | 503                        | 513                        | 5.1                                  | n.d.                                      | n.d.   |

**Scheme 1: Dihydroxylation chemistry of compound 1**

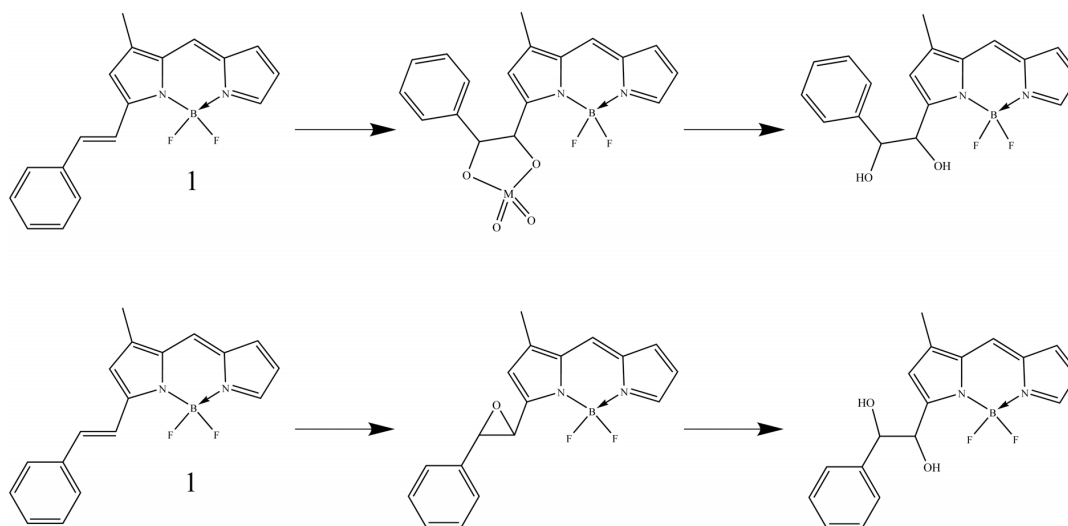


**Figure captions****Figure 1:** Characterization of **1**

- a) Crystallographic structure.
- b) Intensity dependent FCS-curves of **1** in water ( $\lambda_{\text{exc}} = 544$  nm). Both the amplitude for the process on the sub- $\mu\text{s}$ -time scale as well as the decrease of the diffusional time  $\tau_d$  on the sub-ms time scale, are dependent on the excitation intensity [13b].

**Figure 2:** Fluorescence spectroscopy of the oxidation reactions

- a) Reaction of **1** with MCPBA ( $\sim 100\text{x}$  fold excess,  $\lambda_{\text{exc}} = 470$  nm) with the built-up of product fluorescence. Data are normalized to the fluorescence intensity of **1** although its intensity decreased.
- b) Reaction of **1** with  $\text{OsO}_4$  ( $\sim 100\text{x}$  fold excess,  $\lambda_{\text{exc}} = 470$  nm) with the built-up of product fluorescence. Data are normalized to the intensity of **1**.
- c) Reaction of **1** with  $\text{MnO}_4^-$ , followed by thin-layer chromatography ( $\lambda_{\text{exc}} = 365$  nm). Unconsumed **1** was migrating close to the solvent front.  $\text{MnO}_4^-$  and  $\text{MnO}_2$  remain at the stipple spot. The fluorescence emission maxima of **P**<sub>1</sub> and **P**<sub>2</sub> coincided with those of b).

**Figure 3:** Spectroscopic characterization of the products **P**<sub>1</sub> – **P**<sub>3</sub>.

- a) Absorption (black) and fluorescence emission (green) spectra ( $\lambda_{\text{exc}} = 450$  nm) of **P**<sub>1</sub> and **P**<sub>2</sub> in acetone.
- b) Excitation intensity dependent FCS-spectra ( $\lambda_{\text{exc}} = 488$  nm) of **P**<sub>2</sub> in  $\text{H}_2\text{O}$ .
- c) Excitation intensity dependent FCS-spectra ( $\lambda_{\text{exc}} = 488$  nm) of **P**<sub>1</sub> in  $\text{H}_2\text{O}$ .
- d) Fluorescence lifetime data of the green fluorescent products **P**<sub>2</sub> and **P**<sub>3</sub> in acetone.
- e) Infrared spectra of the doubly methylated, non-styryl substituted BDP core structure (black dotted line), **1** (black line), the green (red line) and yellow (red dotted line) oxidation products of the reaction of **1** with  $\text{OsO}_4$  and the oxidation product of the reaction of **1** with MCPBA (green line).

**Figure 1a**

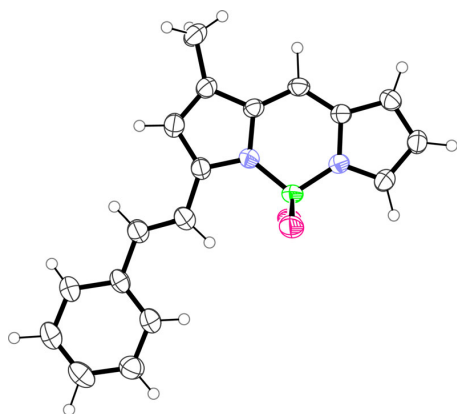


**Figure 1b**

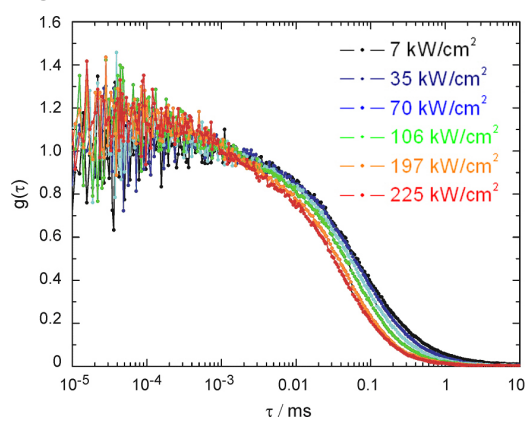


**Figure 2a**

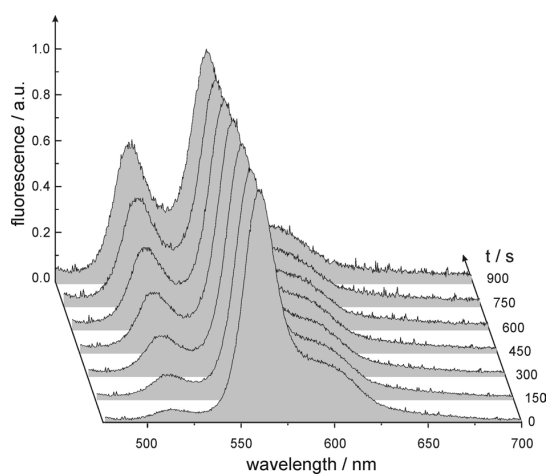


**Figure 2b**

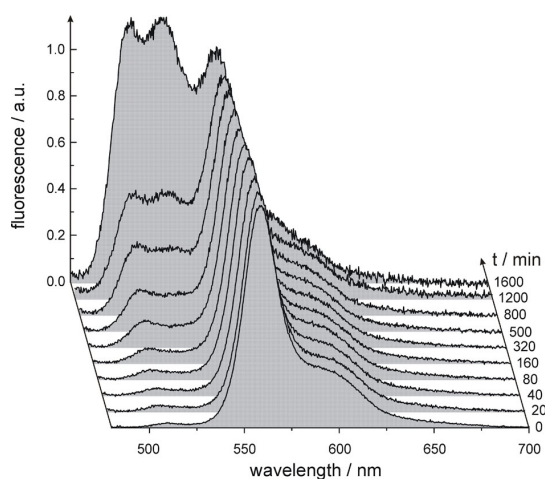
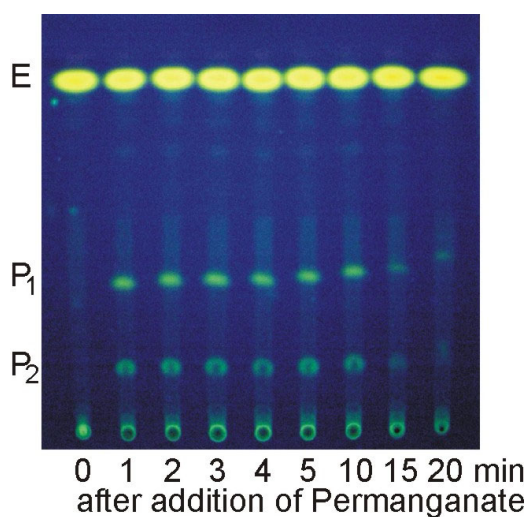
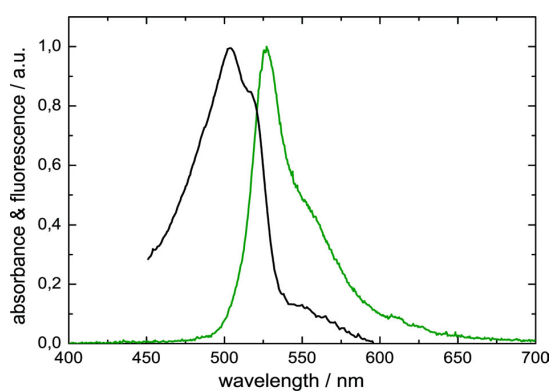
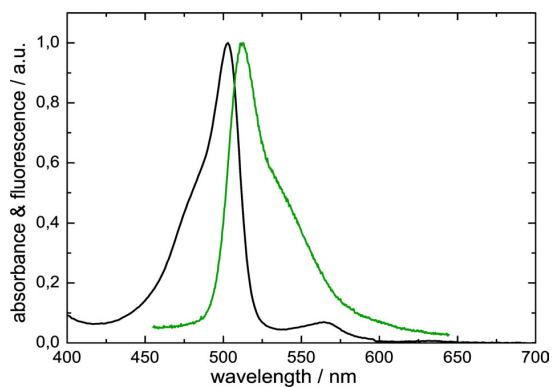


**Figure 2c**

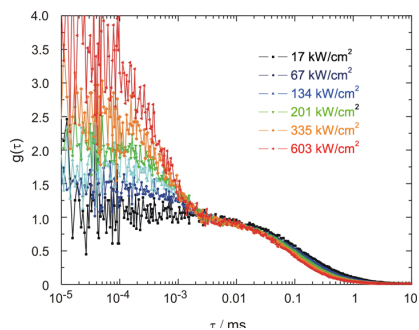


This is a pre-peer reviewed version of the following article: *J Phys. Org. Chem.* (2009), accepted 27-Jun-2009, DOI: 10.1002/poc.1604

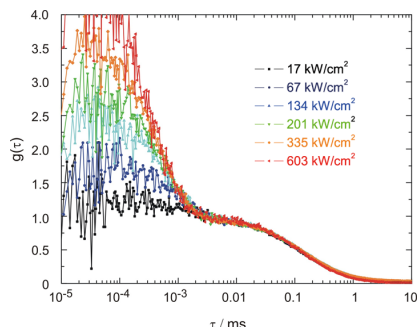
**Figure 3a**



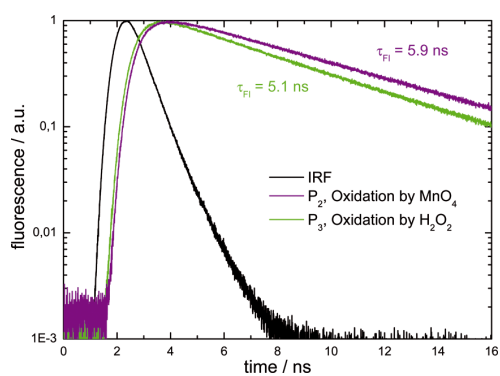
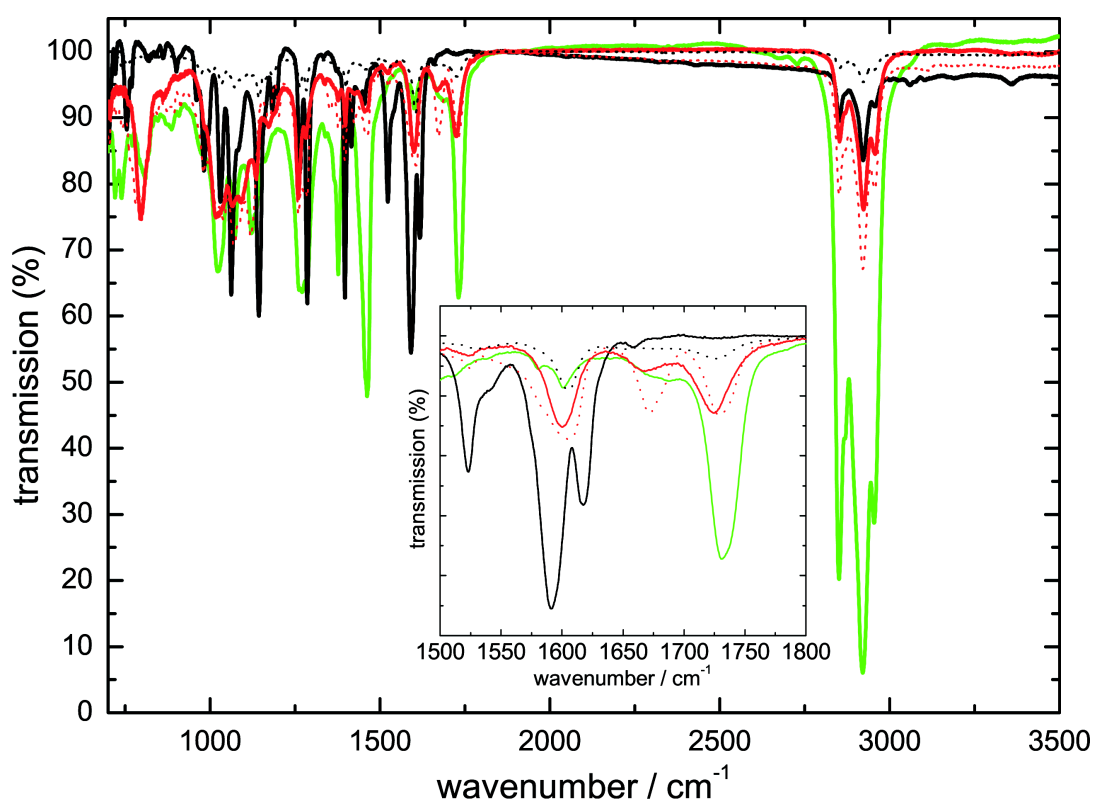
**Figure 3b**



**Figure 3c**



This is a pre-peer reviewed version of the following article: *J Phys. Org. Chem.* (2009), accepted 27-Jun-2009, DOI: 10.1002/poc.1604

**Figure 3d****Figure 3e**

This is a pre-peer reviewed version of the following article: *J Phys. Org. Chem.* (2009), accepted 27-Jun-2009, DOI: 10.1002/poc.1604

**Supporting information:**

Crystallographic data:

"CCDC 693706 contains the supplementary crystallographic data for this paper. These data can be obtained free of charge from The Cambridge Crystallographic Data Centre via [www.ccdc.cam.ac.uk/data\\_request/cif](http://www.ccdc.cam.ac.uk/data_request/cif)"

NMR- Spectroscopic data:

The following spectra show the NMR- spectroscopic characterization of **1**. All signals which are part of the molecule have been identified and assigned. The spectra show the full recorded range. For better overview, important values are represented in the tables.

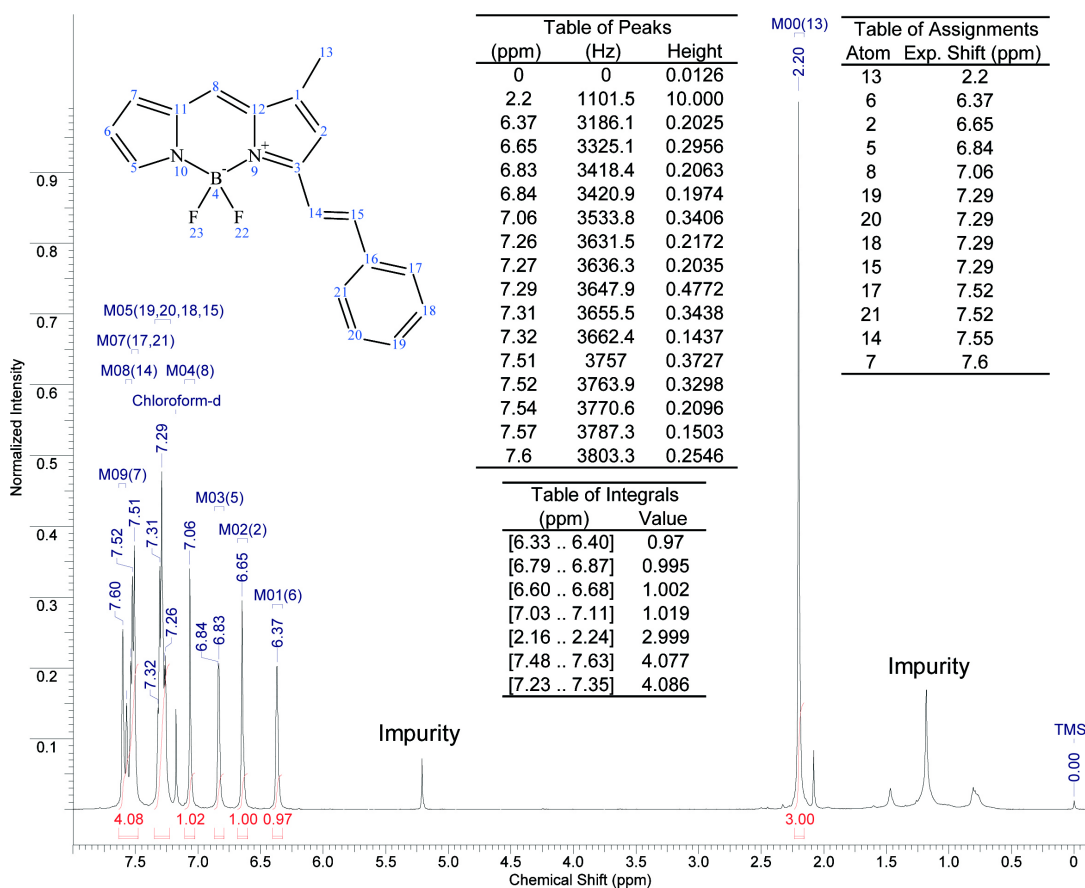
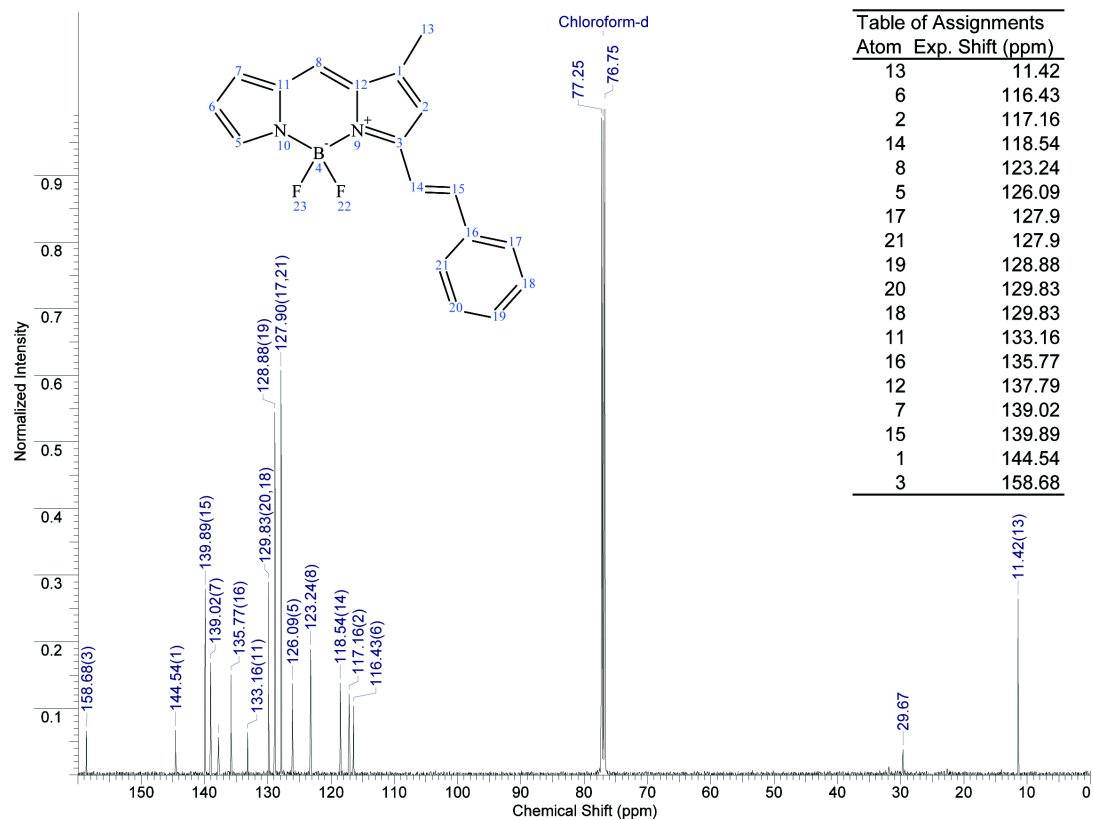
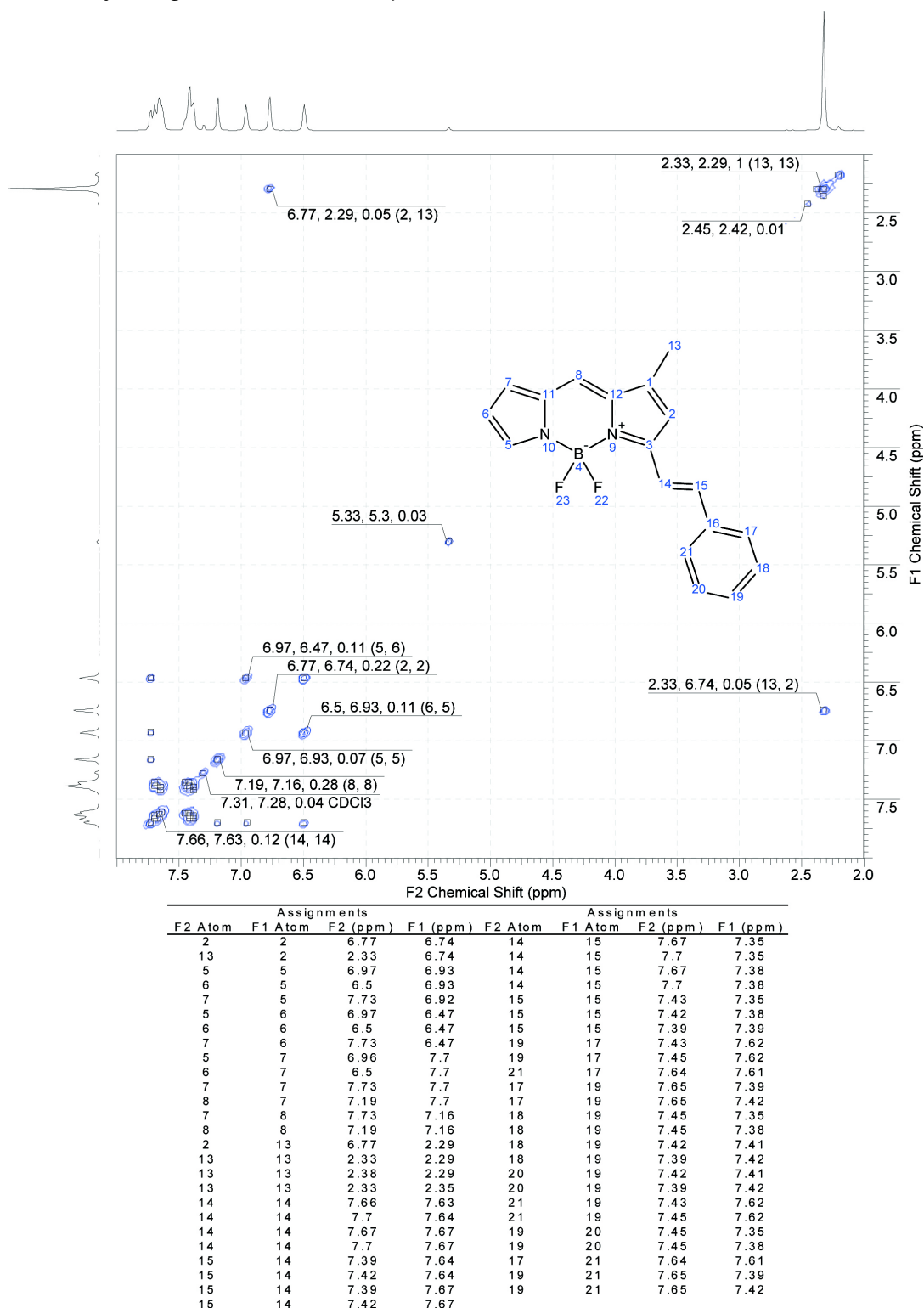


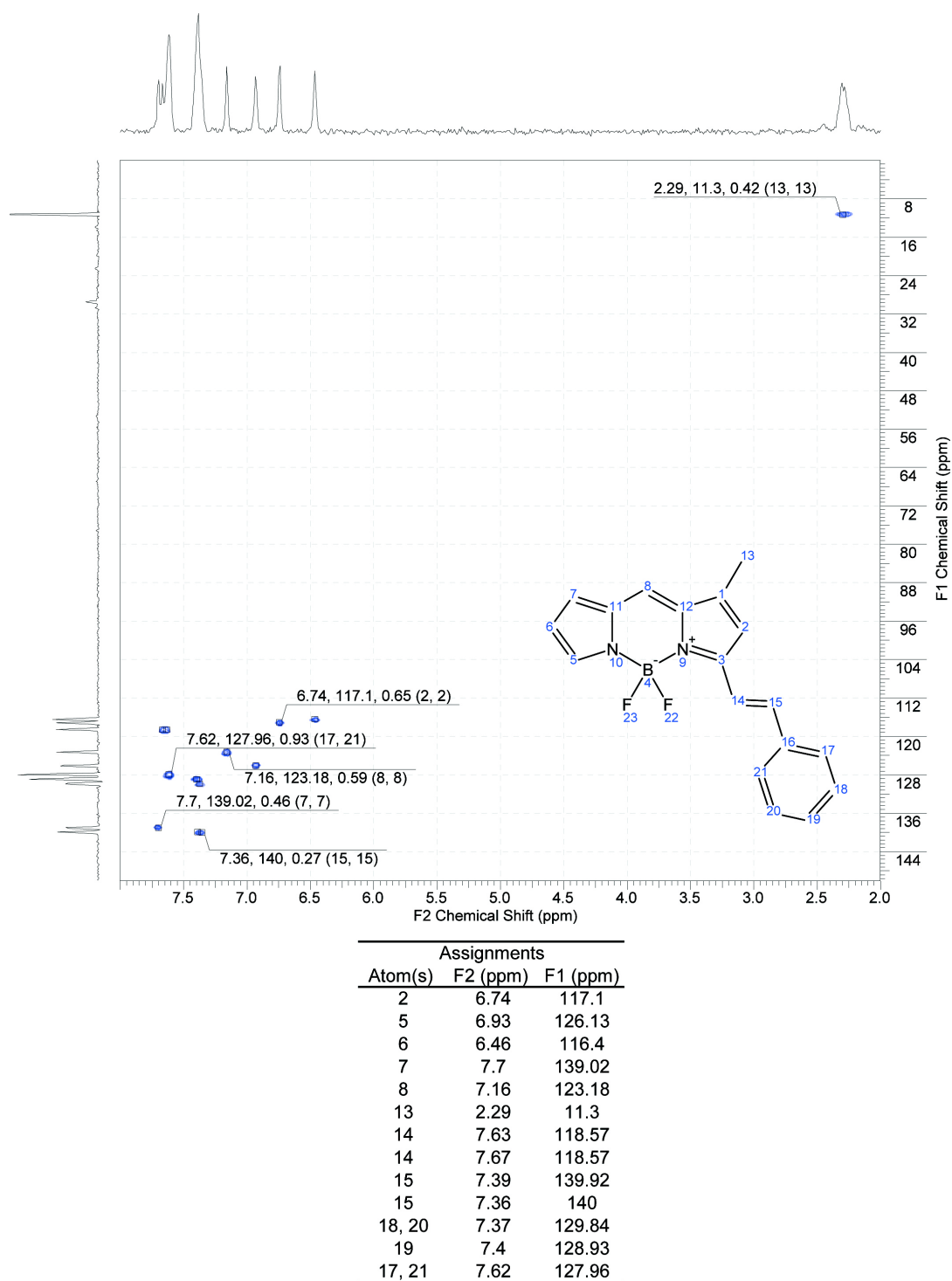
Figure S1: <sup>1</sup>H- NMR- Spectrum of **1**.

This is a pre-peer reviewed version of the following article: *J Phys. Org. Chem.* (2009), accepted 27-Jun-2009, DOI: 10.1002/poc.1604

Figure S2:  $^{13}\text{C}$ -NMR- Spectrum of **1**.

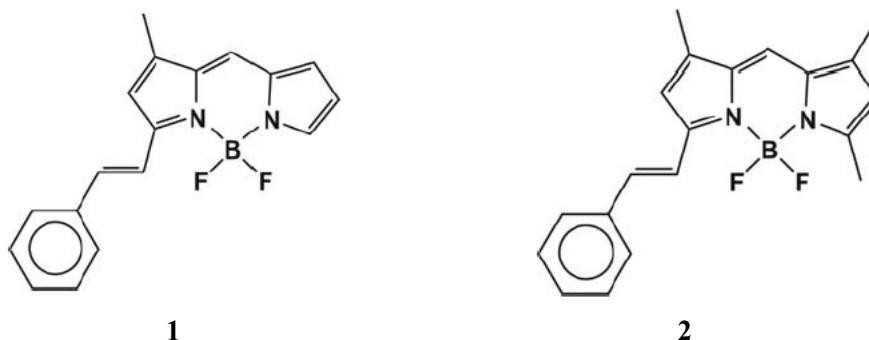
Figure S3: HH-Cosy- NMR- Spectrum of **1**.

This is a pre-peer reviewed version of the following article: *J Phys. Org. Chem.* (2009), accepted 27-Jun-2009, DOI: 10.1002/poc.1604

Figure S4: HC- Cosy- NMR- Spectrum of **1**.

**1,5,7-Trimethyl-3-styryl-4,4'-difluoro-bora-3a-4a-diaza-(s)-indacene (2).**

In addition to the described compound **1** from which we were able to obtain crystals for x-ray diffraction, we also synthesized **2** according to the described procedure. **2** has very similar properties compared to **1** with slightly red-shifted spectra ( $\lambda_{\text{ex}} = 558 \text{ nm}$ ,  $\lambda_{\text{em}} = 566 \text{ nm}$ ).



FCS experiments, which we performed like for **1**, revealed no significant change of the diffusional time  $\tau$ , upon increasing the intensity (see Figure S5). This finding suggests an even higher photostability for **2** than for **1**. This property might become important when the BDP-dyes ought to become immobilized via one of the positions which are methylated in **2** but not in **1**. However, **2** tends to aggregate in aqueous solution as indicated by the curve at the lowest intensity.

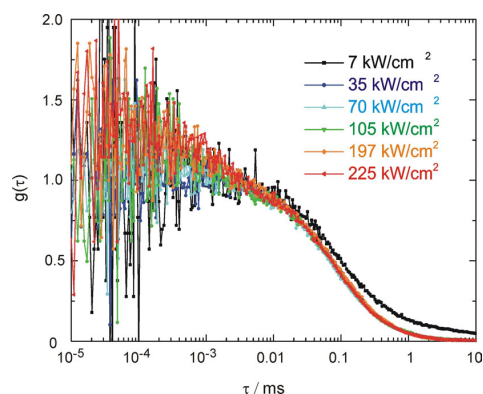


Fig. S5: Intensity dependent FCS-curves of **2** in water ( $\lambda_{\text{ex}} = 544 \text{ nm}$ ).

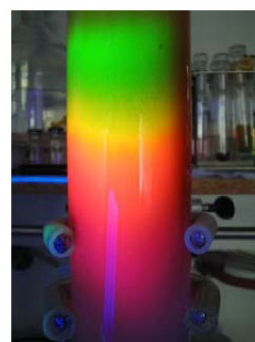


Fig. S6: Column chromatography of **2** (orange). It is followed by the green fluorescent substrate (above) and preceded by the doubly substituted product (red).

Moreover, we renounced at using **2** for our kinetic experiments as the purity of **2** was not as high as that of **1**. The reason is that unconsumed substrate (a green fluorescent BDP), **2** and the doubly substituted BDP (with two Styryl-expansions of the chromophoric system) have obviously similar polarities and, thus, can be hardly separated by column chromatography (see Figure S6).

## 4 Appendix

### 4.1 Research in progress: A BODIPY dye for metathesis screening

To expand the idea of the usage of BODIPY dyes as a probe molecule for chemical agents in order to unravel the dynamics and mechanisms of a chosen reaction on a single-molecule level, a second reaction other than dihydroxylation was brought into focus.

#### 4.1.1 The metathesis reaction

A large research field with a huge perspective in commercial and technical appliance grew in the area of metathesis reactions and the development and design of the employed catalysts [Mil96, Sch96a, Trn01, Sch03].

Metathesis in general means the metal catalyzed exchange of alkylidene or alkylidene units in alkenes or alkynes. These may proceed by homogeneous or heterogeneous catalysis (Figure 4.1).

First observations of the phenomenon have been made with  $\text{TiCl}_4$ , that converted linear olefins in olefins with shorter or longer chain lengths, by Ziegler and Natter in the 1950's. The first metal catalyzed polymerization attempts out of alkenes using the Ziegler catalyst succeeded in 1960 by Truett. Following that experiments were expanded to other metals as catalysts like, tungsten or molybdenum, first in heterogeneous then later in homogeneous catalysis. In 1971 Chauvin proposed a mechanism of metathesis catalysis (Figure 4.1). In 1971, Wilkinson designed his catalyst  $[\text{W}(\text{CH}_3)_6]$ . Five years later the first exchange reaction between a metal methylene and an olefin was observed. This formed the base of the development of the modern metathesis catalysts we know today. In 1980 Schrock designed his catalysts on tungsten and molybdenum base. In 1995 Grubbs developed the first generation of ruthenium-based catalysts. In 2005 Chauvin, Schrock and Grubbs were honoured with the Nobel prize

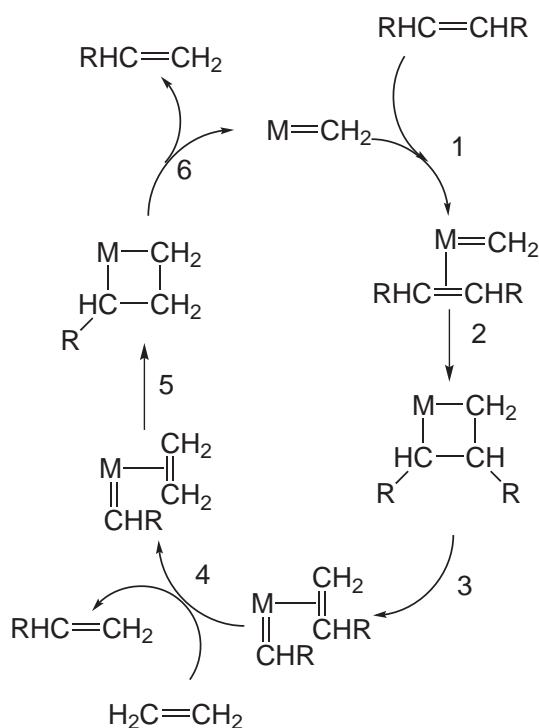


Fig. 4.1: Mechanism of the metathesis reaction as proposed by Chauvin:

1. Coordination of the metal complex to the olefin
2. Formation of a metallacyclobutene intermediate
3. Rearrangement of the metallacyclobutane
4. Exchange of the unsubstituted alkene in the metal complex
5. Formation of a second metallacyclobutene
6. Regeneration of the metal complex and dissociation from the now mixed olefin

for their outstanding achievements in metathesis catalysis technology [Cha06, Sch06, Gru06].

The many different metathesis catalysts which are commercially available these days, and which carry the names of their designers (mostly Schrock and Grubbs) (Figure 4.2) differ in reactivity and tolerance against functional groups in the substrates and selectivity. Nowadays special catalysts for special substrates exist and re-

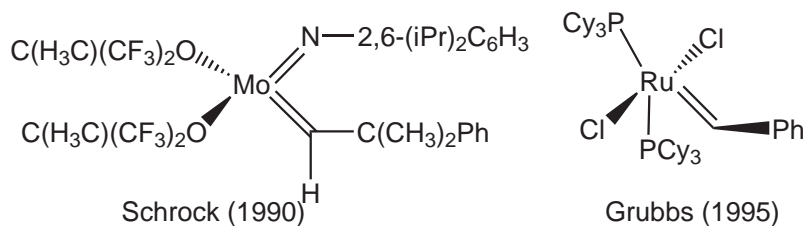


Fig. 4.2: Two popular metathesis catalysts based on molybdenum (Schrock) and ruthenium (Grubbs)

search topics focus on the design of new catalysts that are best suited for their different applications on new substrates [Ald07]. Metathesis catalysts are widely used in oil processing industry, pharmacology, or polymer synthesis. In industrial scales mostly heterogeneous

catalysts are used for convenience of separation from the products. In laboratory and research scale mostly homogeneous catalysts are used. They gain more and more popularity for laboratory syntheses due to some useful properties. They can also be employed in mild reaction conditions (normal pressure, room temperature) and especially ruthenium catalysts are highly stable against air and water compared to tungsten, molybdenum or titanium catalysts.

#### 4.1.2 A BODIPY dye as a probe for metathesis catalysis

Our aim was to design a BODIPY dye as a probe for metathesis catalysis. The dye and its metathesis reaction products should be suitable for single-molecule detection and could be used for ratio-metric screening of metathesis catalysts in combinatoric scales. This could happen by the usage of well plates filled with different metathesis catalysts solutions, where metathesis capable BODIPY would be added and the change of fluorescence colours would be observed by e.g. fluorescence microscopy. A following evaluation of the kinetics and magnitude of these changes could provide valuable information about the effectiveness and suitability of the appropriate catalysts. As a first attempt of such a suitable and metathesis capable BODIPY dye we chose a dye system in analogy to the BODIPY probe dye sensitive to oxidizing species. A BODIPY was synthesized which contained an expanded chromophoric system relative to the core compounds. Part of this expanded chromophore should be the target functional groups. The synthesis of this dye was performed in analogy to the orange fluorescent oxidant probe BODIPY **6** (Figure 4.3) The synthesis involved a Knoevenagel-like condensation

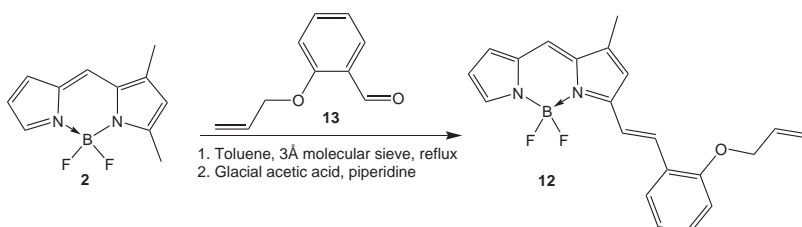


Fig. 4.3: Synthesis of 1-Methyl-3-(2'-Allyloxy-1-styryl)-4-difluorobor-3a,4a-diaza-(S)-indacen (**12**)

of 2-Allyloxy-benzaldehyde (**13**) and BODIPY core compound **2** to yield the orange fluorescent 1-Methyl-3-(2'-Allyloxy-1-styryl)-4-difluorobor-3a,4a-diaza-(S)-indacen (**12**). In addition to this dye the 4-Allyloxy-analogue **14** of dye **12** was synthesized to show that this dye could not undergo a metathesis reaction. Both species have been characterized by NMR spectroscopy and crystallography (Figure 4.4). BODIPY dye **12** has also been characterized by highly

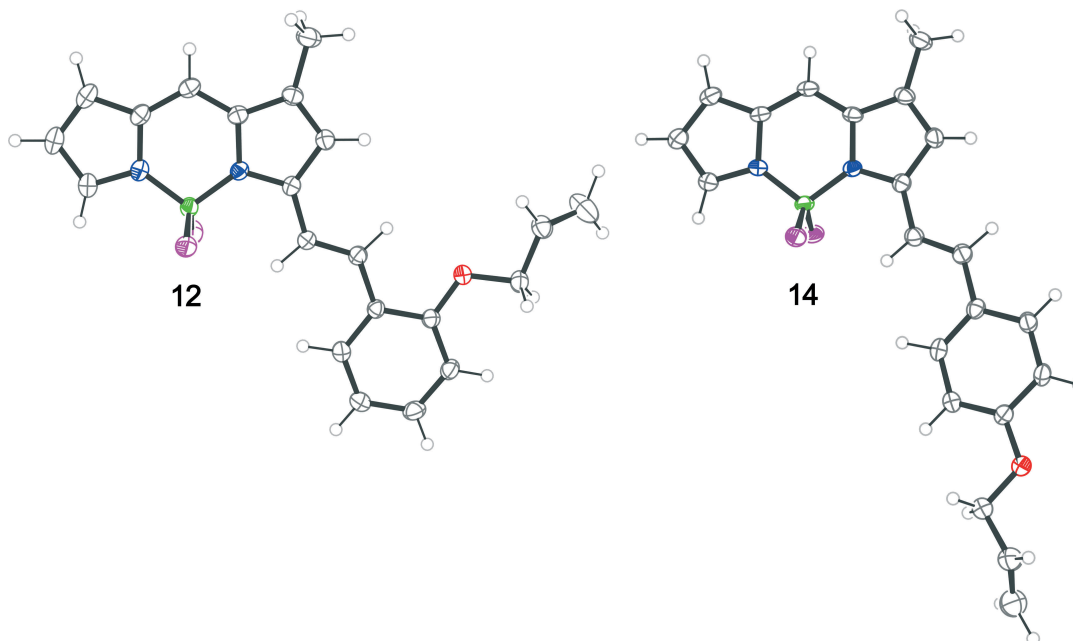


Fig. 4.4: Crystallographic structures of 1-Methyl-3-(2'-Allyloxy-1-styryl)-4-difluorobor-3a,4a-diaza-(S)-indacen (**12**) and 1-Methyl-3-(4'-Allyloxy-1-styryl)-4-difluorobor-3a,4a-diaza-(S)-indacen (**14**)

sensitive optical spectroscopy (excitation/emission (Figure 4.5), TC-SPC and FCS (Figure 4.6)). Photophysical data have been collected as  $\lambda(\text{Ex})_{\text{max}}=560\text{nm}$ ,  $\lambda(\text{Em})_{\text{max}}=571\text{nm}$ ,  $\tau_{\text{Fl}}=5.25\text{ns}$ ,  $k_{23}=170.000\text{ s}^{-1}$  and  $k_{31}=1.042.000\text{ s}^{-1}$ .

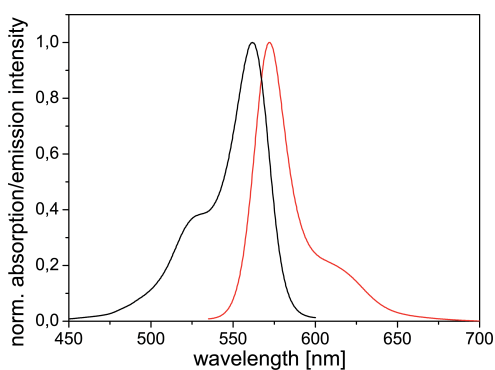


Fig. 4.5: Excitation and emission spectrum of metathesis probe dye **12**

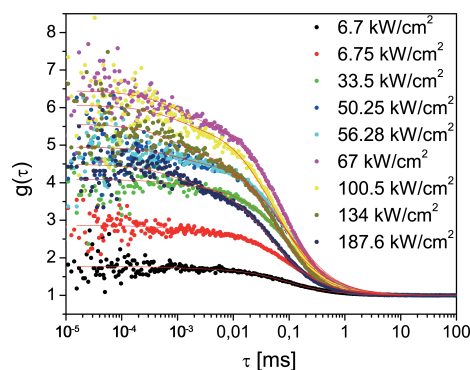


Fig. 4.6: FCS spectrum of metathesis probe dye **12** ( $\lambda_{ex}=544\text{nm}$ )

### 4.1.3 BODIPYs and Grubbs reactions

In presence of a metathesis catalyst, e.g. a Grubbs catalyst, the orange fluorescent dye would undergo an intramolecular alkene exchange that yields two molecules. A green fluorescent BODIPY core compound and a non fluorescent species (Figure 4.7). Unfortunately

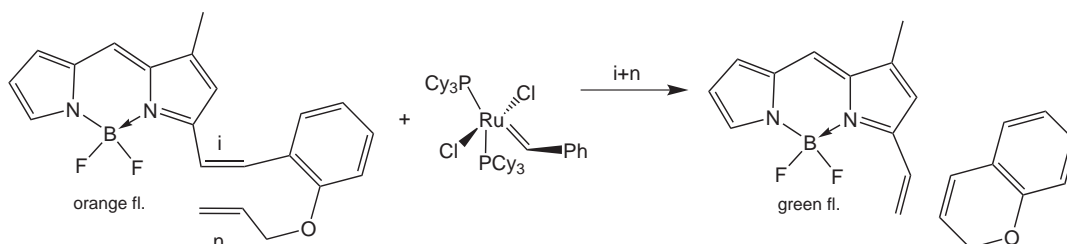


Fig. 4.7: Assumed product generation of a reaction between a metathesis capable BODIPY dye and a Grubbs catalyst

a far more complex product mixture than the expected (Figure 4.7) was obtained, which is related to the reaction conditions and concentration issues. Products could only be characterized by fluorescence and absorption techniques. This is to the low amounts of usable dye and therefore small product yields, in addition with product instability.

Figure 4.8 shows a thin layer chromatography foil where the compounds **12** and **14** were exposed to a qualitative amount of first generation Grubbs catalyst (Grubbs1, G1). Only with compound **12** green/yellowish fluorescent products (emphasized by red circles) appeared. With both dyes, however, multiple spots with orange flu-

orescence were generated. Attempts to isolate these products with

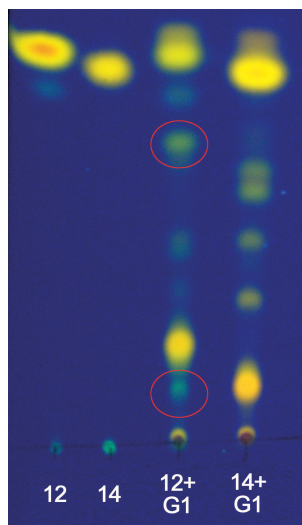


Fig. 4.8: Thin layer chromatography foil under UV light ( $\lambda_{ex}=350\text{nm}$ ) showing the influence of Grubbs1 catalyst to the orange fluorescent dyes **12** and **14**. Fluorescent products with shorter fluorescence wavelengths than the educts appear only with dye **12** (marked by red circles)

hypsochromic emission wavelengths relative to the educt were made. A strong correlation between the amount of catalyst and fluorescent substrate was observed. This circumstance caused many other fluorescent product spots to appear. To accelerate the reaction catalyst was added in excess concentrations. An addition of constant amounts of catalyst resulted in increasing numbers and intensity of new products (Figure 4.9). It is obvious that most of the ap-

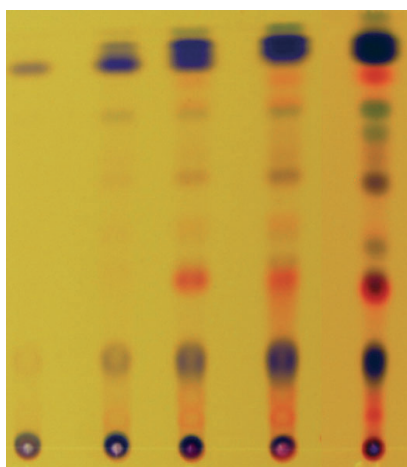


Fig. 4.9: Thin layer chromatography foil under UV light ( $\lambda_{ex}=350\text{nm}$ ) displayed with inverted colours to show the increasing appearance of product spots by addition of constant qualitative amounts of Grubbs1 catalyst to dye **12**

pearing spots are follow-up products of initially formed products. Under the reaction circumstances a number of products is imaginable. These include intermolecular and intramolecular reactions

between dye molecules and their follow-up products among themselves. In addition reactions between these products and the alkene unit of the catalyst molecule are possible. Figure 4.10 shows a selection of possible reactions of alkene unit bearing dye molecules and catalyst molecules. The projected products are marked with numbers and letters to describe the reaction sites and pathways. The

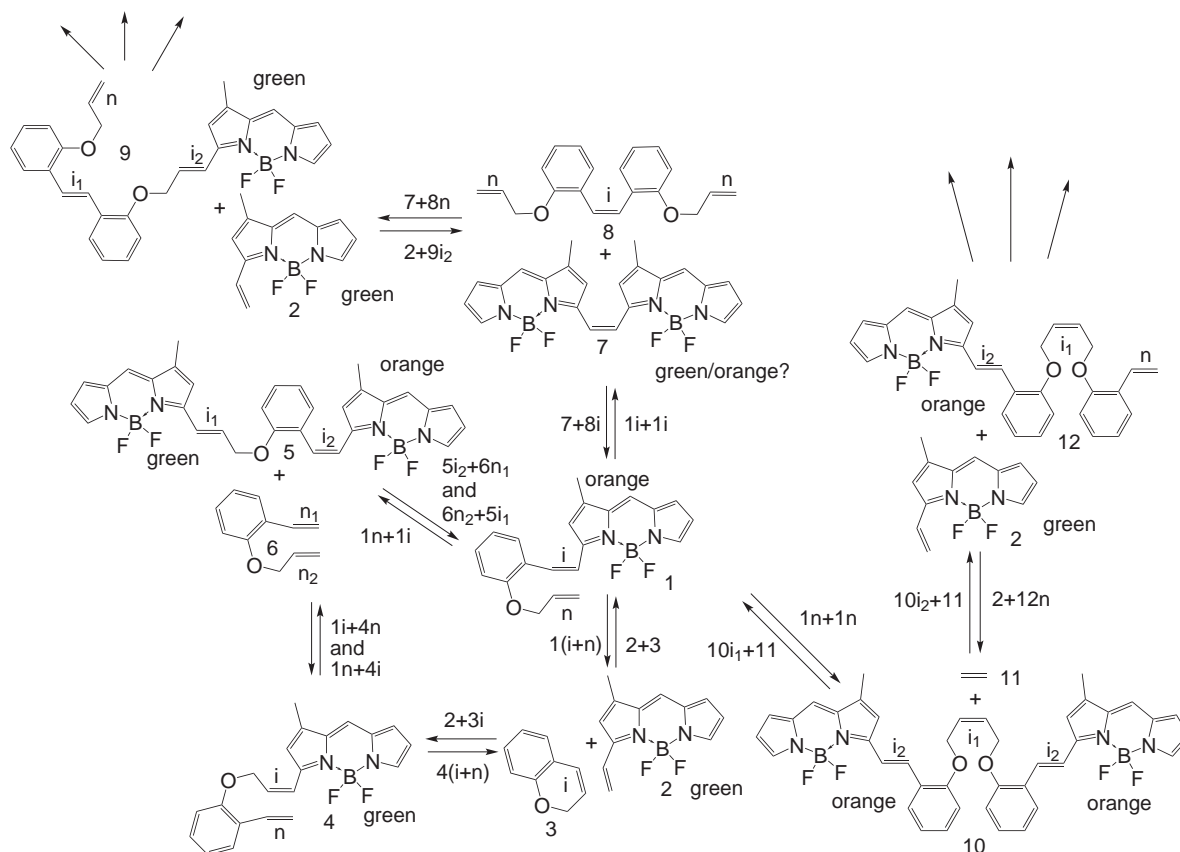


Fig. 4.10: Assumed product generation of a reaction between a metathesis capable BODIPY dye and a Grubbs catalyst (see text for explanation of scheme)

numbers identify the molecules and the letters identify the double bonds which react.  $n$  stands for terminal bonds, and  $i$  for intrinsic bonds. If more than one or unsymmetrical bonds exist in a molecule they are further marked by an index number. A reaction marked as  $5i_2+6n_1$  means that the intrinsic double bond  $i_2$  of molecule 5 reacts with the terminal double bond  $n_1$  of molecule 6. A reaction marked with  $1(i+n)$  means an intramolecular reaction of the intrinsic and terminal double bonds. Also the estimated fluorescence colour of the molecules is noted. This confusing scheme clearly shows one of

the main technical problems that have to be overcome before any screening appliance of the system is thinkable: to control the product generation. In addition the nature of the emerging products is totally unknown. Attempts to isolate interesting products from the reaction of **12** with Grubbs1 were successful, but the products were not stable and structure determinations by means of combination of mass spectroscopy, NMR spectroscopy or crystallography were not yet possible. But it was possible to figure out which of the most intensely emerged product spots could be assigned to be follow-up products. To determine which of the products were follow-up products a new TLC experiment was conducted (Figure 4.11). Here,

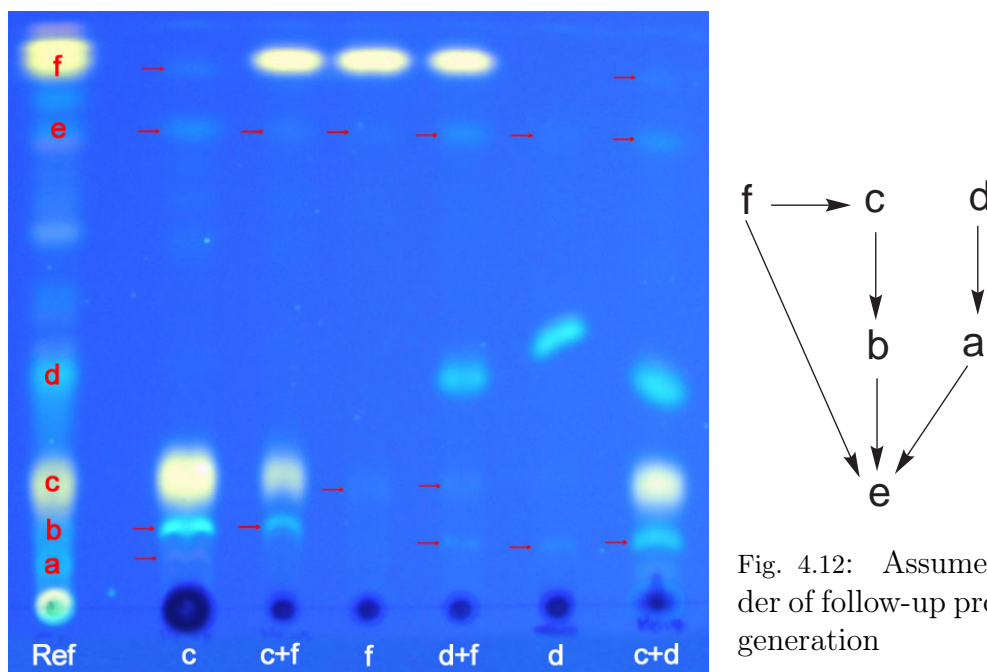


Fig. 4.11: TLC foil showing the intermediate products and their combinations to determine possible follow-up products ( $\lambda_{ex}=350\text{nm}$ )

from the reference compound (Ref), three spots were assigned to be initial products, due to their appearance at the beginning of the reaction (c, yellow, d, green, f, yellow). These spots were isolated by being scratched off individually from the TLC foil with following dissolving. Then the pure products and combinations of the products, as shown in figure 4.11, were exposed to catalyst and applied to TLC. For better visibility spots that are hardly to recognize on

the recorded picture are emphasized by red arrows. It is visible that the spots a, b and e are follow-up products. Product e is formed in every combination of products indicating the formation of a product that can be built up on each of the reaction paths. Product b is clearly a follow-up product of product c. Product a is formed in small amounts, obviously from product d (Figure 4.12). As mentioned the nature of these products is still unknown. But it can be stated that the following analysis concentrated on the initial products c, d and f. These could at least be characterized by high sensitive optical spectroscopy like excitation/emission-, FCS- and TCSPC-spectroscopy. Figures 4.13 and 4.14 show the received data of product c,

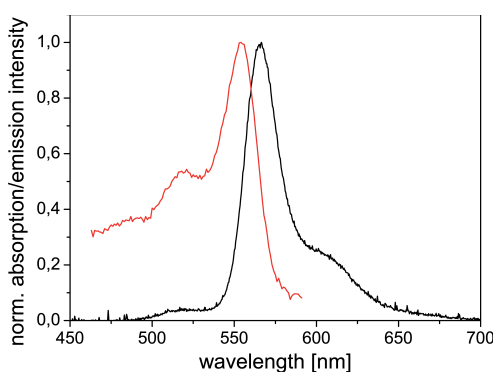


Fig. 4.13: Excitation and emission spectrum of metathesis intermediate c

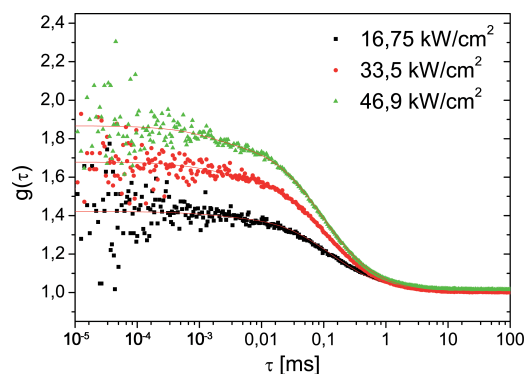


Fig. 4.14: FCS spectrum of metathesis intermediate c ( $\lambda_{ex}=544\text{nm}$ )

figures 4.15 and 4.16 the data of product d and figures 4.17 and 4.18

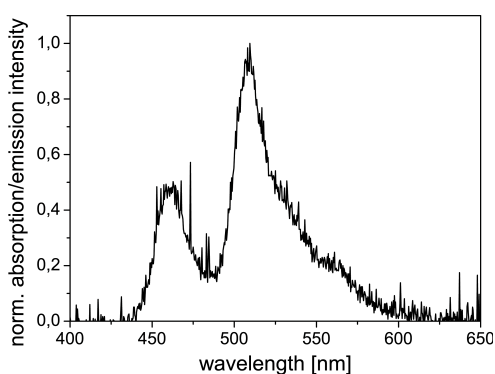


Fig. 4.15: Excitation and emission spectrum of metathesis intermediate d

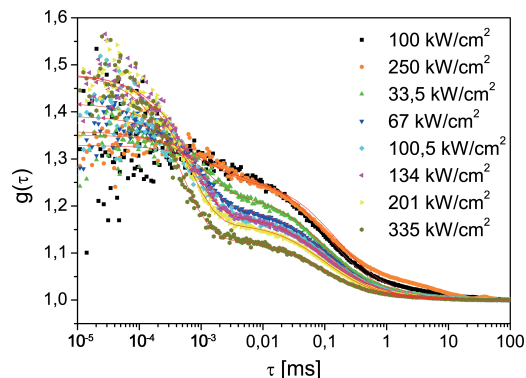


Fig. 4.16: FCS spectrum of metathesis intermediate d ( $\lambda_{ex}=544\text{nm}$ )

the data of product f. The collected data of the three products is

#### 4.1 Metathesis BODIPY

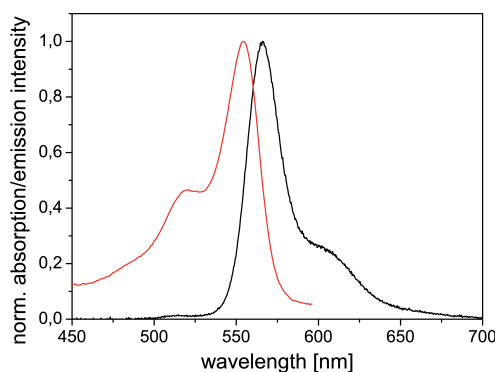


Fig. 4.17: Excitation and emission spectrum of metathesis intermediate f

#### 4.1.3. BODIPY and Grubbs reactions

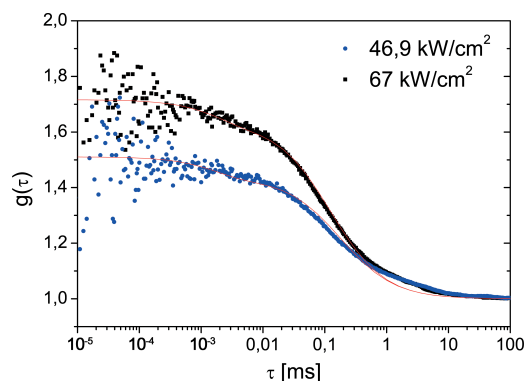


Fig. 4.18: FCS spectrum of metathesis intermediate f ( $\lambda_{ex}=544\text{nm}$ )

shown in figure 4.19.

| Product | $\lambda_{ex}$ [nm] | $\lambda_{em}$ [nm] | $\tau_{fl}$ [ns] | $\tau_{diff}$ [ms] |
|---------|---------------------|---------------------|------------------|--------------------|
| c       | 554                 | 566                 | 4.01             | 0.11               |
| d       | 502                 | 510                 | 5.72             | 0.11               |
| f       | 554                 | 566                 | 4.12             | 0.15               |

Fig. 4.19: Data collected by photophysical means of the metathesis products c, d and f

#### 4.1.4 Conclusion on metathesis

Although technical problems need to be overcome, a proof-of-principle was obtained. A reaction with Grubbs1 catalyst indicated conversion of the educt to a variety of different coloured products. Characterization of these products, however, could only be achieved on a level of assignment of follow-up products, due to an implemented excess of used catalysts. A structural characterization will be crucial for upcoming research and analysis of the occurred mechanism and product generation. To achieve this aim, a well timed qualitative analysis of catalysis is needed and intermediate products need to be synthesized in a more targeted way on a larger scale and structural characterization must be performed quickly. HPLC purification of the reaction products should also be researched and applied to make sure that no more reactive species destroy or convert the reaction products. A structural alteration of the educt might also be proposed to enhance the performance and selectivity of product generation.

## 4.2 Bibliography

- [Agm05] N. Agmon *J. Phys. Chem. A*, **109** (2005), 13–35.
- [Ald07] Aldrich *Aldrichim. acta*, **40** (2007), 1–28.
- [Atk98] P. W. Atkins, *Physical chemistry*, Oxford University Press, Oxford Melbourne Toko, 1998.
- [Bar05] M. Baruah, W. W. Qin, R. A. L. Vallee, D. Beljonne, T. Rohand, W. Dehaen, and N. Boens *Org. Lett.*, **7** (2005), 4377–4380.
- [Bet93] E. Betzig and R. J. Chichester *Science*, **262** (1993), 1422–1425.
- [Bin82] G. Binnig, H. Rohrer, Ch. Gerber, and E. Weibel *Phys. Rev. Lett.*, **49** (1982), 57–61.
- [Bün87] G. Büнау, *Photochemie*, Wiley VCH, Weinheim, 1987.
- [Boy89] J. Boyer, *Patent US 4,779,230*, 1989.
- [Bur03] R. Burgstahler, H. Koegel, F. Rucker, D. Tracey, P. Grafe, and C. Alzheimer *Am. J. Phys.*, **284** (2003), 944–952.
- [Cha06] Y. Chauvin *Angew. Chem. Int. Ed.*, **45** (2006), 3740–3747.
- [Cho06] J. K. Choi, A. Lee, S. Kim, S. Ham, K. No, and J. S. Kim *Org. Lett.*, **8** (2006), 1601–1604.
- [Dap95] J. Dapprich, U. Mets, W. Simm, M. Eigen, and R. Rigler *Exp. Tech. Phys.*, **41** (1995), 259–264.
- [Dem08] A.P. Demchenko, *Introduction to fluorescence sensing*, Springer Netherlands, Dordrecht, 2008.
- [Dru02] G. P. C. Drummen, L. C. M. van Liebergen, J. A. F. Op den Kamp, and J. A. Post *Free Radical Biol. Medicine*, **33** (2002), 473–490.

- [Eer04] O. Eerbeek, E. G. Mik, C. J. Zuurbier, M. van 't Loo, C. Donkersloot, and C. Ince *J. Appl. Phys.*, **97** (2004), 2042–2050.
- [Egg98] C. Eggeling, J. Widengren, R. Rigler, and C. A. M. Seidel *An. Chem.*, **70** (1998), 2651–2659.
- [Egg05] C. Eggeling, A. Volkmer, and C. A. M. Seidel *Chemphyschem*, **6** (2005), 791–804.
- [Ehr74] W. Ehrenberg and R. Rigler *Chem. Phys.*, **4** (1974), 390–401.
- [Els74] E. L. Elson and D. Magde *Biopolymers*, **13** (1974), 1–27.
- [End05] J. Enderlein, I. Gregor, D. Patra, T. Dertinger, and U. B. Kaupp *Chemphyschem*, **6** (2005), 2324–2336.
- [För49] Th. Förster *Naturwiss.*, **36** (1949), 186.
- [För50] Th. Förster *Elektrochem.*, **54** (1950), 42.
- [För51] Th. Förster, *Fluoreszenz organischer verbindungen*, Vandenhoeck & Ruprecht, Göttingen, 1951.
- [Gab04] Y. Gabe, Y. Urano, K. Kikuchi, H. Kojima, and T. Nagano *J. Am. Chem. Soc.*, **126** (2004), 3357–3367.
- [Gar01] S. Garfield, *How one man invented a color that changed the world*, W. W. Norton & Company, New York, 2001.
- [Gre05] K. O. Greulich *Chemphyschem*, **6** (2005), 2458–2471.
- [Gro94] E. Gross, R. S. Bedlack, and L. M. Loew *Biophys. J.*, **67** (1994), 208–216.
- [Gru06] R. H. Grubbs *Angew. Chem. Int. Ed.*, **45** (2006), 3760–3765.
- [Gry85] G. Grynkiewicz, M. Poenie, and R. Y. Tsien *J. Biol. Chem.*, **260** (1985), 3440–3450.

## 4.2 Bibliography

- [Hau88] R. P. Haughland and H. C. Kang, *Patent US 4,774,339*, 1988.
- [Hau02] R. P. Haughland, *The handbook- a guide to fluorescent probes and labeling technologies*, <http://www.invitrogen.com/site/us/en/home/References/Molecular-Probes-The-Handbook.html>.
- [Hua05] Q. Huang and W. L. Fu *Clin. Chem. Lab. Med.*, **43** (2005), 841–842.
- [Jun01] G. Jung, *Zweifارben-Fluoreszenzkorrelationsspektroskopie am Grün Fluoreszierenden Protein und seinen Mutanten*, Ph.D. thesis, L. M. Univ. München, 2001.
- [Kab99] B. Kaboudin *J. Chem. Res.*, (1999), 402–403.
- [Kam76] M. J. Kamlet and R. W. Taft *J. Am. Chem. Soc.*, **98** (1976), 377–383.
- [Kam77] M. J. Kamlet, J. L. Abboud, and R. W. Taft *J. Am. Chem. Soc.*, **99** (1977), 6027–6038.
- [Kam83] M. J. Kamlet, M. H. Abraham, and R. W. Taft *J. Org. Chem.*, **48** (1983), 2877–2887.
- [Kan93] H. C. Kang and R. P. Haughland, *Patent US 5,187,288*, 1993.
- [Kol99] M. Kollmannsberger, *Bor- Dipyrrromethenfarbstoffe als Fluoreszenz- und Redoxschalter*, Ph.D. thesis, Univ. Regensburg, 1999.
- [Kon82] H. Kondo, I. Miwa, and J. Sunamoto *J. Phys. Chem.*, **86** (1982), 4826–4831.
- [Lak99] J. R. Lakowicz, *Principles of fluorescence spectroscopy*, Kluwer, New York, 1999.
- [Lau94] C. Laurence, P. Nicolet, M. T. Dalati, J. L. M. Abboud, and R. Notario *J. Phys. Chem.*, **98** (1994), 5807–5816.

- [Laz92] S. Lazar and G. Guillaumet *Synth. Comm.*, **22** (1992), 923–931.
- [Lea06] M. C. Leake, J. H. Chandler, and G. H. Wadhams *Nature*, **443** (2006), 355–358.
- [Lee05] S. H. Lee, S. H. Kim, S. K. Kim, J. H. Jung, and J. S. Kim *J. Org. Chem.*, **70** (2005), 9288–9295.
- [Lew39] G.N. Lewis and M. Calvin *Chemical Reviews*, **25** (1939), 273–328.
- [Li98] F. R. Li, S. I. Yang, Y. Z. Ciringh, J. Seth, D. F. Bocian, D. Holten, and J. S. Lindsey *J. Am. Chem. Soc.*, **120** (1998), 10001–10017.
- [Lip57] E. Lippert *Z. f. Elektroch.*, **61** (1957), 962–975.
- [Lou07] A. Loudet and K. Burgess *Chem. Rev.*, **107** (2007), 4891–4932.
- [Mag72] D. Magde, W. W. Webb, and E. Elson *Phys. Rev. Lett.*, **29** (1972), 705.
- [Mag74] D. Magde, E. L. Elson, and W. W. Webb *Biopolymers*, **13** (1974), 29–61.
- [Mar01] J. March and M. B. Smith, *Advanced organic chemistry*, Wiley Interscience, New York, 2001.
- [Mil96] S. J. Miller, H. E. Blackwell, and R. H. Grubbs *J. Am. Chem. Soc.*, **118** (1996), 9606–9614.
- [Moe89] W. E. Moerner and L. Kador *Phys. Rev. Lett.*, **62** (1989), 2535–2538.
- [Moh05] O. F. Mohammed, D. Pines, J. Dreyer, E. Pines, and E. T. J. Nibbering *Science*, **310** (2005), 83–86.
- [Mon89] F. J. Monsma, A. C. Barton, H. C. Kang, D. L. Brassard, R. P. Haugland, and D. R. Sibley *J. Neurochemistry*, **52** (1989), 1641–1644.

## 4.2 Bibliography

- [Mor93] R. Morgan and J. Boyer, *Patent US 5,446,157*, 1993.
- [Nie94] S. M. Nie, D. T. Chiu, and R. N. Zare *Science*, **266** (1994), 1018–1021.
- [Orr90] M. Orrit and J. Bernard *Phys. Rev. Lett.*, **65** (1990), 2716–2719.
- [Par85] J. A. Pardoen, J. Lugtenburg, and G. W. Canters *J. Phys. Chem.*, **89** (1985), 4272–4277.
- [Pet49] S. Petersen *Z. Angew. Chem.*, **61** (1949), 17.
- [Pic90] C. L. Picou, E. D. Stevens, M. Shah, and J. H. Boyer *Acta Cryst.*, **46** (1990), 1148–1150.
- [Pro00] Molecular Probes, Oregon, USA, <http://www.invitrogen.com>.
- [Qin06] W. W. Qin, T. Rohand, M. Baruah, A. Stefan, M. Van der Auweraer, W. Dehaen, and N. Boens *Chem. Phys. Lett.*, **420** (2006), 562–568.
- [Rei03] C. Reichardt, *Solvents and solvent effects in organic chemistry*, Wiley VCH, Weinheim, 2003.
- [Roh06a] T. Rohand, M. Baruah, W. W. Qin, N. Boens, and W. Dehaen *Chem. Comm.*, (2006), 266–268.
- [Roh06b] T. Rohand, W. W. Qin, N. Boens, and W. Dehaen *Eur. J. Org. Chem.*, (2006), 4658–4663.
- [Sat94] G. Sathyamoorthi, L. T. Wolford, A. M. Haag, and J. H. Boyer *Heteroatom Chem.*, **5** (1994), 245–249.
- [Sch96a] P. Schwab, R. H. Grubbs, and J. W. Ziller *J. Am. Chem. Soc.*, **118** (1996), 100–110.
- [Sch96b] P. Schwille, *Fluoreszenz-Korrelations-Spektroskopie: Analyse biochemischer Systeme auf Einzelmolekülebene*, Ph.D. thesis, Techn. Univ. Braunschweig, 1996.

- [Sch03] B. Schmidt *Angew. Chem. Int. Ed.*, **42** (2003), 4996–4999.
- [Sch06] R. R. Schrock *Angew. Chem. Int. Ed.*, **45** (2006), 3748–3759.
- [Sil96] L. J. Silverberg, J. L. Dillon, and P. Vemishetti *Tetrahedron Lett.*, **37** (1996), 771–774.
- [Sol98a] K. M. Solntsev, D. Huppert, and N. Agmon *J. Phys. Chem. A*, **102** (1998), 9599–9606.
- [Sol98b] K. M. Solntsev, D. Huppert, L. M. Tolbert, and N. Agmon *J. Am. Chem. Soc.*, **120** (1998), 7981–7982.
- [Sol99] K. M. Solntsev, D. Huppert, and N. Agmon *J. Phys. Chem. A*, **103** (1999), 6984–6997.
- [Sot07] M. Sotomayor and K. Schulten *Science*, **316** (2007), 1144–1148.
- [Spr07] D. B. Spry and M. D. Fayer *J. Chem. Phys.*, **127** (2007), 204501.
- [Sun97] W. C. Sun, K. R. Gee, D. H. Klaubert, and R. P. Haugland *J. Org. Chem.*, **62** (1997), 6469–6475.
- [Taf76] R. W. Taft and M. J. Kamlet *J. Am. Chem. Soc.*, **98** (1976), 2886–2894.
- [Tol02] L. M. Tolbert and K. M. Solntsev *Accounts Chem. Research*, **35** (2002), 19–27.
- [Tre68] A. Treibs and F. H. Kreuzer *Liebigs Ann. Chem.*, **718** (1968), 208.
- [Trn01] T. M. Trnka and R. H. Grubbs *Acc. Chem. Res.*, **34** (2001), 18–29.
- [Tsi98] R. Y. Tsiens *Ann. Rev. Biochem.*, **67** (1998), 509–544.
- [Ulr04] G. Ulrich and R. Ziessel *J. Org. Chem.*, **69** (2004), 2070–2083.

## 4.2 Bibliography

- [Ulr08] G. Ulrich, R. Ziessel, and A. Harriman *Angew. Chem. Int. Ed.*, **47** (2008), 1184–1201.
- [Upp99] J. Uppenbrink and D. Clery *Science*, **283** (1999), 1667.
- [Wan03] C. W. Wan, A. Burghart, J. Chen, F. Bergstrom, L. B. A. Johansson, R. M. Hochstrasser, and K. Burgess *Chem. Eur. J.*, **9** (2003), 4430–4441.
- [Wid95] J. Widengren, U. Mets, and R. Rigler *J. Phys. Chem.*, **99** (1995), 13368–13379.
- [Xie06] X. S. Xie, J. Yu, and W. Y. Yang *Science*, **312** (2006), 228–230.
- [Yu06] J. Yu, J. Xiao, and X. S. Xie *Science*, **311** (2006), 1600–1603.

### 4.3 List of Figures

|      |   |    |
|------|---|----|
| 2.1  | BODIPY fluorophore with atom numbering . . . . .  | 7  |
| 2.2  | Relative polarisation of the atoms in the BODIPY core framework [Kol99] . . . . .   | 7  |
| 2.3  | 2D-HH-COSY-NMR-spectrum of the BODIPY core compound and its crystallographic structure with atom numbering . . . . .  | 8  |
| 2.4  | Synthesis of symmetric BODIPY dyes from pyrroles and acid chlorides or anhydrides . . . . .   | 9  |
| 2.5  | Synthesis of BODIPY dyes from pyrroles and aldehydes, involving an additional oxidation step . . . . .  | 9  |
| 2.6  | Performed synthesis of BODIPY core compounds via the symmetric route . . . . .  | 10 |
| 2.7  | Synthesis of asymmetric BODIPY dyes from carbonyl-pyrroles and pyrroles . . . . .   | 10 |
| 2.8  | Performed synthesis of BODIPY core compounds via the asymmetric route . . . . .   | 11 |
| 2.9  | Applied synthesis of BODIPY dyes with expanded chromophoric system derived from the BODIPY core compound <b>2</b> . . . . .   | 12 |
| 2.10 | Applied synthesis of BODIPY dyes with expanded chromophoric system derived from the <i>meso</i> -substituted BODIPY core compound <b>4</b> . . . . .  | 12 |
| 2.11 | Green-yellow fluorescent Rhodamine 110 and orange-red fluorescent Rhodamine B as competitor dyes to the applied BODIPY dye system . . . . .   | 14 |
| 2.12 | Structures of the used fluorescein dyes . . . . .   | 16 |
| 2.13 | Structures of the used BODIPY dyes . . . . .  | 16 |
| 2.14 | Disabling PeT in BODIPY <b>5</b> . By lowering the energy of the highest occupied molecular orbital in the donor moiety (D), i.e. raising the oxidation potential, electron transfer to the singly occupied molecular orbital of the accepting moiety (A) is disabled . . . . . | 17 |
| 2.15 | Pyranines used for reinvestigation of their solvatochromism   | 18 |

#### 4.3 List of Figures

|      |  |    |
|------|--|----|
| 2.16 | Dihydroxylation chemistry of compound <b>6</b> . . . . .   | 18 |
| 2.17 | Assumed product generation of a reaction between a metathesis capable BODIPY dye and a Grubbs catalyst (i stands for the intrinsic double bond and n for the terminal double bond which react with one another) . . . . .  | 19 |
| 2.18 | Schematic setup of the absorption (UV/Vis) spectrometer Perkin Elmer Lambda 5 . . . . .  | 22 |
| 2.19 | Simplified Jablonski diagram showing the most important transitions and their rate constants. The electronic states are supplemented with vibrational states. . . . .  | 23 |
| 2.20 | Schematic representation of the configuration of the fluorescence spectrometer used in this work, Jasco FP-6500 . . . . .  | 24 |
| 2.21 | Typical experimental FCS setup . . . . .   | 25 |
| 2.22 | Schematic representation of the confocal principle . . . . .   | 26 |
| 2.23 | Recorded FCS spectrum of BODIPY <b>2</b> at two different excitation intensities. . . . .  | 28 |
| 2.24 | Schematic setup of an TCSPC experiment . . . . .   | 29 |
| 2.25 | Recorded TCSPC spectrum of BODIPY <b>5</b> and its phosphorylated analogon <b>5a</b> . The lowered donor energy level by phosphorisation explains the prolongation of the fluorescence lifetime from <b>5</b> ( $\tau_{Fl}=0,7\text{ns}$ ) to <b>5a</b> ( $\tau_{Fl}=3,7\text{ns}$ ) . . . . . | 30 |
| 2.26 | Emission spectra of carboxy SNARF-1 in 50 mM potassium phosphate buffers at various pH values. Samples were excited at 488 nm. . . . .   | 31 |
| 2.27 | Diagram of the Förster-cycle [Tol02] . . . . .   | 33 |
| 2.28 | Spectral transitions of the pyrenes used by Förster, and the pH range where they occur . . . . .   | 34 |
| 2.29 | Differential solvatochromism of 5CN relative to its methoxyderivative in different solvents. Emission is represented by circles and excitation by filled circles. . . . .  | 38 |

|      |   |     |
|------|---|-----|
| 4.1  | Mechanism of the metathesis reaction as proposed by Chauvin: 1. Coordination of the metal complex to the olefin 2. Formation of a metallacyclobutene intermediate 3. Rearrangement of the metallacyclobutane 4. Exchange of the unsubstituted alkene in the metal complex 5. Formation of a second metallacyclobutane 6. Regeneration of the metal complex and dissociation from the now mixed olefin . . . . . | 164 |
| 4.2  | Two popular metathesis catalysts based on molybdenum (Schrock) and ruthenium (Grubbs) . . . . .   | 164 |
| 4.3  | Synthesis of 1-Methyl-3-(2'-Allyloxy-1-styryl)-4-difluorobor-3a,4a-diaza-(S)-indacen ( <b>12</b> ) . . . . .  | 165 |
| 4.4  | Crystallographic structures of 1-Methyl-3-(2'-Allyloxy-1-styryl)-4-difluorobor-3a,4a-diaza-(S)-indacen ( <b>12</b> ) and 1-Methyl-3-(4'-Allyloxy-1-styryl)-4-difluorobor-3a,4a-diaza-(S)-indacen ( <b>14</b> ) . . . . .  | 166 |
| 4.5  | Excitation and emission spectrum of metathesis probe dye <b>12</b> . . . . .  | 167 |
| 4.6  | FCS spectrum of metathesis probe dye <b>12</b> ( $\lambda_{ex}=544\text{nm}$ )  | 167 |
| 4.7  | Assumed product generation of a reaction between a metathesis capable BODIPY dye and a Grubbs catalyst  | 167 |
| 4.8  | Thin layer chromatography foil under UV light ( $\lambda_{ex}=350\text{nm}$ ) showing the influence of Grubbs1 catalyst to the orange fluorescent dyes <b>12</b> and <b>14</b> . Fluorescent products with shorter fluorescence wavelengths than the educts appear only with dye <b>12</b> (marked by red circles)  | 168 |
| 4.9  | Thin layer chromatography foil under UV light ( $\lambda_{ex}=350\text{nm}$ ) displayed with inverted colours to show the increasing appearance of product spots by addition of constant qualitative amounts of Grubbs1 catalyst to dye <b>12</b> . . . . .   | 168 |
| 4.10 | Assumed product generation of a reaction between a metathesis capable BODIPY dye and a Grubbs catalyst (see text for explanation of scheme) . . . . .   | 169 |

### 4.3 List of Figures

|      |  |     |
|------|--|-----|
| 4.11 | TLC foil showing the intermediate products and their combinations to determine possible follow-up products ( $\lambda_{ex}=350\text{nm}$ ) . . . . . | 170 |
| 4.12 | Assumed order of follow-up product generation . . . . .  | 170 |
| 4.13 | Excitation and emission spectrum of metathesis intermediate c . . . . .  | 171 |
| 4.14 | FCS spectrum of metathesis intermediate c ( $\lambda_{ex}=544\text{nm}$ )  | 171 |
| 4.15 | Excitation and emission spectrum of metathesis intermediate d . . . . .  | 171 |
| 4.16 | FCS spectrum of metathesis intermediate d ( $\lambda_{ex}=544\text{nm}$ )  | 171 |
| 4.17 | Excitation and emission spectrum of metathesis intermediate f . . . . .  | 172 |
| 4.18 | FCS spectrum of metathesis intermediate f ( $\lambda_{ex}=544\text{nm}$ )  | 172 |
| 4.19 | Data collected by photophysical means of the metathesis products c, d and f . . . . .  | 172 |

## 4.4 List of Equations

- 2.1 Beer-Lambert law:  

$$E = -lg \frac{I}{I_0} = \epsilon \cdot c \cdot d$$
 ..... 21
- 2.2 Fluorescence decay rate  $k_{Fl}$ :  

$$k_{Fl} = (k_{rad} + k_{IC}) + k_{23} = k_{21} + k_{23}$$
 ..... 23
- 2.3 Fluorescence emission rate  $k_{Em}$ :  

$$k_{Em} = \frac{k_{12} \cdot \Phi_{Fl}}{1 + \frac{k_{12}}{k_S}} ; k_S = k_{21} + k_{23}$$
 ..... 23
- 2.4 Fluorescence auto correlation function  $g^2(\tau)$ :  

$$g^2(\tau) = \frac{[S(0)S(0 + \tau)]}{[S(t)]^2} = 1 + \frac{[\delta S(0)\delta S(0 + \tau)]}{[S(t)]^2}$$
 ..... 27
- 2.5 Fluorescence auto correlation function  $G(\tau)$  with photophysical parameters:  

$$G(\tau) = 1 + \frac{1}{N} \left( \frac{1}{1 + \frac{\tau}{\tau_D}} \right) \left( 1 + \frac{k_{23}^{eff}}{k_{31}} \exp \left[ - \left( k_{23}^{eff} + k_{31} \right) \tau \right] \right)$$
 ..... 27
- 2.6 Fluorescence lifetime as a function of state population:  

$$N(t) = N_0 \cdot \exp \left( -\frac{t}{\tau_{Fl}} \right)$$
 ..... 30
- 2.7 Fluorescence lifetime as a function of fluorescence intensity:  

$$F(t) = F_0 \cdot \exp \left( -\frac{t}{\tau_{Fl}} \right)$$
 ..... 30

#### 4.4 List of Equations

2.8 Förster equation:

$$pK_a^* = pK_a - \frac{(h\nu_1 - h\nu_2)}{\ln 10 RT} \quad 34$$

2.9 Kamlet-Taft equation:

$$\nu_i = \nu_{i0} + p_i\pi^* + b_i\beta + a_i\alpha \quad 36$$

2.10 Principle of differential solvatochromism:

$$\Delta\nu = \nu(ROMe) - \nu(ROH) \approx b_i\beta \quad 37$$

2.11 Altered Kamlet-Taft equation for the determination of  $\mathbf{p_i}$ :

$$\nu_i - \nu_{i0} - b_i\beta = p_i\pi^* \quad 38$$

2.12 Altered Kamlet-Taft equation for the determination of  $\mathbf{a_i}$ :

$$\nu_i - \nu_{i0} - b_i\beta - p_i\pi^* = a_i\alpha \quad 39$$

2.13 Orientation polarisability  $\Delta f$ :

$$\Delta f = \frac{\varepsilon - 1}{2\varepsilon + 1} - \frac{n^2 - 1}{2n^2 + 1} \quad 40$$

2.14 Orientation polarisability  $\Delta f$  as a function of dipole moments:

$$\Delta\nu = \frac{2\Delta f}{a^3hc}(\vec{\mu}_e - \vec{\mu}_g)^2 \quad 40$$

2.15 Ooshika-Lippert-Mataga equation:

$$\Delta\nu = \nu_{abs} - \nu_{em} = \frac{2}{a^3hc}\Delta\vec{\mu}^2 \left[ \frac{\varepsilon_r - 1}{2\varepsilon_r + 1} - \frac{n^2 - 1}{2n^2 + 1} \right] \quad 40$$